

September 2022
DRAFT

**MODELING
EUTROPHICATION
PROCESSES IN THE
DELAWARE RIVER ESTUARY
THREE-DIMENSIONAL
WATER QUALITY MODEL**

Technical Report No. 2022-X



Managing, Protecting and Improving
the Water Resources of the
Delaware River Basin since 1961



This report was prepared by the following staff with the Delaware River Basin Commission, as well as the United States Geological Survey, who performed the work described herein.

Li Zheng, PhD (primary author)	Senior Water Resource Modeler
Thomas Amidon, BCES	Manager, Water Resource Modeling
Sarah Beganskas, PhD	Water Resource Scientist
Jake Bransky	Aquatic Biologist
Fanghui Chen, PhD, PE	Senior Water Resource Engineer
Vince DePaul	Hydrologist
Elaine Panuccio	Water Resource Scientist
Namsu Suk, PhD	Director, Science and Water Quality Management
John Yagecic, PE	Manager, Water Quality Assessment

Cite report as:

Delaware River Basin Commission. 2022. *Modeling Eutrophication Processes in the Delaware River Estuary: Three-Dimensional Water Quality Model*. September 2022 Draft.

ACKNOWLEDGEMENTS

This work was funded in part by generous grants from the William Penn Foundation, the United States Environmental Protection Agency, the New Jersey Department of Environmental Protection, and the Pennsylvania Department of Environmental Protection. Critical datasets, without which this work could not have been performed, were obtained from the National Oceanic and Atmospheric Administration’s National Climatic Data Center as well as the United States Geological Survey.

The DRBC is grateful for the technical support and direction provided by its Expert Panel, composed of internationally renowned modelers: Dr. Steve Chapra, Dr. Carl Cerco, Dr. Bob Chant, and Tim Wool. In addition to the model expert panel, DRBC acknowledges with appreciation its hydrodynamics modeling consultant, Dr. Hugo Rodrigues of GHD. Finally, DRBC acknowledges with appreciation the invaluable guidance received from the day-to-day interactions with its water quality modeling consultants, Dr. Victor Bierman and Scott Hinz of LimnoTech.

Finally, DRBC acknowledges the various NPDES permit-holders within the tidal estuary that provided critical discharge data for this work.

EXECUTIVE SUMMARY

[to be written when report is finalized]



TABLE OF CONTENTS

Acknowledgements..... ii

Executive Summary..... iii

Table of Contents..... iv

 List of Appendices v

 List of Tables..... vi

 List of Figures vii

 List of Acronyms/Abbreviations x

1. Background and Introduction 1

 1.1 Purpose and Objective of the Modeling Study 1

 1.2 Study Area 3

 1.3 Processes Affecting Dissolved Oxygen..... 5

 1.4 Overview of Technical Approach 6

2. Sampling Program and Results..... 7

 2.1 Sampling Program Description 7

 2.2 Sampling Results 25

 2.3 Characterization of Loads..... 31

 2.4 Additional Field Data 39

3. Water Quality Model Development 43

 3.1 Model Description 43

 3.2 Water Quality Model Calibration 80

 3.3 Model Summary 152

References 153

LIST OF APPENDICES

Appendix A: Monitoring Results

Appendix B: Transect Profile Data

Appendix C: Verification of Transport Fidelity

Appendix D: Enhancement in Reaeration Simulation

Appendix E: State Variable Calculation

Appendix F: Model to Data Comparisons

Appendix G: Diagnostic Analyses

Appendix H: Sensitivity Analysis



LIST OF TABLES

Table 2-1 Boat Run monitoring dates	11
Table 2-2 Boat Run locations	11
Table 2-3 Boat Run parameters	12
Table 2-4: Continuous monitoring locations.....	15
Table 2-5 Monitored treatment plant discharges.....	18
Table 2-6 Effluent monitoring parameters	20
Table 2-7 Tributary monitoring locations	23
Table 2-8 Tributary Monitoring Parameters	24
Table 2-9 Mean effluent concentrations of key nutrients.....	26
Table 2-10 Mean concentrations of key nutrients at monitored tributaries.....	30
Table 3-1: Water quality model state variables.....	46
Table 3-2: CSO effluent concentrations	64
Table 3-3: Nutrient concentrations from WOA18 near mouth of Estuary	67
Table 3-4 NOAA NADC weather stations	68
Table 3-5: SOD and benthic flux model inputs from survey data	70
Table 3-6: USGS Transect Surveys during 2012, 2018, and 2019	81
Table 3-7: Key calibration parameters.....	84
Table 3-8: Average statistical metrics at 22 Boat Run Stations, 2018–2019	87
Table 3-9: Statistical Metrics of Dissolved Oxygen at USGS Stations and PWD-Buoys, 2018–2019	121
Table 3-10: Statistical Metrics of Phytoplankton at USGS Stations and PWD-Buoys, 2018–2019.	121
Table 3-11: Parameters Chosen in Sensitivity Analysis.....	142

LIST OF FIGURES

Figure 1-1: DO at Ben Franklin Bridge during July and August from 1965–2022	2
Figure 1-2: Delaware River Basin	4
Figure 2-1 Overview of sampling programs	8
Figure 2-2: Boat Run sampling and continuous in-situ monitoring locations.....	10
Figure 2-3: Monitored point source discharges.....	17
Figure 2-4: Tributary monitoring locations	22
Figure 2-5 Long-term monitoring within the Estuary (example results)	26
Figure 2-6 Effluent Ammonia Concentrations – Ranked Boxplots.....	29
Figure 2-7 Tributary ammonia concentrations - ranked boxplots	31
Figure 2-8 Ammonia loads from monitored treatment plants and tributaries	32
Figure 2-9: Effluent ammonia loads – ranked boxplots	33
Figure 2-10: Tributary ammonia loads – ranked boxplots.....	34
Figure 2-11 Total phosphorus from monitored treatment plants and tributaries	35
Figure 2-12 Total nitrogen from monitored treatment plants and tributaries	35
Figure 2-13 Total organic carbon from monitored treatment plants and tributaries	36
Figure 2-14 Tributary total phosphorus loads – ranked boxplots.....	37
Figure 2-15 Tributary total nitrogen loads - ranked boxplots.....	38
Figure 2-16 Tributary total organic carbon loads - ranked boxplots	38
Figure 2-17 Dissolved oxygen profiles	40
Figure 2-18 Primary productivity estimates.....	42
Figure 3-1: Numerical grid and projected bathymetry	45
Figure 3-2: Water quality model kinetics.....	46
Figure 3-3: Location maps of (a) WOA18 data on 1° grid; and (b) Monitoring stations near mouth.....	66
Figure 3-4: Weather stations used to characterize climatic boundaries	69
Figure 3-5: SOD and benthic flux survey locations	71
Figure 3-6: Spatial distribution of observed benthic nutrient flux and SOD.....	72
Figure 3-7: Temporal variation of sediment ammonia flux, summer vs. non-summer.....	73
Figure 3-8: Temporal variation of sediment nitrate flux, summer vs. non-summer.	74
Figure 3-9: Temporal variation of sediment phosphate flux, summer vs. non-summer.	75
Figure 3-10: Temporal variation of SOD, summer vs. non-summer.	76
Figure 3-11: Spatial distribution of benthic flux and SOD summarized to bins.....	77

Figure 3-12 Daily flow by year at Delaware River at Trenton NJ 79

Figure 3-13: Daily flow by year at Schuylkill River at Philadelphia PA 79

Figure 3-14: Annual Precipitation at Philadelphia 80

Figure 3-15: Calibration data locations 82

Figure 3-16: Model to Boat Run data comparisons – DOC during summer..... 89

Figure 3-17: Model to Boat Run data comparison – DOC at Navy Yard, 2018–2019 89

Figure 3-18: Model to Boat Run data comparisons – ammonia during summer 91

Figure 3-19: Model to Boat Run data comparison – ammonia at Navy Yard, 2018–2019 91

Figure 3-20: Model to Boat Run data comparisons – nitrate during summer..... 92

Figure 3-21: Model to Boat Run data comparison – nitrate at Navy Yard, 2018–2019..... 92

Figure 3-22: Model to Boat Run data comparisons – TN during summer 93

Figure 3-23: Model to Boat Run data comparison – TN at Navy Yard, 2018–2019 93

Figure 3-24: Model to Boat Run data comparisons – phosphate during summer 95

Figure 3-25: Model to Boat Run data comparison – phosphate at Navy Yard, 2018–2019 95

Figure 3-26: Model to Boat Run data comparisons – TP during summer..... 96

Figure 3-27: Model to Boat Run data comparison – TP at Navy Yard, 2018–2019..... 96

Figure 3-28: Model to Boat Run data comparisons – solids during summer..... 98

Figure 3-29: Model to Boat Run data comparison – solids at Navy Yard, 2018–2019 98

Figure 3-30: Model to Boat Run data comparisons – phytoplankton during summer 99

Figure 3-31: Model to Boat Run data comparison – phytoplankton at Navy Yard, 2018–2019..... 100

Figure 3-32: Light extinction – July 2018, 2019, and 2012..... 102

Figure 3-33: Seasonal phytoplankton comparisons, 2018–2019..... 103

Figure 3-34: Seasonal Phytoplankton Comparisons, 2012 104

Figure 3-35: Model to Boat Run data comparisons – DISOX during summer..... 105

Figure 3-36: Model to Boat Run data comparison – DISOX at Navy Yard, 2018–2019..... 106

Figure 3-37: Model to Boat Run data comparisons – DOSAT during summer..... 107

Figure 3-38: Model to Boat Run data comparison – DOSAT at Navy Yard, 2018–2019 107

Figure 3-39: Model to Continuous Data Comparison – DO at Pennypack Woods during 2018–2019 109

Figure 3-40: Model to Continuous Data Comparison – DO at Ben Franklin Bridge during 2018–2019 .. 110

Figure 3-41: Model to Continuous Data Comparison – DO at Buoy B during 2018–2019..... 111

Figure 3-42: Model to Continuous Data Comparison – DO at Chester during 2018–2019 112

Figure 3-43: Model to Continuous Data Comparison – DO at Buoy P during 2018–2019..... 113

Figure 3-44: Model to Continuous Data Comparison – DO at Reedy Island during 2018–2019 114

Figure 3-45: Phytoplankton at Ben Franklin Bridge during 2018–2019..... 118

Figure 3-46: Phytoplankton DO at Buoy B during 2018–2019..... 119

Figure 3-47: Phytoplankton at Buoy P during 2018–2019 120

Figure 3-48: Target Diagram for Predicted DO at at Continuous Stations, 2018–2019..... 122

Figure 3-49: Target Diagram for Predicted Phytoplankton at Continuous Stations, 2018–2019 122

Figure 3-50: Model to Transect Data Comparisons at Pennypack Woods and Ben Franklin Bridge 124

Figure 3-51: Model to Transect Data Comparisons at Ben Franklin and Delaware Memorial Bridges ... 125

Figure 3-52: Model to Transect Data Comparisons at Reedy Island..... 126

Figure 3-53: DO Component Analyses – February and July 2018 128

Figure 3-54: Alga Growth Limiting Factors at Ben Franklin Bridge during 2019 – Water Surface..... 130

Figure 3-55: Algal Growth Limiting Factors at Ben Franklin Bridge during 2019 – Depth-averaged 131

Figure 3-56: Temperature Limiting Factors at Eddystone during 2019 132

Figure 3-57: Figure 3 from McSweeney et al. 2017 133

Figure 3-58: Chlorophyll at Ben Franklin Bridge and River Discharge Flow at Trenton, 2019..... 134

Figure 3-59: Comparisons between Base Case and Seasonal Adjustment – Ke 136

Figure 3-60: Comparisons between Base Case and Seasonal Adjustment - Phytoplankton 137

Figure 3-61: Base Case and Seasonal Adjustment Comparisons – Phytoplankton and DO..... 138

Figure 3-62: Base Case and Seasonal Adjustment Comparisons – DO at Ben Franklin Bridge..... 139

Figure 3-63: Sensitivity Test: Phytoplankton Maximum Growth Rate Constant (Group 2)..... 143

Figure 3-64: Sensitivity Test: Phytoplankton Maximum Growth Rate Constant (Group 1, 2, 3)..... 144

Figure 3-65: Sensitivity Test: Phytoplankton Respiration Rate Constant (Group 1, 2, 3) 145

Figure 3-66: Sensitivity Test: Optimal Temperature for Growth (Group 1, 2, 3)..... 146

Figure 3-67: Sensitivity Test: Phytoplankton Optimal Light Saturation (Group 1, 2, 3)..... 147

Figure 3-68: Comparisons of SOD Data Collected during 2012—2018 vs. 1986 149

Figure 3-69: DO Components for July 2018: Base case vs. no phytoplankton growth..... 151

LIST OF ACRONYMS/ABBREVIATIONS

2D	Two Dimensional
3D	Three Dimensional
Boat Run	DRBC's Delaware Estuary Water Quality Monitoring Program
BOD5	5-day Biochemical Oxygen Demand
CBOD	Carbonaceous Biochemical Oxygen Demand (CBODU indicates ultimate CBOD)
C&D Canal	Chesapeake and Delaware Canal
Chla	Chlorophyll-a
CSO	Combined Sewer Overflow
D-DIP	Inorganic Phosphate
DET-C	Detrital Carbon
DET-N	Detrital Nitrogen
DET-P	Detrital Phosphorus
DET-Si	Detrital Silica
DISOX	Dissolved Oxygen
DO	Dissolved Oxygen
DOC	Dissolved Organic Carbon
DON	Dissolved Organic Nitrogen
DOP	Dissolved Organic Phosphorus
DOSi	Dissolved Organic Silica
DOSAT	Dissolved Oxygen Saturation
DRB	Delaware River Basin
DRBC	Delaware River Basin Commission
DW	Dry Weight
EFDC	The Environmental Fluid Dynamics Code
ETM	Estuary Turbidity Maxima
Hr	Hour
IN-SI	Inorganic Silica
Ke	light extinction coefficient
LOADEST	Load Estimator
MDLs	Method Detection Limits
MEP	Model Expert Panel

MS4	Municipal Separate Storm Sewer System
NADP	National Atmospheric Deposition Program
NH34	Ammonia Nitrogen
NO3O2	Nitrite plus Nitrate Nitrogen
NOAA	National Oceanic and Atmospheric Administration
NPS	Non-Point Source
NSE	Nash-Sutcliffe coefficients
NWQP	National Water Quality Portal
Org-N	Dissolved Organic Nitrogen
Org-P	Dissolved Organic Phosphorus
Org-Si	Dissolved Organic Silica
PAR	Photosynthetically Active Radiation
PWD	Philadelphia Water Department
R2	Coefficient of determination
RM	River Mile
SOD	Sediment Oxygen Demand
SPW	Special Protection Waters
SRP	Soluble Reactive Phosphorus
TDS	Total Dissolved Solids
TSS	Total Suspended Solids
TDN	Total Dissolved Nitrogen
TKN	Total Kjeldahl Nitrogen
TN	Total Nitrogen
TP	Total Phosphorus
ubRMSD	unbiased Root Mean Square Difference
USACE	U.S. Army Corps of Engineers
USEPA	U.S. Environmental Protection Agency (or EPA)
USGS	U.S. Geological Survey
UV	Ultraviolet
WASP	Water Quality Analysis Simulation Program
WQAC	Water Quality Advisory Committee
WRDB	Water Resources Database
WRTDS	Weighted Regressions on Time, Season, and Discharge Tool

1. BACKGROUND AND INTRODUCTION

The Delaware River Basin Commission (“DRBC” or “Commission”) adopted a Resolution No. 2017-4 recognizing the significant water quality improvements in the Delaware River Estuary (“Delaware Estuary” or “the Estuary”) and the vital importance of determining the appropriate designated aquatic life uses and water quality criteria necessary to support these uses. The resolution specifically requires the development and calibration of a eutrophication model for the Delaware Estuary¹, as well as the formation of an Expert Panel to provide input and advice to the DRBC.

The DRBC convened a Eutrophication Model Expert Panel (MEP) in a regular basis since November of 2016. Under the guidance of the MEP, DRBC staff developed a eutrophication model for the Delaware Estuary. Broadly, the goal of the project was to develop and calibrate a water quality model of dissolved oxygen and eutrophication processes in the Delaware Estuary from the head of the tidal Delaware River at Trenton, NJ to the outlet of the Delaware Bay into the ocean between Cape May, NJ and Lewis, DE. In addition to enhancing our understanding of the impact of carbon, nitrogen and phosphorus loads on dissolved oxygen conditions in the tidal Delaware River and Bay, this project provides the scientific basis for the DRBC to evaluate feasible scenarios of controlling various sources of these loads into Delaware Estuary in order to achieve higher dissolved oxygen concentrations.

This effort includes: 1) the convening of an expert panel to guide the development of the eutrophication model; 2) the completion of a two-year monitoring program in partnership with wastewater authorities in order to obtain data on nutrient loadings from point sources; 3) field studies on primary productivity in the lower Delaware Estuary; and 4) development of a linked hydrodynamic model and eutrophication model. The DRBC previously published a Quality Assurance Project Plan (QAPP) for this project (DRBC, 2019) as well as a draft hydrodynamics model calibration report (DRBC, 2021). This report documents the development and calibration of the water quality model, which simulates eutrophication processes that impact dissolved oxygen.

1.1 PURPOSE AND OBJECTIVE OF THE MODELING STUDY

Dissolved oxygen is among the most critical environmental parameters directly affecting fish communities. When the Delaware River Basin Commission was created in 1961, little or no dissolved oxygen was present in the Delaware River Estuary from Wilmington to Philadelphia for periods of up to six months each year, preventing the survival of resident fish and the passage of anadromous fish through these waters. The water quality and aquatic life uses of the Delaware Estuary have substantially improved since DRBC adopted designated uses and water quality criteria for these reaches in 1967, specifically due

¹ This report uses the term Delaware Estuary broadly to include the entire tidal Delaware River as well as the Delaware Bay. In some other contexts, the tidal Delaware River is referred to as the Delaware River Estuary.

to wastewater treatment plant upgrades to meet organic wastewater discharge criteria. These improvements over the years are schematically illustrated in Figure 1-1. Nonetheless, significant dissolved oxygen sags still occur in Zones 3 (River Mile [RM] 95 - 108) and 4 (RM 79 - 95), especially during summer periods, limiting the degree of propagation amongst resident fish populations. Note that the mouth of the Delaware Bay is referred to as RM 0.

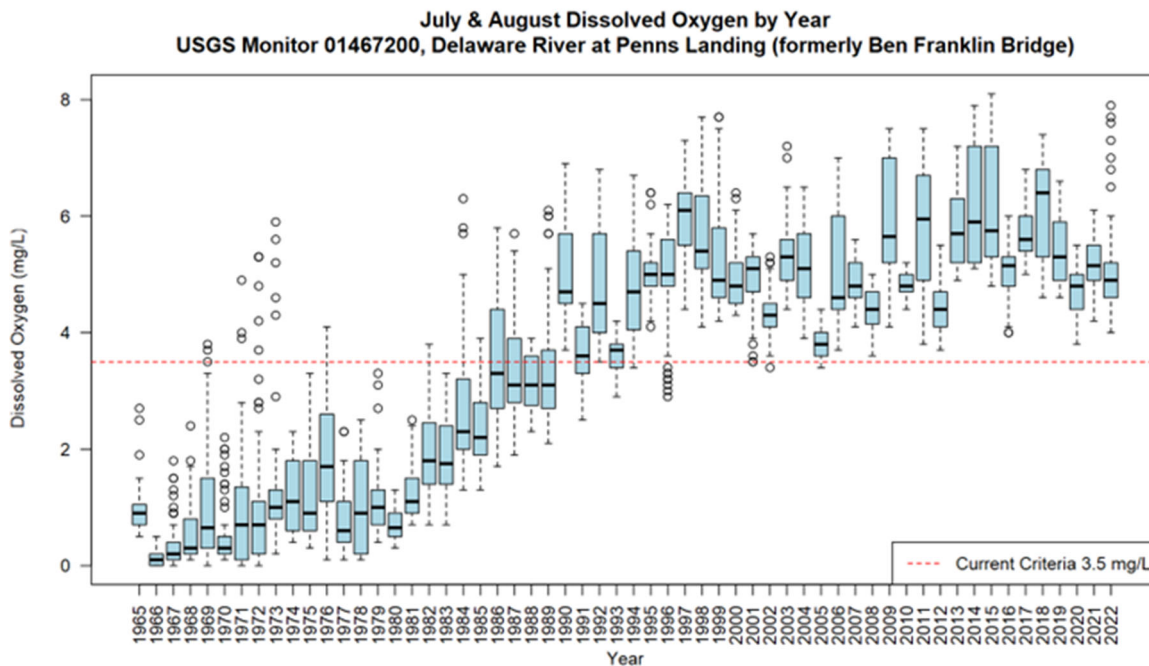


Figure 1-1: DO at Ben Franklin Bridge during July and August from 1965–2022

The DRBC approved a resolution in September 2017 recognizing the significant water quality improvements in the Delaware River Estuary and the vital importance of determining the appropriate designated aquatic life uses and water quality criteria necessary to support these uses in a 38-mile section of the tidal Delaware River stretching from Wilmington to Philadelphia. In accordance with DRBC Resolution No. 2017-4, which affirms the important goal of continued water quality improvement, the DRBC is conducting a comprehensive scientific and engineering evaluation of water quality to determine the "highest attainable use" of this reach of the river and to provide data and information to establish revised water quality criteria to protect that use. DRBC is leading this groundbreaking effort through a collaborative process informed by an Expert Panel comprised of nationally recognized water resource scientists and engineers, and in close consultation with its Water Quality Advisory Committee (WQAC), a stakeholder advisory group representing state and federal co-regulators, NGOs, academic institutions, and municipal and industrial dischargers. DRBC will perform an "analysis of attainability" to determine the highest attainable dissolved oxygen condition that can be achieved.

In support of the overall evaluation of highest attainable dissolved oxygen conditions to support the revised aquatic life designated use as described above, the goal of this modeling project is to develop a technically sound eutrophication model for the Delaware Estuary and Bay, from the head of the tide at Trenton, NJ to the ocean, utilizing an appropriate level of complexity within the current state of the science and within the timeframe established by the Commission. The eutrophication model being developed by the DRBC will enhance our understanding of the impact of carbon, nitrogen and phosphorus loads including nitrogenous and carbonaceous oxygen demand and effects from phytoplankton photosynthesis and respiration, on dissolved oxygen conditions in the tidal Delaware River and Bay. The model also accounts for reaeration, sediment oxygen demand impacts to ensure processes affecting water column dissolved oxygen levels are adequately represented. Given the complexity of tidal dynamics and input loads, the spatial extent of the model includes the entire tidal Delaware River and Bay. The model is designed to estimate ambient dissolved oxygen levels that can be expected for various levels of input load reductions using a dynamic (time-varying), long-term simulation of diurnal dissolved oxygen patterns.

1.2 STUDY AREA

The study area encompasses the entire Delaware River drainage basin, while the Delaware Estuary (the tidal Delaware River and Bay) defines the water quality model extent.

1.2.1 DELAWARE RIVER DRAINAGE BASIN

The Delaware River extends 330 miles from the Catskill Mountains in New York to the mouth of the Delaware Bay where it enters the Atlantic Ocean between Cape May, New Jersey and Cape Henlopen, Delaware (Figure 1-2). It is the longest un-dammed river on the Atlantic coast of the United States. The entire Delaware River basin comprises 13,539 square miles in four states (New York, New Jersey, Pennsylvania, and Delaware), including the 782 square miles of the Delaware Bay itself. The East and West Branches of the Delaware River combine at Hancock, New York to form the mainstem Delaware River, which flows 200 miles south to the head of tide at Trenton, New Jersey. Below Trenton, the river is tidally influenced for 133 miles down to the mouth of the Delaware Bay. The drainage area at Trenton, New Jersey is approximately 6,780 square miles. The total watershed downstream of Trenton to the mouth of the bay is 6,060 square miles, including the Schuylkill River (1,911 square miles) and Christina River (755 square miles) basins; these are the second and third largest tributaries (behind the Delaware River itself) in terms of freshwater flow contributed to the mainstem. The hydrodynamics and water quality model domain extends from the head of tide at Trenton to the mouth of the bay into the Atlantic Ocean.

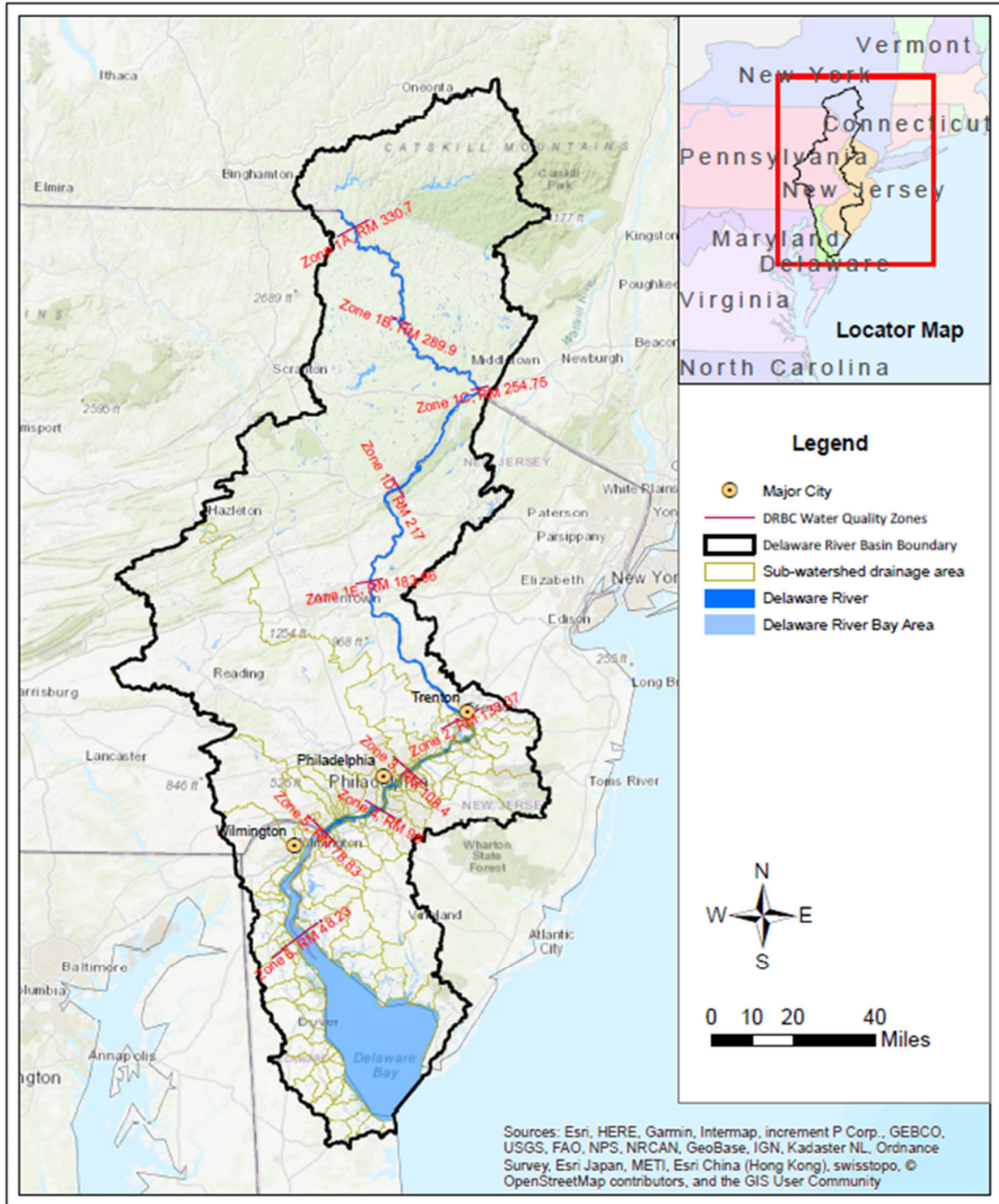


Figure 1-2: Delaware River Basin

The average annual water discharge at Trenton is about 20,290 cfs based on data from 1913 to 2019. The monthly statistics of river discharge show a clear flow seasonality, with the two highest monthly mean

flows in March and April (20,400 and 21,900 cfs, respectively) and the two lowest in July and August (6,420 and 6,680 cfs, respectively). The average annual water discharge in the Schuylkill River over the period 1932–2018 is approximately 2,850 cfs. According to a U.S. Geological Survey (USGS) study prepared for the Federal Emergency Management Agency (FEMA) in 2008, the flood frequencies at Delaware River at Trenton, N.J. are estimated as follows: 94,900 (2-year), 138,000 (5-year), 169,000 (10-year), 211,000 (25-year), 245,000 (50-year), and 280,000 (100-year) in units of cfs (Schopp and Firda, 2008).

Monitoring demonstrates that the dissolved oxygen levels and water quality in the non-tidal Delaware (i.e., north of Trenton, N.J.) are already better than standards. A Special Protection Waters (SPW) Program was initially adopted by the DRBC in 1992 and expanded in 1994 and 2008 for the non-tidal portion of Delaware River, designed to prevent degradation in streams and rivers where existing water quality is better than the established water quality standards. The program states that there will be no measurable change in existing water quality of SPW except towards natural conditions. Simply, the goal of SPW program is to keep the clean water clean.

1.2.2 DELAWARE ESTUARY

The tidal portion of the Delaware River is a typical coastal plain estuary with a relatively homogeneous shallow depth of about 26 to 33 feet. Eighty percent of the estuary has a depth of less than 30 feet, except for the Federal Navigation Channel, which was deepened most recently in 2016 to a depth of 45 feet below Mean Lower Low Water (MLLW) level. The width of the Delaware Bay at its mouth is 11 miles, and the widest part of the bay is about 27 miles. Channel width decreases precipitously in the upstream direction: 2.4 miles wide in the reach from Delaware City just inland of the Chesapeake and Delaware Canal (C&D Canal) around RM 60; 1/2 -mile wide in Philadelphia at the Ben Franklin Bridge (RM 100); about ¼-mile wide at Burlington (RM 117.5); and less than 1,000 feet wide at Trenton (RM 134). Additional hydro-physical characterization of the Delaware Estuary is found in the draft hydrodynamics model calibration report (DRBC, 2021).

1.3 PROCESSES AFFECTING DISSOLVED OXYGEN

Dissolved oxygen is controlled by a series of complex physical, chemical, and biological processes, which is summarized on Figure 3-2 and represented in the WASP8 model framework as discussed in Section 3.1.2. Physical processes represented in the model include advection, dispersion or mixing, reaeration, settling, and sorption. The model chemical processes consist of ammonia nitrification, CBOD oxidation, sediment oxygen demand, dissolution, and mineralization. Last, the modeled biological processes involve photosynthesis, respiration, phytoplankton growth, death, and uptake of nutrients. Of these processes, reaeration and photosynthesis contribute to the dissolved oxygen production; nitrification, sediment oxygen demand, CBOD oxidation, and respiration cause dissolved oxygen consumption. In addition, water temperature and salinity influence the levels of dissolved oxygen in equilibrium with the atmosphere;

warmer water contains less oxygen than colder water at saturation, while saltier water (higher salinity) carries less oxygen than fresh water.

1.4 OVERVIEW OF TECHNICAL APPROACH

The DRBC's overall modeling approach is as follows.

- Develop a linked hydrodynamic and water quality model of the system using Environmental Fluid Dynamics Code (EFDC) and Water Quality Analysis Simulation Program (WASP8).
- Assess available nutrient and auxiliary environmental data and conduct additional monitoring of both sources and ambient water to fill gaps as needed.
- Calibrate linked hydrodynamic and water quality model to our intensive monitoring period (2018-2019), and corroborate against historical periods, primarily 2012. Together these periods represent a wide range of hydrologic conditions.

The primary purpose of the study is to develop a calibrated EFDC-WASP8 model appropriate for conducting forecast simulations to determine the input load reductions needed to achieve varying levels of ambient dissolved oxygen conditions in the Delaware River Estuary, and in particular the urban estuary.

2. SAMPLING PROGRAM AND RESULTS

The development of a spatially explicit eutrophication model for the entire Delaware Estuary represents an ambitious undertaking that requires a significant amount of data.

2.1 SAMPLING PROGRAM DESCRIPTION

The following monitoring programs were expanded and initiated in 2017 to support this study as shown in Figure 2-1:

- Delaware Estuary Water Quality Monitoring Program (Boat Run);
- Tributary Monitoring including the Delaware River at Trenton and the Schuylkill River at Philadelphia;
- Enhancements to selected USGS monitors; and
- Additional wastewater treatment plant effluent monitoring for Tier 1 and 2 facilities from March 2018 to February 2020. Tier 1 facilities comprise 95% of the cumulative point discharge load for ammonia, TKN, and BOD5 based on the data set collected between 2011 and 2015. Tier 2 facilities include facilities contributing to the 95% cumulative load for phosphorus, SRP, nitrate, and TN that were not already included in Tier 1. Tier 3 facilities were those facilities not included in Tiers 1 or 2. More information is available [here](#).
- For Tier 3 facilities, two-year effluent data collected from 2011 to 2015 and states' electronic Discharge Monitoring Record were used to characterize effluent conditions for the model calibration period.

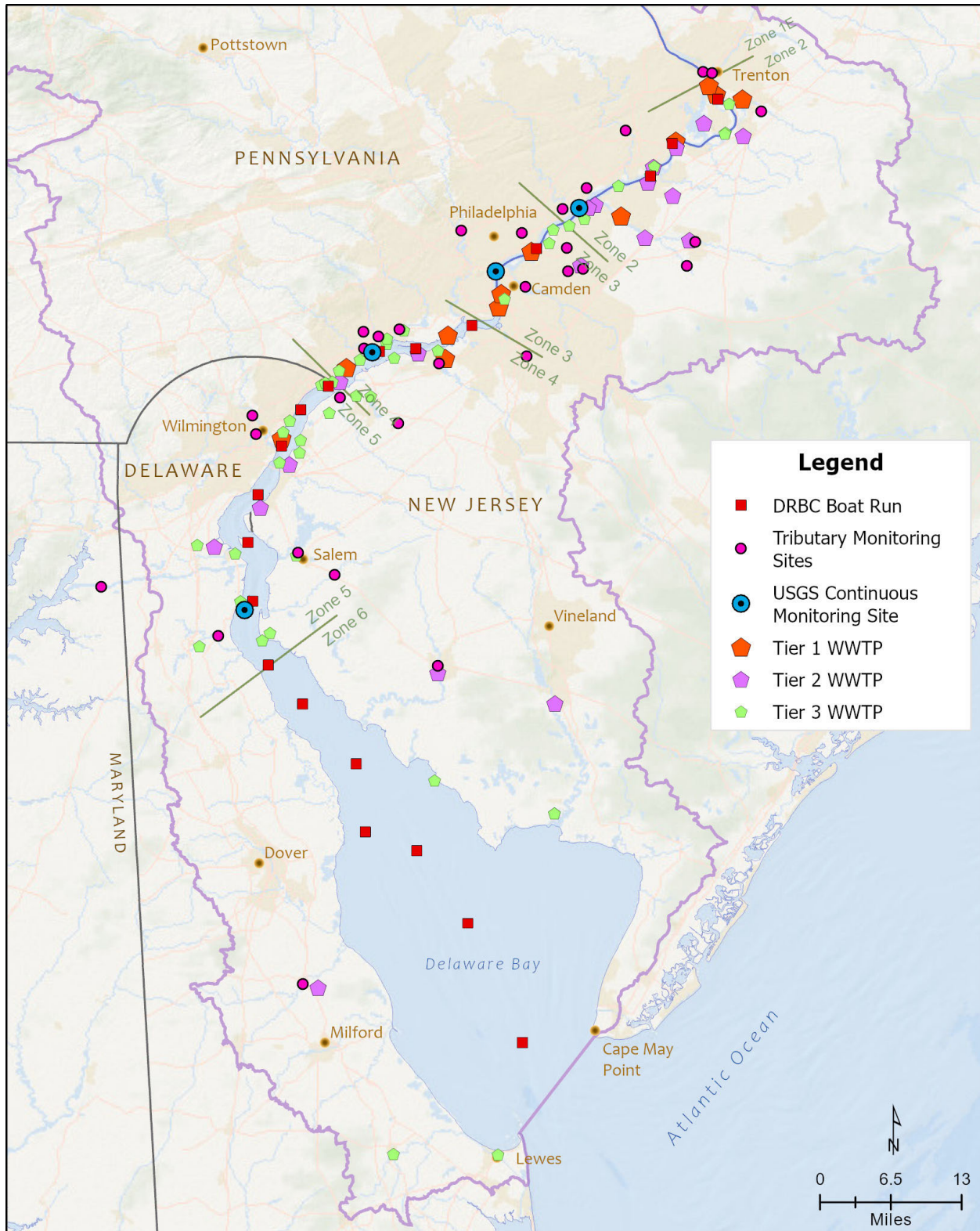


Figure 2-1 Overview of sampling programs

2.1.1 DELAWARE ESTUARY WATER QUALITY MONITORING

Delaware Estuary water quality monitoring consisted of primarily event-based Delaware Estuary Water Quality Monitoring Program (Boat Run) monitoring and enhancements to USGS water quality meters, as shown in Figure 2-2. Boat Run monitoring involved the collection of discrete samples on specific sample collection days at 22 stations with analysis of an extended parameter list. USGS monitors are deployed at several fixed locations where they measure and report a shorter list of parameters on a continuous basis. These ambient data were used as model calibration targets by comparing with model outputs.



Figure 2-2: Boat Run sampling and continuous in-situ monitoring locations

2.1.1.1 DRBC BOAT RUN

Historically, boat runs have been performed approximately monthly beginning in March or April and continuing through October. During the period from 2017 through 2020, the Boat Run was expanded to nearly year-round (weather permitting). Boat Run monitoring was performed on the dates shown in Table 2-1 below.

Table 2-1 Boat Run monitoring dates

CY2017	CY2018	CY2019	CY2020
18-Jan-17		26-Feb-19	
6-Feb-17		11-Mar-19	24-Feb-20
13-Mar-17	19-Mar-18	25-Mar-19	9-Mar-20
10-Apr-17	23-Apr-18	22-Apr-19	
22-May-17	7-May-18	20-May-19	
12-Jun-17	11-Jun-18	17-Jun-19	
10-Jul-17	9-Jul-18	15-Jul-19	
7-Aug-17	13-Aug-18	27-Aug-19	24-Aug-20
26-Sep-17	17-Sep-18	9-Sep-19	14-Sep-20
9-Oct-17	8-Oct-18	7-Oct-19	5-Oct-20
6-Nov-17	7-Nov-18	4-Nov-19	
18-Dec-17		9-Dec-19	

The Boat Run program samples 22 stations near surface in the center channel of the Delaware Estuary from just below the head of tide to just above the mouth of the Bay. Sample locations are shown in

Figure 2-2 and listed in Table 2-2 below.

Table 2-2 Boat Run locations

Sample Location Description	River Mile (from Mouth of Bay)	Coordinates (Latitude and Longitude)
South Brown Shoal	6.5	38.932187, -75.103146
South Joe Flogger Shoal	15.5	39.068639, -75.177453

Sample Location Description	River Mile (from Mouth of Bay)	Coordinates (Latitude and Longitude)
Elbow of Crossledge Shoal	22.75	39.144737, -75.239596
Mahon River	31	39.229606, -75.300302
Ship John Light	36.6	39.296339, -75.375902
Smyrna River	44	39.380387, -75.472996
Liston Point	48.2	39.425987, -75.525838
Reedy Island	54.9	39.511917, -75.553137
Pea Patch Island	60.6	39.592357, -75.564242
New Castle	66	39.655110, -75.545412
Cherry Island	71	39.720878, -75.505794
Oldmans Point	74.9	39.774134, -75.467938
Marcus Hook	78.1	39.800655, -75.425245
Eddystone	84	39.844852, -75.342034
Paulsboro	87.9	39.848061, -75.267146
Navy Yard	93.2	39.881679, -75.180190
Benjamin Franklin Bridge	100.2	39.955502, -75.135818
Betsy Ross Bridge	104.75	39.984701, -75.066603
Torresdale	110.7	40.040199, -74.988048
Burlington Bristol Bridge	117.8	40.081067, -74.868852
Florence Bend	122.4	40.128025, -74.816028
Biles Channel	131.04	40.181566, -74.746191

Beginning in 2017 additional parameters related to the eutrophication study were included. Analytical parameters analyzed during boat run events are shown in **Error! Reference source not found.** below.

Table 2-3 Boat Run parameters

Analytical Parameter	Units	Filtration	Sample Type
Salinity	ppt	Unfiltered	in-situ surface water grab
Specific Conductance	µS/cm	Unfiltered	in-situ surface water grab

Analytical Parameter	Units	Filtration	Sample Type
Salinity	ppt	Unfiltered	near-surface water grab
Dissolved Oxygen	mg/L	Unfiltered	in-situ surface water grab
Dissolved Oxygen Saturation	% Saturation	Unfiltered	in-situ surface water grab
pH, Field	1-14 S.U.	N/A	in-situ surface water grab
Secchi Depth	meters	N/A	in-situ surface water grab
Temperature, Water	°C	N/A	in-situ surface water grab
Turbidity (Nephelometric)	NTU	Unfiltered	near-surface water grab
Light Attenuation	m ⁻¹	N/A	in-situ ship level grab
Light Attenuation	m ⁻¹	N/A	in-situ 1-meter depth grab
Color Dissolved Organic Material (CDOM)	RFU	Unfiltered	near-surface water grab
Chlorophyll-a	µg/L	0.70 µm filter	near-surface water grab
UV 254	cm ⁻¹	Unfiltered	near-surface water grab
Alkalinity (titrimetric, pH 4.5)	mg/L	Unfiltered	near-surface water grab
Hardness as CaCO ₃	mg/L	Unfiltered	near-surface water grab
Chloride, Total	mg/L	Unfiltered	near-surface water grab
Sodium	mg/L	Unfiltered	near-surface water grab
Calcium	mg/L	Unfiltered	near-surface water grab
Magnesium (Mg 2+)	mg/L	Unfiltered	near-surface water grab
Potassium (K+)	mg/L	Unfiltered	near-surface water grab
Sulfate	mg/L	0.45 µm filter	near-surface water grab
Dissolved Organic Carbon (DOC)	mg/L	0.45 µm filter	near-surface water grab
Particulate Organic Carbon (POC)	mg/L	0.45 µm filter	near-surface water grab
Silica, Dissolved	mg/L	0.45 µm filter	near-surface water grab
Silica, Total	mg/L	Unfiltered	near-surface water grab
Nitrogen, Total	mg/L	Unfiltered	near-surface water grab
Nitrogen, Total Dissolved	mg/L	0.45 µm filter	near-surface water grab
Nitrate as N, Dissolved	mg/L	0.45 µm filter	near-surface water grab

Analytical Parameter	Units	Filtration	Sample Type
Nitrate/Nitrite as N, Dissolved	mg/L	0.45 µm filter	near-surface water grab
Nitrite as N, Dissolved	mg/L	0.45 µm filter	near-surface water grab
Nitrogen, Particulate	mg/L	0.45 µm filter	near-surface water grab
Ammonia Nitrogen (NH3-N)	mg/L	0.45 µm filter	near-surface water grab
Phosphorus, Particulate Organic	mg/L	0.45 µm filter	near-surface water grab
Phosphorus, Particulate Inorganic	mg/L	0.45 µm filter	near-surface water grab
Orthophosphorus, Soluble	mg/L	0.45 µm filter	near-surface water grab
Phosphorus, Total	mg/L	Unfiltered	near-surface water grab
Phosphorus, Dissolved Total	mg/L	0.45 µm filter	near-surface water grab
Total Dissolved Solids (TDS)	mg/L	Unfiltered	near-surface water grab
Total Suspended Solids (TSS)	mg/L	Unfiltered	near-surface water grab
Fixed Suspended Solids (FSS)	mg/L	Unfiltered	near-surface water grab
Volatile Suspended Solids (VSS)	mg/L	Unfiltered	near-surface water grab

2.1.1.2 CONTINUOUS *IN-SITU* MONITORING

Continuous monitoring data were available from four USGS water quality monitors in the Delaware Estuary: Pennypack Woods, Penn’s Landing, Chester, and Reedy Island. Detailed information is provided in Table 2-4, while locations are shown in

Figure 2-2. DRBC augmented the monitoring at Chester beginning in May 2018, adding nitrite plus nitrate and dissolved organic carbon (DOC). Not all parameters were available at all stations for the full model calibration period. The Penn’s Landing gage was relocated from end of Pier 12 about 150 ft upstream of Ben Franklin Bridge (formerly called Ben Frankling Bridge Station) to approximately 2,500 ft downstream from Ben Franklin bridge, at Penn's Landing in January 2020. More information about each USGS monitoring station, as well as data retrieval, is available at <https://waterdata.usgs.gov/nwis>.

Philadelphia Water Department (PWD) with the support of Woods Hole Group conducted a water quality measurement program in the Delaware Estuary from 2017—2020 (Lavallee, 2021). Near-continuous 12-minute water quality data were collected at two stations: Buoy B near the Schuylkill River entrance and Buoy P at about 4 miles upstream of C&D Canal entrance. Station locations and measured parameters are summarized in Table 2-4.

Table 2-4: Continuous monitoring locations

Station ID	Name	Latitude Longitude	River Mile	Relevant Parameters
USGS/PWD 14670261	Delaware River at Pennypack Woods, PA	40°02'19" N -74°59'37" W	110.0	water temperature specific conductance dissolved oxygen dissolved oxygen % of saturation chlorophyll relative fluorescence turbidity
PWD Buoy B	Delaware River near Schuylkill River confluence	39° 52' 48" N 75° 10' 14" W	93.7	water temperature dissolved oxygen dissolved oxygen % of saturation chlorophyll relative fluorescence
USGS 1467200	Delaware River at Penn's Landing, Philadelphia, PA*	39°56'47" N -75°08'23" W	99.5 current 100.05 during calibration	water temperature specific conductance dissolved oxygen dissolved oxygen % of saturation chlorophyll relative fluorescence turbidity
USGS 1477050	Delaware River at Chester, PA	39°50'44" N -75°21'03" W	83.6	water temperature specific conductance dissolved oxygen dissolved oxygen % of saturation turbidity nitrate plus nitrite dissolved organic carbon
PWD Buoy P	Delaware River at Pea Patch Island	39° 36' 49" N 75° 34' 24" W	62.2	water temperature dissolved oxygen dissolved oxygen % of saturation chlorophyll relative fluorescence
USGS 1482800	Delaware River at Reedy Island Jetty, DE	39°30'03" N -75°34'07" W	54.1	water temperature specific conductance dissolved oxygen turbidity

*During model calibration period (prior to January 2020), located at end of Pier 12, ~150 ft upstream of Ben Franklin Bridge

2.1.2 POINT-DISCHARGE NUTRIENT MONITORING

Resolution No. 2010-5 authorized DRBC to require point source dischargers to the Delaware Estuary to perform monthly data collection for nutrients and related parameters for 24 months. Starting in 2011, data were obtained over a two-year period from 75 facilities; this first round of point-discharge monitoring was conducted to rank facilities by nutrient loadings and assign to Tiers accordingly. In March 2018, DRBC initiated a second round of point-discharge monitoring, a 2-year intensive nutrient monitoring program to obtain model input data for the calibration period based on Resolution for the Minutes adopted on September 13, 2017. Based on the first round of monitoring, facilities that contributed the top 95% of total load for ammonia, TKN, or BOD-5 (Tier 1 facilities) were monitored weekly between 2018 and 2020, while facilities that contributed top 95% of total load for TP, SRP, Nitrate-N, or TN (Tier 2 facilities) were monitored monthly. For the 2018–2020 point-discharge nutrient monitoring period, 32 facilities monitored and submitted data to DRBC; Twelve Tier 1 facilities and twenty Tier 2 facilities. The remaining 43 facilities are classified as Tier 3, for which the first round of monitoring data and states' electronic Discharge Monitoring Record was used for characterization. In addition to the submittal of results from an approved laboratory, facilities also submitted directly monitored effluent data, such as flow and temperature, during the intensive monitoring period. Discharge facilities by Tiers are shown in

Figure 2-3 and listed in **Error! Reference source not found.** below.

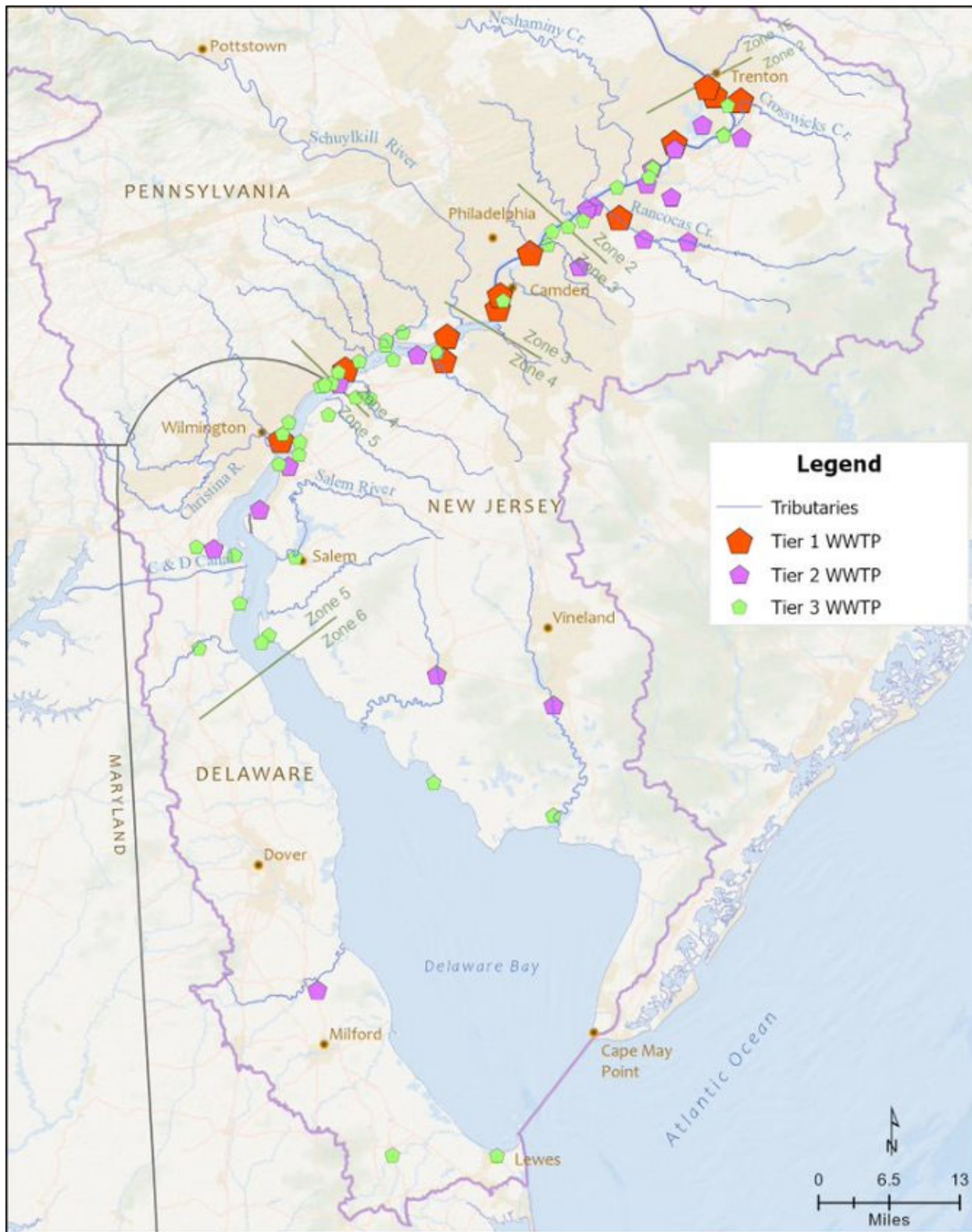


Figure 2-3: Monitored point source discharges

Table 2-5 Monitored treatment plant discharges

Facility Name	NPDES	Tier 1
Camden County Municipal Utilities Authority	NJ0026182-001A	Tier 1
City of Wilmington, Department of Public Works	DE0020320-001	Tier 1
DELCORA	PA0027103-001	Tier 1
Gloucester County Utilities Authority	NJ0024686-001A	Tier 1
Hamilton Township - Wastewater Utility	NJ0026301-001A	Tier 1
Lower Bucks County Joint Municipal Authority	PA0026468-001	Tier 1
Morrisville Borough Municipal Authority	PA0026701-201	Tier 1
Philadelphia Water Department Northeast	PA0026689-001	Tier 1
Philadelphia Water Department Southeast	PA0026662-001	Tier 1
Philadelphia Water Department Southwest	PA0026671-001	Tier 1
Trenton Sewer Utility	NJ0020923-001A	Tier 1
Willingboro Municipal Utilities Authority	NJ0023361-001A	Tier 1
Bordentown Sewerage Authority	NJ0024678-001A	Tier 2
Bristol Borough Water & Sewer Authority	PA0027294-001	Tier 2
Burlington City STP	NJ0024660-002A	Tier 2
Burlington Township Public Works	NJ0021709-002A	Tier 2
Chemours Chambers Works	NJ0005100-662A	Tier 2
Cinnaminson Sewerage Authority	NJ0024007-001A	Tier 2
City of Millville Sewage Treatment Authority	NJ0029467-001A	Tier 2
Cumberland County Utilities Authority	NJ0024651-001A	Tier 2
Delaware City Refining	DE0000256-601	Tier 2
Delran Sewerage Authority	NJ0023507-001A	Tier 2
Florence Township STP	NJ0023701-001A	Tier 2
GROWS Landfill, Waste Management	PA0043818-001	Tier 2
Kent County Department of Public Works	DE0020338-001	Tier 2
Moorestown Township WWTP	NJ0024996-001A	Tier 2
Mt. Holly Municipal Utilities Authority	NJ0024015-001A	Tier 2



Facility Name	NPDES	Tier 1
Mt. Laurel Municipal Utilities Authority	NJ0025178-001A	Tier 2
Paulsboro Refining Company	NJ0005029-001A	Tier 2
Pennsville Sewerage Authority	NJ0021598-001A	Tier 2
Riverside Water Reclamation Authority	NJ0022519-001A	Tier 2
Valtris Specialty Chemicals	NJ0005045-001A	Tier 2
Beverly Sewerage Authority	NJ0027481-001	Tier 3
Boeing	PA0013323-001	Tier 3
Bridgeport Disposal LLC	NJ0005240-001A	Tier 3
Calpine Mid-Atlantic Generation	DE0000558-016	Tier 3
Canton Village STP	NJ0062201-001A	Tier 3
Carneys Point STP	NJ0021601-001A	Tier 3
Chemours Company Repauno	NJ0004219-001	Tier 3
City of Lewes	DE0021512-001	Tier 3
Delaware City STP	DE0021555-001	Tier 3
DuPont Edgemoor	DE0000051-001	Tier 3
Evonik Degussa	PA0051713-001	Tier 3
Exelon Generating Company, Eddystone	PA0013714-107	Tier 3
Former BP Paulsboro Terminal No. 4555	NJ0005584-003A	Tier 3
Formosa Plastics	DE0000612-001	Tier 3
FPL Energy Marcus Hook	PA0244449-001	Tier 3
General Chemical	DE0000655-001	Tier 3
Hoeganaes Corporation	NJ0004375-001A	Tier 3
Hope Creek Generating Station	NJ0025411-461A	Tier 3
Logan Township MUA	NJ0027545-001A	Tier 3
MAFCO Worldwide Corp	NJ0004090-001A	Tier 3
Menu Food Inc	NJ0031216-001B	Tier 3
Mercer Generating Station	NJ0004995-441A	Tier 3
Mexichem Specialty Resins	NJ0004286-001	Tier 3

Facility Name	NPDES	Tier 1
Middletown-Odessa-Townsend	DE0050547-001	Tier 3
Milton STP	DE0021491-001	Tier 3
Monroe Energy	PA0012637-201	Tier 3
Occidental	DE0050911-001	Tier 3
Palmyra STP	NJ0024449-001A	Tier 3
Penns Grove Sewerage Authority	NJ0024023-001A	Tier 3
Port Penn STP	DE0021539-001	Tier 3
PSEG Fossil Burlington Generating Station	NJ0005002-WTPA	Tier 3
PSEG Nuclear Salem Generating Station	NJ0005622-048C	Tier 3
Riverton STP	NJ0021610-001A	Tier 3
Rohm & Haas Chemicals, Bristol	PA0012769-009	Tier 3
Salem City Wastewater Treatment Facility	NJ0024856-001A	Tier 3
Surfside Products LLC	NJ0004766-001A	Tier 3
Tinicum TWP	PA0028380-001A	Tier 3
US Steel, Fairless-103	PA0013463-103	Tier 3
US Steel, Fairless-203	PA0013463-203	Tier 3

The DRBC required facilities to monitor the parameters listed in Table 2-6 below between March 2018 and February 2020. Parameters were monitored weekly for Tier 1 facilities and monthly for Tier 2 facilities. Based on the results obtained during the first round of sampling performed beginning in 2011, Tier 3 facilities were not required to monitor during the second round of sampling for this study (i.e., the 2018–2020 period).

Table 2-6 Effluent monitoring parameters

Analytical Parameter	Units	Filtration	Sample Type
Total Phosphorus (TP)	mg/L as P	Unfiltered	24-hour composite
Total Kjeldahl Nitrogen (TKN)	mg/L as N	Unfiltered	24-hour composite
Nitrate Nitrogen (NO3-N)	mg/L as N	Unfiltered	24-hour composite
Nitrite Nitrogen (NO2-N)	mg/L as N	Unfiltered	24-hour composite

Analytical Parameter	Units	Filtration	Sample Type
20-day Biochemical Oxygen Demand (BOD ₂₀)	mg/L	Unfiltered	24-hour composite
5-day Carbonaceous Biochemical Oxygen Demand (CBOD ₅)*	mg/L	Unfiltered	24-hour composite
Chemical Oxygen Demand (COD)	mg/L	Unfiltered	24-hour composite
Total Organic Carbon (TOC)	mg/L	Unfiltered	24-hour composite
Dissolved Organic Carbon (DOC)*	mg/L	0.45 µm filter	24-hour composite
Total Suspended Solids (TSS)	mg/L	Unfiltered	24-hour composite
Soluble Reactive Phosphorus (SRP)	mg/L as P	0.45 µm filter	24-hour composite
Ammonia Nitrogen (NH ₃ -N)	mg/L as N	0.45 µm filter	24-hour composite
Discharge Flow	MGD	N/A	daily average
Water Temperature	°C	N/A	24-hour mean
Dissolved Oxygen	mg/L	N/A	24-hour mean
pH	1-14 S.U.	N/A	24-hour mean
Specific Conductance or TDS	µS/cm or mg/L	N/A	24-hour mean

*Added in April 2019

Note that unfiltered ammonia, standard method 20-day Carbonaceous Biochemical Oxygen Demand (CBOD₂₀), and a DRBC-amended method of CBOD₂₀ were dropped from the parameter list in April 2019.

2.1.3 TRIBUTARY NUTRIENT MONITORING

Nutrient sampling at the head of tide of Delaware River and major tributaries within Zones 2 through 5 was conducted from 2018 through 2019. In 2018, DRBC sampled 24 tributaries and the C&D Canal once per month from April through November. In 2019, the same locations were monitored once per month from March through August, with two sampling events in September. Tributaries that are tidally influenced were monitored near-low tide to minimize influence from the Delaware Estuary. The Delaware River at Calhoun Street Bridge and the Schuylkill River at East Falls Bridge were monitored twice per month January through December in both 2018 and 2019 as they are the largest freshwater inflows to the Delaware Estuary. The monitoring locations are shown in

Figure 2-4 and listed in Table 2-7 below.

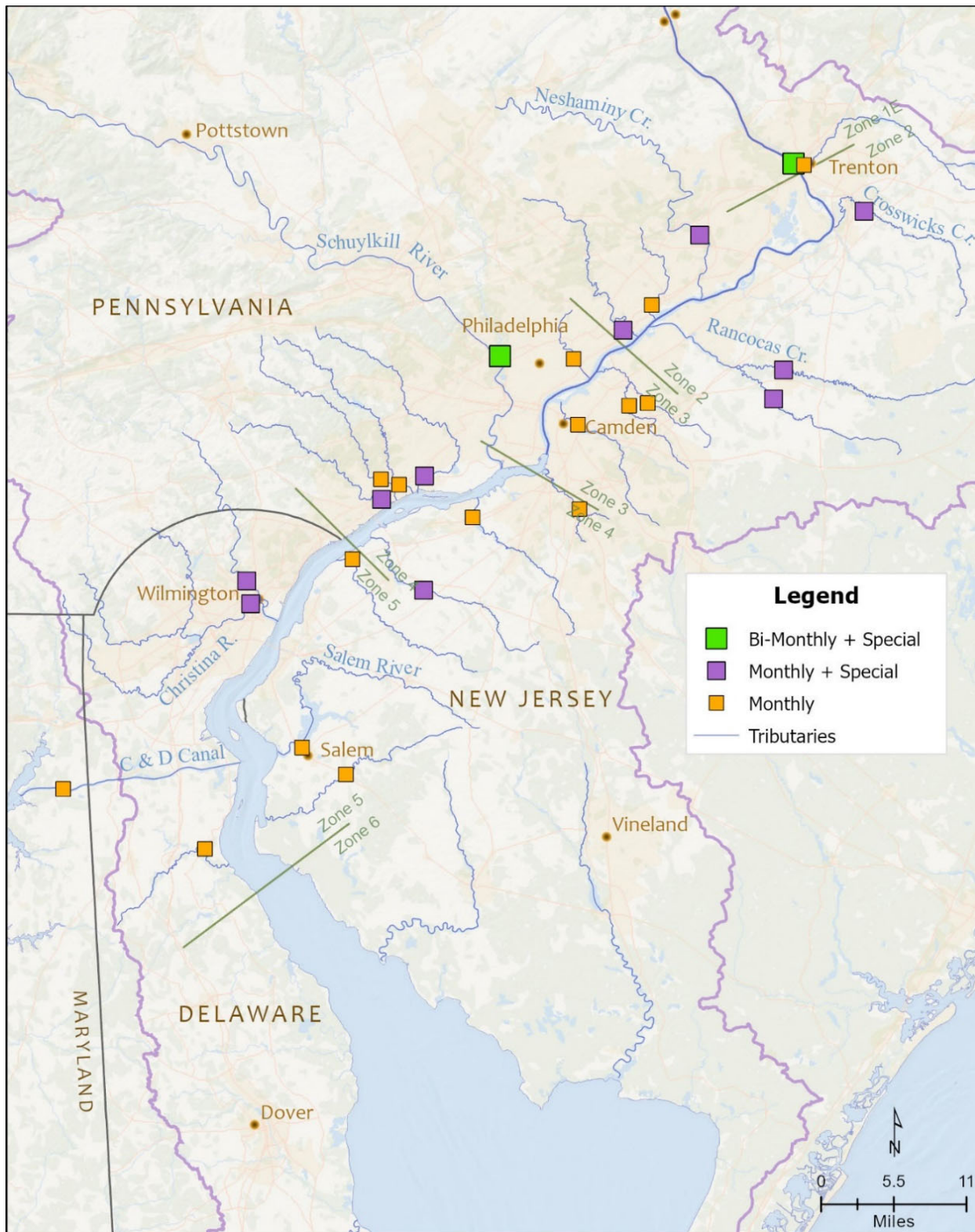


Figure 2-4: Tributary monitoring locations

Table 2-7 Tributary monitoring locations

Location	Site ID	DRBC Zone	State	Latitude	Longitude
Delaware River at Trenton	1343ICP	2	NJ	40.219819	-74.778107
Neshaminy Creek	NUTR-NESH	2	PA	40.141561	-74.912438
Rancocas South Branch	NUTR-RANS	2	NJ	39.961358	-74.807316
Rancocas North Branch	NUTR-RANN	2	NJ	39.993224	-74.792997
Crosswicks Creek	NUTR-CROS	2	NJ	40.167267	-74.677339
Pennypack Creek	NUTR-PNNY	2	PA	40.037176	-75.021786
Poquessing Creek	NUTR-POQU	2	PA	40.06486	-74.98098
Assunpink Creek	NUTR-ASSU	2	NJ	40.21826	-74.763063
Mantua Creek	NUTR-MANT	3	NJ	39.831246	-75.236045
Big Timber Creek	NUTR-BIGT	3	NJ	39.840497	-75.08392
Cooper River	NUTR-COOP	3	NJ	39.933259	-75.086351
Frankford Creek	NUTR-FRAN	3	PA	40.00545	-75.092486
Pennsauken North Branch	NUTR-PENO	3	NJ	39.957043	-74.986672
Pennsauken South Branch	NUTR-PESO	3	NJ	39.954196	-75.013308
Schuylkill River	DRBC-SCHU	4	PA	40.008405	-75.197454
Darby Creek	NUTR-DARB	4	PA	39.87655	-75.30453
Chester Creek	NUTR-CHES	4	PA	39.85073	-75.36554
Raccoon Creek	NUTR-RACC	4	NJ	39.751019	-75.3053
Ridley Creek	NUTR-RIDL	4	PA	39.87274	-75.366612
Crum Creek	NUTR-CRUM	4	PA	39.866919	-75.340823
Brandywine River	NUTR-BRAN	5	DE	39.76035	-75.556779
Christina River	NUTR-CHRI	5	DE	39.735236	-75.551033
Salem River	NUTR-SALE	5	NJ	39.57768	-75.47687
Oldmans Creek	NUTR-OLDS	5	NJ	39.784815	-75.406687
Alloway Creek	NUTR-ALLO	5	NJ	39.548457	-75.414473
C&D Canal	NUTR-CDCA	5	MD	39.530372	-75.815058
Appoquinimink River	NUTR-APPO	5	DE	39.465765	-75.613544

Parameters analyzed, shown in Table 2-8 below, include nutrients, solids, conventional parameters, and others relevant to eutrophication processes and model development needs. Samples were collected by DRBC staff and analyzed by New Jersey Department of Health Environmental Chemical Laboratory Services. In addition to laboratory analyzed samples: dissolved oxygen, water temperature, specific conductance, and pH readings were collected by DRBC personnel at each location with a Eureka Manta multiprobe water quality meter, and turbidity measured with a Hach Turbidimeter 2100Q.

Table 2-8 Tributary Monitoring Parameters

Analytical Parameter	Units	Filtration	Sample Type
Specific Conductance	µS/cm	Unfiltered	in-situ surface water grab
Dissolved Oxygen - Optical Electrode	mg/L	Unfiltered	in-situ surface water grab
Dissolved Oxygen	% Saturation	Unfiltered	in-situ surface water grab
pH, Field	1-14 S.U.	N/A	in-situ surface water grab
Turbidity (Nephelometric)	NTU	Unfiltered	near-surface water grab
Temperature, Water	°C	N/A	in-situ surface water grab
Suspended Chlorophyll-a	µg/L	0.70 µm filter	near-surface water grab
Chemical Oxygen Demand	mg/L	Unfiltered	near-surface water grab
Chloride, Total	mg/L	Unfiltered	near-surface water grab
Ammonia as N, Dissolved	mg/L	0.45 µm filter	near-surface water grab
Nitrate + Nitrite as N, Dissolved	mg/L	0.45 µm filter	near-surface water grab
Total Kjeldahl Nitrogen (TKN)	mg/L	Unfiltered	near-surface water grab
Alkalinity (titrimetric, pH 4.5)	mg/L	Unfiltered	near-surface water grab
Total Suspended Solids (TSS)	mg/L	Unfiltered	near-surface water grab
Total Solids (TS)	mg/L	Unfiltered	near-surface water grab
Fixed Suspended Solids (FSS)	mg/L	Unfiltered	near-surface water grab
Total Volatile Solids (TVS)	mg/L	Unfiltered	near-surface water grab
Organic Carbon, Total	mg/L	Unfiltered	near-surface water grab
Organic Carbon, Dissolved	mg/L	0.45 µm filter	near-surface water grab
Organic Carbon, Particulate	mg/L	0.45 µm filter	near-surface water grab
Orthophosphate, Dissolved	mg/L	0.45 µm filter	near-surface water grab
Total Phosphorus as P, Total	mg/L	Unfiltered	near-surface water grab

Analytical Parameter	Units	Filtration	Sample Type
Total Phosphorus as P, Dissolved	mg/L	0.45 µm filter	near-surface water grab
Silica, Total	mg/L	Unfiltered	near-surface water grab
Silica, Dissolved	mg/L	0.45 µm filter	near-surface water grab
CBOD20, standard method	mg/L	Unfiltered	near-surface water grab
Acid-Hydrolyzable Phosphorus, Dissolved	mg/L	0.45 µm filter	near-surface water grab
Acid-Hydrolyzable Phosphorus, Total	mg/L	Unfiltered	near-surface water grab
Particulate Inorganic Phosphorus	mg/L	0.45 µm filter	near-surface water grab
Sulfate	mg/L	Unfiltered	near-surface water grab

2.2 SAMPLING RESULTS

2.2.1 LONG-TERM WATER QUALITY MONITORING RESULTS

Two long-term water quality datasets were used in the model. Data from DRBC’s Boat Run Monitoring Program was accessed via the National Water Quality Portal (NWQP). Data from USGS continuous monitors in the Delaware Estuary was accessed via the USGS National Water Information System (NWIS). Data from both datasets were downloaded using the Data Retrieval package in R. Figure 2-5 below shows box and whisker plots for the period 2010–2021 by river mile for a) ammonia from the Boat Run and b) dissolved oxygen from USGS monitors. The box and whisker plot is a graphical illustration of numerical data to show the distribution of data through their quartiles (box) and data ranges (whiskers and circles). This report employed the standard box and whisker plot definition to summarize the data spread. The structure of each box indicates the following: bottom portion of the box = the first quartile (Q1 = 25th percentile); mid-point line on box = median (or 50th percentile); uppermost portion of the box = the third quartile (Q3 = 75th percentile); entirety of the box = interquartile range (IQR = the distance between the upper (Q3) and the lower quartiles (Q1)); and the whiskers is based on the 1.5 IQR value. From above the upper quartile (Q3), a distance of 1.5 times the IQR is measured out and a whisker is drawn up to the largest observed data point from the dataset if that largest point falls within this distance. Similarly, a distance of 1.5 times the IQR is measured out below the lower quartile (Q1) and a whisker is drawn down to the lowest observed data point from the dataset if that lowest point falls within this distance. All other observed data points outside the boundary of the whiskers, if any, are plotted as symbols such as circles.

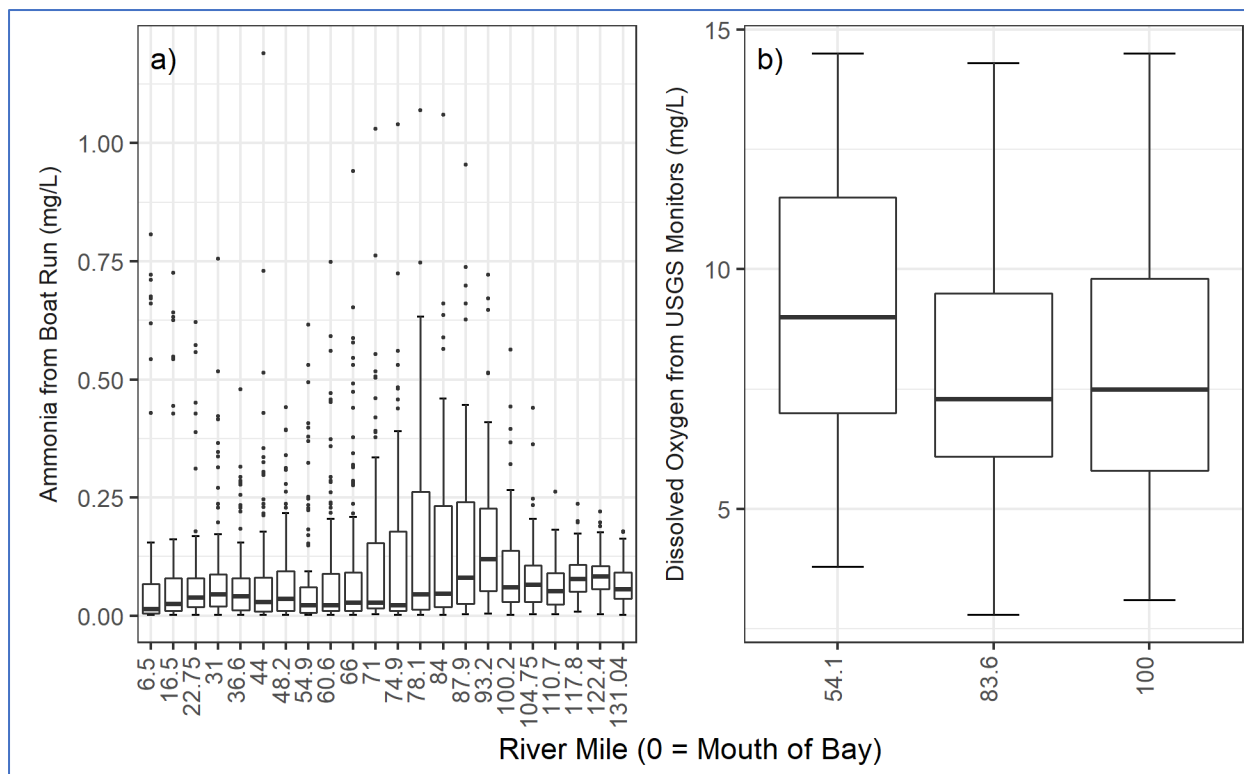


Figure 2-5 Long-term monitoring within the Estuary (example results)

2.2.2 POINT-DISCHARGE MONITORING RESULTS

Point-discharge nutrient monitoring occurred over a 2-year period from March 2018 (for Tier 1 facilities) and April 2018 (for Tier 2 facilities) up to February and March 2020. In order to properly represent point-discharge loadings in the model, substantial data is required for the calibration period (2018–2019). Tier 1 facilities monitored weekly, while Tier 2 facilities monitored once per month, with all being monitored for the same suite of parameters (see Table 2-8). Mean concentrations of Total Phosphorus as P, Total Organic Carbon, Ammonia, and Total Nitrogen (Total Kjeldahl Nitrogen as N [TKN] + Nitrate [NO₃-N] + Nitrite [NO₂-N]) are provided in Table 2-9 below, along with mean daily flows on the days sampled.

Table 2-9 Mean effluent concentrations of key nutrients

Facility	NPDES-Outfall	Total Phosphorus mg/L	Total Organic Carbon mg/L	Ammonia Nitrogen mg/L	Total Nitrogen mg/L	Effluent MGD
Philadelphia Water Dept NE	PA0026689-001	0.37	7.95	5.26	9.43	179.8
Philadelphia Water Dept SW	PA0026671-001	0.27	8.67	18.61	21.56	178.0

Facility	NPDES-Outfall	Total Phosphorus mg/L	Total Organic Carbon mg/L	Ammonia Nitrogen mg/L	Total Nitrogen mg/L	Effluent MGD
Philadelphia Water Dept SE	PA0026662-001	0.21	7.71	8.47	10.29	78.91
City of Wilmington DPW	DE0020320-001	0.87	12.97	11.54	18.39	71.03
Camden County MUA	NJ0026182-001A	1.79	11.97	16.85	21.99	53.03
DELCORA	PA0027103-001	1.51	14.26	7.83	15.76	34.80
Gloucester County UA	NJ0024686-001A	2.28	15.23	22.35	28.67	18.92
Kent County DPW	DE0020338-001	0.22	5.33	0.44	4.38	13.08
Trenton DWS	NJ0020923-001A	2.48	14.83	4.71	19.48	11.69
Delaware City Refining	DE0000256-601	0.97	11.64	0.33	33.54	10.15
Paulsboro Refining Company	NJ0005029-001	1.82	11.02	0.18	5.82	8.98
Hamilton Township Dept WPC	NJ0026301-001A	3.47	15.72	26.70	29.85	8.28
Lower Bucks County JMA	PA0026468-001	2.13	11.18	20.19	24.59	7.23
Chemours Chambers Works	NJ0005100-662A	0.51	6.74	0.16	6.79	5.79
Morrisville Borough MA	PA0026701-201	2.21	14.43	11.27	25.79	5.08
Mt. Laurel MUA	NJ0025178-001A	0.62	5.34	1.43	12.35	4.12
Willingboro MUA	NJ0023361-001A	1.50	13.66	3.39	21.00	3.77
Mt. Holly MUA	NJ0024015-001A	2.62	10.13	0.97	20.23	3.31
Cumberland County UA	NJ0024651-001A	1.41	11.03	6.90	14.35	3.26
Moorestown Township WWTP	NJ0024996-001	1.41	5.76	1.07	18.44	2.33

Facility	NPDES-Outfall	Total Phosphorus mg/L	Total Organic Carbon mg/L	Ammonia Nitrogen mg/L	Total Nitrogen mg/L	Effluent MGD
City of Millville DPW	NJ0029467-001A	2.94	12.35	26.76	26.67	2.28
Delran SA	NJ0023507-001A	2.44	5.08	0.15	15.88	2.07
Burlington City STP	NJ0024660-002A	2.37	11.60	0.99	17.97	2.02
Bordentown SA	NJ0024678-001A	4.31	5.15	0.21	29.37	1.67
Burlington Township DPW	NJ0021709-002A	1.59	5.54	0.38	2.96	1.52
Florence Township STP	NJ0023701-001A	0.99	14.15	3.25	15.25	1.48
Cinnaminson SA	NJ0024007-001A	2.81	11.81	17.87	22.75	1.45
Bristol Borough WSA	PA0027294-001	2.22	10.03	1.00	15.30	1.44
Pennsville SA	NJ0021598-001A	1.50	11.53	0.61	14.56	1.41
Valtris Specialty Chemicals	NJ0005045-001A	17.94	12.21	1.33	9.16	0.93
Riverside WRA	NJ0022519-001A	4.18	11.58	0.54	24.04	0.68
Waste Management - GROWS	PA0043818-001	0.31	61.83	0.25	231.39	0.15

The range of Total Phosphorus (TP) concentration data is non-detect to 64.0 mg/L (Method Detection Limits [MDLs] of non-detect results range from 0.007-0.1 mg/L); the mean TP concentration overall is 1.92 mg/L, and the median is 1.48 mg/L. The range of Total Nitrogen (TN) concentration data is 1.11-566.0 mg/L; the mean TN concentration overall is 22.6 mg/L, and the median is 19.7 mg/L. The range of Total Organic Carbon (TOC) concentration data is non-detect to 155.0 mg/L (MDLs of non-detect results range from 0.5-2.5 mg/L); the mean TOC concentration overall is 12.34 mg/L, and the median TOC concentration is 11.50 mg/L.

Point discharge ammonia concentrations range from non-detect to 37.8 mg/L (MDLs for non-detects range from 0.008-0.5 mg/L). The mean ammonia concentration overall is 10.7 mg/L, and the median is 8.47 mg/L. Ranked boxplots of effluent ammonia concentrations are provided in Figure 2-6.

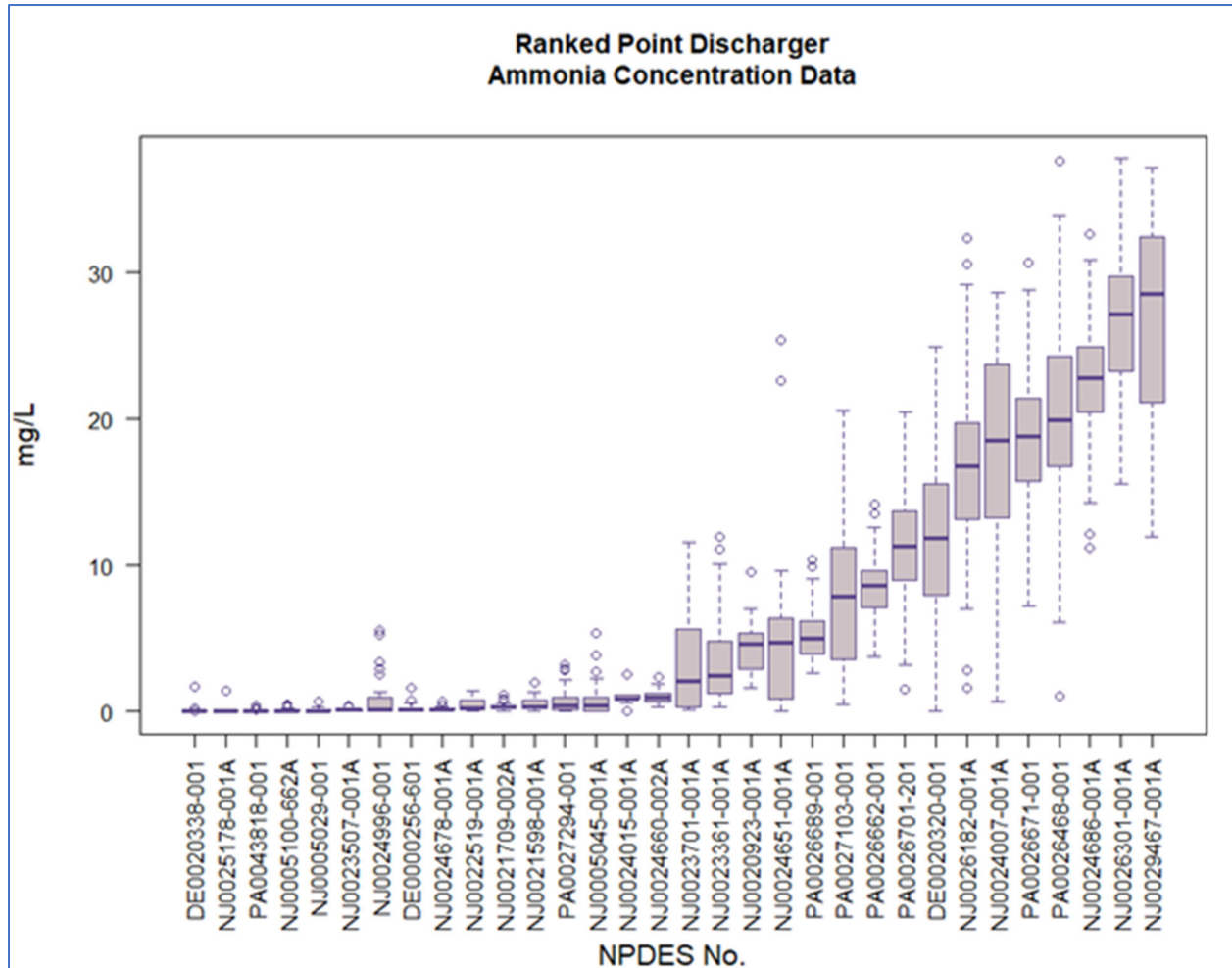


Figure 2-6 Effluent Ammonia Concentrations – Ranked Boxplots

2.2.3 TRIBUTARY NUTRIENT MONITORING RESULTS

Tributary nutrient monitoring occurred twice monthly for nearly a 3-year period from January 2018 through December 2020 at Delaware River at Trenton and Schuylkill River monitoring locations. For the 25 other tributary locations, including the C&D Canal, which was monitored as a boundary condition for the model, monitoring occurred monthly for 8 months in both 2018 and 2019, and extra samples were collected August through October 2020. The same suite of parameters was collected across all sites (see the list in the Sampling Program Description for Tributary Nutrient Monitoring). For this section of the report, Total Phosphorus as P, Total Organic Carbon, Ammonia, and Total Nitrogen (Total Kjeldahl Nitrogen as N + Nitrate (NO₃-N) + Nitrite (NO₂-N)) are examined. Mean concentrations of these parameters were assessed and are shown in Table 2-10 below.

Table 2-10 Mean concentrations of key nutrients at monitored tributaries

Tributary Monitoring Location	Total Phosphorus mg/L	Total Nitrogen mg/L	Ammonia Nitrogen mg/L	Total Organic Carbon mg/L	Discharge cfs
Alloway Creek	0.13	1.18	0.04	7.25	53.7
Appoquinimink River	0.16	1.44	0.06	4.14	58.2
Assunpink Creek	0.37	3.81	0.09	5.17	220
Big Timber Creek	0.15	0.94	0.09	4.42	52.6
Brandywine River*	0.05	3.07	0.02	2.48	756.6
Chester Creek*	0.15	4.06	0.03	2.73	150
Christina River*	0.07	1.93	0.04	4.73	569.8
Cooper River*	0.1	0.98	0.07	5.1	76.7
Crosswicks Creek	0.16	1.14	0.05	6.54	216.5
Crum Creek	0.03	1.72	0.04	2.99	72.9
Darby Creek*	0.09	2.01	0.14	3.63	163.7
Delaware River at Trenton	0.06	1.88	0.03	2.85	17,870
Frankford Creek*	0.09	2.31	0.13	3.2	54.7
Mantua Creek	0.13	1.55	0.09	4.09	85.8
Neshaminy Creek	0.13	2.12	0.05	3.89	525.9
Oldmans Creek	0.15	1.73	0.04	4.47	68.6
Pennsauken Creek, North Branch	0.08	1.04	0.16	5.11	37.5
Pennsauken Creek, South Branch	0.15	2.72	0.11	4.46	34.0
Pennypack Creek*	0.17	3.49	0.03	2.83	137.0
Poquessing Creek*	0.05	1.84	0.03	2.87	43.6
Raccoon Creek	0.17	1.99	0.08	4.57	65.8
Rancocas Creek, North Branch	0.14	1.09	0.16	11.05	259.5
Rancocas Creek, South Branch	0.19	1.35	0.09	12.8	294.2
Ridley Creek*	0.15	3.19	0.02	2.56	78.1
Salem River	0.15	1.49	0.07	4.24	144.8
Schuylkill River*	0.16	2.7	0.07	2.77	5,173

*Upstream CSOs influence water quality under some conditions

The range of TP concentration data is 0.014-0.96 mg/L; the mean TP concentration overall is 0.13 mg/L, and the median is 0.11 mg/L. The range of TN concentration data is 0.47-12.39 mg/L; the mean TN concentration overall is 2.08 mg/L, and the median is 1.74 mg/L. The range of TOC concentration data is 1.58-20.1 mg/L; the mean TOC concentration overall is 4.30 mg/L, and the median TOC concentration is 3.54 mg/L.

Tributary ammonia concentrations range from non-detect to 0.76 mg/L (MDLs for non-detects range from 0.004-0.023 mg/L). The mean ammonia concentration overall is 0.071 mg/L, and the median is 0.05 mg/L. Ranked boxplots of ammonia concentrations at monitored tributaries are shown in Figure 2-7 below.

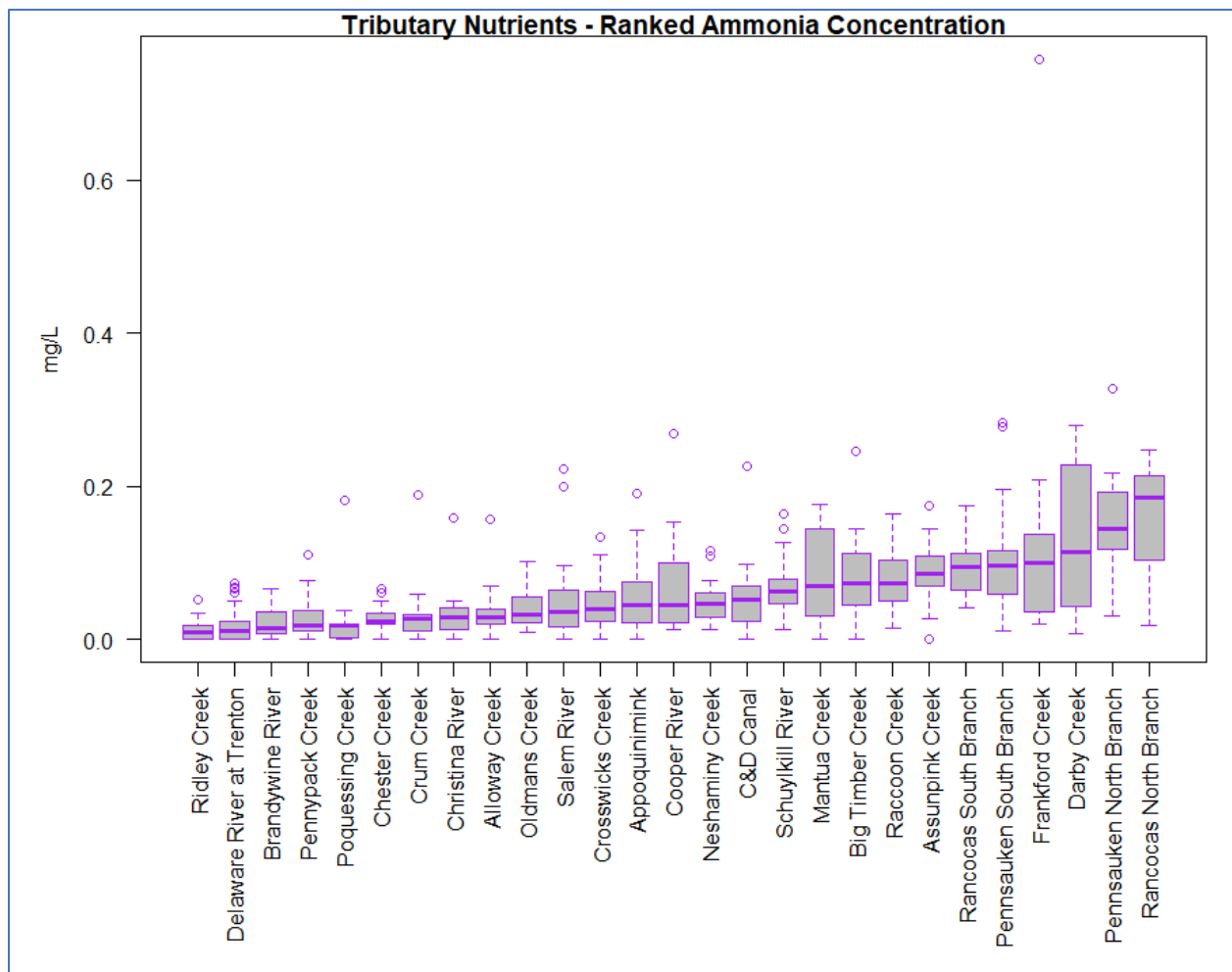


Figure 2-7 Tributary ammonia concentrations - ranked boxplots

2.3 CHARACTERIZATION OF LOADS

In addition to water quality constituent concentration data, nutrient loadings were also assessed. To compute nutrient loadings from the Point-Discharge Nutrient Monitoring data, concentration data was

multiplied by the effluent flow for each given sampling day for each facility and converted to kg/day. Similarly, to compute nutrient loading estimates from the Tributary Nutrient Monitoring dataset, concentration data was multiplied by the daily discharge flow for each given sampling day for each site and converted to kg/day. Tributary discharge flows were taken from the hydrodynamics model (DRBC, December 2021) on which this study is based. The average (kg/day) of the estimated loads were calculated and multiplied by 365 (average days in a year) to obtain annual loading estimates.

Figure 2-8 shows the relative ammonia loads from monitored point discharges, the upstream Delaware River (at Trenton), Schuylkill River, and all other monitored tributaries. Point discharges clearly comprise the largest category of ammonia loads into the Delaware Estuary. Note that this loading assessment reflects only the point sources and tributaries that were intensively monitored for this effort from 2018–2020.

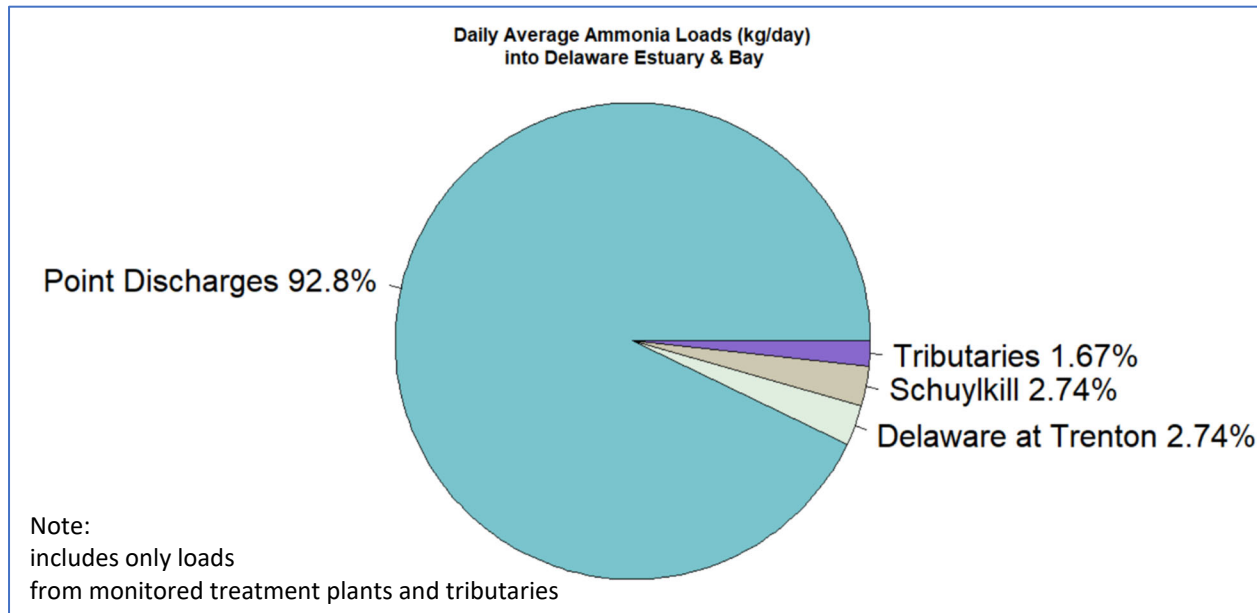


Figure 2-8 Ammonia loads from monitored treatment plants and tributaries

Figure 2-9 and Figure 2-10 show ranked ammonia loading boxplots for monitored point source discharges and monitored tributaries, respectively.

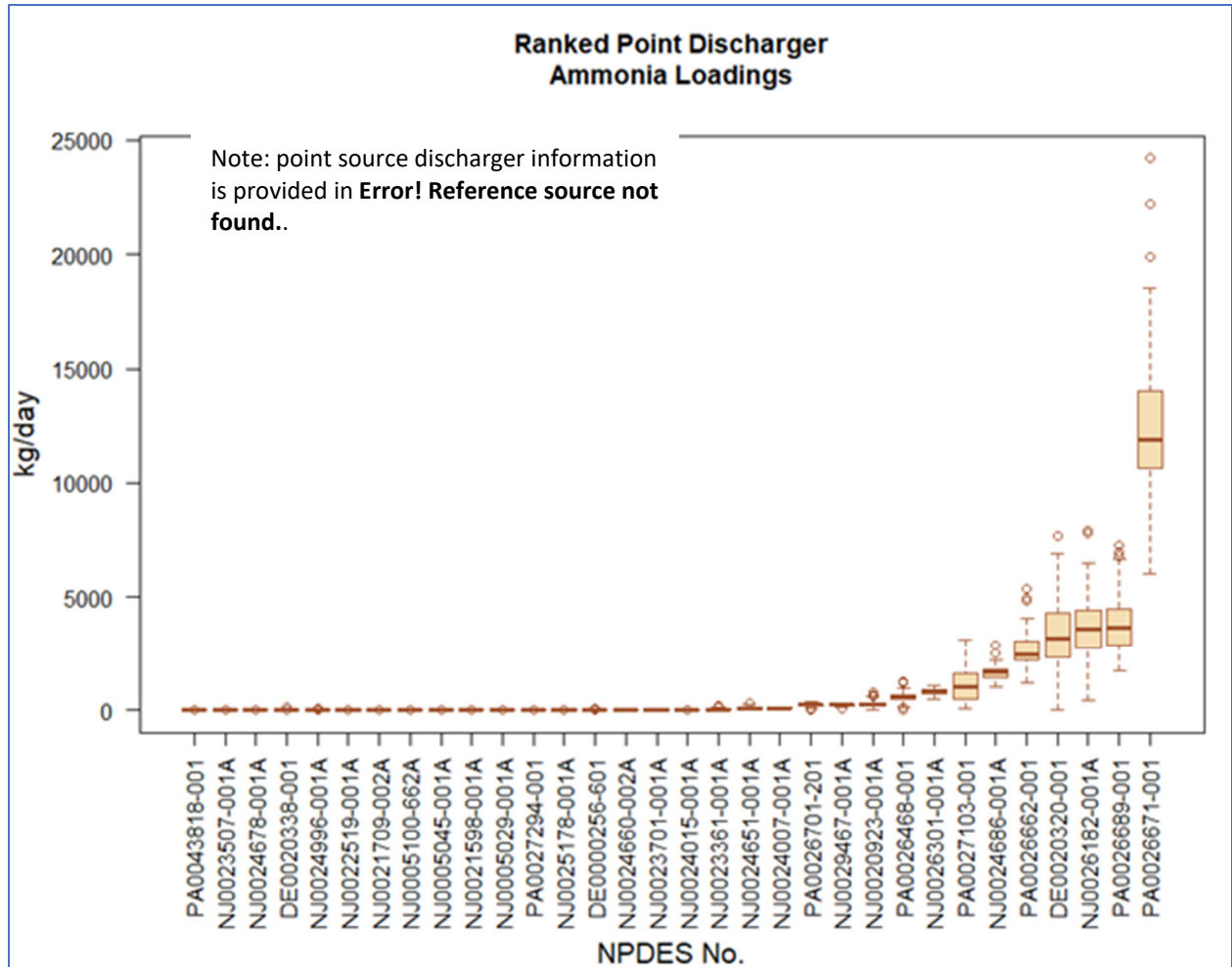


Figure 2-9: Effluent ammonia loads – ranked boxplots

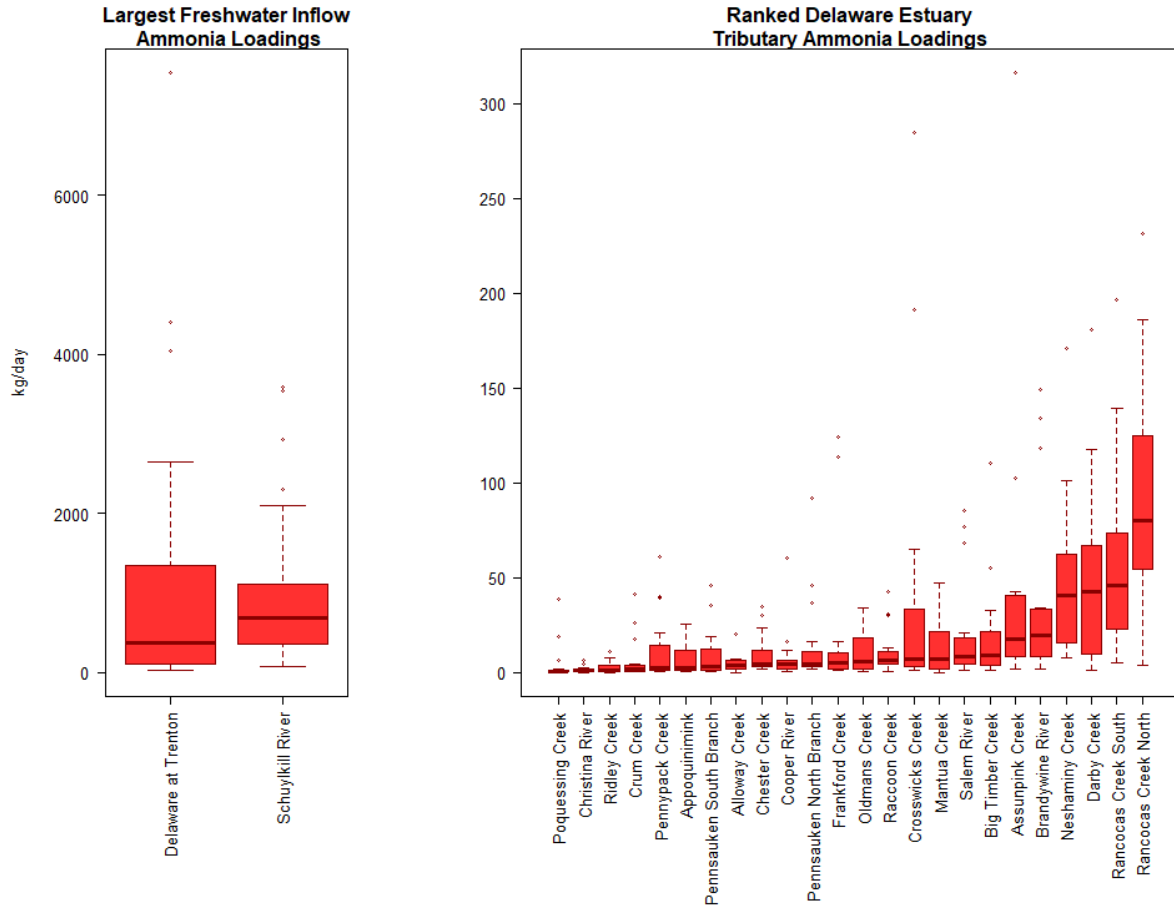


Figure 2-10: Tributary ammonia loads – ranked boxplots

TP and TN estimated loadings (Figure 2-11 and Figure 2-12, respectively) indicate that the relative impacts are comparable among point sources, the Delaware River at Trenton, the Schuylkill River, and other tributaries. Note that the pie charts separate the tributary contributions into “Delaware at Trenton,” “Schuylkill,” and “Other Tributaries.” By contrast, the Delaware River at Trenton contributes about 50% of TOC loads relative to the other sources assessed (Figure 2-13), while the point sources are estimated to contribute only 11% of the total assessed TOC load.

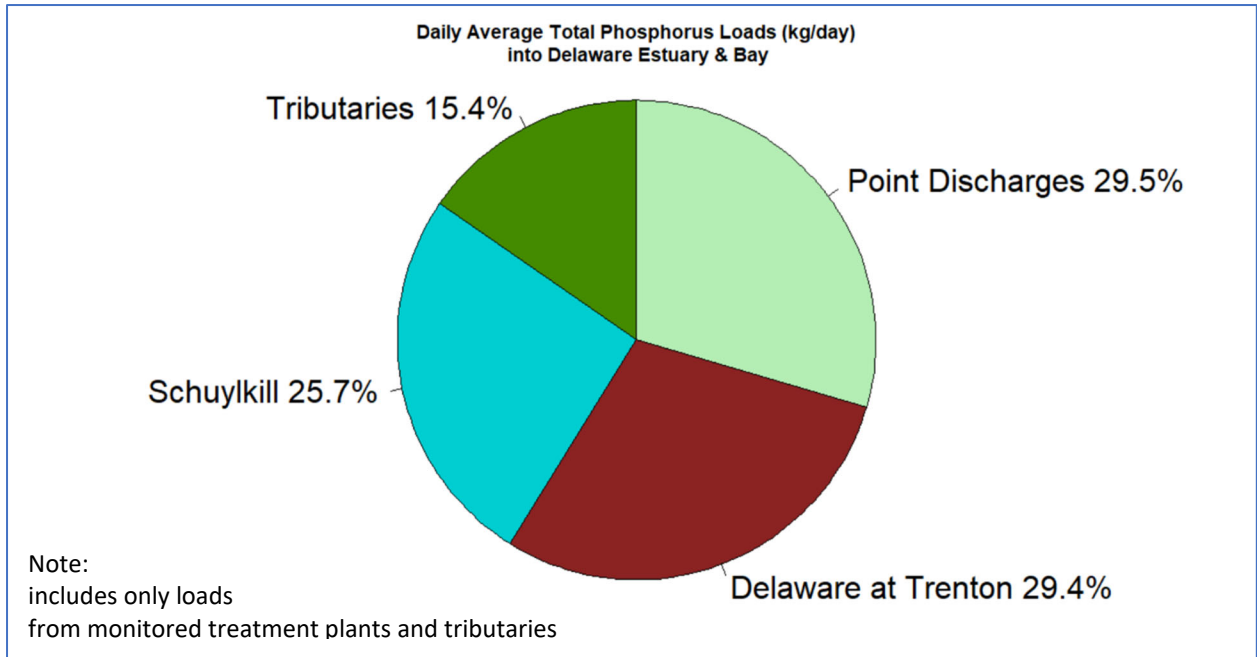


Figure 2-11 Total phosphorus from monitored treatment plants and tributaries

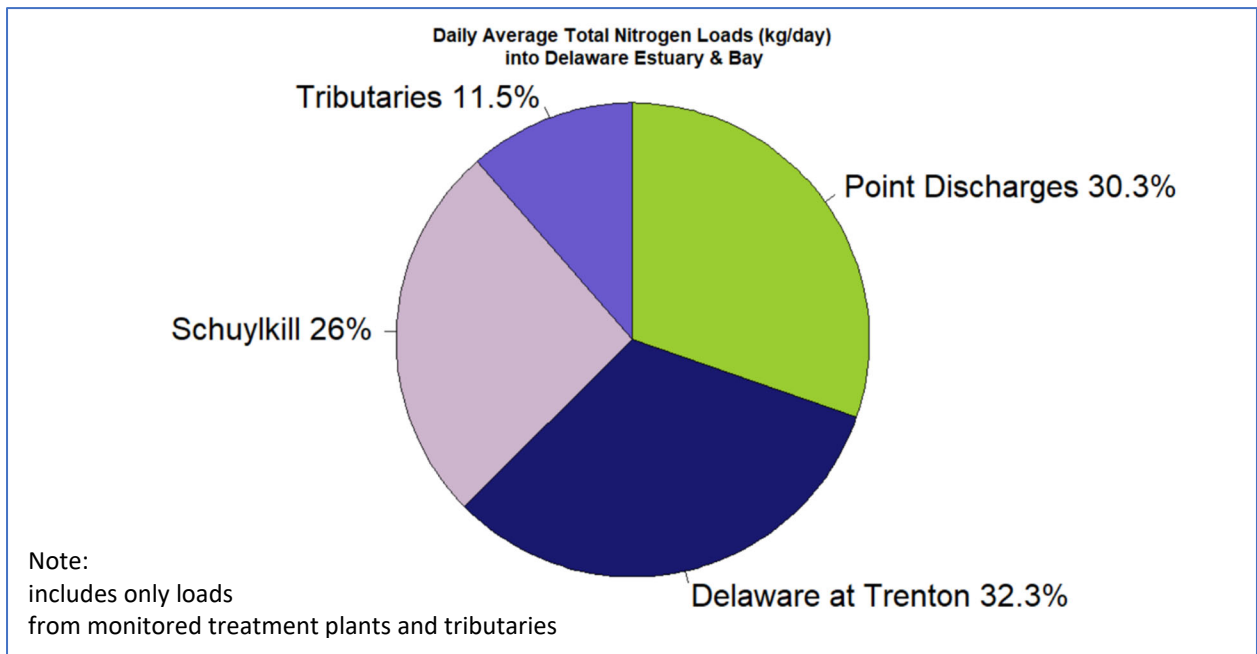


Figure 2-12 Total nitrogen from monitored treatment plants and tributaries

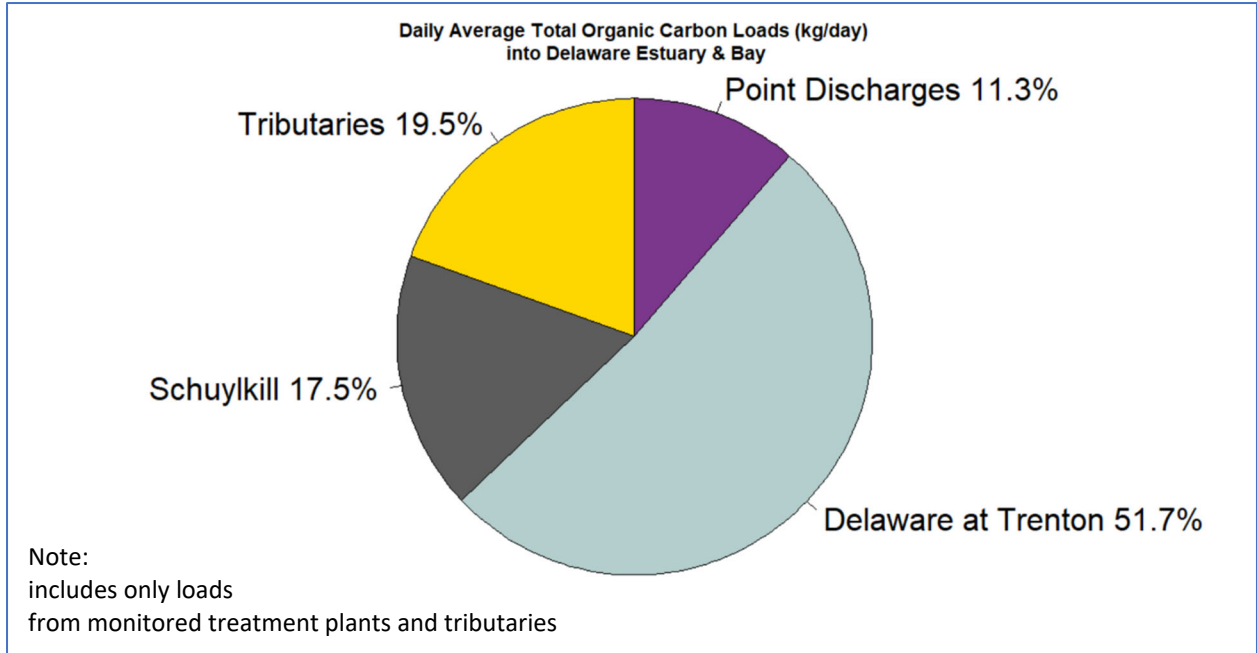


Figure 2-13 Total organic carbon from monitored treatment plants and tributaries

Ranked boxplots of TP, TN, and TOC loads from monitored tributaries are shown in Figure 2-14, Figure 2-15, and

Figure 2-16, respectively. Boxplots of all monitored parameters are included in **Error! Reference source not found..**

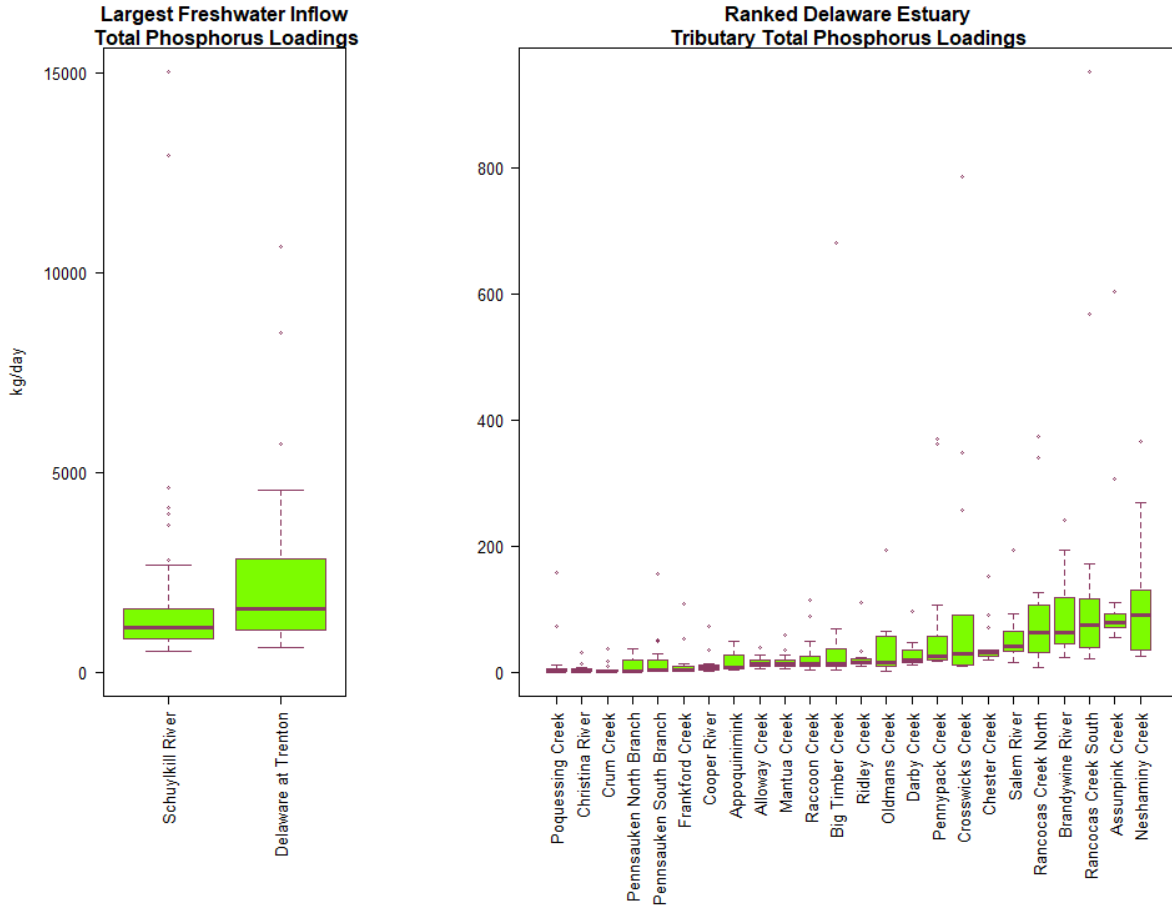


Figure 2-14 Tributary total phosphorus loads – ranked boxplots

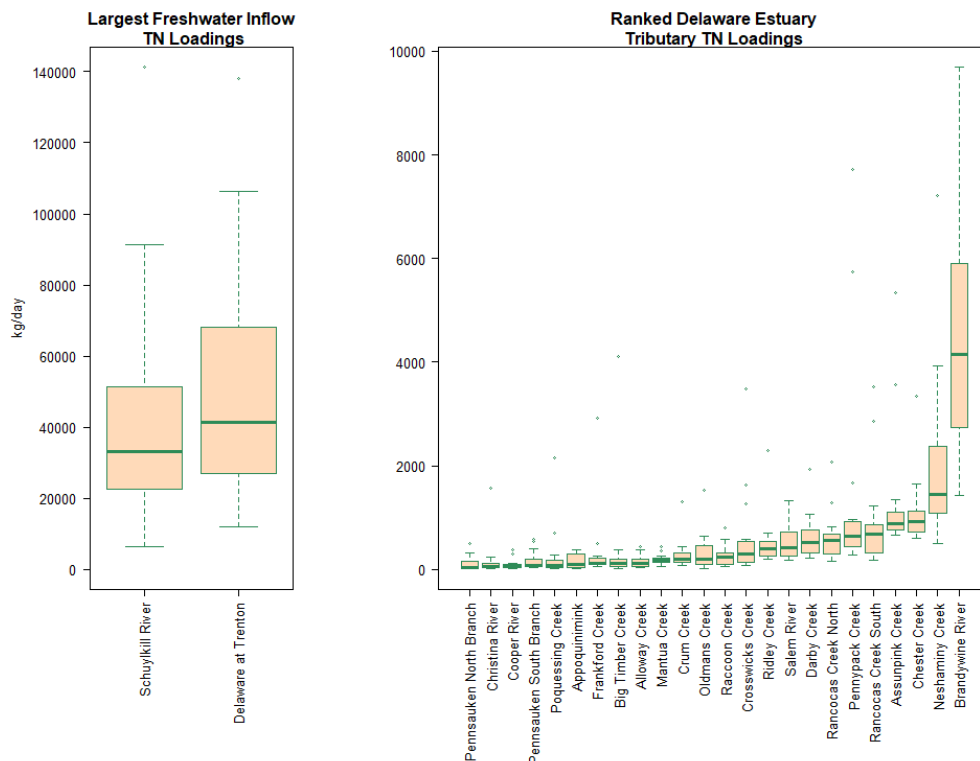


Figure 2-15 Tributary total nitrogen loads - ranked boxplots

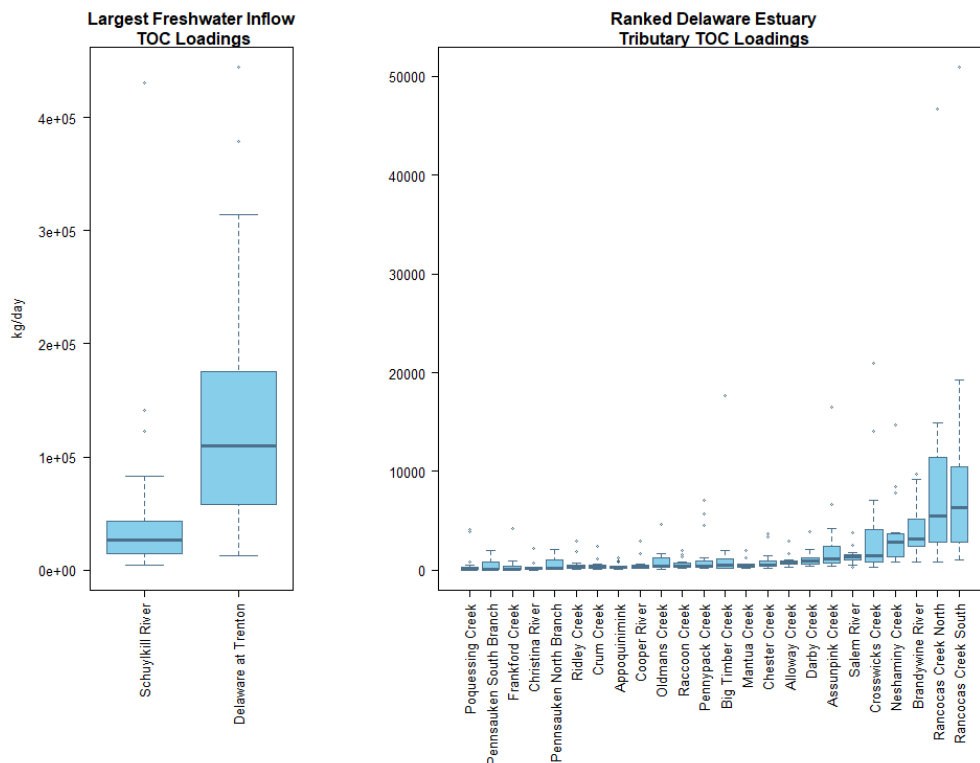


Figure 2-16 Tributary total organic carbon loads - ranked boxplots

2.4 ADDITIONAL FIELD DATA

Additional water quality data were compiled and used for the model input conditions. See the Section 3.1.4 for characterization of nonpoint source, atmospheric deposition and Combined Sewer Overflow (CSO) sources.

2.4.1 DISSOLVED OXYGEN TRANSECT PROFILES

To assess the degree of dissolved oxygen stratification in the Delaware Estuary, vertical dissolved oxygen profiles were collected via boat on three occasions in Summer 2021 across two transects at Ben Franklin and Chester. The Ben Franklin transects were conducted just downstream of the Ben Franklin Bridge in Philadelphia, PA; the Chester transects were conducted just downstream of Chester Island in Chester, PA. At each location a series of five profiles was collected along a transect spanning the width of the river. At each profile collection point, a dissolved oxygen reading was taken at the surface and the bottom. If a difference of greater than 5% was seen between the two readings, additional readings were taken throughout the water column. At both transect locations, the navigational channel runs along the Pennsylvania side of the river. Additionally, at both transect locations, the easternmost point (i.e., the point closest to the New Jersey bank) occurred on a shallow shoal with depths less than 2 m. At these locations, only a surface reading was taken. In addition to dissolved oxygen, water temperature, specific conductance, and pH readings were collected at each location. All readings were taken with a Eureka Manta water quality meter.

Dissolved oxygen transect profiles were conducted at Ben Franklin and Chester monitoring locations in May, July, and September 2021, spanning a range of conditions. May dissolved oxygen readings were high and ranged from 8.91–9.41 mg/L at Ben Franklin Bridge and 10.06–11.27 mg/L at Chester. July dissolved oxygen readings were lower and ranged from 5.92–6.27 mg/L at Ben Franklin Bridge and 4.50–6.09 mg/L at Chester. September dissolved oxygen readings ranged from 7.09–7.68 mg/L at Ben Franklin Bridge and 6.15–6.60 mg/L at Chester.

Dissolved oxygen stratification was not observed between bottom and surface readings collected in the Delaware Estuary in Summer 2021 (Figure 2-17). The difference between top and bottom readings was always within 5% and almost always within the level of accuracy of the water quality meter (± 0.2 mg/L). On two instances top/bottom dissolved oxygen differences were greater than 0.2 mg/L. Both instances occurred at the second

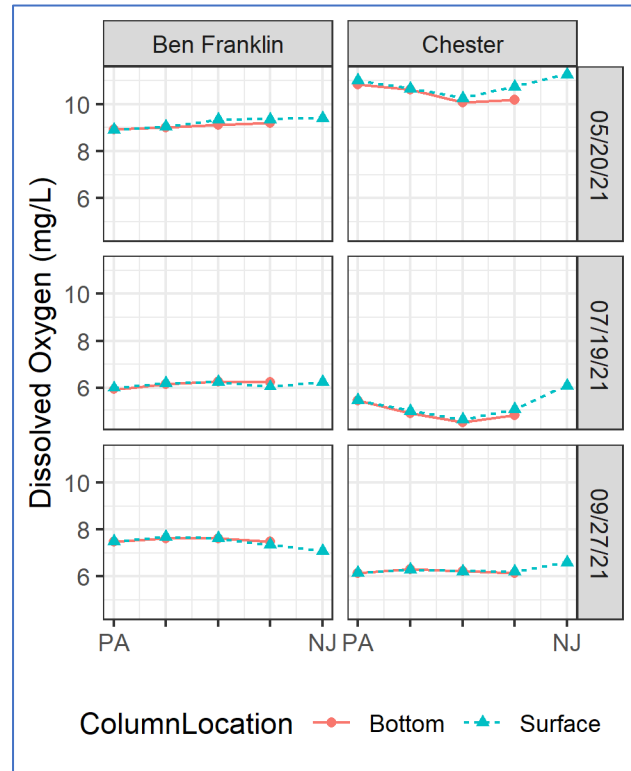


Figure 2-17 Dissolved oxygen profiles

station from the New Jersey bank along the Chester transect where a large shallow shoal mixes with the main river channel. In both instances, dissolved oxygen levels on this shallow shoal were higher than levels in the main channel and likely influenced the surface reading at this station. Both instances represented minor differences of approximately 5% from top to bottom.

USGS has conducted transect profile surveys at selected locations adjacent to USGS stations, where dissolved oxygen and its percent saturation, pH, conductivity, and water temperature were measured along the transects and at different depths. Profile data collected during the periods of model calibration and corroboration (Table 3-6) are used to evaluate model performance. Profile data collected in other years are presented in Appendix B. These profile data indicate that Delaware Estuary is weakly stratified, especially in the urban area.

2.4.2 ESTIMATES OF PRIMARY PRODUCTION IN THE DELAWARE ESTUARY

Field sampling studies to estimate primary production in the Delaware Estuary were conducted in 2014, 2018, and 2019 (Fisher and Gustafson, 2015, 2019, and 2020). Sampling was conducted by boat on two dates each year, once in May and once in July. Sampling in 2014 focused on the Delaware Bay while sampling in 2018 and 2019 focused on the upper estuary. DRBC staff collected surface and bottom water

samples along lateral transects at river miles 10, 25, and 40 in 2014 and at river miles 71, 86, 101, 116, and 131 in 2018 and 2019. In 2014, samples were collected at five sites on each lateral transect. In 2018 and 2019, samples were collected at three sites on each lateral transect.

More information on primary production including site mapping is available on the DRBC website at:

- https://www.nj.gov/drbc/library/documents/nutrients/nutrients-chlor-a_DelawareBay_UMd2015_rev012519.pdf
- https://www.nj.gov/drbc/library/documents/nutrients/nutrients-chlor-a_DelawareEstuary_UMd_feb2019.pdf
- https://www.nj.gov/drbc/library/documents/nutrients/nutrients-chlor-a_DelawareEstuary_UMd_sept2020.pdf

Field data were collected by DRBC personnel. Salinity, temperature, and dissolved oxygen data at the surface and bottom were obtained using a Eureka Manta water quality meter. Light extinction measurements were made using a LiCor LI-1400 data logger connected to a LI-190 surface PAR sensor and a LI-192 underwater sensor. These measurements were made *in situ* on the vessel when the water samples were taken for subsequent analysis of nutrients, respiration, and primary production in our laboratory. Collected water samples were maintained at ambient bay or estuary water temperature at 60% light (surface samples) or in darkness (bottom water samples) while on the ship. At the dock the samples were transferred to staff from University of Maryland Center for Environmental Science (UMCES) for analysis.

Within 1.5 h of the ship's arrival at the dock, the samples were transferred to a BOD box at the Horn Point Laboratory maintained at 16.3°C in May and 25.7°C in July to approximate the median bay temperatures observed (range = 16.1-18.0°C in May, 25.5-27.0°C in July). Lights within the box simulated the appropriate day/night cycle for the month. Bottom samples were wrapped in black bags within the BOD box to maintain darkness and ambient temperature. On the morning following sample collection, aliquots of the samples were placed in incubation bottles for measurements of respiration (all samples) and ¹⁴C-based primary production (surface samples only).

For this report, primary productivity is represented as an integrated rate of carbon fixation in the water column. Rates of primary production were averaged by river mile with sites in the bay collected in 2014 consisting of N=5 data points and sites in the upper estuary collected in 2018 and 2019 consisting of N=6 data points.

River mile-averaged primary production ranged from 0.13 – 4.93 gC/m²/d throughout the estuary (Figure 2-18). Samples downstream of river mile 40 were collected in 2014 while samples upstream of river mile 71 were collected in 2018 and 2019. Generally, rates of primary production were considerably higher downstream of river mile 25 than at upstream sites. Mean production was as high as 4.93 gC/m²/d at river mile 25 while mean production never exceeded 0.63 gC/m²/d at any site upstream of river mile 40. Mean primary production was variable between May and July samples. At sites in the bay collected in 2014, primary production was higher in July than May. At upstream sites collected in 2018 and 2019, primary production was similar in May and July.

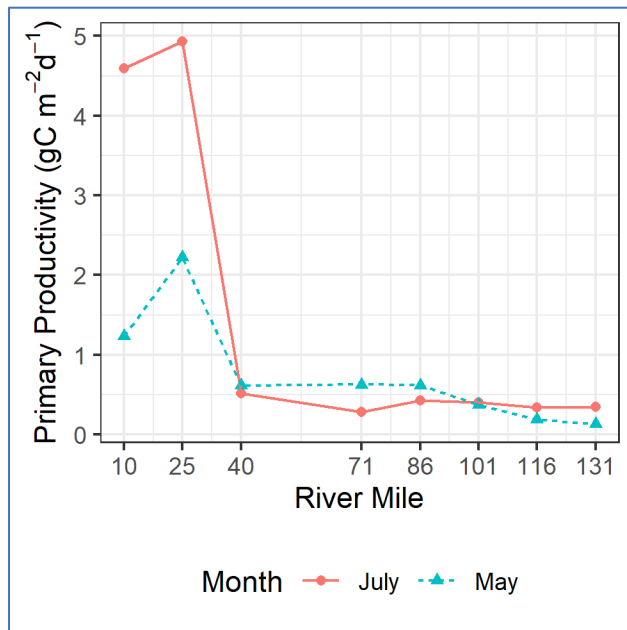


Figure 2-18 Primary productivity estimates

For a more detailed analysis of primary production in the estuary along with estimates of nutrients, chlorophyll a, dissolved oxygen, and respiration from this sampling see reports from UMCES (Fisher and Gustafson 2015, 2019, and 2020).

3. WATER QUALITY MODEL DEVELOPMENT

The goal of this modeling project is to develop a technically sound eutrophication model for the Delaware Estuary, from the head of the tide at Trenton, NJ, to the ocean, utilizing an appropriate level of complexity within the current state of the science and within the timeframe established by the Commission. This model will be used to address the impacts on dissolved oxygen from nutrients loads and carbonaceous oxygen demanding organic inputs.

DRBC is leading this effort through a collaborative process informed by an Expert Panel comprised of nationally recognized water resource scientists and engineers: Dr. Steve Chapra, Dr. Carl Cerco, Dr. Bob Chant, and Tim Wool. In addition to the model expert panel, DRBC benefits from day-to-day interaction with modeling consultants, Dr. Victor Bierman and Scott Hinz.

3.1 MODEL DESCRIPTION

The water quality model used in this study is the Water Quality Analysis Simulation Program (WASP) with the Advanced Eutrophication sub-model. The WASP model was originally developed by HydroScience (Di Toro et al. 1983; Connolly and Winfield 1984) and has remained under continuous development and support by the U.S. Environmental Protection Agency (USEPA). This model has been widely applied throughout the United States and worldwide to investigate water quality issues (Wool et al., 2003 and 2020; Ambrose et al., 2009; Petrus, 2015; Tetra Tech, 2015 and 2016; and Camacho et al., 2019). It has a user database with over 15,000 users. WASP8.32 is a recent version of WASP (released April 2, 2019) and has many upgrades to the user interface and to the model capabilities. WASP can be downloaded at <http://epawasp.twool.com/>. Technical documents are accessible at the USEPA website (2021).

A three-dimensional mass-conservation equation used in WASP is given as:

$$\frac{\partial C}{\partial t} = -\frac{\partial}{\partial x}(U_x C) - \frac{\partial}{\partial y}(U_y C) - \frac{\partial}{\partial z}(U_z C) + \frac{\partial}{\partial x}\left(E_x \frac{\partial C}{\partial x}\right) + \frac{\partial}{\partial y}\left(E_y \frac{\partial C}{\partial y}\right) + \frac{\partial}{\partial z}\left(E_z \frac{\partial C}{\partial z}\right) \pm S_c \quad (3-1)$$

where:

C = concentration of a particular water quality constituent;

t = time;

x , y , and z = spatial dimensions of fluid movement;

U_x , U_y , and U_z = lateral, longitudinal, and vertical advective velocities;

E_x , E_y , and E_z = lateral, longitudinal, and vertical diffusional coefficients; and

S_c = all sources and sinks of water quality constituent.

3.1.1 MODEL DOMAIN AND NUMERICAL GRID

The water-quality model in this study covers the same model domain and utilizes the same numerical grid as the hydrodynamic model (DRBC 2021). The model domain extends from the mouth of the Delaware Bay (River Mile [RM] 0) to the head of tide on the Delaware River near Trenton (RM 134.3). The C&D Canal westward to the NOAA tide gage station at Chesapeake City is included in the domain. Orthogonal curvilinear numerical grids were created to represent the geometry and shoreline of the river and estuary. The numerical grids consist of 1876 horizontal cells and utilize a generalized vertical coordinate (GVC) system, in which the number of active model layers is variable. The number of vertical layers ranges from a single layer at the upstream boundary at Trenton to 12 near the mouth of the Bay, resulting in a total of 11,490 water-column segments (Figure 3-1). Grid cell resolution is greater in the tidal river than in the Bay with average grid cell sizes in the river channel upstream of RM 70 of 580 m and 190 m in the longitudinal and lateral directions, respectively. The tidal river channel was generally delineated by 4 to 6 grid cells in the cross-channel direction, and the navigational channel was typically represented by one cell in the horizontal plane and ten cells (layers) in the vertical. Grid cells in Zone 6 are much coarser, with average lengths in the longitudinal and lateral directions of 2020 m and 1900 m, respectively. Additional details regarding the model domain and numerical grid system are described in Section 2 of the Hydrodynamic Model Report (DRBC, 2021).

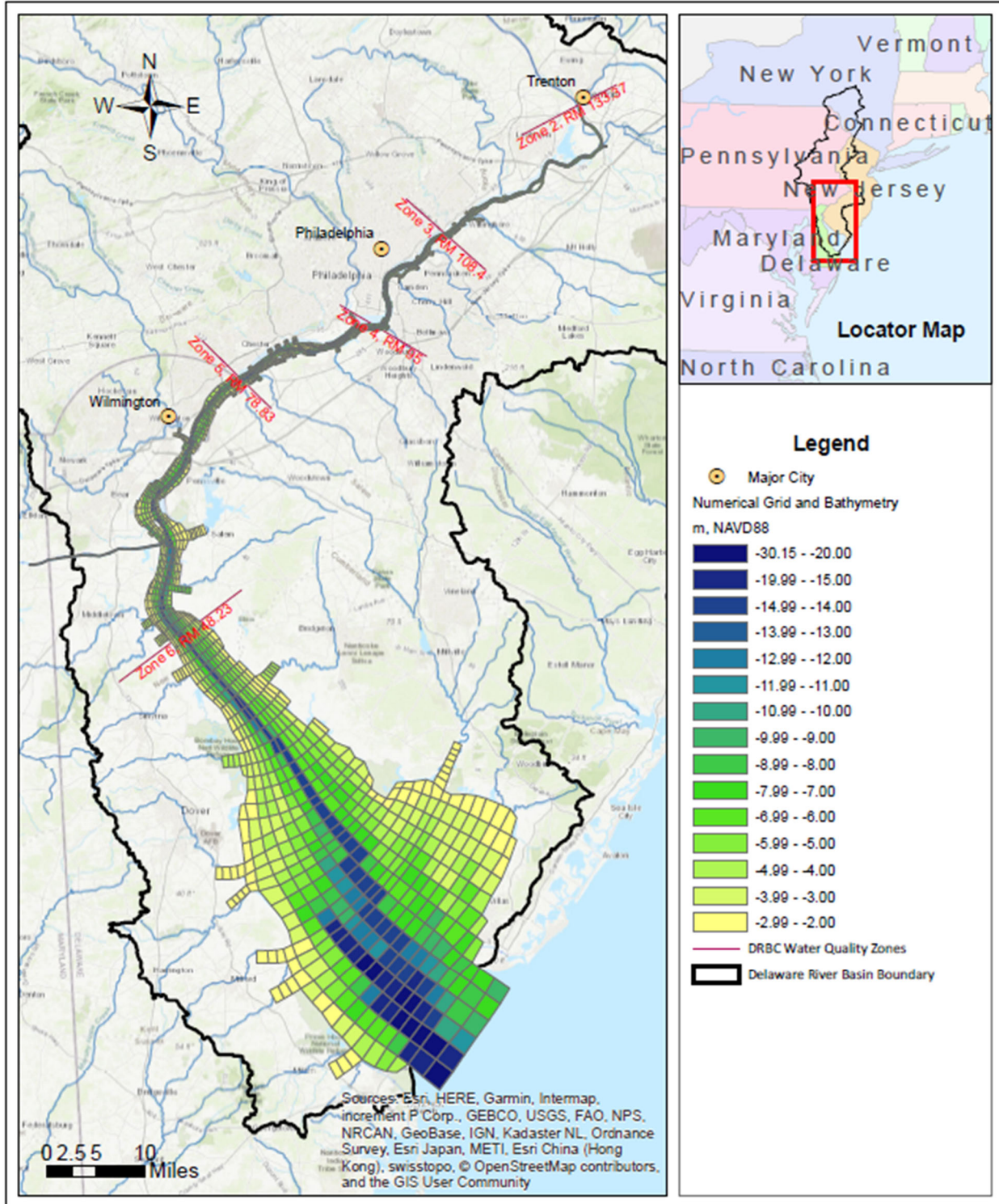


Figure 3-1: Numerical grid and projected bathymetry

3.1.2 MODEL KINETICS

Figure 3-2 presents the major physical, chemical, and biological processes for nutrient cycling and dissolved oxygen in the WASP model for the Delaware Estuary. These kinetic interactions provide sources and sinks in Equation (3-1). Principal kinetics are discussed below.

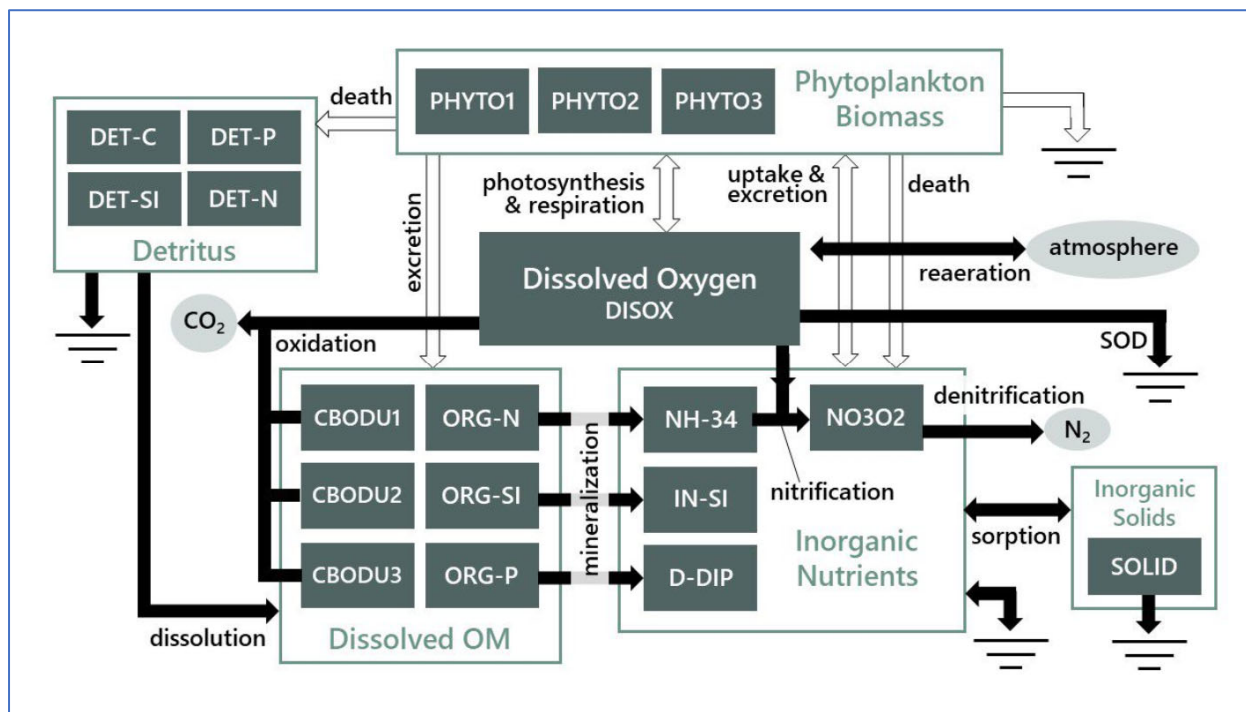


Figure 3-2: Water quality model kinetics

3.1.2.1 STATE VARIABLES

The WASP model as applied to the Delaware Estuary consists of 20 state variables (Table 3-1). The state variable is a water quality parameter that the model simulates its mass (concentration) for each cell for each model calculation time step through physical, chemical, and biological processes.

Table 3-1: Water quality model state variables

Group	Symbol	Description	Unit
Dissolved: Gases	DISOX	Dissolved Oxygen	mg-O ₂ /L
Dissolved: Inorganic Nutrients	NH-34	Ammonia Nitrogen	mg-N/L
	NO3O2	Nitrite + Nitrate Nitrogen	mg-N/L
	D-DIP	Inorganic Phosphate	mg-P/L
	IN-SI	Inorganic Silica	mg-Si/L

Group	Symbol	Description	Unit
Dissolved: Organic Nutrients	CBODU1	Ultimate CBOD from streams	mg-O ₂ /L
	CBODU2	Ultimate CBOD from point sources	mg-O ₂ /L
	CBODU3	Refractory CBOD	mg-O ₂ /L
	ORG-N	Dissolved Organic Nitrogen	mg-N/L
	ORG-P	Dissolved Organic Phosphorus	mg-P/L
	ORG-SI	Dissolved Organic Silica	mg-Si/L
Particulate: Phytoplankton Biomass	PHYTO1	Spring Marine Diatom Community	µg-Chla/L
	PHYTO2	Summer Freshwater Diatom Community	µg-Chla/L
	PHYTO3	Summer Marine Diatom Community	µg-Chla/L
Particulate: Detritus	DET-C	Detrital Carbon	mg-C/L
	DET-N	Detrital Nitrogen	mg-N/L
	DET-P	Detrital Phosphorus	mg-P/L
	DET-SI	Detrital Silica	mg-Si/L
Particulate: Other Solids	SOLID	Inorganic Solid	mg-DW/L
	TOTDE	Particulate Detrital Organic Material	mg-DW/L

Notes: "DW" represents Dry Weight

"CBOD" represents Carbonaceous Biochemical Oxygen Demand

3.1.2.2 KINETIC PROCESSES

3.1.2.2.1 Carbonaceous Oxidation

The decomposition of carbonaceous matter consumes oxygen, which can be expressed as the carbonaceous biochemical oxygen demand (CBOD). Oxidation provides sinks to both CBOD and dissolved oxygen. A general chemical representation of carbonaceous oxidation is (Chapra, 1997):



Equation (3-2) indicates that six moles of oxygen are required to oxidate one mole of carbonaceous organic matter into carbon dioxide and water. This equation also provides a simplified expression of the life/death cycle, i.e., the reverse reaction represents photosynthesis and the forward reaction represents respiration and decomposition (Chapra, 1997).

The kinetic expression for carbonaceous oxidation in WASP contains three terms: a first-order rate constant, a temperature correction term, and a low-DO correction term (Wool et al., 2018 and 2006). The third term represents the decline of the aerobic oxidation rate as DO levels approach 0. The user may specify the half-saturation constant that represents the DO level at which the oxidation rate is reduced by half.

$$S_{CBOD} = k_d \theta_d^{T-20} \left(\frac{C_{DO}}{K_{CBOD} + C_{DO}} \right) C_{CBOD} \quad (3-3)$$

where:

S_{CBOD} = CBOD decay rate (mg-O₂/L-day);

k_d = CBOD decay rate constant at 20°C (1/day);

θ_d = CBOD decay rate temperature correction coefficient;

T = water temperature (°C);

K_{CBOD} = CBOD half saturation oxygen limit (mg-O₂/L);

C_{DO} = concentration of dissolved oxygen (mg/L);

C_{CBOD} = concentration of CBOD (mg-O₂/L).

3.1.2.2.2 Nitrification

Nitrification is a process mediated by specialized groups of autotrophic bacteria that obtain energy through the oxidation of ammonium to nitrite and oxidation of nitrite to nitrate (Cercio and Noel, 2017). Thus, nitrification provides sinks to ammonium nitrogen and dissolved oxygen, and a source to nitrate nitrogen. A simplified expression for complete nitrification is (Cercio and Noel, 2017; Chapra et al., 2012; and Chapra, 1997):



Equation (3-4) indicates that two moles of oxygen are required to nitrify one mole of ammonium into nitrate.

The kinetics of nitrification in WASP are modeled as a function of available ammonium, dissolved oxygen, and water temperature (Wool et al., 2018 and 2006):

$$S_{NIT} = k_{nitr} \theta_{nitr}^{T-20} \left(\frac{C_{DO}}{K_{NIT} + C_{DO}} \right) C_{NH_4} \quad \text{when } T \geq T_{nitr} \quad (3-5)$$

$$S_{NIT} = 0 \quad \text{when } T < T_{nitr} \quad (3-6)$$

where:

S_{NIT} = nitrification rate (mg-N/L-day);

k_{nitr} = nitrification rate constant at 20°C (1/day);

θ_{nitr} = nitrification temperature coefficient (dimensionless);

K_{NIT} = half saturation constant for nitrification oxygen limit (mg-O₂/L);

C_{NH4} = concentration of ammonium nitrogen (mg-N/L);

T_{nitr} = minimum water temperature for nitrification reaction (°C).

3.1.2.2.3 Phytoplankton Processes

Theory and application of phytoplankton production and metabolism in WASP8 are provided by Wool et al. (2004). A high-level summary is provided here.

Up to 5 groups of phytoplankton can be simulated in the current version of WASP8, with kinetics expressed as:

$$S_{k,i} = (G_{p,i} - R_{p,i} - D_{p,i} - k_{s,i})C_{alg,i} \quad (3-7)$$

where:

$S_{k,i}$ = reaction term for phytoplankton group i (mg-C/L-day);

$C_{alg,i}$ = concentration of phytoplankton population group i (mg-C/L);

$G_{p,i}$ = specific growth rate constant (1/day);

$R_{p,i}$ = respiration rate constant (1/day);

$D_{p,i}$ = death rate constant (1/day);

$K_{s,i}$ = settling rate constant (1/day).

3.1.2.2.3.1 Phytoplankton growth due to photosynthesis

The specific growth rate constant, $G_{p,i}$, for group i is related to $k_{c,i}$, the maximum 20°C growth rate at optimum light and nutrients:

$$G_{p,i} = k_{c,i}X_{RT,i}X_{RI,i}X_{RN,i} \quad (3-8)$$

where:

$X_{RT,i}$ = the temperature adjustment factor (dimensionless);

$X_{RI,i}$ = the light limitation factor (dimensionless);

$X_{RN,i}$ = the nutrient limitation factor as a function of dissolved inorganic phosphorus, nitrogen, and silica (dimensionless).

The temperature adjustment is based on the approach of Cerco and Cole (1994):

$$X_{RT,i} = e^{-\kappa_{1,i}(T-T_{opt,i})^2} \quad \text{when } T \leq T_{opt,i} \quad (3-9)$$

$$X_{RT,i} = e^{-\kappa_{2,i}(T-T_{opt,i})^2} \quad \text{when } T > T_{opt,i} \quad (3-10)$$

where:

$T_{opt,i}$ = optimum temperature for phytoplankton group i growth ($^{\circ}\text{C}$);

$\kappa_{1,i}$ = effect of temperature below $T_{opt,i}$ on growth ($^{\circ}\text{C}^{-2}$);

$\kappa_{2,i}$ = effect of temperature above $T_{opt,i}$ on growth ($^{\circ}\text{C}^{-2}$).

The light limitation is based on Steele light limitation function integrated over depth:

$$X_{RI,i} = \frac{ef}{K_e H} \left[\exp \left\{ -\frac{I_a}{I_{s,i}} \exp(-K_e D) \right\} - \exp \left\{ -\frac{I_a}{I_{s,i}} \right\} \right] \quad (3-11)$$

where:

$e = 2.718$;

I_a = light intensity at top of segment (W/m^2);

$I_{s,i}$ = saturating light intensity for the i th phytoplankton group (W/m^2);

K_e = segment light extinction coefficient ($1/\text{m}$). A site-specific light attenuation model was developed in this study. Details are provided in Section 3.1.3.3.

f = fraction of day that is daylight (dimensionless);

H = depth of water column or water segment (m).

The nutrient limitation factor is given below, based on Monod growth kinetics:

$$X_{RN,i} = \text{Min} \left(\frac{C_{DIN}}{K_{MN,i} + C_{DIN}}, \frac{C_{PO4}}{K_{MP,i} + C_{PO4}}, \frac{C_{SiO4}}{K_{MSi,i} + C_{SiO4}} \right) \quad (3-12)$$

where:

DIN , $PO4$, $SiO4$ represent inorganic nitrogen, phosphate, and silica, respectively;

DIN includes both ammonia and nitrate-nitrogen (the sum of the two concentrations);

$K_{MN,i}$, $K_{MP,i}$, $K_{MSi,i}$ represent the half-saturation constants of phytoplankton group i for nitrogen, phosphorus, and silica uptake, respectively.

Phytoplankton growth provides sinks to dissolved inorganic nutrients through plant uptake. The kinetic processes are summarized in Equations (3-13) to (3-17) (Wool et al., 2018 and 2006). For notational simplicity, the transport terms are dropped in the equations below.

$$\frac{\partial C_{PO4}}{\partial t} = - \sum_{i=1}^{nalg} G_{p,i} C_{alg,i} a_{pc,i} \quad (3-13)$$

$$\frac{\partial C_{SiO4}}{\partial t} = - \sum_{i=1}^{nalg} G_{p,i} C_{alg,i} a_{sic,i} \quad (3-14)$$

$$\frac{\partial C_{NH4}}{\partial t} = - \sum_{i=1}^{nalg} G_{p,i} C_{alg,i} P_{NH4,i} a_{nc,i} \quad (3-15)$$

$$\frac{\partial C_{NO3}}{\partial t} = - \sum_{i=1}^{nalg} G_{p,i} C_{alg,i} (1 - P_{NH4,i}) a_{nc,i} \quad (3-16)$$

$$P_{NH4,i} = \frac{C_{NH4} C_{NO3}}{(K_{MN,i} + C_{NH4})(K_{MN,i} + C_{NO3})} + \frac{C_{NH4} K_{MN,i}}{(C_{NH4} + C_{NO3})(K_{MN,i} + C_{NO3})} \quad (3-17)$$

where:

$a_{pc,i}$ = phytoplankton phosphorous to carbon ratio of phytoplankton group i ;

$a_{sic,i}$ = phytoplankton silica to carbon ratio of phytoplankton group i ;

$a_{nc,i}$ = phytoplankton nitrogen to carbon ratio of phytoplankton group i ;

P_{NH4} = preference for ammonia uptake term;

$nalg$ = number of phytoplankton groups.

Phytoplankton growth also provides a source to dissolved oxygen through photosynthesis, which is summarized in sub-section of Dissolved Oxygen Processes.

3.1.2.2.3.2 Phytoplankton respiration

Phytoplankton respiration rate is temperature dependent and is determined by:

$$R_{p,i} = K_{R,i} \theta_{R,i}^{T-20} \quad (3-18)$$

where:

$K_{R,i}$ = the endogenous respiration rate at 20 °C for phytoplankton group i (1/day);

$\theta_{R,i}$ = temperature coefficient (dimensionless).

Phytoplankton respiration provides sources to both inorganic and organic matter. The kinetic processes are summarized in Equations (3-19) to (3-21) (Wool et al., 2018 and 2006).

$$\frac{\partial C_{PO4}}{\partial t} = \sum_{i=1}^{nalg} R_{p,i} C_{alg,i} (1 - f_{OP,i}) a_{pc,i}; \quad \frac{\partial C_{DOP}}{\partial t} = \sum_{i=1}^{nalg} R_{p,i} C_{alg,i} f_{OP,i} a_{pc,i} \quad (3-19)$$

$$\frac{\partial C_{SiO4}}{\partial t} = \sum_{i=1}^{nalg} R_{p,i} C_{alg,i} (1 - f_{OSi,i}) a_{sic,i}; \quad \frac{\partial C_{DOSi}}{\partial t} = \sum_{i=1}^{nalg} R_{p,i} C_{alg,i} f_{OSi,i} a_{sic,i} \quad (3-20)$$

$$\frac{\partial C_{NH4}}{\partial t} = \sum_{i=1}^{nalg} R_{p,i} C_{alg,i} (1 - f_{ON,i}) a_{nc,i}; \quad \frac{\partial C_{DON}}{\partial t} = \sum_{i=1}^{nalg} R_{p,i} C_{alg,i} f_{ON,i} a_{nc,i} \quad (3-21)$$

where:

DON , DOP , $DOSi$ = dissolved organic nitrogen, phosphorus, and silica, respectively;

$f_{OP,i}$ = fraction of respired phytoplankton group i recycled to the organic phosphorus pool;

$f_{OSi,i}$ = fraction of respired phytoplankton group i recycled to the organic silica pool;

$f_{ON,i}$ = fraction of respired phytoplankton group i recycled to the organic nitrogen pool.

Phytoplankton respiration also provides a sink to dissolved oxygen, which is summarized in sub-section on Dissolved Oxygen Processes.

3.1.2.2.3.3 Phytoplankton death

Phytoplankton death consists of natural death, grazing by herbivorous zooplankton, salinity toxicity for freshwater diatom community, and freshwater toxicity for marine diatom community. The natural death term is represented by a first-order rate constant that is not temperature corrected. The death of freshwater algae introduced to a saline environment is referred to as salinity toxicity, and freshwater toxicity refers to the death of saltwater algae introduced to a freshwater environment. In this study, death rates and threshold values due to salinity and freshwater toxicity were assigned to the appropriate phytoplankton class. The kinetic processes are summarized in Equations (3-27) to (3-30) (T. Wool, written communication, 2022).

$$D_{p,i} = K_{D,i} + K_{GZ,i} + K_{ST,i}X_{ST,i} + K_{FT,i}X_{FT,i} \quad (3-22)$$

$$X_{ST,i} = 1 - \exp[\text{Log}_{10}(0.5) \times \left(\frac{\text{Sal} - \text{Sal}_{1,i}}{\text{Sal}_{1,i} - K_{H1,i}}\right)^2] \quad \text{when } \text{Sal} > \text{Sal}_{1,i} \quad (3-23)$$

$$X_{ST,i} = 0 \quad \text{when } \text{Sal} \leq \text{Sal}_{1,i} \quad (3-24)$$

$$X_{FT,i} = 1 - \exp[\text{Log}_{10}(0.5) \times \left(\frac{\text{Sal}_{2,i} - \text{Sal}}{\text{Sal}_{2,i} - K_{H2,i}}\right)^2] \quad \text{when } \text{Sal} < \text{Sal}_{2,i} \quad (3-25)$$

$$X_{FT,i} = 0 \quad \text{when } \text{Sal} \geq \text{Sal}_{2,i} \quad (3-26)$$

where:

$D_{p,i}$ = total death rate for phytoplankton group i (1/day);

$K_{D,i}$ = natural death rate for phytoplankton group i (1/day);

$K_{GZ,i}$ = loss rate due to grazing by zooplankton for phytoplankton group i (1/day);

$K_{ST,i}$ = mortality rate due to salinity toxicity for phytoplankton group i (1/day);

$K_{FT,i}$ = mortality rate due to freshwater toxicity for phytoplankton group i (1/day);

Sal = salinity (ppt);

$\text{Sal}_{1,i}$ = salinity mortality threshold (freshwater to saltwater) concentration for phytoplankton group i (ppt);

$K_{H1,i}$ = sustainable salinity level due to salinity toxicity for phytoplankton group i (ppt);

$\text{Sal}_{2,i}$ = salinity mortality threshold (saltwater to freshwater) concentration for phytoplankton group i (ppt);

$K_{H2,i}$ = sustainable salinity level due to freshwater toxicity for phytoplankton group i (ppt).

Phytoplankton death provides a source to the estuarine detrital pool. The kinetic processes are summarized in Equations (3-27) to (3-30) (Wool et al., 2018 and 2006).

$$\frac{\partial C_{detP}}{\partial t} = \sum_{i=1}^{nalg} D_{p,i} C_{alg,i} a_{pc,i} \quad (3-27)$$

$$\frac{\partial C_{detSi}}{\partial t} = \sum_{i=1}^{nalg} D_{p,i} C_{alg,i} a_{sic,i} \quad (3-28)$$

$$\frac{\partial C_{detN}}{\partial t} = \sum_{i=1}^{nalg} D_{p,i} C_{alg,i} a_{nc,i} \quad (3-29)$$

$$\frac{\partial C_{detC}}{\partial t} = \sum_{i=1}^{nalg} D_{p,i} C_{alg,i} \quad (3-30)$$

where:

detP, *detSi*, *detN*, *detC* = detrital phosphorus, silica, nitrogen, and carbon, respectively.

3.1.2.2.4 Reaeration

Reaeration is the transport of oxygen entering or leaving the system across the air-water interface. It provides a source or sink to the dissolved oxygen, depending on the dissolved oxygen deficit in the water column. Reaeration rate is a function of the difference between oxygen saturation and the interface oxygen concentration, mass transfer coefficient, and temperature (Chapra, 1997).

$$R_O = AK_L(C_{DO,sat} - C_{DO}) \quad (3-31)$$

where:

R_O = reaeration rate (mg-O₂/day);

A = surface area (m²);

$C_{DO,sat}$ = oxygen saturation (mg-O₂/L);

C_{DO} = dissolved oxygen concentration at the air-water interface (mg-O₂/L);

K_L = mass transfer coefficient of oxygen (m/day).

WASP provides several options for simulating reaeration, including hydraulic-driven reaeration in rivers and streams, wind-driven reaeration, and dam reaeration (Wool et al., 2018 and 2006). In this study, an enhancement in reaeration simulation was developed utilizing turbulence dissipation rate near the air-water interface. Details on this enhancement is provided in Section 3.1.3.2 and Appendix D.

3.1.2.2.5 Sediment Oxygen Demand (SOD) and Nutrient Benthic Fluxes

Oxygen demand by and nutrient release from sediment due to the mineralization (diagenesis) of organic matter can contribute to surface water quality. WASP provides options to either prescribe (via input flux rates) or predict SOD and sediment nutrient releases (Martin and Wool, 2017). The latter option, i.e., a sediment diagenesis model in WASP, was based on Di Toro's (2001) framework. The prescriptive option was used in this study based on the extensive SOD and sediment benthic flux data available for 2012–2013 and 2016–2018 (see Section 3.1.4.6).

3.1.2.2.6 Dissolved Oxygen Processes

Dissolved oxygen processes include multiple kinetics discussed in the previous sub-sections. The kinetic expression for the dissolved oxygen process is given as (Wool et al., 2018 and 2006):

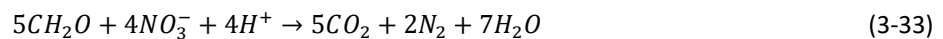
$$\frac{\partial C_{DO}}{\partial t} = \frac{K_L}{H} (C_{DO,sat} - C_{DO}) - S_{CBOD} - \frac{64}{14} S_{nitr} - \frac{SOD}{H} \theta_{SOD}^{T-20} \quad (3-32)$$

$$+ \sum_{i=1}^{nalg} G_{p,i} \left[\frac{32}{12} + \left(\frac{3}{2} \times \frac{32}{14} \times a_{nc,i} \right) (1 - P_{NH_4}) \right] C_{alg,i} - \sum_{i=1}^{nalg} \frac{32}{12} R_{p,i} C_{alg,i}$$

where the terms on the right-hand-side of Equation (3-32) represent: (1) dissolved oxygen (DO) gain from the reaeration (where H is the water depth or segment depth); (2) DO loss due to carbonaceous oxidation; (3) DO loss resulted from nitrification; (4) DO loss caused by SOD; (5) DO gain from photosynthesis using NH_4 and NO_3 , respectively; and (6) DO loss caused by respiration.

3.1.2.2.7 Denitrification

Under low dissolved oxygen conditions (i.e., hypoxic or lower), nitrate can be reduced to nitrite and nitrite converted to free nitrogen in gaseous form by denitrification (Chapra, 1997). This process also consumes dissolved organic carbon. Thus, the denitrification reaction provides sinks to both nitrate nitrogen and CBOD. A chemical representation of denitrification is (Chapra et al., 2012, and Wool et al., 2006):



Equation (3-33) indicates that for each mg of nitrate-nitrogen reduced, 5/4 (12/14) mg of carbon are consumed, which reduces CBOD by 5/4 (12/14) (32/12) mg. Denitrification is not a significant loss in the water column but can be important when simulating anaerobic benthic conditions (Wool et al., 2006).

The kinetic expression for denitrification in WASP contains three terms: a first order rate constant (with appropriate stoichiometric ratios), a temperature correction term, and a DO correction term (Wool et al., 2018 and 2006). The third term represents the decline of the denitrification rate as DO levels rise above 0. The user may specify the half-saturation constant, which represents the DO level at which the denitrification rate is reduced by half.

$$S_{DNIT} = k_{dnit} \theta_{dnit}^{T-20} \left(\frac{K_{NO_3}}{K_{NO_3} + C_{DO}} \right) C_{NO_3} \quad (3-34)$$

where:

S_{DNIT} = denitrification rate (mg-N/L-day);

k_{dnit} = denitrification rate constant at 20°C (1/day);

θ_{dnit} = denitrification temperature coefficient (dimensionless);

K_{NO_3} = half saturation constant for denitrification oxygen limit (mg-O₂/L);

C_{NO_3} = concentration of nitrate nitrogen (mg-N/L).

Denitrification rate in Equation (3-34) is related to the nitrate nitrogen. For CBOD, the loss due to denitrification is: $\frac{5.32}{4.14} S_{DNIT}$

3.1.2.2.8 Dissolution of Nutrients Associated with Particulate Organic Matter

Particulate organic matter (POM or simply detritus) is derived from algal death, but also from allochthonous external loads. This detrital matter transforms into dissolved organic matter through bacterial dissolution. Dissolved organic matter is further mineralized to inorganic forms, as discussed in the following section. Transformation of detrital carbon (including associated organic nitrogen, phosphorus and silica) to dissolved forms in WASP follows a temperature-corrected first-order kinetic process. For algal nutrients these transformation terms are as follows:

$$S_{disP} = k_{disDet} \theta_{disDet}^{T-20} C_{DetP} \quad (3-35)$$

$$S_{disN} = k_{disDet} \theta_{disDet}^{T-20} C_{DetN} \quad (3-36)$$

$$S_{disSi} = k_{disDet} \theta_{minSi}^{T-20} C_{DetSi} \quad (3-37)$$

where:

S_{disP} , S_{disN} , and S_{disSi} = dissolution rates of particulate organic matter (mg-P, N, Si/L-day);

k_{disDet} = dissolution rate constant at 20°C (1/day);

θ_{disDet} = dissolution rate temperature correction coefficient (dimensionless);

C_{DetP} , C_{DetN} , C_{DetSi} = concentration of detrital P, N and Si (mg-P, N, Si /L).

3.1.2.2.9 Mineralization of Dissolved Organic Nitrogen, Phosphorus, and Silica

Mineralization is a process whereby dissolved organic compounds are converted to dissolved inorganic products (Chapra, 1997; Cerco and Noel, 2017). Direct mineralization of particulate organic matter

(detritus) does not occur, but this material does undergo a process of dissolution (see previous section) to dissolved organic forms which may then be mineralized. Thus, mineralization provides sinks to the dissolved organic matters and sources to the dissolved inorganic nutrients. The mineralization rates in WASP are related to a first order rate constant, a temperature correction term, and a phytoplankton concentration correction term. The third term slows the mineralization rate if the phytoplankton population is small but does not permit the rate to increase continuously as phytoplankton increase (Wool et al., 2018 and 2006).

$$S_{minP} = k_{minP} \theta_{minP}^{T-20} \frac{C_{algT}}{K_{mpc} + C_{algT}} C_{DOP} \quad (3-38)$$

$$S_{minN} = k_{minN} \theta_{minN}^{T-20} \frac{C_{algT}}{K_{mpc} + C_{algT}} C_{DON} \quad (3-39)$$

$$S_{minSi} = k_{minSi} \theta_{minSi}^{T-20} \frac{C_{algT}}{K_{mpc} + C_{algT}} C_{DOSi} \quad (3-40)$$

where:

S_{minP} , S_{minN} , and S_{minSi} = mineralization rates of dissolved organic matter (mg-P, N, Si/L-day);

k_{minP} , k_{minN} , and k_{minSi} = mineralization rate constants at 20°C (1/day);

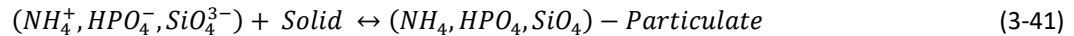
θ_{minP} , θ_{minN} , and θ_{minSi} = mineralization temperature coefficients (dimensionless);

K_{mpc} = algal half saturation constant for mineralization (mg-C/L);

C_{algT} = concentration of total phytoplankton (mg-C/L).

3.1.2.2.10 Sorption

There is an adsorption–desorption interaction between dissolved inorganic nutrients and suspended particulate matters in the water column. The subsequent settling of the suspended solids together with the sorbed inorganic nutrients can act as a loss mechanism in the water column and is a source of nutrients to the sediment (Wool et al., 2018 and 2006). Sorption kinetics is summarized below:



$$K_d = \frac{C_p}{C_{solid} C_{dis}} \quad (3-42)$$

$$f_s = \frac{C_p}{C_{dis} + C_p} = \frac{K_d C_{solid}}{1 + K_d C_{solid}} \quad (3-43)$$

where:

K_d = partition coefficient for inorganic nutrients (e.g., NH_4 , PO_4 , and SiO_4) (m^3/g);

C_p = particulate inorganic nutrient concentrations (g/m^3);

C_{dis} = dissolved inorganic nutrient concentrations (g/m^3);

C_{solid} = suspended solid concentration (g/m^3);

f_s = particulate fractions of inorganic nutrients (dimensionless).

3.1.2.2.11 Settling

Settling rate in WASP is expressed as (Wool et al., 2018 and 2006):

$$k_s = \frac{v_s}{H} \quad (3-44)$$

where:

k_s = settling rate (1/day);

v_s = net settling velocity associated with solids, phytoplankton, and detritus, respectively (m/day);

“Net settling” represents gross settling minus gross resuspension.

H = water depth or segment depth (m).

Settling causes the loss of state variables from the system to the sediment. The loss term is expressed as: $-k_s C$, which includes the losses associated with 1) solid, $-k_s C_{solid}$; 2) detritus, $-k_s C_{detP}$, $-k_s C_{detSi}$, $-k_s C_{detN}$, and $-k_s C_{detC}$, respectively; 3) particulate inorganic matters, $-k_s f_{s,PO_4} C_{PO_4}$, $-k_s f_{s,SiO_4} C_{SiO_4}$, and $-k_s f_{s,NH_4} C_{NH_4}$; and 4) phytoplankton related, $-k_s a_{pc,i} C_{alg,i}$, $-k_s a_{sic,i} C_{alg,i}$, $-k_s a_{nc,i} C_{alg,i}$, and $-k_s C_{alg,i}$ for phytoplankton group i .

3.1.3 MODEL ENHANCEMENTS

Three enhancements were made during this study to improve the water quality model (WASP) accuracy and reliability: (1) a thorough investigation of WASP model integration with the hydrodynamic model EFDC, (2) reaeration simulation, and (3) light extinction formulation.

3.1.3.1 INTEGRATION WITH HYDRODYNAMIC MODEL

Application of a three-dimensional hydrodynamic model (EFDC) and a water quality model (WASP) to a complex system requires thorough examination of model integration. Information from EFDC, such as

water volume, current velocity, flow rate, mixing coefficient, salinity, water temperature, and turbulence dissipation rate, is transferred to WASP via stored output (or linkage file) for use in simulating water column transport of constituents. The two models perform simulations on the same numerical grid, so spatial collapsing of EFDC output is not necessary. Temporally, WASP can use a larger time step than EFDC. Key parameters for preparing the linkage file include (1) the coupling interval NTSMMT, i.e., the number of time steps for EFDC to average and output variables to the linkage file; and (2) the upper limit on the vertical mixing ABMAX, aiming at capping larger vertical mixing coefficient values and maintaining numerical stability in WASP. Determining these parameters needs to consider: 1) the capability for WASP to reproduce conservative tracer transport by EFDC; 2) maintaining mass balance in WASP; 3) controllable WASP computation time; and 4) a manageable linkage file size.

Time step in WASP model is related to the EFDC coupling interval NTSMMT. Generally, smaller NTSMMT results in a smaller time step in WASP and consequent longer computation time. Smaller NTSMMT also brings about better conservative tracer transport, improved mass balance, and a correspondingly larger linkage file. From a practical perspective, we would choose a NTSMMT as large as possible, as long as the WASP model can maintain a good mass balance and reproduce the conservative tracer transport predicted by EFDC. A series of numerical tests suggested that NTSMMT = 30, combined with an adequate ABMAX value, could provide a good balance among the factors discussed above. Appendix C presents the results of conservative tracer transport and mass balance with NTSMMT = 30. Results of numerical tests with other NTSMMT values are not included in the report. In this application, the time step for EFDC was 10 seconds (DRBC, 2021), NTSMMT = 30 resulted in a linkage output every 300 seconds (every 5 minutes) and a linkage file of 45 Gigabyte for one year simulation.

In theory, WASP model should honor the vertical mixing predicted by EFDC. However, in practice, the “Timestep Optimization” algorithm in WASP, without which computation time may become double or triple, is sensitive to the ABMAX, i.e., larger vertical mixing coefficient forces the algorithm to adopt a smaller time step in WASP for maintaining numerical stability. For example, a WASP model with ABMAX = 0.01 m²/s and NTSMMT = 30 takes about 100 hours for one year simulation with 20 state variables, whereas a WASP model with ABMAX = 0.001 m²/s and NTSMMT = 30 takes about 32 hrs. for the same simulation. The value of 0.01 m²/s corresponds to about 80th percentile and up to 30th percentile of vertical mixing coefficients in the Bay and tidal river, respectively. Numerical tests presented in Appendix C indicated that a combination of NTSMMT = 30 and ABMAX = 0.01 m²/s produced reasonable agreement in conservative tracer transports between EFDC and WASP, as well as adequate mass balance from WASP (e.g., 2% or lower yearly averaged error along navigation channel, and 5% or lower instantaneous error at main stem cells), even though the linkage file removed the top 70% of vertical mixing coefficient values in the tidal river. This is in part because a vertical mixing coefficient of 0.01 m²/s is sufficient to generate vertically well mixing in the tidal river under the model spatial and temporal scales. Another combination of NTSMMT = 30 and ABMAX = 0.001 m²/s generated comparable downstream transport but less desirable upstream transport as those in the first combination with ABMAX = 0.01 m²/s (Appendix C). The

second combination also resulted in mass balance errors double but three times faster than the first combination.

Furthermore, numerical tests in Appendix C demonstrated that $ABMAX = 0.01$ and $0.001 \text{ m}^2/\text{s}$ generate insignificant differences in simulated DO concentrations. All other parameters in the tests were identical as in the final calibration. To balance mass transport accuracy and computation time, we used the combination of $NTSMMT = 30$ and $ABMAX = 0.001 \text{ m}^2/\text{s}$ in the model calibration production runs and the combination of $NTSMMT = 30$ and $ABMAX = 0.01 \text{ m}^2/\text{s}$ for the final water quality model calibration.

3.1.3.2 REAERATION

Reaeration is a process of dissolved oxygen (DO) transfer at the air–water interface in both ways depending on DO concentration gradients. DO component analysis (see Section 3.2.5.1) indicates that reaeration is an important contributor to DO gain in the tidal river. Conventional options for reaeration simulation in WASP model, such as O’Connor-Dobbins (1958), categorize the reaeration process into (1) hydraulic-driven reaeration for streams or rivers where current effect is a predominant factor, and (2) wind-driven reaeration for lakes or bays where wind effect is dominant. Depth-averaged velocity and water column depth are used in the hydraulic-driven formulation for estimating the mass transfer coefficient, whereas wind speed is used in the wind-driven formulation. In both cases, DO concentrations are usually represented by the ones at surface segments. However, the Delaware Estuary is a complex environment with deep-water, high energy, flow reversals (tides), potential stratification, and geometry varying from relatively narrow river to relatively wide estuary, suggesting there was an opportunity for the representation of surface DO concentration in the reaeration formulation to be improved. Furthermore, advancement in turbulence modeling in recent decades may help improve quantification of the mass transfer at the air–water interface. In this study, reaeration simulation was enhanced in two aspects: (1) extrapolating DO concentrations from surface layer centers to the air–water interface for proper representation of gas transfer across the interface; and (2) utilizing the turbulence dissipation rate at the air–water interface for estimating the mass transfer coefficient (Zappa et al. 2007). Zappa’s approach incorporates the comprehensive effects of current velocity, wind speed, and water temperature on reaeration into the key input parameters. Thus, users do not need to decide whether to use hydraulic- or wind-driven formulations. Details regarding the reaeration simulation enhancement, including comparisons between the Zappa and O’Connor-Dobbins’ approaches, are discussed in Appendix D.

3.1.3.3 LIGHT EXTINCTION

Light extinction in water refers to the loss of light in the water column due to absorption and scattering. Light extinction in aquatic environments plays an important role in controlling important water quality parameters such as temperature and dissolved oxygen (via photosynthesis). Understanding the dynamics of light extinction is essential to accurately modelling dissolved oxygen dynamics in the Delaware Estuary. Water quality constituents that affect light extinction include suspended solids, phytoplankton, and detritus (Di Toro 1978). Ideally, all these parameters could be used to predict light extinction, however,

to develop a dynamic light model for use within the eutrophication model, light extinction needed to be predicted using only model state variables. This limited the parameters available to model light extinction.

2018 and 2019 data from DRBC's Boat Run Monitoring Program were used to model light extinction in the Delaware Estuary. The Boat Run provided a valuable dataset for the purpose of this exercise, as it has broad spatial and temporal coverage of the Estuary and includes important parameters for modelling light extinction including photosynthetically active radiation (PAR, collected at the surface and 1 meter depth) along with several model state variables. Observed light extinction (K_e) was calculated from PAR data using the following equation (Chapra, 1997):

$$K_e = \ln\left(\frac{PAR_{surface}}{PAR_{1\text{ meter}}}\right) \quad (3-45)$$

The model state variables that were chosen to predict light extinction were chlorophyll a, dissolved organic carbon, and salinity. Salinity, while not a direct driver of light extinction, acted as a surrogate for suspended solids for the purposes of our model. Suspended solids are the main driver of light extinction in the Delaware Estuary and are also a model state variable, however they were unable to be used as explanatory variable as several of the processes driving sediment dynamics in the Estuary are not incorporated in the model (e.g., erosion and resuspension of sediments). This leads to underpredictions of sediment loads in the model. Salinity was chosen as a surrogate for sediment because its gradient in the Estuary inversely resembles that of solids. Suspended solids are highest near the Estuarine Turbidity Maximum (ETM) zone, around river mile 55, and lowest at the mouth of the Bay. Salinity follows an inverse pattern showing highest concentrations at the mouth of the Bay and concentrations approaching zero at the upstream extent of the ETM. Therefore, an inverse relationship with salinity was able to be used as a surrogate for suspended solids up to the upper extent of the ETM. To accurately capture this dynamic, data from the mouth of the Bay to the lower end of the ETM (RM 36) was used to parametrize the salinity coefficient in the model. Since salinity values are near-zero upstream of the ETM, this parameter would have little to no influence on K_e predictions upstream of the ETM. Suspended sediments are the dominant driver of light extinction near the ETM, however chlorophyll and DOC are important drivers upstream and downstream of this reach. Because the effects of these secondary parameters are difficult to observe at the ETM, we parametrized these variables using only data from upstream and downstream of the ETM (RM 0-36, 80-131). Finally, to capture light extinction dynamics more accurately throughout the Estuary, we calculated spatially variable intercepts for each Boat Run station. This allowed for a model that captures consistent large-scale spatial differences in K_e throughout the estuary (i.e., K_e is higher at the ETM than at the mouth or head of tide) while still retaining the dynamic capabilities of using modeled state variables to predict K_e . The final predictive function for K_e is below:

$$K_e = \text{Intercept} + (0.345 * DOC) + (0.014 * Chlorophyll\ a) + (-0.097 * Salinity) \quad (3-46)$$

$$\text{Intercept} = 3.5944e^{-0.016 \times RM} + \text{Max}[0, (1.7549 - 0.069 \times |54.9 - RM|)] \quad (3-47)$$

3.1.4 MODEL INPUTS

All flows, salinity and water temperature information are provided by the hydrodynamic model (DRBC, 2021) through a linkage file. The water quality model requires concentration specification for inflow boundaries and open boundaries. Also, requires assignment of loads/fluxes for certain source categories. The time-series model input files for each state variable are prepared based on the compiled monitoring data as presented in Section 2.2 and model input conditions described in this section. Methodologies used to develop the model input file are described for following list of source categories.

- Tributary and watershed (MS4s and NPS Runoffs) inflow concentrations
- Wastewater Treatment and CSOs effluent concentrations
- Ocean and C&D Canal open boundary concentrations
- Atmospheric loads
- Meteorologic boundaries
- Sediment Oxygen Demand (SOD) and benthic nutrient fluxes

Procedures for calculating state variable concentrations from analytical parameters are described in Appendix E. The concentration values were used to specify the boundary conditions or calibration parameters. All boundary conditions were compiled into a Water Resources Database (WRDB) for being used by the WASP model.

Initial conditions of the model and hydrologic conditions of the model calibration and model corroboration periods are discussed in last two subsections.

3.1.4.1 TRIBUTARY AND WATERSHED INFLOW CONCENTRATIONS

Concentrations must be assigned for freshwater inflows, including flows from upstream boundaries, tributaries (gaged and ungaged), non-point sources (NPS), and Municipal Separate Storm Sewer Systems (MS4) discharges. Groundwater/surface water interaction was not considered in this study.

Several approaches were used to assign advective nutrient loading to the tidal Delaware River and Estuary. The primary approach utilizes the compilation and direct assignment of discrete or continuous observational data acquired from various agencies including the DRBC, USGS New Jersey, Pennsylvania, and Maryland Water Science Centers, Delaware Department of Natural Resources and Environmental Control (DNREC), New Jersey Department of Environmental Protection (NJDEP), Pennsylvania Department of Environmental Protection (PADEP), and U.S. Army Corps of Engineers (USACE). Discrete data were widely available during the 2018–2019 simulation period but less so during 2012. The frequency of data

for each water-quality parameter varied from monthly to quarterly, except for The Delaware River at Trenton, where data were collected on an approximate biweekly basis. Water-quality boundaries were augmented with continuous DO collected at USGS gages located on selected tributaries (Delaware River at Trenton, Brandywine Creek, Christina River, Appoquinimink River, and Murderkill River). Additionally, sensory monitoring of chlorophyll-a at Trenton provided hourly input time series at the model upstream boundary.

At selected tributaries, water-quality boundaries were temporally enhanced using standard USGS regression techniques. Regression methods were implemented through two USGS-developed packages, Load Estimator (LOADEST) and the Weighted Regressions on Time, Season, and Discharge (WRTDS) tool. Both packages employ logarithms of daily discharge, decimal time, and sine and cosine transformations of decimal time (season) to estimate concentration. The basic form of the LOADEST model consists of a seven-parameter model in which log-transformed daily concentrations are related to second-order polynomials of log-transformed daily flow, decimal time, and seasonal factors derived from transformations of decimal time (Cohn et al., 1989; Runkel et al., 2004). WRTDS resolves variations in constituent concentration using five terms, excluding the squared terms that are used in LOADEST. A fundamental difference between the models is the manner in which coefficients are estimated. WRTDS estimates parameter coefficients for each estimation point (any given combination of discharge and time) using a unique weighted regression for each day of the estimation period, applying greater weight to observations closer in time, discharge, and season to the estimation point (Hirsch et al., 2010). In contrast, LOADEST estimates parameter coefficients once for the entire dataset. Both packages were combined into a single script, implemented using the R language, such that input requirements are common to both. Statistical models using both methods were run for NO₂+NO₃, NH-34, TDN, DIP, TDP, DSI, TP, TN, DOC, TOC, and TSS for each tributary with a sufficient sample size (60+) and a representative range of hydrologic conditions. Model performance was assessed both graphically and statistically; if the model was deemed acceptable, these data were used at the appropriate water-quality boundary.

In sparsely monitored or unmonitored portions of the watershed, environmental classification was used to transfer water-quality information between measured and unmeasured sites. A hierarchical agglomerative cluster analysis was used to group sub-watersheds with similar physical and hydrologic attributes into general landscape regions, providing the basis for assigning water-quality values to catchments lacking data. Hierarchical agglomerative clustering successively combines smaller clusters into larger ones while maintaining a minimal merge cost at each stage; similarity among clusters was determined using Ward's method of linkage with squared Euclidean distances.

The cluster analysis identified four general groups of watersheds: small to medium-sized urbanized basins with mixed geology, moderate slopes, and low base flow indices (BFI); medium-to-larger size, gently-sloped basins underlain by unconsolidated sand/silts with significant BFI; medium-to-larger size, steeper-sloped basins with forested uplands, underlain by consolidated bedrock; and small, low fluvial energy, coastal plain basins containing higher percentages of agricultural land use and wetlands.

Associated data from the control watersheds were composited into four matrices by season and streamflow condition and subsequently assigned to unmonitored watersheds on the basis of cluster membership. Time series for most state variables were compiled at a daily time step and applied to NPS and MS4 boundaries. Where a daily time series could not be prescribed, constant values, derived from averaging 2018–2019 tributary data, were used.

3.1.4.2 WASTEWATER TREATMENT PLANT EFFLUENT CONCENTRATIONS

Seventy-one (71) point discharge facilities (see

Figure 2-3 and **Error! Reference source not found.**) are included in this study. Constituent concentrations from these point source discharges during the model calibration period 2018–2019 were specified based on the second round of monitoring data depicted in Sections 0 and 2.2.2. If the concentration of a state variable was not measured directly, it was then calculated based on other measured data, following the procedures listed in Appendix E. The input intervals of boundary conditions for Tier-1 and -2 facilities are weekly and monthly, respectively, consistent with the monitoring frequencies for the 2018-2019 period. The effluent concentrations from Tier-3 facilities are set to constant values for simplification, based on the medians of collected data. For the model corroboration period 2012, effluent concentrations from the point discharges were specified based on the first round of monitoring initiated in 2011 (see Section 0). The boundary condition intervals are monthly for both Tier-1 and -2 facilities. The boundary condition intervals for Tier-3 facilities are coarser due to less available data.

Freshwater inflows from CSOs during the model calibration and corroboration periods were provided to various degrees of resolution by four municipalities: Philadelphia Water Department (PWD), Camden County Municipal Utilities Authority (CCMUA), Delaware County Regional Water Quality Control Authority (DELCORA), and City of Wilmington (CoW). For simplification, all CSO outfalls were aggregated to 14 locations: five for PWD CSOs; three for CCMUA CSOs; three for DELOCRA CSOs; and three for CoW CSOs. CSO outfalls located upstream of tributary monitoring locations were excluded to avoid double counting of flows and loads. Constant effluent concentrations were assumed for each state variable (limited CSO sampling data provided by DELCORA. These concentrations were compared with PWD’s CSO modeling methodology, and DRBC’s concentrations assignments generally fall within the range PWD assumed for stormwater and wastewater, respectively.

Table 3-2), based on limited CSO sampling data provided by DELCORA. These concentrations were compared with PWD’s CSO modeling methodology, and DRBC’s concentrations assignments generally fall within the range PWD assumed for stormwater and wastewater, respectively.

Table 3-2: CSO effluent concentrations

State Variable	Effluent Concentration	Units
NH-34	6.9	mg-N/L

State Variable	Effluent Concentration	Units
NO3O2	0.5	mg-N/L
ORG-N	2.9	mg-N/L
DET-N	4.1	mg-N/L
D-DIP	0.8	mg-P/L
ORG-P	0.2	mg-P/L
DET-P	1.8	mg-P/L
STR-CBODU	0.0	mg-O ₂ /L
PS-CBODU	38.4	mg-O ₂ /L
CDOM	4.3	mg-O ₂ /L
DET-C	18.9	mg-C/L
DISOX	5.9	mg-O ₂ /L
PHYTO	0.0	ug-Chla/L
IN-SI	9.4	mg-Si/L
ORGSi	0.0	mg-Si/L
DETSi	1.9	mg-Si/L
SOLID	57.0	mg-DW/L
TOTDE	0.0	mg-DW/L

3.1.4.3 OCEAN AND C&D CANAL BOUNDARY CONCENTRATIONS

NOAA National Centers for Environmental Information's World Ocean Atlas 2018 (WOA18) provides a statistical analysis of long-term data collected since 1960 on a 1° grid resolution (Garcia et al., 2019). The monthly-mean and depth-averaged nutrient concentrations at the grid cell closest to the mouth of Delaware Estuary were chosen as the ocean boundary conditions (Figure 3-3a). These nutrient concentrations include phosphate, nitrate, silicate, and dissolved oxygen (

Table 3-3). NJDEP grab samples collected at BMWM-3826A station (Figure 3-3b) provided supplemental information for characterizing phosphate and ammonia concentrations for the ocean boundary. Remaining state variable concentrations at the ocean boundary were specified based on the data collected by the DRBC Boat Run (see Section 2.1.1.1) at South Brown Shoal during the calibration and corroboration periods.

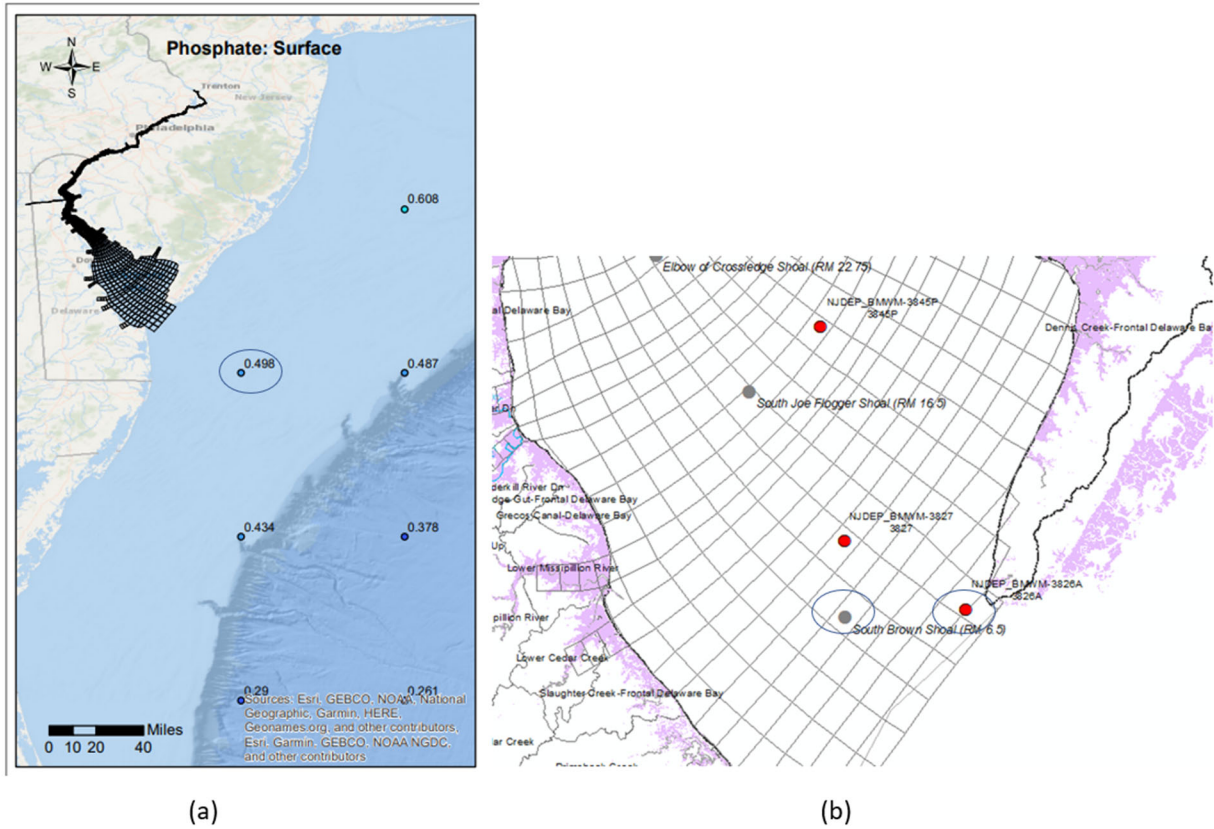


Figure 3-3: Location maps of (a) WOA18 data on 1° grid; and (b) Monitoring stations near mouth

Table 3-3: Nutrient concentrations from WOA18 near mouth of Estuary

Month	Nitrate (mg-N/L)	Phosphate (mg-P/L)	Silicate (mg-Si/L)	Dissolved Oxygen (mg-O ₂ /L)
January	0.035	0.015	0.005	8.555
February	0.029	0.023	0.015	8.989
March	0.046	0.016	0.008	9.689
April	0.018	0.008	0.028	10.569
May	0.006	0.005	0.047	9.242
June	0.007	0.008	0.045	9.591
July	0.007	0.011	0.039	8.470
August	0.013	0.012	0.048	8.258
September	0.010	0.010	0.053	7.708
October	0.007	0.007	0.030	8.019
November	0.024	0.011	0.015	8.305
December	0.021	0.009	0.051	8.781

Source: [The World Ocean Atlas \(WOA\) 2018](#)

Concentrations at the C&D canal boundary were based on the data collected during the DRBC Tributary Nutrient Monitoring Program (Section 2.2.3), and supplemented with data collected by the Maryland Department of Natural Resources and Delaware Department of Natural Resources and Environmental Control.

3.1.4.4 ATMOSPHERIC LOADS

Nutrient data collected by the National Atmospheric Deposition Program (NADP) from 2012 through 2019 provided the basis for estimating atmospheric nutrient loading to the tidal Delaware River and Estuary. Wet deposition rates were calculated using precipitation and nutrient data (NH-34, NO₃O₂) measured at Washington's Crossing, NJ and Wye, MD according to the methods of Ullman and others (2010). Dry deposition rates were estimated using NADP Total Deposition Maps (Schwede and Lear, 2014) in conjunction with wet deposition rates, whereby ratios of wet-to-dry deposition were estimated at each station. The ratios were then applied to the calculated wet deposition rates to estimate dry and ultimately total deposition rates. The rates are applied to all surface segments as a time-varying function (mg/m²/d) throughout the 2012 and 2018–19 simulation periods.

3.1.4.5 CLIMATE / METEOROLOGICAL BOUNDARIES

As detailed in Section 2.4.4 of the Hydrodynamic Model Report (DRBC, 2021), climate/meteorological data, such as air temperature and pressure, dew point, cloud conditions, wind speed, wind direction, precipitation, and net shortwave solar radiation, were used in EFDC to calculate the heat flux at the water surface and water temperature in the water column. Although predicted water temperature values were transferred from the hydrodynamic model to the water quality model through a linkage file, some of the meteorological data (e.g., wind speed and solar radiation) are still required by WASP as inputs for calculating reaeration and PAR. Similar to the hydrodynamic model, the meteorological inputs to WASP were provided from four weather stations as shown in Figure 3-4 and summarized in Table 3-4. Temporal variations in meteorological data for 2018 and 2019 were presented in the Hydrodynamic Model Report (DRBC, 2020, Appendix B).

Table 3-4 NOAA NADC weather stations

Count	STATION	USAF	LAT	LON	Coverage
1	TRENTON MERCER AIRPORT	724095	40.277	-74.816	RM > 108.5
2	PHILADELPHIA INTERNATIONAL AIR	724080	39.873	-75.227	79 < RM < 108.5
3	NEW CASTLE COUNTY AIRPORT	724180	39.674	-75.606	48.5 < RM < 79
4	DOVER AFB AIRPORT	724088	39.133	-75.467	RM < 48.5

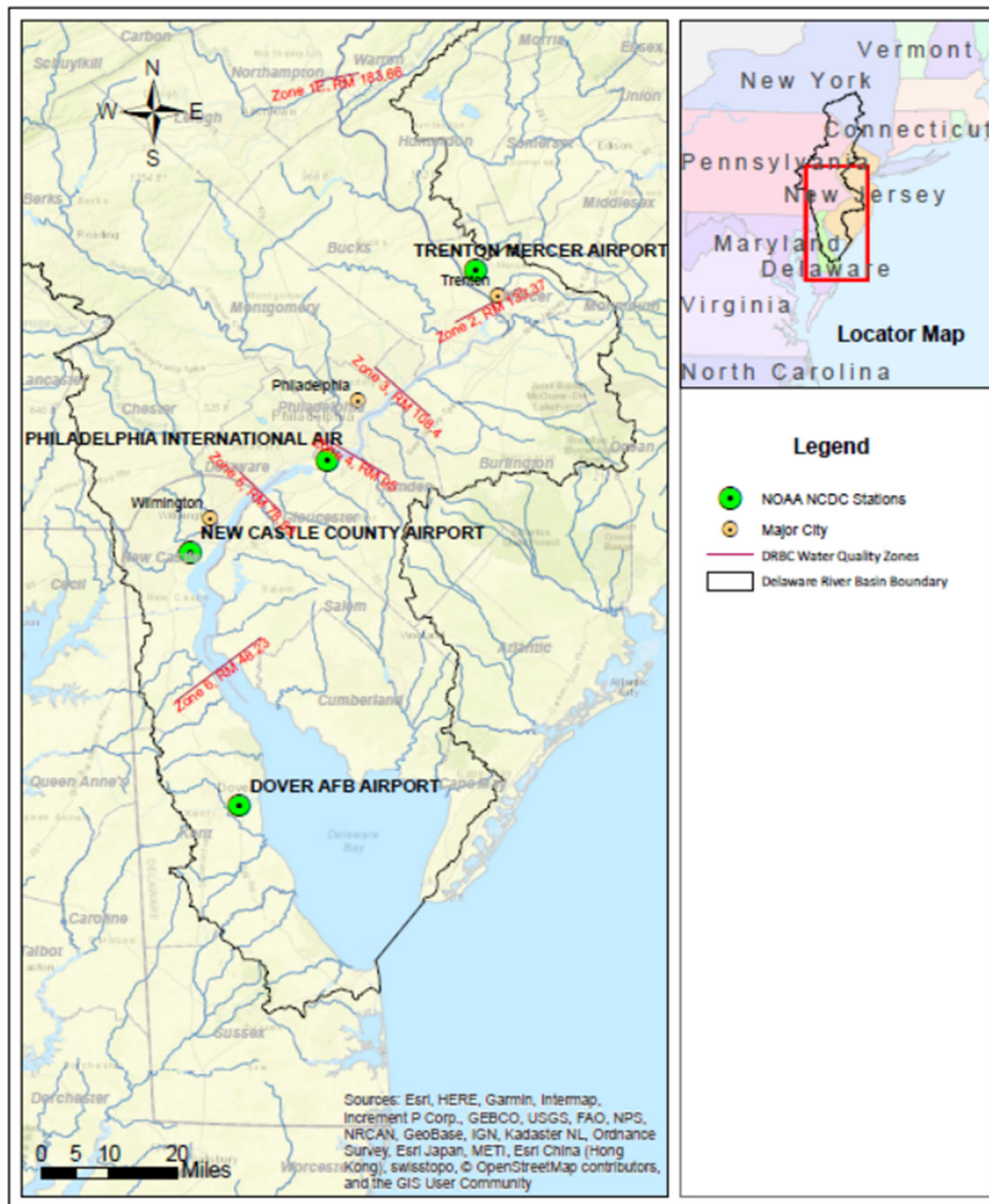


Figure 3-4: Weather stations used to characterize climatic boundaries

3.1.4.6 SEDIMENT OXYGEN DEMAND (SOD) AND BENTHIC FLUXES

SOD and nutrient fluxes from the sediment layer were prescribed as model inputs using available data, rather than employing a sediment diagenesis model (see Section 3.1.2.2). PWD, along with Woods Hole Group, The Academy of Natural Sciences of Drexel University, and Chesapeake Biogeochemical Associates, designed and conducted a field data collection program to measure SOD and benthic nutrient fluxes in RM 63–128 in the Delaware Estuary during 2012–2013 and 2016–2018 (Philadelphia Water Department, 2015 and 2022; Woods Hole Group, 2016). The data include 237 measurements of SOD and 158 measurements of benthic ammonia-nitrogen, nitrite-nitrogen + nitrate-nitrogen, and inorganic phosphate

fluxes (Figure 3-5). SOD raw data were converted to values at 20°C using a temperature correction factor of 1.065 (Chapra 1997). This same temperature correction was used in the WASP model calibration so that the temperature-normalized SOD at 20°C values were adjusted based on the EFDC-simulated water temperatures which linked to WASP. Hereafter, the SOD data and model inputs are expressed as temperature-corrected values in this report. If a location contained replicate or triplicate samples during a single survey, the average value was used in the analysis.

All benthic nutrient flux and SOD data are displayed by river mile on Figure 3-6. Comparing repeated SOD and benthic flux observations at five locations in 2012–2013 and 2016–2018, no apparent temporal trends were observed (Figure 3-7 to Figure 3-10). Box plots display the minimum (bottom whisker), 25th-percentile (bottom edge), median (middle line), 75th-percentile (upper edge), and maximum (upper whisker) value among data collected at each location. For model SOD and benthic flux input assignment, data were grouped into relatively coarse bins (Figure 3-11). First, bins were delineated centered at each Boat Run station, then adjacent bins were combined so that each bin had at least 5 unique benthic flux measurements and at least 14 unique SOD measurements. As temperature correction factors for benthic fluxes are not available in WASP, only benthic flux data collected in August were included. This is a conservative approximation, considering that August data are generally have the highest observed upward fluxes. In the lower portion of Zone-5 (RM 48–63) where no measured data are available, SOD and benthic fluxes were assigned to values from the adjacent bin (data collected from RM 63–73). In Zone-6 (RM < 48), where no data were collected, model inputs were adjusted from those at Zone-5 based on sediment organic carbon ratios. During model calibration, SOD and benthic flux inputs were adjusted within the 10th and 90th percentiles of the available data to improve model-data comparisons for water column DO and nutrient concentrations. Final model inputs are shown as blue lines in Figure 3-11 and described in Table 3-5.

Table 3-5: SOD and benthic flux model inputs from survey data

Flux	Data included	Bay / Zone-6 (RM < 48)	ETM (RM 48–73)	Urban River (RM 73–115)	Upper River (RM > 115)
NH3-N	August	25 mg N/m ² /day	Median*	50–75 th percentile*	75 th percentile*
NO3-N	August	0 mg N/m ² /day	10 th percentile*	10 th percentile*	10 th percentile*
DIP	August	6 mg P/m ² /day	Median*	25 th percentile*	Median*
SOD	All	0.75 g O ₂ /m ² /day	75 th percentile*	75–95 th percentile*	90 th percentile*

*Among measured values in each bin

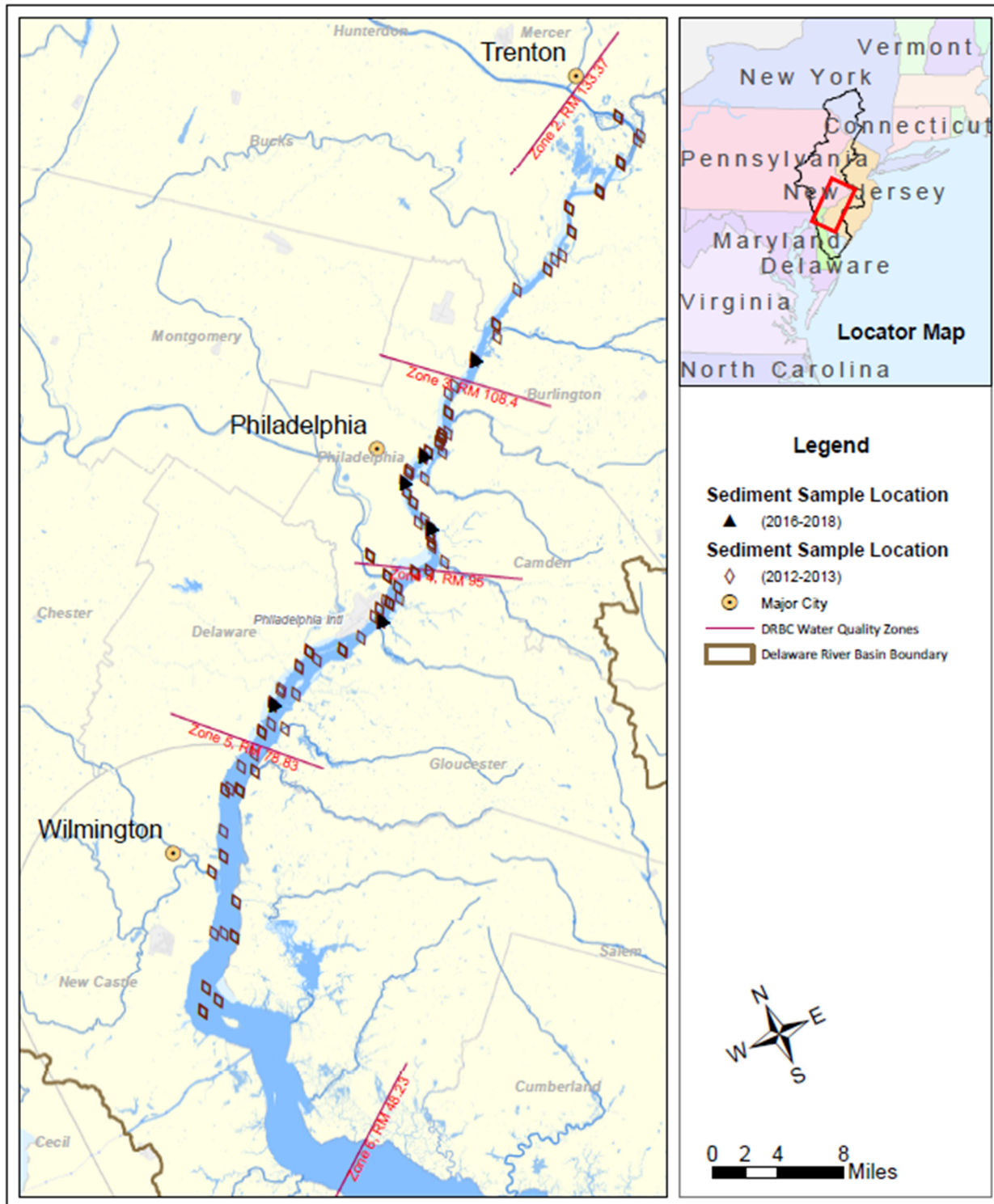


Figure 3-5: SOD and benthic flux survey locations

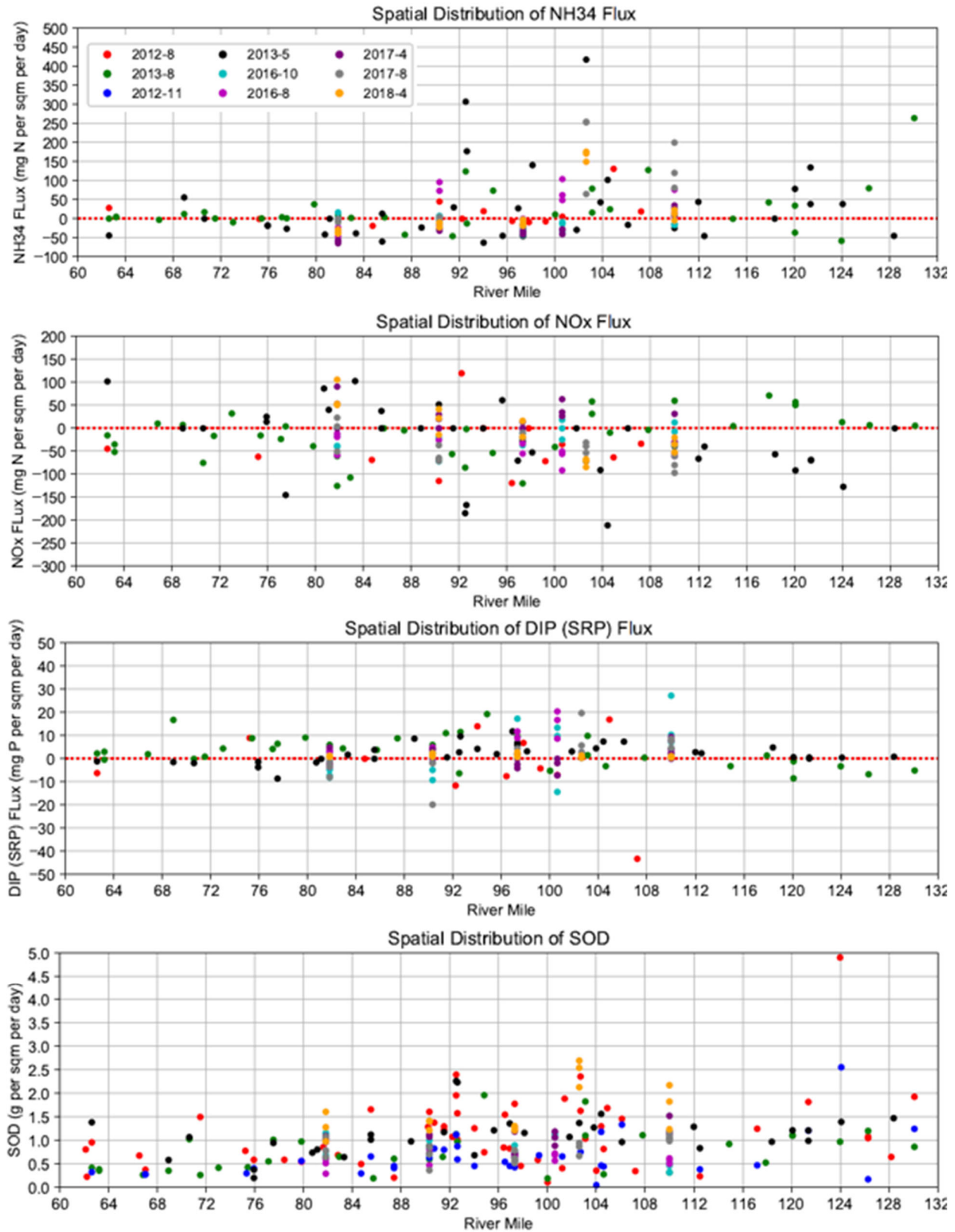


Figure 3-6: Spatial distribution of observed benthic nutrient flux and SOD

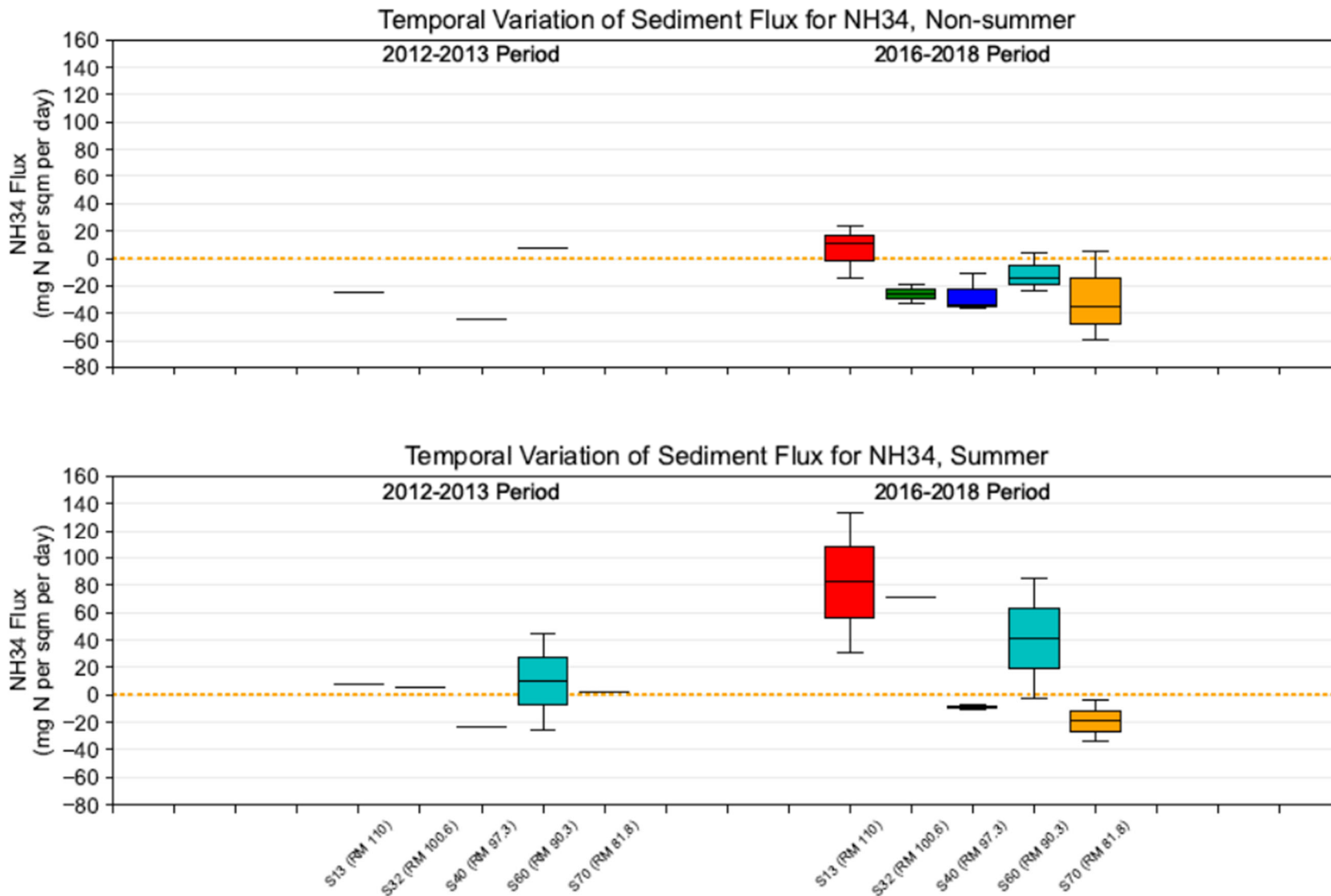


Figure 3-7: Temporal variation of sediment ammonia flux, summer vs. non-summer.

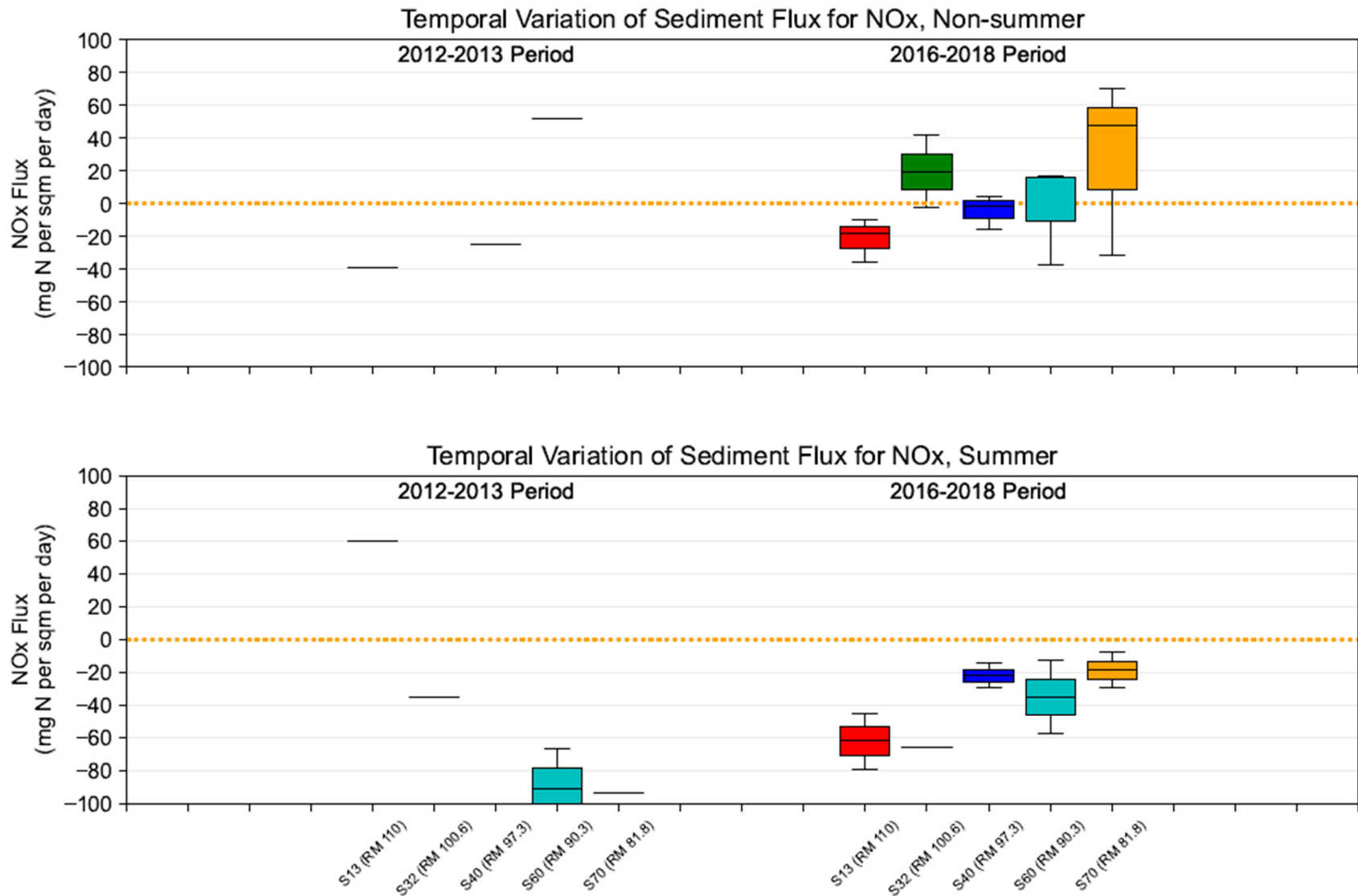


Figure 3-8: Temporal variation of sediment nitrate flux, summer vs. non-summer.

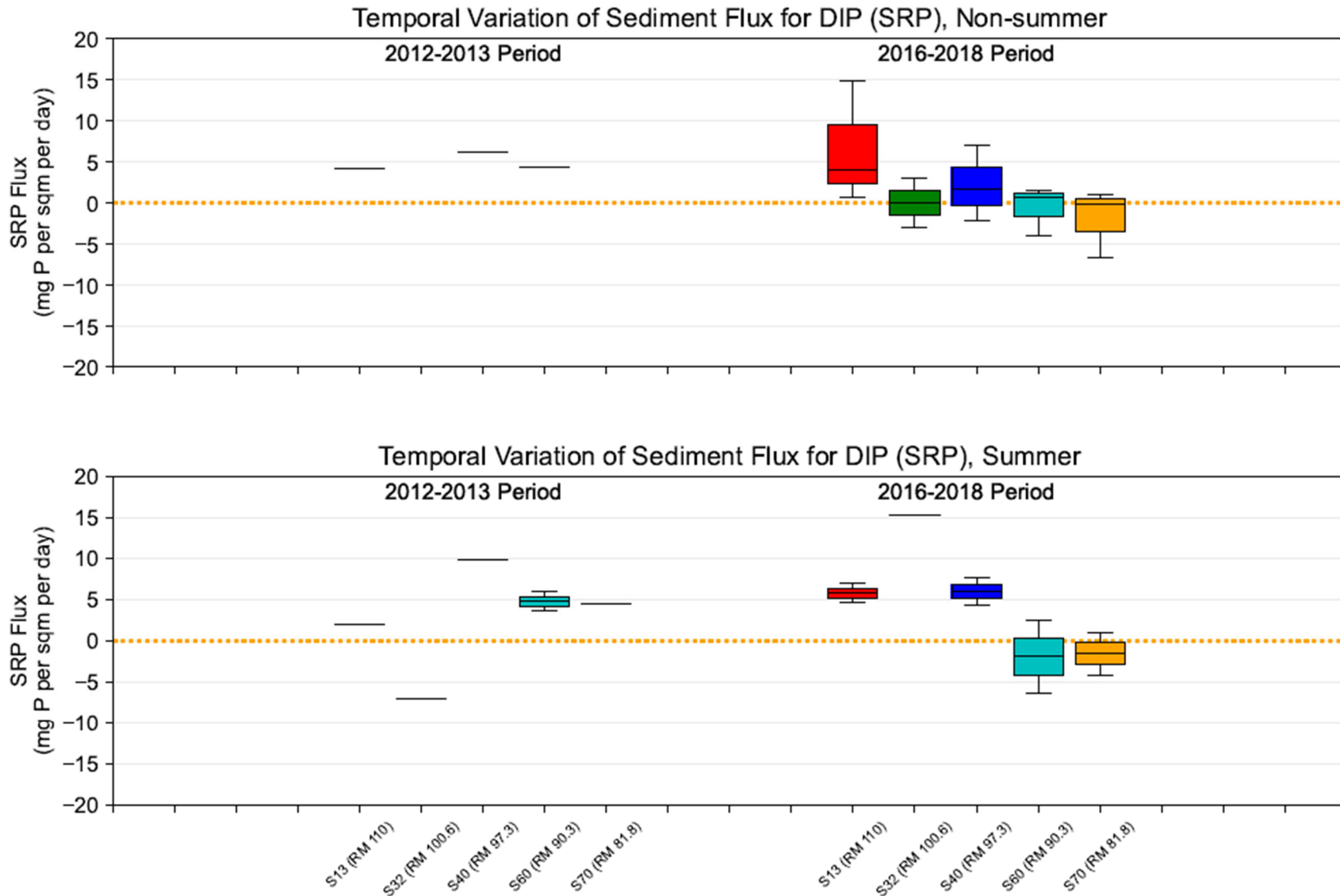


Figure 3-9: Temporal variation of sediment phosphate flux, summer vs. non-summer.

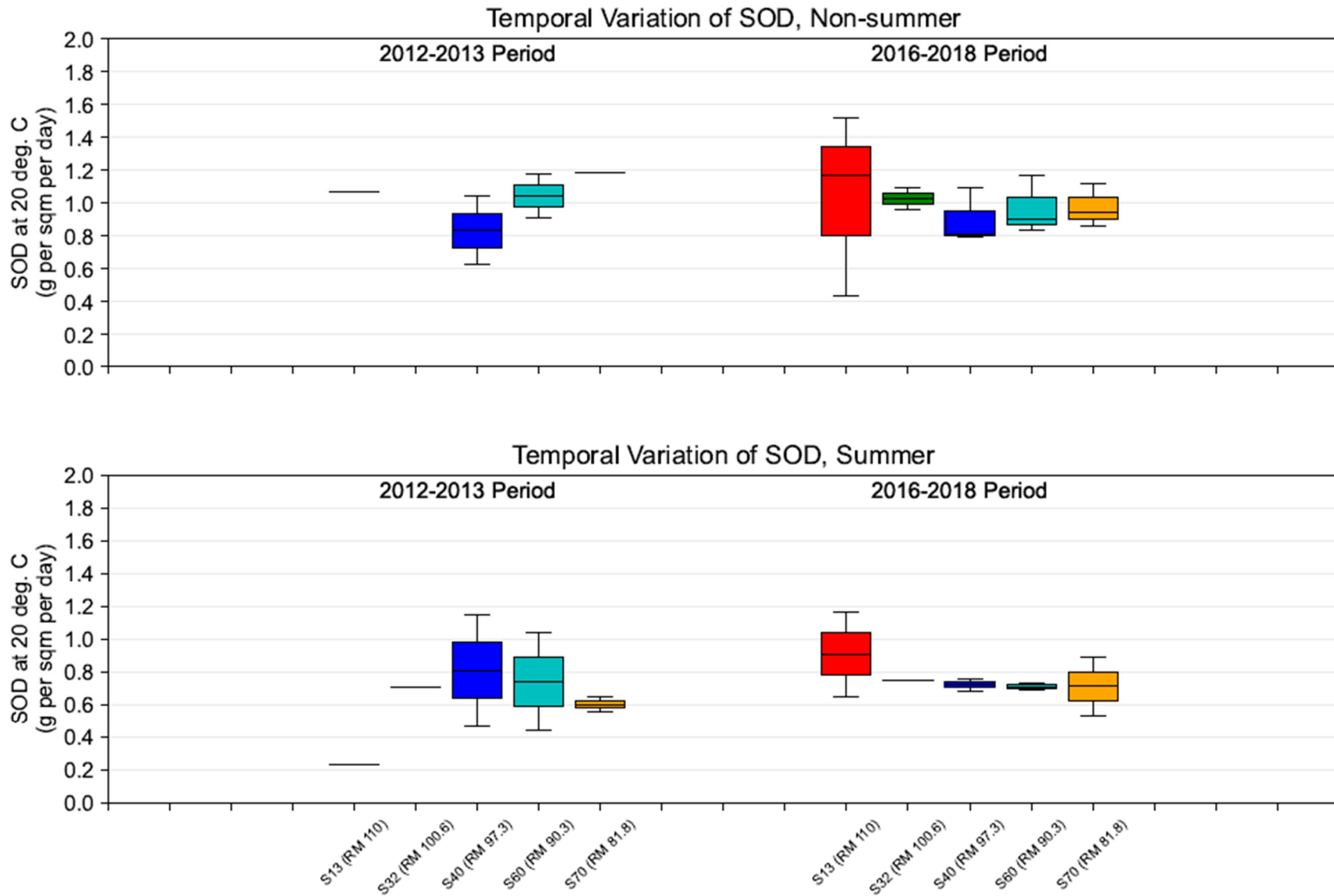


Figure 3-10: Temporal variation of SOD, summer vs. non-summer.

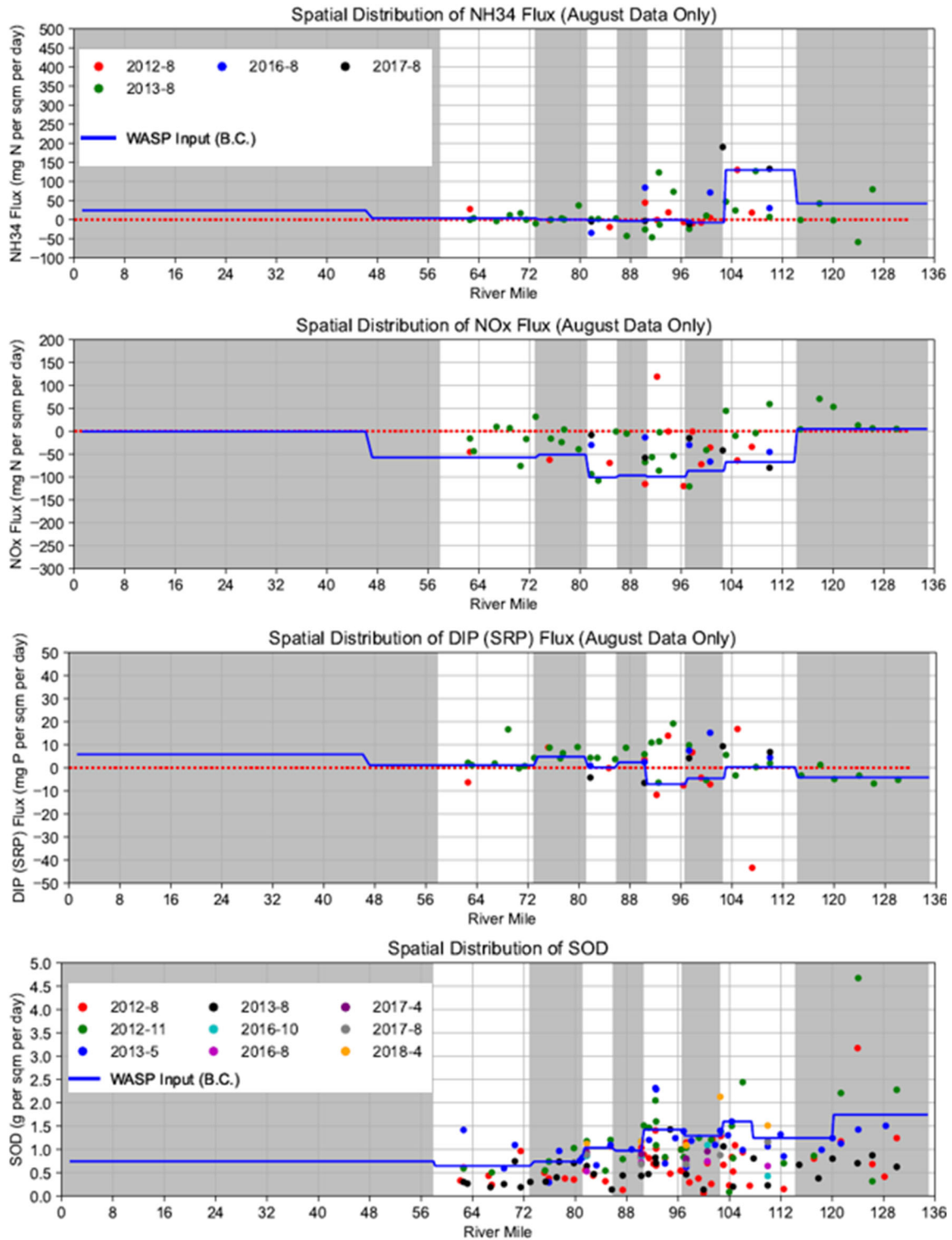


Figure 3-11: Spatial distribution of benthic flux and SOD summarized to bins

3.1.4.7 INITIAL CONDITIONS

Initial conditions or concentrations are assigned for each water-quality state variable at each model segment, including salinity, water temperature, and components of flow, which are transferred through the hydrodynamic linkage routines.

Initial conditions for each state variable were derived from data collected in the Estuary during the winter and early spring of 2012 and 2017–18; values were assigned to each model segment using a proximity analysis. To minimize initial condition effects, the model was brought to a dynamic equilibrium by determining spin-up time and constituent behavior. Model spin-up time was determined by calculating the amount of time the model needed to reach equilibrium for a conservative tracer applied at each boundary. Simulations show that spin-up time within the model domain is highly variable; at and near significant tributary inflows in the Upper Tidal River spin-up is relatively quick (2 to 4 days); downstream in the Estuary, the spin-up period increases and can range from two to ten weeks, with maxima coinciding with areas of greatest water age or residence time. Multiple, recursive 10-week runs were made with the fully loaded model for the 2018 and 2012 simulation periods, with output for each state variable subsequently reinitialized for the next run. The process was repeated until a quasi-steady state for concentrations of N, P, C, Si, and DO was achieved. The resulting state variable concentrations were then applied as initial water column conditions. For the 2019 simulation year, state variable output from the 2018 simulation was used.

3.1.4.8 HYDROLOGIC CONDITIONS

The model calibration period was established for 2018-2019 based on the intensive data collection efforts to develop model input loads and to establish model calibration targets in ambient waters for that period. Annual statistics of daily discharges over the past two decades at the two largest inflows, which contribute over 65% of freshwater inflows into the Delaware River Estuary, Delaware River at Trenton, NJ (USGS 01463500) and Schuylkill River at Philadelphia, PA (USGS 01474500), are shown in Figure 3-12 and Figure 3-13. The two-year model calibration period of 2018-2019 is relatively wet. Due to this reason, the project team determined to corroborate the model for year 2012 which has relatively lower flow conditions especially in a summer season. These flow patterns are generally consistent with the precipitation pattern shown in Figure 3-14. Details information of hydrologic conditions for 2012 and 2018-2019, such as time series of flow rates, is provided in the Hydrodynamic Model Report (DRBC, 2021).

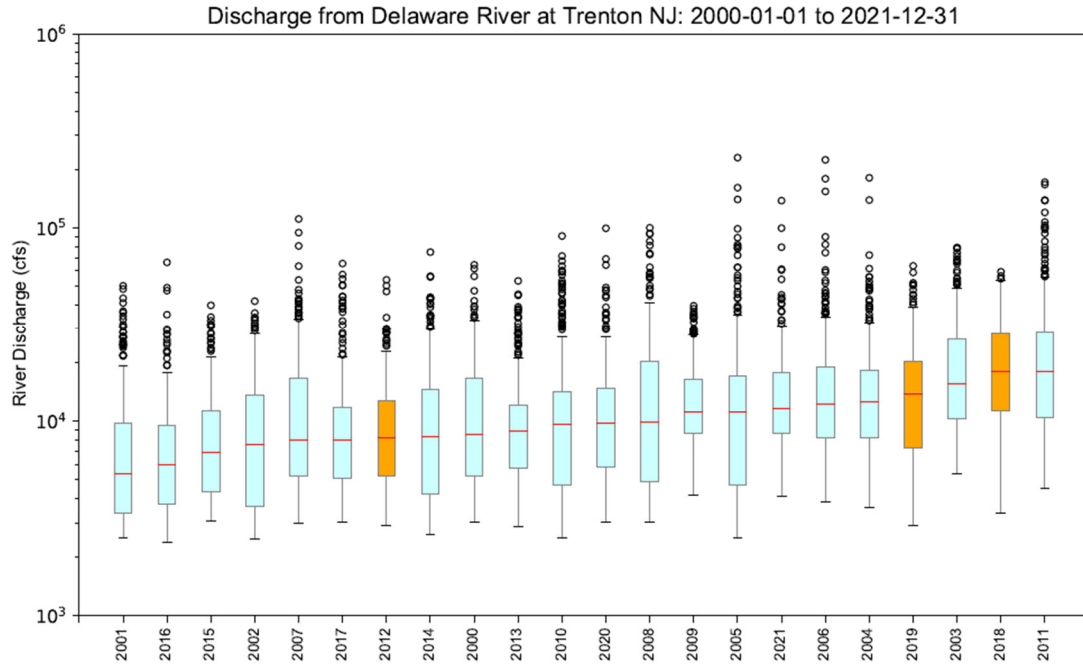


Figure 3-12 Daily flow by year at Delaware River at Trenton NJ

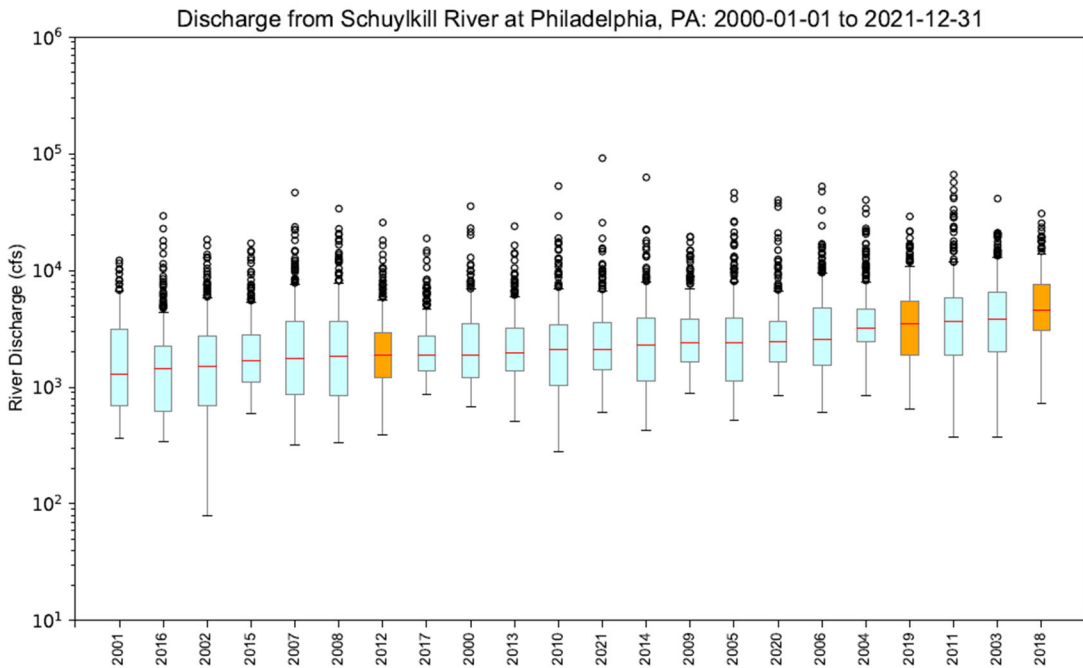


Figure 3-13: Daily flow by year at Schuylkill River at Philadelphia PA

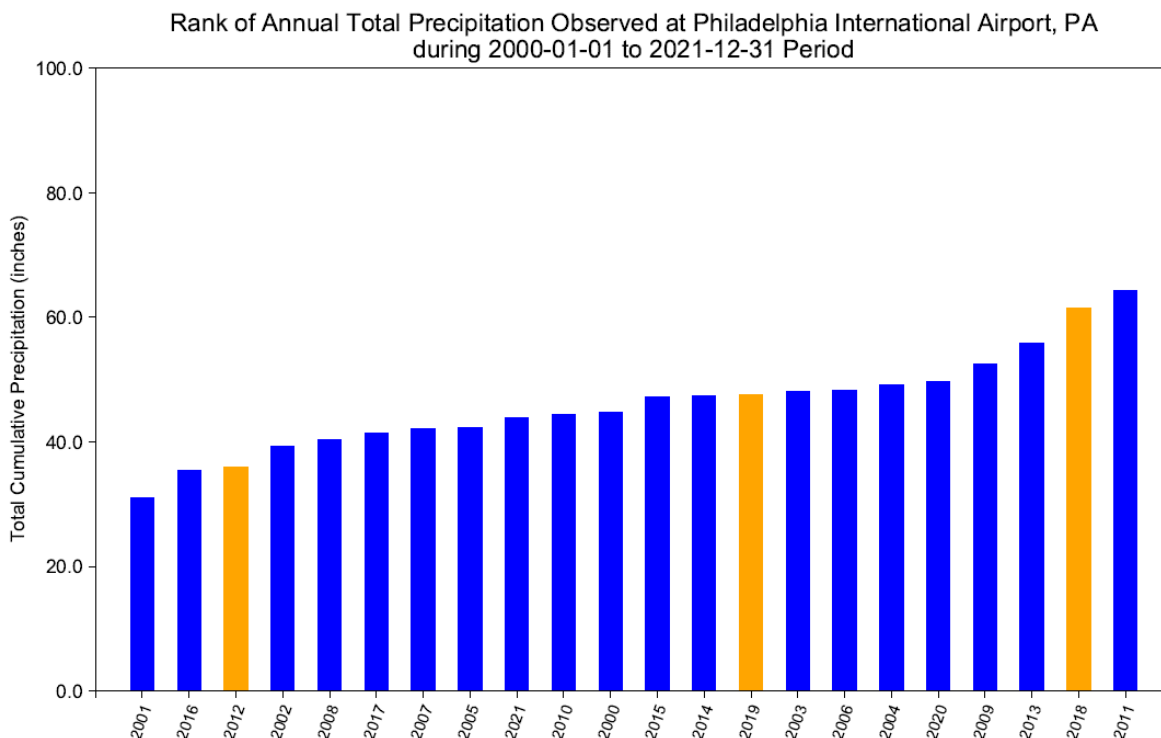


Figure 3-14: Annual Precipitation at Philadelphia

3.2 WATER QUALITY MODEL CALIBRATION

After external loads for twenty state variables and fluxes are assigned, Delaware Estuary specific physical and kinetic processes need to be identified through comparisons of the observed and the simulated results for each state variable, sensitivity simulations, previous modeling studies, and professional judgement based on current science. This process is called model calibration process. The primary focus of the model and data evaluation is the period of April through October for Zones 2 through 5 where low dissolved oxygen conditions usually occur.

The utility of the model for making realistic projections of future conditions rests on its ability to represent the physical, biochemical, and biological processes that control the dynamics of all state variables. The ability of the model to simulate these processes was assessed by evaluating the performance of the model relative to measured water quality constituents.

Model calibration was conducted for the intensive monitoring period of 2018–2019. Next, the model was corroborated for 2012 without changing coefficients. Year 2012 was selected because it was one of the “dry” summers with low DO concentrations and sufficient flow and nutrient data collected from the point source discharges. Note that lesser data was collected during 2012 as compared to 2018–2019 calibration period for setting up boundary conditions and assessing model performance.

3.2.1 CALIBRATION DATA

Model–data comparison locations are shown in Figure 3-15, which include: DRBC Boat Run sampling stations, USGS continuous *in-situ* monitoring locations, and two additional continuous *in-situ* buoys deployed by the PWD during the calibration period.

Multiple parameters collected by the DRBC Boat Run (depicted in Section 2.1.1.1) were selected to calibrate and corroborate the model, including: dissolved organic carbon (DOC), ammonia nitrogen (NH₃), nitrite and nitrate nitrogen (NO₃O₂), total nitrogen (TN), orthophosphate (D-DIP), total phosphorus (TP), chlorophyll-a (PHYTO), inorganic suspended solids (SOLID), dissolved oxygen (DISOX), and dissolved oxygen percent saturation (DOSAT). There are about 21 and 7 monitoring events for each parameter at a given station during calibration years 2018–2019 and corroboration year 2012, respectively. All data were collected at the water surface at a monthly interval.

Continuous dissolved oxygen and chlorophyll-a data collected by USGS (Section 2.1.1.2) were also used to assess model performance. These data were reported at a 15-minute interval. Chlorophyll-a data were available only at the Ben Franklin Bridge station for the calibration period 2018–2019. Dissolved oxygen observations at the Pennypack Woods station started in October 2018. USGS sondes are typically deployed at two to three feet below water surface during low tide (personal communication with USGS staff).

The buoy survey program conducted by PWD and Woods Hole Group collected continuous dissolved oxygen, chlorophyll-a, and other parameters along the Delaware Estuary (Section 2.1.1.2). These parameters were measured at about one meter below the water surface and reported at a 12-minute interval. Data from Buoys B and P (Figure 3-15) covered the model calibration period 2018–2019 and were used to help calibrate the model.

Transect profile surveys have been conducted by USGS at selected locations adjacent to USGS stations, where dissolved oxygen and other parameters were measured along the transects and at different depths. Five surveys were included during the period of model calibration and corroboration (Table 3-6). Dissolved oxygen data from these surveys were used to evaluate model performance.

Table 3-6: USGS Transect Surveys during 2012, 2018, and 2019

Date	Location	River Mile
July 24, 2019	Pennypack Woods	110.5
December 4, 2019	Ben Franklin Bridge	100.0
October 11, 2012	Ben Franklin Bridge	100.0
July 19, 2018	Delaware Memorial Bridge	68.9
June 7, 2019	Reedy Island	54.0



Figure 3-15: Calibration data locations

3.2.2 CALIBRATION APPROACH

In accordance with the established Quality Assurance Project Plan (DRBC, 2019) for this project, a “weight of evidence” approach was used in close coordination with the Expert Panel and DRBC’s modeling consultants in order to judge the acceptability of the model for its intended purpose. Model calibration was managed through the processes below:

- Initial model testing was performed to examine whether the nutrient loads into the system were specified correctly. This was accomplished by disabling off kinetics, rates, and settling velocities, but leaving all the boundary conditions, with the goal of ensuring more than sufficient predicted dissolved organic carbon, total nitrogen, and total phosphorous concentrations were present throughout the system in comparison to observations. This testing was essentially used to flag and correct possible issues with boundary mass loadings being underestimated.
- A two-dimensional (2D) depth-averaged model was used as a surrogate to guide three-dimensional (3D) calibration testing, considering: (1) The urban area of the Estuary is well-mixed, and (2) There is a significant difference in computation time between the two models, i.e., 1.5-hr per simulation year for the 2D model, compared to 32-hr per simulation year for the 3D model.
- A series of upfront sensitivity analyses were conducted with the 2D model to test the response of key parameters and processes and to identify the calibration parameters to which the model responses would be most sensitive.
- Iterative processes with incremental calibration of rate constants were carried out, starting with preliminary calibration of dissolved organic carbon, nitrogen, phosphorus, and dissolved oxygen without phytoplankton, next incorporating phytoplankton, and then introducing spatial variation of sediment oxygen demand and benthic fluxes.
- Dissolved oxygen component analyses were used to understand the model behavior and identify the relative importance of dissolved oxygen-impacting processes over space and time within the entire estuary.
- Phytoplankton outputs were grouped to the growth seasons of the three modeled algal communities and compared with *in-situ* data and long-term trends.
- Model–data comparisons were comprehensively evaluated, including: (1) Spatial and longitudinal plots for individual Boat Run sampling events; (2) Time series plots, 1-to-1 plots, cumulative frequency distributions, target diagrams, and statistical metrics for individual stations; and (3) Lateral and vertical profiles of dissolved oxygen for individual surveys. The judgment of model calibration fit used both qualitative and quantitative methods.
- Model parameters were adjusted based on site-specific field and laboratory data, published literature, results from model applications to other similar sites, and guidance from the Model Expert Panel, based on their many decades of collective experience with water quality model development and application. Thus, the final set of model parameters resulted in a model that is consistent with scientific understanding of the underlying processes, field and laboratory studies of these processes, and the particular conditions of Delaware Estuary.

3.2.3 CALIBRATION PARAMETERS

Values for model physical and kinetic processes were adjusted within logical ranges to improve the ability of the model to match the calibration data. A complete description of the model parameters and their final calibration values are listed in Appendix F. Key parameters are shown in Table 3-7.

Table 3-7: Key calibration parameters

Parameter	Value
Nitrification Rate Constant @20°C (1/day)	0.6
Nitrification Temperature Coefficient (dimensionless)	1.1
CBOD Decay Rate Constant @20°C (1/day)*	0.033 / 0.087 / 0.001
CBOD Decay Rate Temperature Correction Coefficient (dimensionless)*	1.065 / 1.065 / 1.065
Phytoplankton Maximum Growth Rate Constant @20°C (1/day)**	4 / 3.75 / 4
Phytoplankton Carbon to Chlorophyll Ratio (mg C/mg Chl)**	40 / 30 / 40
Phytoplankton Respiration Rate Constant @20°C (1/day)**	0.03 / 0.05 / 0.03
Phytoplankton Death Rate Constant (Non-Zoo Predation) (1/day)**	0.02 / 0.08 / 0.05
Phytoplankton Settling Velocity (m/day)**	0.1 / 0.1 / 0.2
POM Settling Velocity (m/day)	0.2
Solid Settling Velocity (m/day)	1
SOD and Benthic Fluxes of Ammonia and Phosphate	Spatially variable (see Table 3-5)

* Three types of CBODU (stream/ point source/ refractory) are simulated

** Three classes of phytoplankton assemblages (spring marine/ summer freshwater/ summer marine diatom community) were calibrated independently

3.2.4 CALIBRATION RESULTS

Overall model performance should be evaluated both qualitatively and quantitatively, and that model acceptance is a decision that involves evaluating both approaches. For efficient post-processing, model results were extracted every two hours and compared to observational data (resampled to a two-hour interval to match model output. Longer intervals (e.g., daily or seasonal) were used when comparing phytoplankton concentrations, given the associated uncertainty (e.g., transient light attenuation and water clarity).

3.2.4.1 COMPARISONS TO DRBC BOAT RUN DATA

Model computed results at the surface layer of Boat Run stations were extracted and compared to the observed Boat Run data. Spatial and temporal comparisons for key state variables are presented in this Section.

For spatial comparisons, each Boat Run event for the summer months (i.e., June to August) for the calibration years 2018–2019 and corroboration year 2012 are graphically presented. The complete set of comparisons for the three-year period are available in Appendix F. Each panel in the plots represents a single survey event, with the observed Boat Run data displayed as red solid circles, and the computed daily ranges and medians on the survey dates shown as shaded-areas and dashed lines, respectively. The spatial plot provides a snap-shot of spatial comparison of the interested state variable. Overall, the absolute magnitudes and spatial patterns of the state variables/parameters are reproduced reasonably well by the model.

Model computed results were also compared to the observed Boat Run data at a fixed station for two-year calibration period for the listed variable. Considering the large number of plots (22 stations for 20 state variables) that can be generated in this format, one station (RM 93.2) around The Navy Yard station is selected because the dissolved oxygen sag is usually located around this station. Three additional stations (RM 100.2, RM 87.9, and RM 78.1) within the urban area of the Delaware Estuary are presented in Appendix F. The top left panel illustrates time series of model predictions with the observed data overlaid as individual points. The top right panel displays scatter plots (also known as 1-to-1 plots) comparing the paired model predictions and observed data points with a best-fitting linear regression line (dashed red line) and 1:1 line (blue line). In an ideal perfect match between model and data, all points lay on the 45° 1:1 line and the red dashed line overlays with the blue line. The bottom left panel shows the cumulative frequency distribution curves for the paired model predictions (black line) and observed data (red line). A cumulative frequency distribution reveals how good the model predictions are compared with data at the low end, mid-range, and high end, respectively. The bottom right panel reports several common summary and goodness of fit statistics, as well as maps showing the station locations. Overall, the absolute magnitudes of the state variables/parameters, their seasonal patterns, and their cumulative frequency distributions are adequately reproduced by the model.

A series of statistical metrics summarized by USEPA Region 4 (Davis, 2019, Appendix B) are applied to provide statistical assessment in this study. An overview of selected metrics is provided below. See Appendix F for additional details on the interpretation of all the statistical metrics.

- Coefficient of determination (R^2) – Assesses the strength of the linear relationship between observed and simulated data. Describes the proportion of variation in the observed data that is explained by a simple linear regression relating observed and simulated data. Values of R^2 range from 0 to 1, with better fitting models possessing higher R^2 values.

$$R^2 = \left[\frac{\sum_{i=1}^N (O_i - \bar{O})(P_i - \bar{P})}{\sqrt{\sum_{i=1}^N (O_i - \bar{O})^2} \times \sqrt{\sum_{i=1}^N (P_i - \bar{P})^2}} \right]^2 \quad (3-48)$$

where O and P represent “Observation” (i.e., data) and “Predicted”, respectively.

- **Nash–Sutcliffe Coefficient (NSE)** – This metric is closely related to mean square error and root mean square error. Using the mean of the observed data as a baseline, it assesses the magnitude of the difference in observed and simulated data relative to residual variance (i.e., natural variation) of observed data. This unitless metric indicates how well the linear fit of observed versus simulated data fits a 1:1 line. Values range from -Infinity to 1, whereby $NSE = 1$ represents a perfect match of simulated and observed data, $NSE = 0$ indicates that model predictions are as accurate as the mean of observed data, while $NSE = -\text{Infinity}$ indicates that the mean of observed values is a better predictor than simulated data.

$$NSE = 1 - \frac{\sum_{i=1}^N (S_i - O_i)^2}{\sum_{i=1}^N (O_i - \bar{O})^2} \quad (3-49)$$

- **Root Mean Square Error (RMSE)** – Measures the difference (i.e., error) between observed and simulated data. This metric provides assurance that the model is matching the frequency, magnitude, and duration of water quality changes. However, it does not account for natural variability in observed data. Values of RMSE range from 0 to infinity, with $RMSE = 0$ indicating a perfect match between observed and simulated data.

$$RMSE = \sqrt{\frac{1}{N} \sum_{i=1}^N (S_i - O_i)^2} \quad (3-50)$$

- **Index of Agreement, or Skill Factor (d)** – Provides a measure of model error relative to natural variability (i.e., error). Values range from 0 to 1, with an index of agreement = 1 indicating a perfect fit of simulated and observed data, and a value of 0 indicating no agreement between them.

$$d = 1 - \frac{\sum_{i=1}^N (S_i - O_i)^2}{\sum_{i=1}^N (|S_i - \bar{O}| + |O_i - \bar{O}|)^2} \quad (3-51)$$

Table 3-8: Average statistical metrics at 22 Boat Run Stations, 2018–2019 lists the average values of statistical metrics over all 22 Boat Run stations for each parameter during the calibration period 2018–2019. The complete statistical metrics for all parameters at each Boat Run station are available in Appendix F.

Table 3-8: Average statistical metrics at 22 Boat Run Stations, 2018–2019

Metric	D-DIP	DISOX	DOC	DOSAT	NH-34	NO3O2	PHYTO	TN	TP
Number Observation	21	21	21	21	21	21	21	21	21
Observed Mean	0.04	8.97	3.03	91.47	0.11	1.19	10.46	1.60	0.09
Observed Variance	0.00	4.71	0.44	68.84	0.01	0.18	114.59	0.16	0.00
Simulation Mean	0.05	8.89	3.00	89.23	0.06	1.22	6.79	1.71	0.09
Simulation Variance	0.00	5.15	0.36	79.35	0.00	0.12	38.04	0.14	0.00
Mean Error	0.01	-0.08	-0.03	-2.23	-0.04	0.03	-3.67	0.11	0.00
Mean Absolute Error	0.01	0.45	0.36	4.88	0.06	0.17	6.34	0.21	0.02
RMSE	0.02	0.57	0.49	6.16	0.08	0.24	9.76	0.26	0.03
NRMSE %	26.30	8.65	23.39	23.18	26.61	16.98	27.89	19.50	26.25
R2	0.59	0.94	0.47	0.60	0.56	0.63	0.21	0.64	0.35
Spearman Coeff.	0.74	0.95	0.63	0.69	0.57	0.77	0.58	0.77	0.48
PBias	12.27	-0.92	-1.35	-2.53	-45.00	2.93	-35.65	7.17	1.70
Nash	0.14	0.91	0.11	0.11	0.05	0.56	-0.25	0.43	-0.02
Index of Agreement	0.81	0.98	0.76	0.81	0.68	0.85	0.59	0.85	0.68
Kling-Gupta Effic. Modified	0.64	0.90	0.60	0.63	0.27	0.67	0.22	0.72	0.40
Kling-Gupta Pear. Coeff.	0.76	0.97	0.65	0.73	0.66	0.77	0.42	0.79	0.49
Kling-Gupta Beta (Ratio Means)	1.12	0.99	0.99	0.97	0.55	1.03	0.64	1.07	1.02
Kling-Gupta Gamma (Ratio CV)	0.96	1.06	0.99	1.13	0.99	0.83	0.99	0.89	0.82

These statistical metrics were computed for all paired model-data values at the Boat Run survey stations. The values of statistical metrics varied noticeably in locations, state variables/parameters, and metric themselves. Of all state variables/parameters, dissolved oxygen has the highest values of R^2 (0.94), Nash-Sutcliffe Coefficient (0.91), and index of agreement (0.98). The value of 1 in these metrics indicates a perfect fit of model predictions and observed data (Davis, 2019, Appendix B). On the other end, phytoplankton has the lowest values of R^2 (0.21), Nash-Sutcliffe Coefficient (-0.25), and index of agreement (0.59). Note that a value of 0 in the Nash-Sutcliffe Coefficient indicates that model predictions are as accurate as the mean of observed data, and a value of 0 in the index of agreement indicates no agreement between predictions and observations (Davis, 2019, Appendix B). Chlorophyll-a levels in the Estuary are highly variable in general as phytoplankton populations respond to light, nutrient, water temperature, and hydrodynamic flow patterns. Further investigation on phytoplankton dynamics and growth limitations are discussed in the next section. For the dissolved organic carbon (DOC), nitrogen (NH-34, NO₃O₂, and TN), and phosphorus (D-DIP and TP), R^2 ranges from 0.35 to 0.64; Nash-Sutcliffe Coefficient ranges from -0.02 to 0.56; and index of agreement ranges from 0.68 to 0.85 indicating reasonably good agreement between the predicted and the observed. In a tidal environment, model predictions lead or lag by a relatively short time (e.g., a few hours), the resulting values of R^2 , Nash-Sutcliffe Coefficient, and index of agreement can be highly affected. Moreover, the model reasonably well captures the absolute concentrations, as well as the spatial and temporal trends of these state variables/parameters indicating that the model adequately reflects inter-annual changes of C/N/P in the system.

In the following section, spatial and temporal, graphical comparisons between the computed and the observed are presented by key state variables, DOC, NH₃4, NO₂3, TN, D-DIP, TP, solids, phytoplankton, DISOX, and DOSAT together with brief descriptions of key calibration processes.

3.2.4.1.1 Dissolved Organic Carbon (DOC)

- Calibration approach: WASP model employed CBOD as a state variable and DOC is computed internally. Three types of CBODs are simulated and assignment of CBOD decay rates were guided based on a 90-day BOD experiment. Temperature correction coefficients for CBOD decay rates were fine-tuned to get optimum agreement between predictions and observations for dissolved organic carbon.
- Spatial plots for individual sampling events: DOC predicted by the model matched the data reasonably well, both in absolute concentrations and spatial patterns, e.g., relatively high levels in the tidal river and relatively low levels in the Bay.
- Temporal plots for individual Boat Run location: The model tended to slightly over-estimated DOC concentrations at Navy Yard. One exception was the survey during August 2019 when the computed result (about 2.6 mg/L) was substantially below observation (about 9 mg/L).

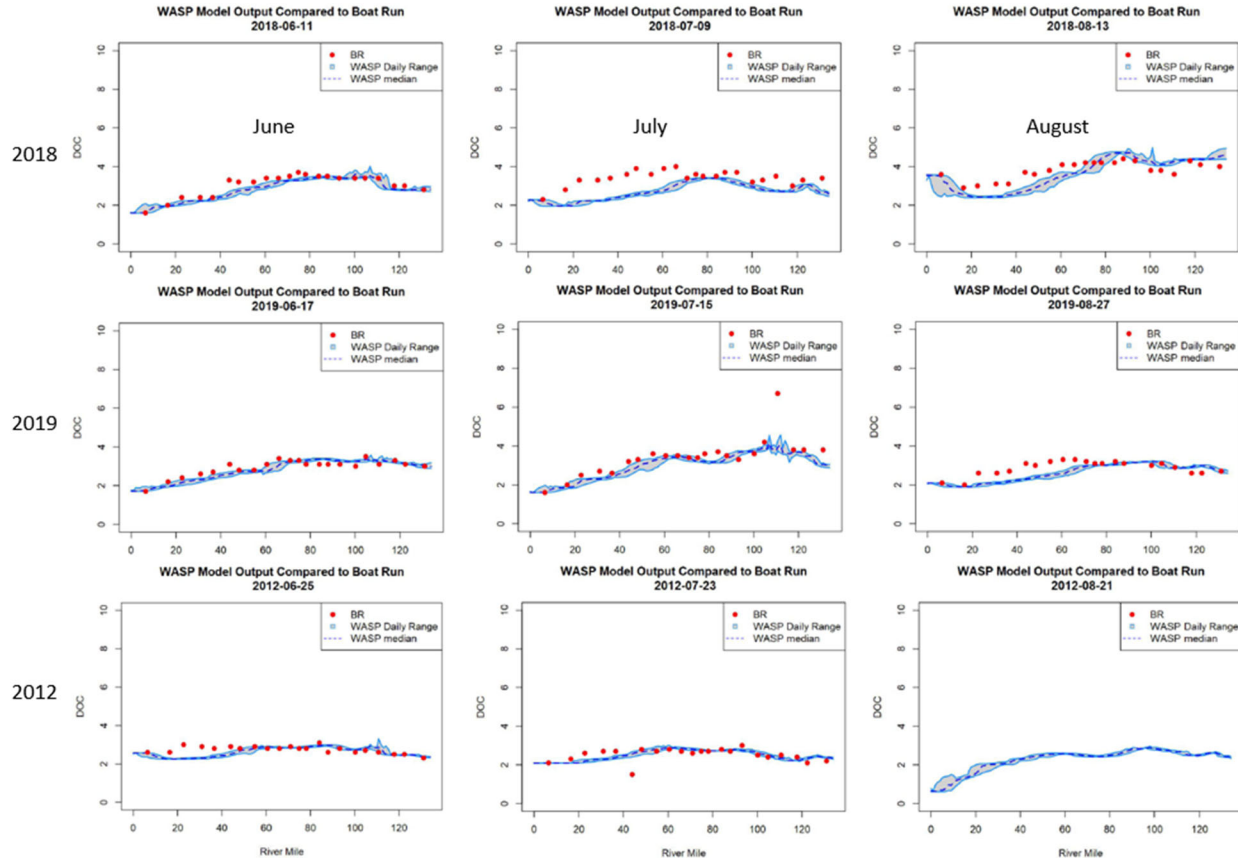


Figure 3-16: Model to Boat Run data comparisons – DOC during summer

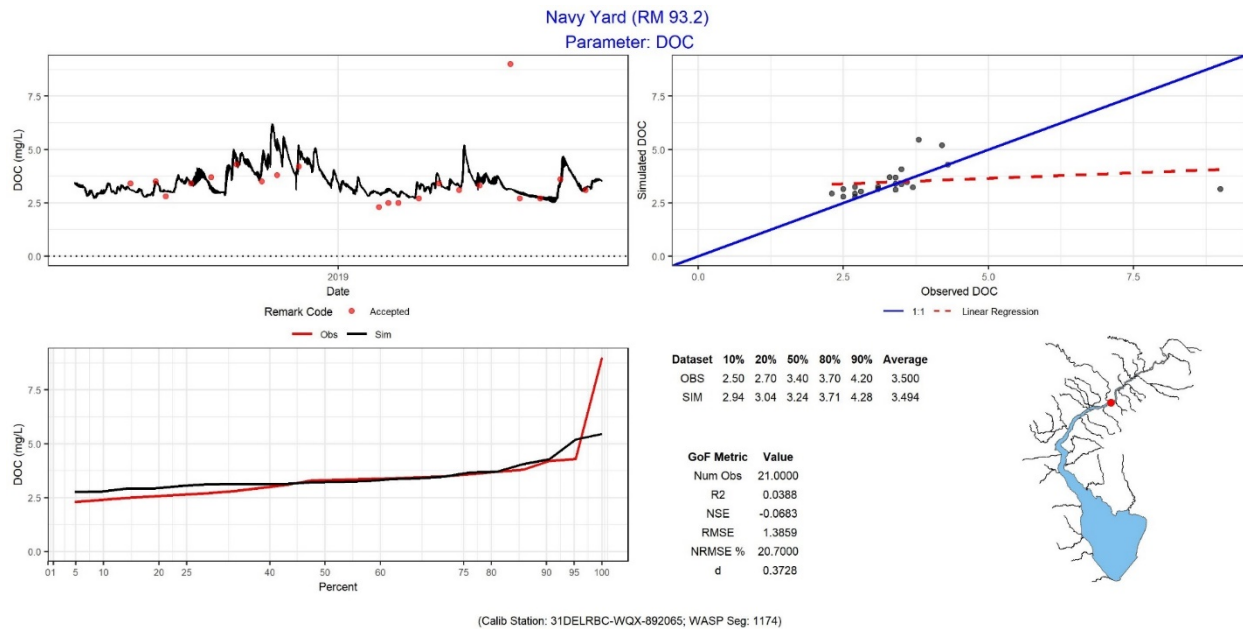


Figure 3-17: Model to Boat Run data comparison – DOC at Navy Yard, 2018–2019

3.2.4.1.2 Nitrogen ((NH₃, NO₃O₂, and TN)

- Calibration Approach: The nitrification rate together with temperature correction factor was determined within a range of uncertainty to match observed ammonium and nitrite + nitrate levels for entire model domain and throughout the season.
- Spatial plots for individual sampling events: The simulated NH-34 concentrations compared generally well with the data during summer. The observed and computed concentrations of NH-34 were elevated in the urban area (e.g., RM 80–110). A single nitrification rate with water temperature correction, rather than spatial variation of reaction rates, was employed in WASP. As a result, the model might over-predict the nitrification process around RM 20–80 during spring (see relevant figures in Appendix F). The model was able to capture the absolute concentrations and spatial patterns of NO₃O₂ and TN during multiple surveys across three years, except for the June 2018 event. Both model and data demonstrated that the peak concentrations of NO₃O₂ and TN were in the urban area around RM 70–110. The model slightly over-predicted the TN concentrations in mid-section of the estuary in 2012. The uncertainty in loading assignment for 2012 seemed to be a major contributor.
- Temporal plots for individual Boat Run location: The observed and computed NH-34 concentrations and seasonal patterns were similar, elevated in spring and winter and declined in summer due to the temperature impact on nitrification rate. The model prediction did not go as high as the data at the high end of NH-34 concentration, perhaps due to a single nitrification rate employed in WASP or/and an inexact representation of temperature effects on nitrification. In general, the model reproduced the NO₃O₂ and TN concentrations, seasonal patterns, and cumulative frequency distributions quite well. Both observed and computed concentrations reach peak values in summer or early fall.

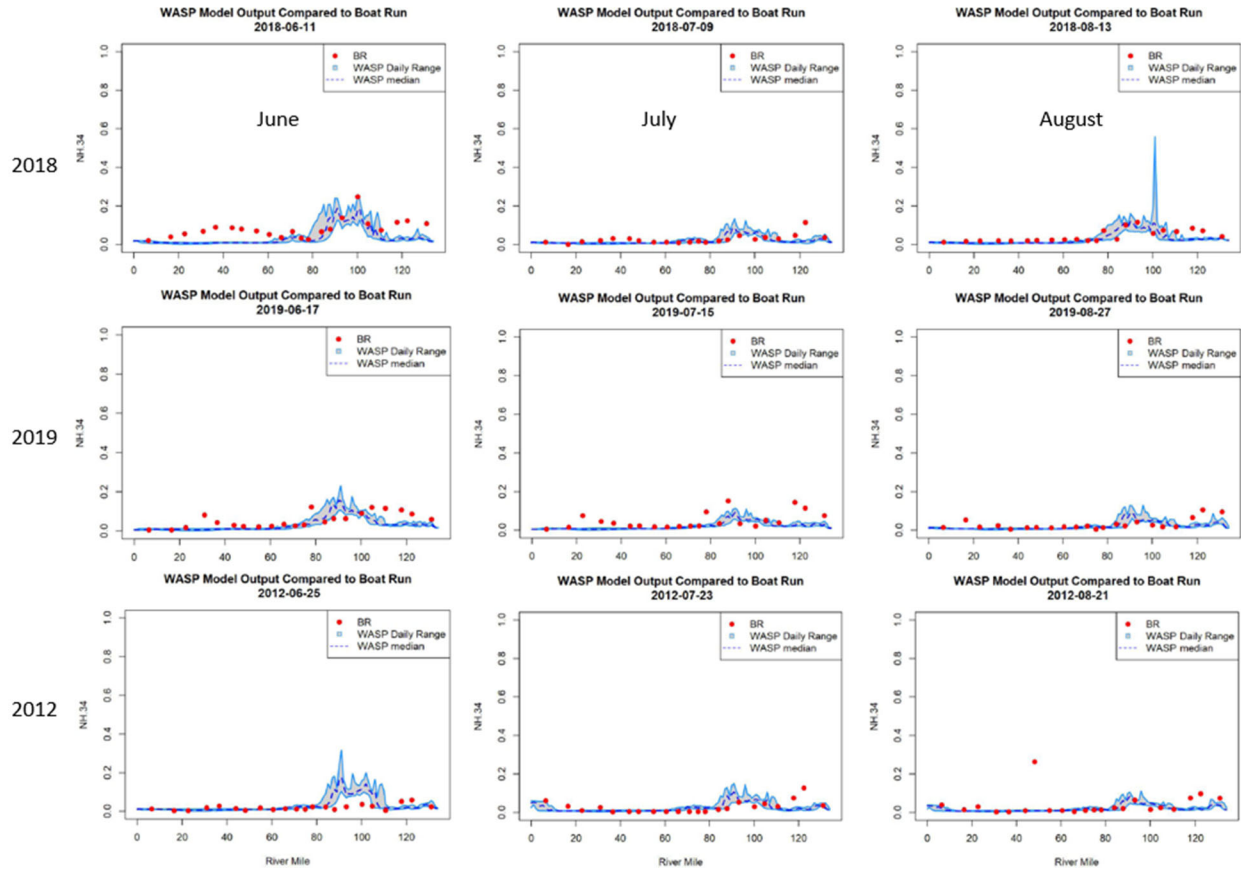


Figure 3-18: Model to Boat Run data comparisons – ammonia during summer

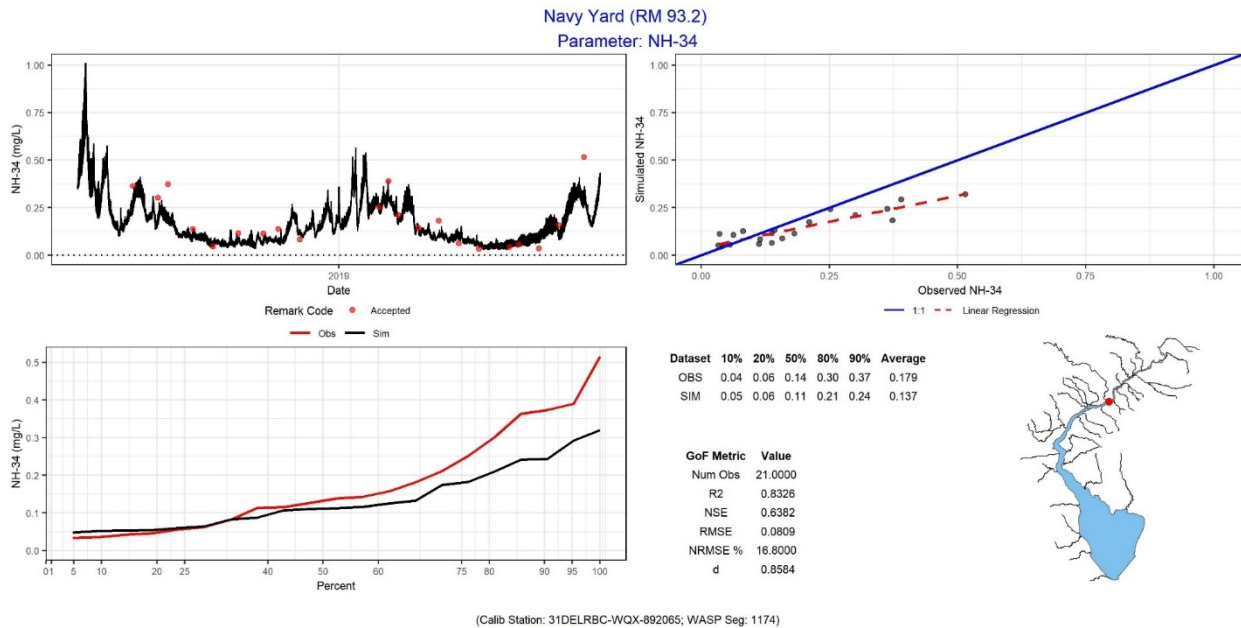


Figure 3-19: Model to Boat Run data comparison – ammonia at Navy Yard, 2018–2019

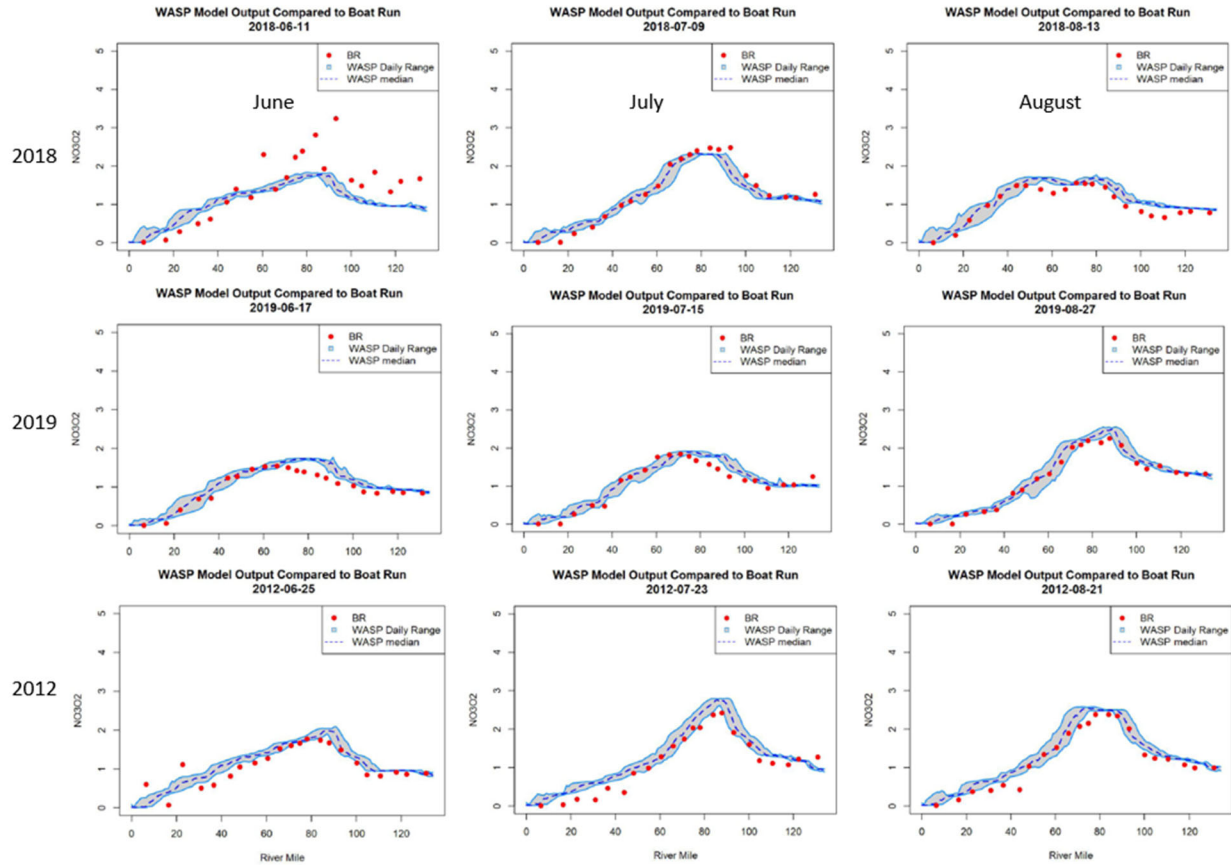


Figure 3-20: Model to Boat Run data comparisons – nitrate during summer

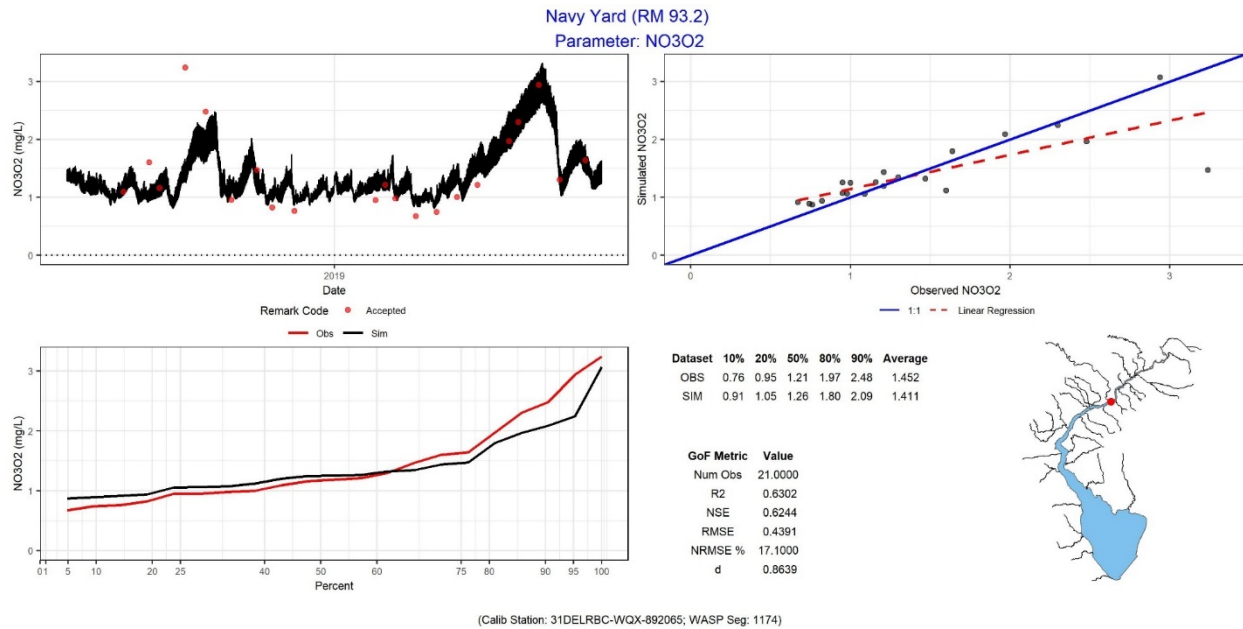


Figure 3-21: Model to Boat Run data comparison – nitrate at Navy Yard, 2018–2019

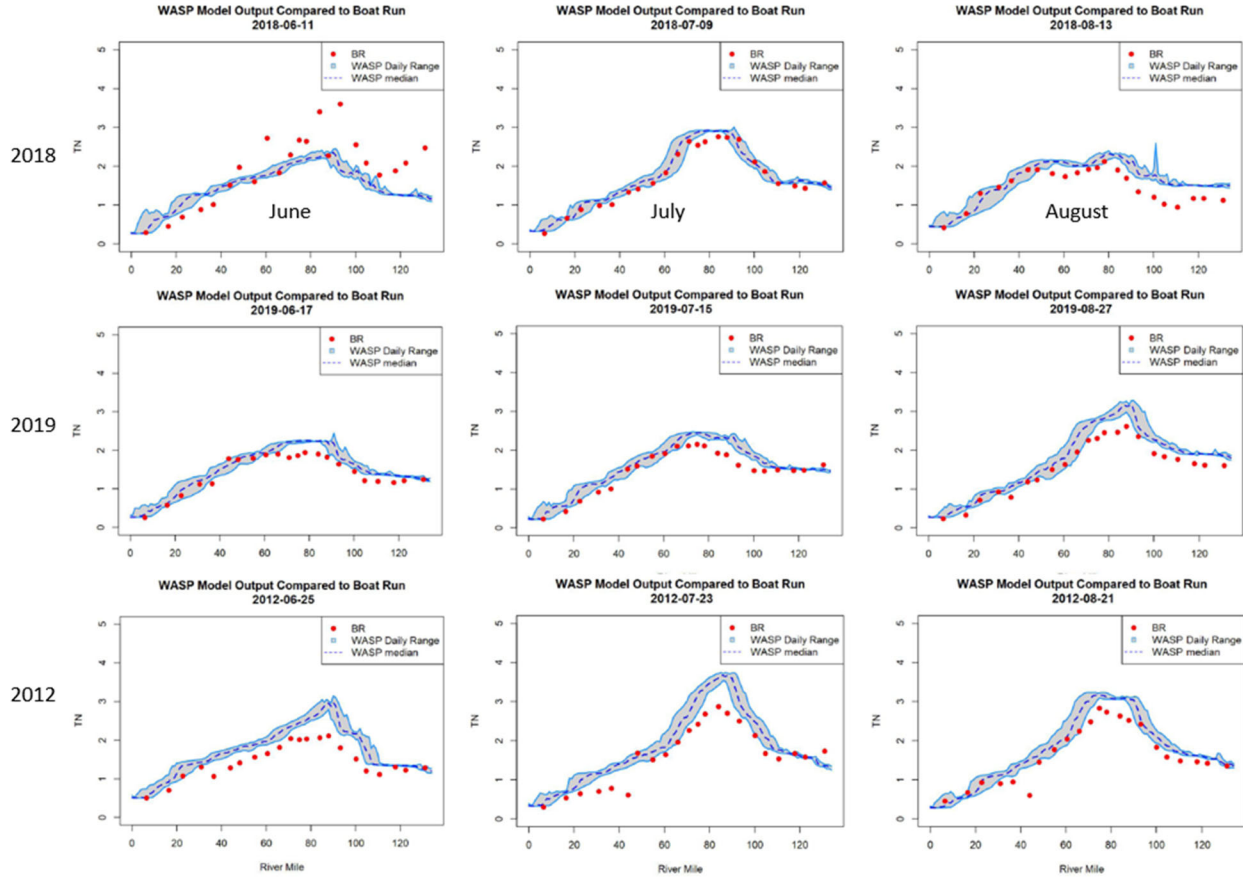


Figure 3-22: Model to Boat Run data comparisons – TN during summer

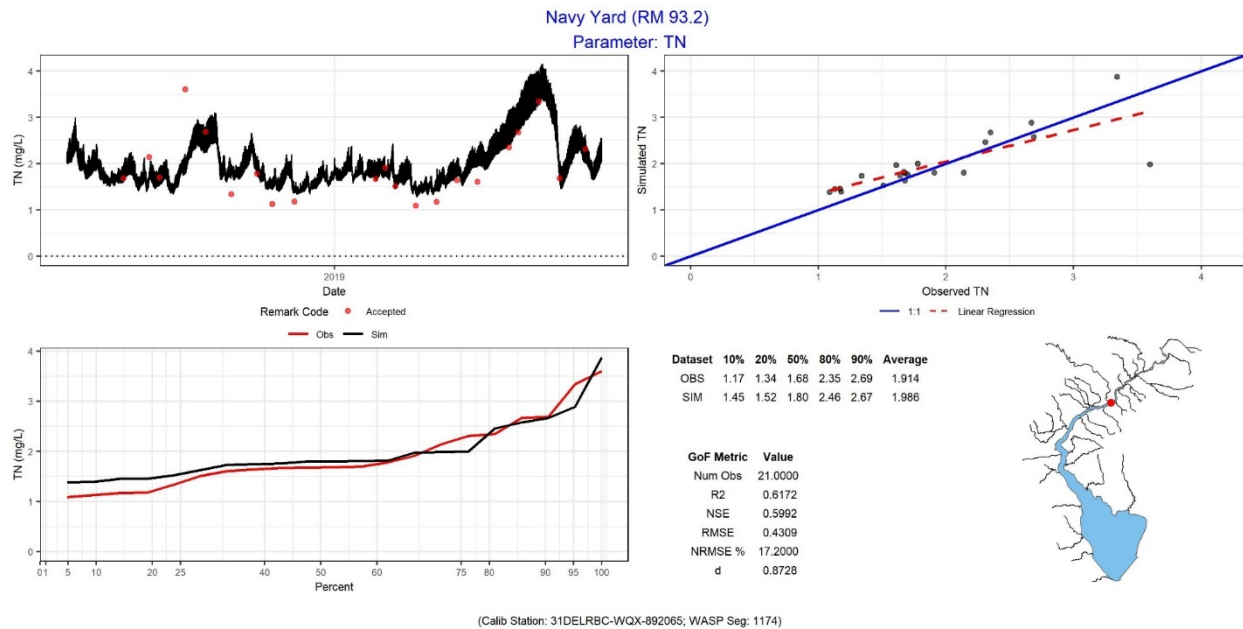


Figure 3-23: Model to Boat Run data comparison – TN at Navy Yard, 2018–2019

3.2.4.1.3 Phosphorus (D-DIP and TP)

- Calibration approach: The partition coefficient of phosphate to water column solid, settling speeds of solid, uptake by phytoplankton, and its death are all contribute to phosphorus dynamics. Phosphate fluxes from the sediment layer were also assigned as described in Table 3-5.
- Spatial plots for individual sampling events: The observed and computed concentrations of D-DIP were elevated in the tidal river. The model simulation over-estimated the peak concentrations of D-DIP in the urban area during some summer surveys but showed a better match for the spring and winter seasons (see relevant figures in Appendix F). D-DIP is more readily sorbed to solid particles compared to nitrogen and fully functional sediment transport model is not included in this study. This could in part cause some mismatch between predictions and observations. Furthermore, this mismatch is not critical to the overall model simulation because algae growth in the Delaware Estuary is not phosphorus limited (see Section 3.2.5.2). The concentrations and spatial patterns of TP were reproduced by the model reasonably well for most of the surveys, indicating phosphorous loads into the system were reasonably accounted for. Both the observed and computed concentrations of TP were elevated at the urban area around RM 60-110.
- Temporal plots for individual Boat Run location: The concentrations, seasonal patterns, and cumulative frequency distributions of D-DIP and TP were reproduced by the model reasonably well. Both observed and computed D-DIP and TP concentrations were elevated in the summer and early fall. D-DIP concentration is over-estimated at the high end, perhaps due to the sorption process not being captured adequately as discussed in the previous section.

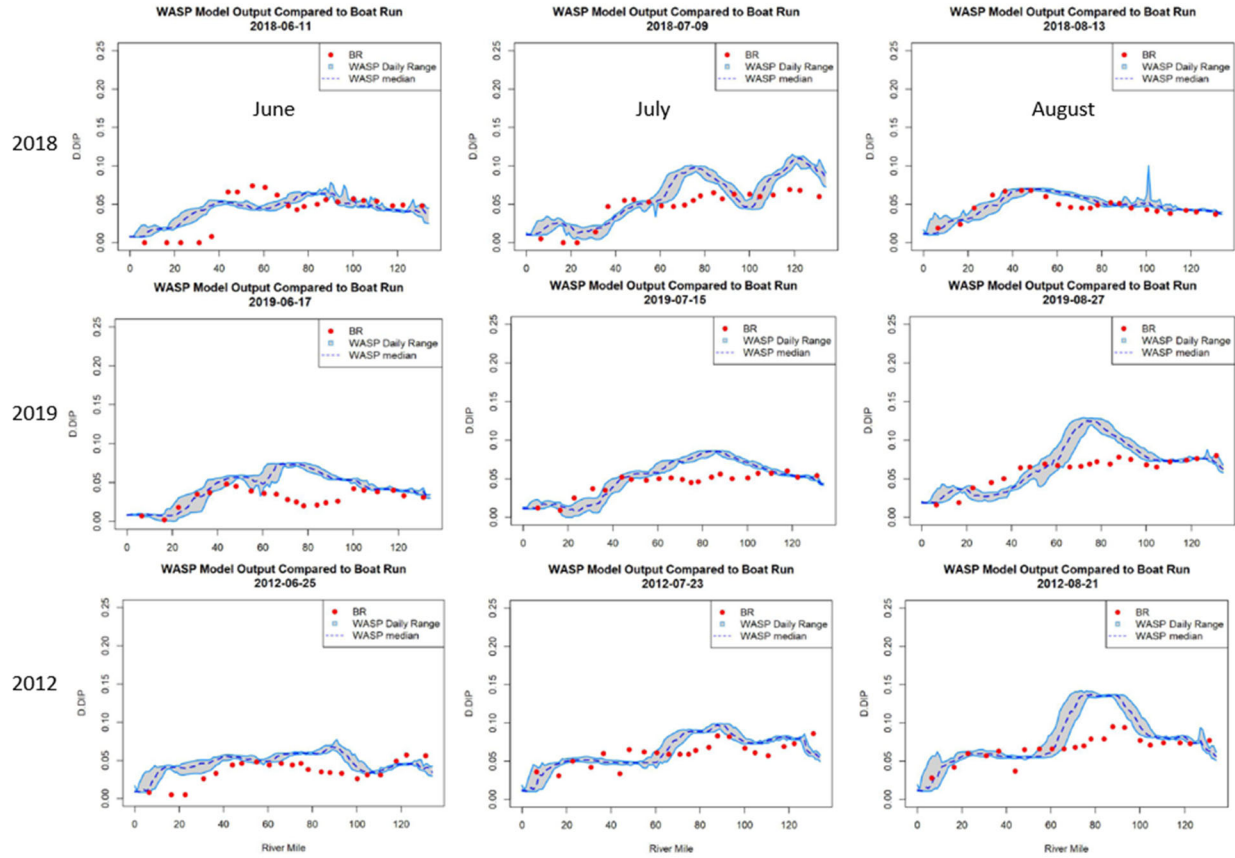


Figure 3-24: Model to Boat Run data comparisons – phosphate during summer

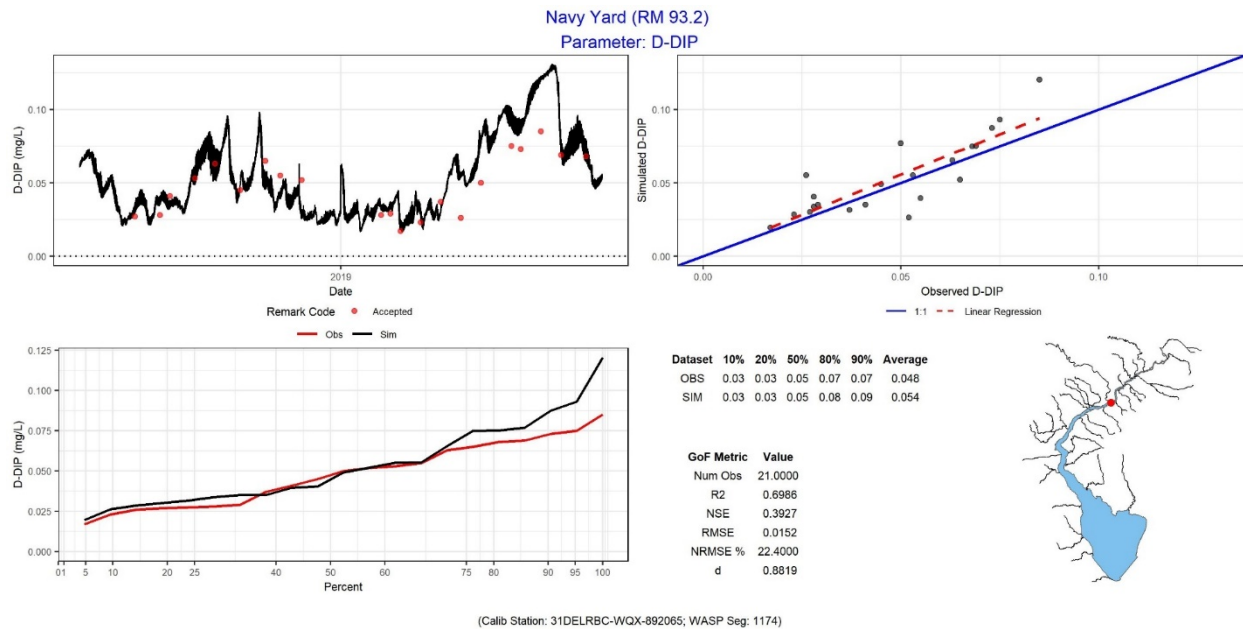


Figure 3-25: Model to Boat Run data comparison – phosphate at Navy Yard, 2018–2019

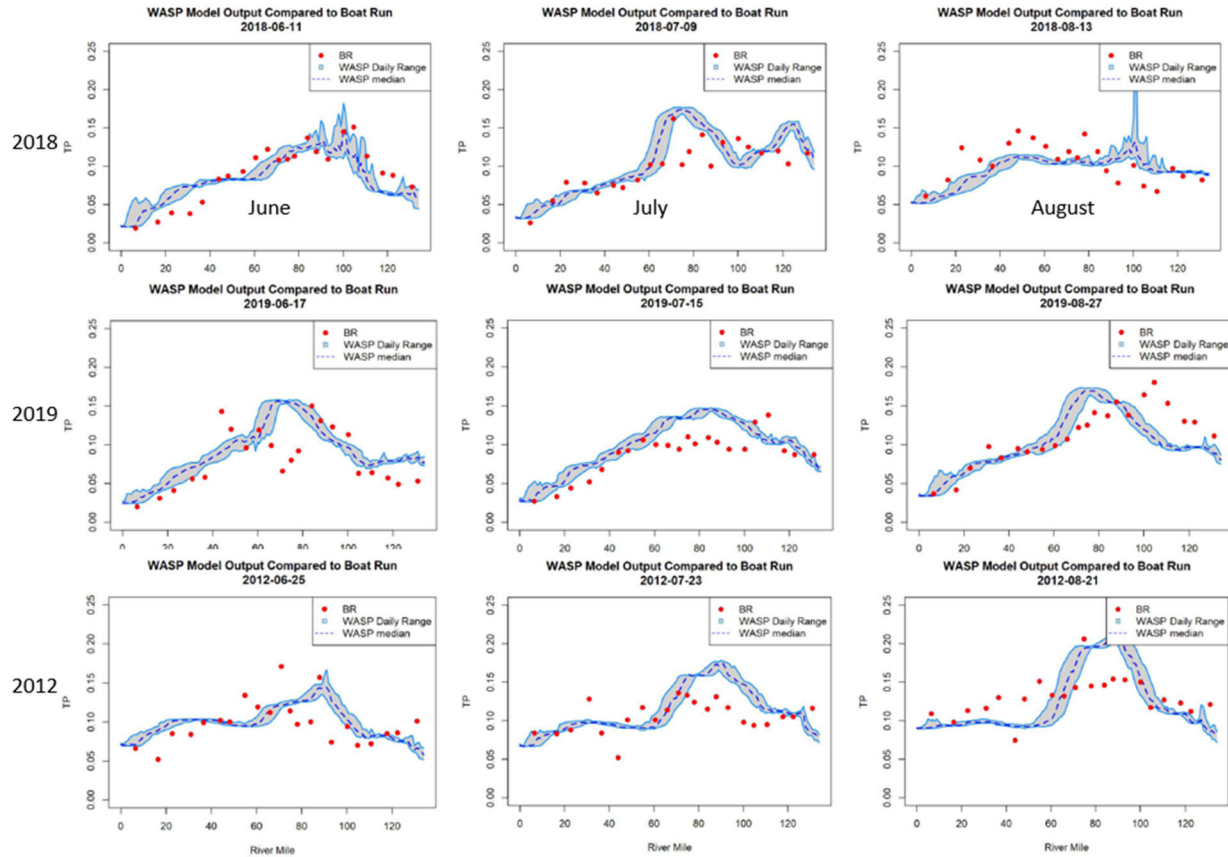


Figure 3-26: Model to Boat Run data comparisons – TP during summer

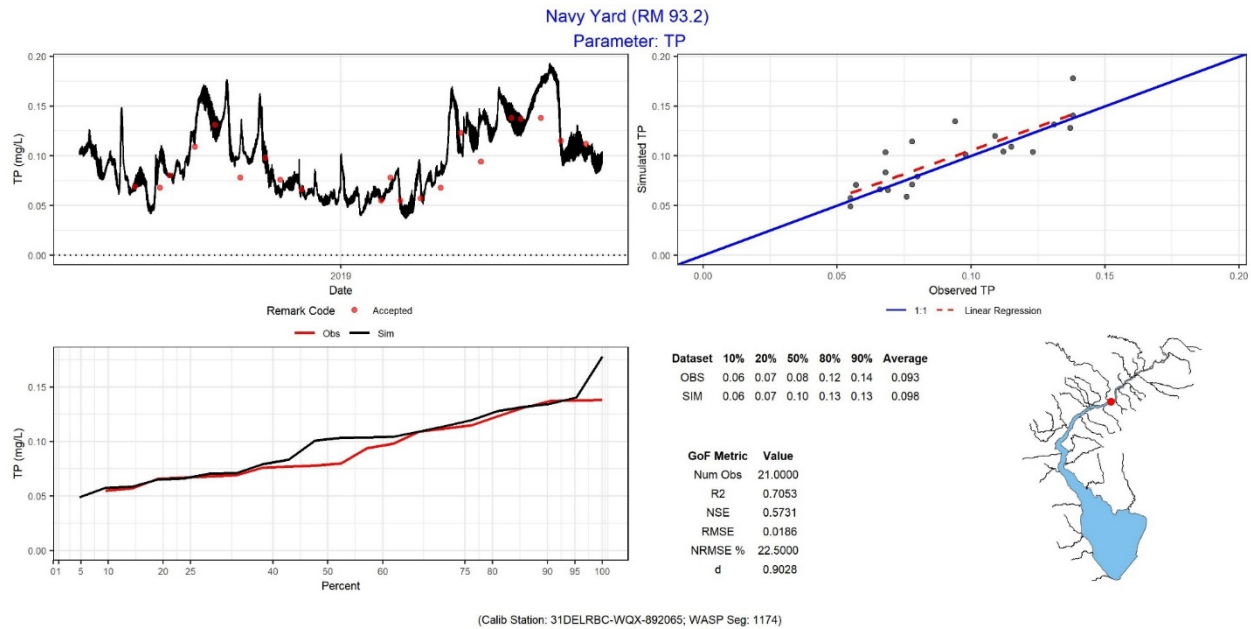


Figure 3-27: Model to Boat Run data comparison – TP at Navy Yard, 2018–2019

3.2.4.1.4 Solids

- Calibration approach: A fully functional sediment transport model with resuspension process is not included in this study due to uncertainty in accounting for all of the sediment loads, complexity of sediment transport models, and the time frame of the study. The solid particles are treated in a way similar to a dissolved tracer but with settling speed. A consequence of this operational approach was that computed suspended solids concentrations were much lower than observed ones, especially in the ETM area. This would cause under-prediction of particulate phosphorus and over-prediction of phosphate and total phosphorus in the water column. To overcome this issue, inorganic suspended solid loads from major tributaries and selected wastewater outfalls were adjusted such that computed and observed suspended solid concentrations matched.
- Spatial plots for individual sampling events: The model reasonably compute the solid concentration, as shown below. This was done solely to provide an operational framework for the suspended solids concentrations required for the sorption-desorption processes in the model.
- Temporal plots for individual Boat Run location: The computed solid concentrations were elevated to the observed levels reasonably well by the model.

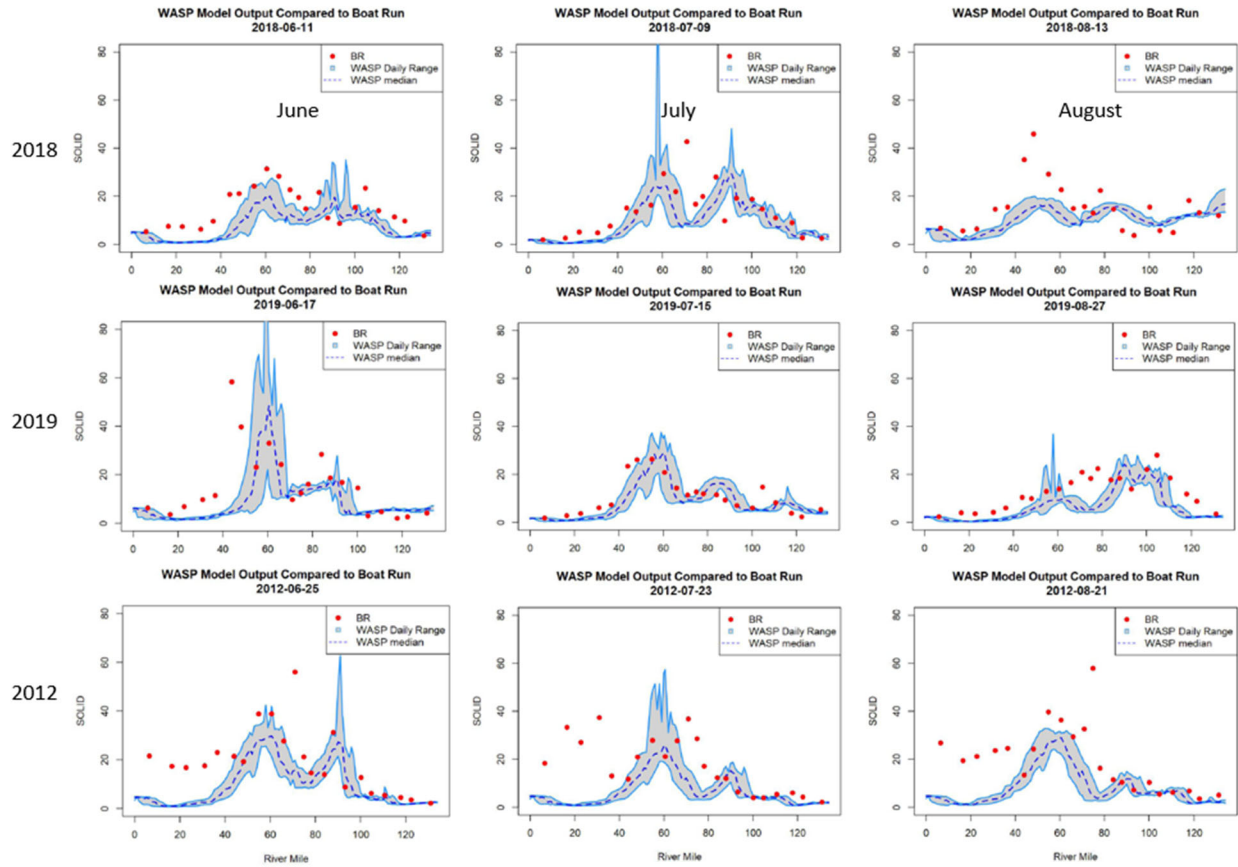


Figure 3-28: Model to Boat Run data comparisons – solids during summer

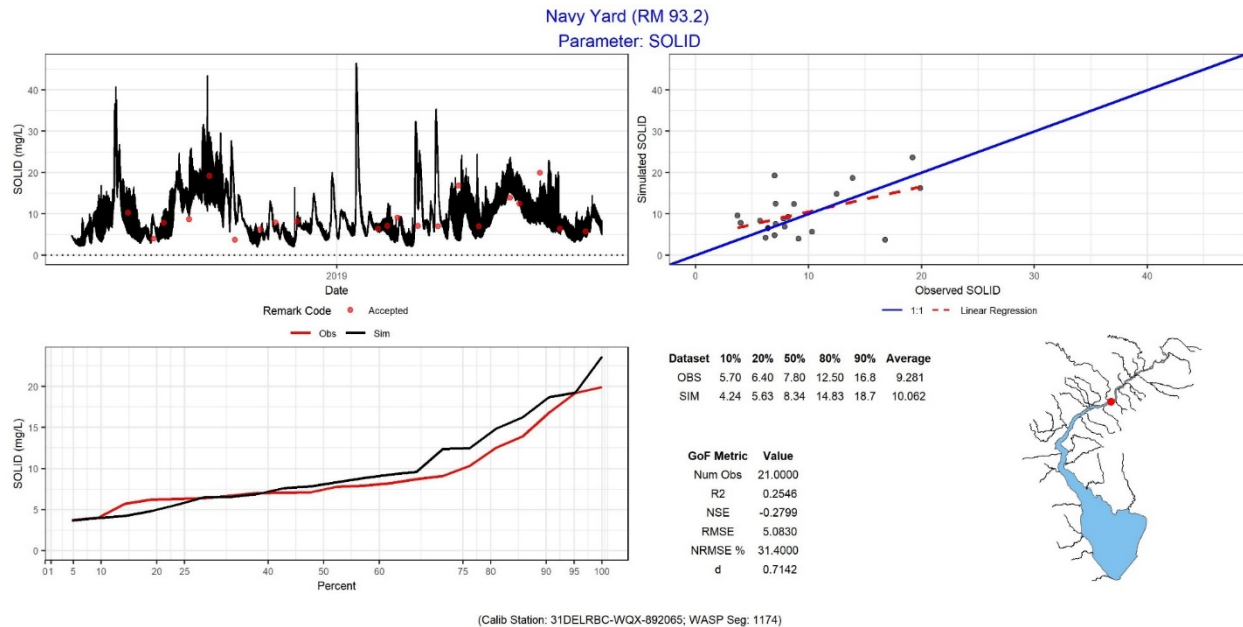


Figure 3-29: Model to Boat Run data comparison – solids at Navy Yard, 2018–2019

3.2.4.1.5 Phytoplankton

- Calibration approach: Phytoplankton maximum growth rates, carbon to chlorophyll ratios, respiration rates, death rates, optimal light saturation, and half-saturation constants for nutrient uptake, were set to match observed seasonal patterns in chlorophyll-a levels in the Bay and tidal river. Optimal temperature and shape parameters for phytoplankton growth were adjusted to represent the timing of the algal blooms.
- Spatial plots for individual sampling events: The model reasonably well captured the algal blooms in the Bay but missed observed blooms in the tidal river during summer of 2018–2019. The inability of the model to match summer blooms is further investigated in the following sub-section of “Phytoplankton”.
- Temporal plots for individual Boat Run location: The model prediction did not go as high as the data during the bloom in the summer of 2018 and did not predict a bloom in the summer of 2019. These mismatches are further investigated in the section 3.2.4.1.3.

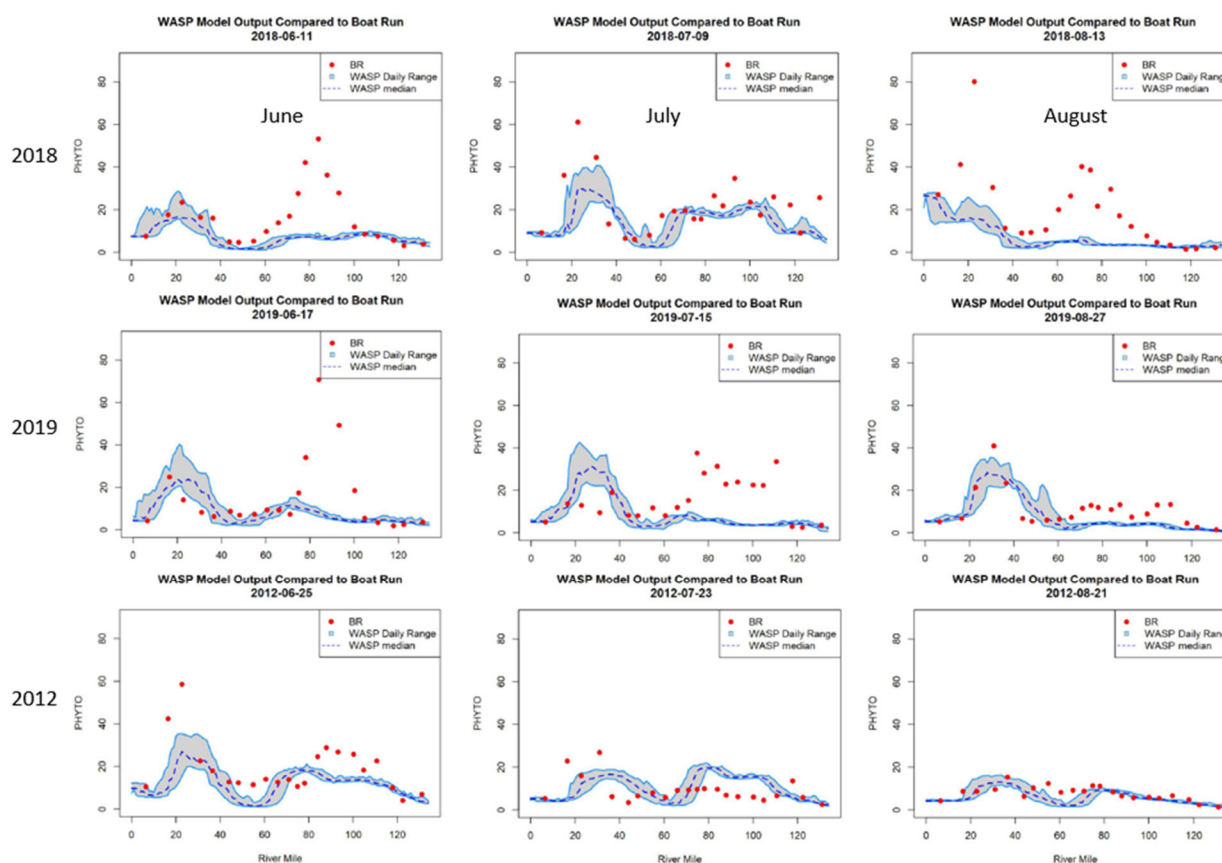


Figure 3-30: Model to Boat Run data comparisons – phytoplankton during summer

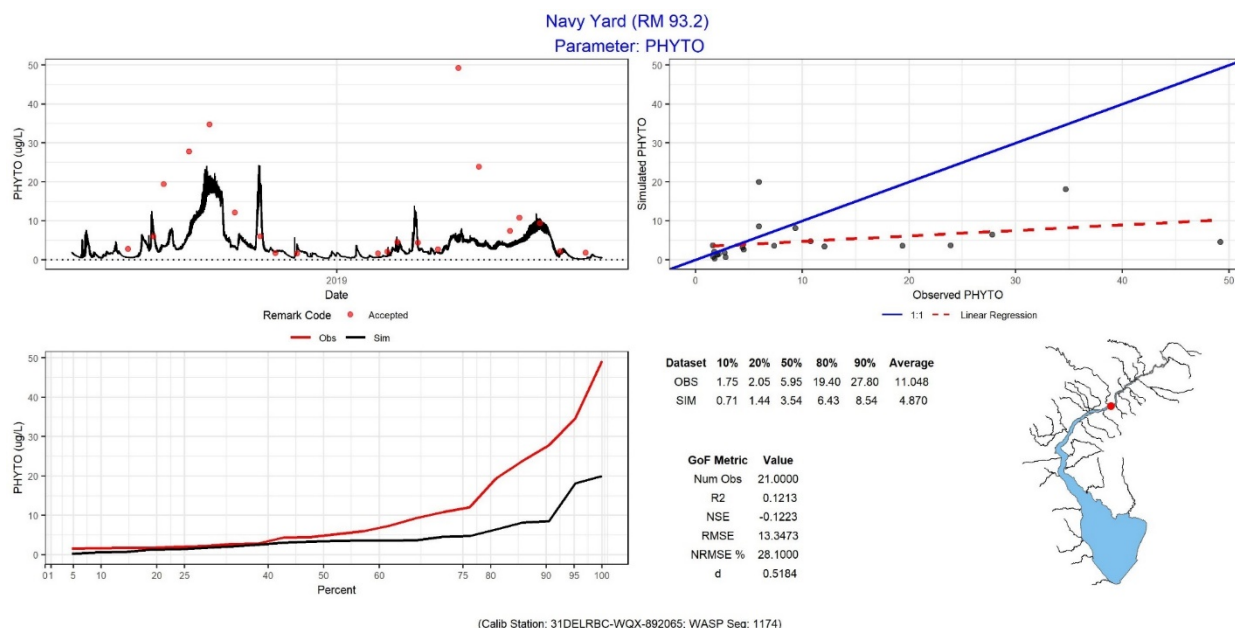


Figure 3-31: Model to Boat Run data comparison – phytoplankton at Navy Yard, 2018–2019

As noted above, both spatial and time series model-data comparisons of phytoplankton indicated that model did not capture the algal blooms all the time in the tidal river during summer 2018–2019. One hypothesis for this is that the model may not be simulating the light attenuation properly. Phytoplankton growth in the Delaware Estuary is extremely sensitive to light attenuation due to its turbid environment (Pennock, 1985; McSweeney et al., 2017). In this section, we evaluate model predictions of light extinction coefficient K_e against observations, which were estimated from light intensity collected at the surface and 1-meter depth during DRBC Boat Run survey (see Section 3.1.3.3). We also examine the predicted seasonal pattern of phytoplankton with observed long-term trend.

Figure 3-32 shows the model to data comparisons of the light extinction coefficient K_e in the surface layer by river mile during the July Boat Run survey in 2018, 2019, and 2012. The complete comparison plots for K_e from all surveys during the calibration years 2018–2019 and corroboration year 2012 are provided in Appendix F. The red lines and gray-shaded area in the spatial plots represent the means and daily ranges of the predicted K_e on the survey dates, respectively. The yellow vertical dashed lines corresponded to the station locations of Reedy Island and Ben Franklin Bridge. If light intensity data were not available for a given survey, observed K_e values were supplemented using Secchi depth data (i.e., the open circles) based on the equation below (Chapra, 1997):

$$K_e = \frac{1.8}{SD} \tag{3-52}$$

where SD = Secchi-disk depth (m).

As described in Section 3.1.3.3, minimum light penetrates at $K_e > 3.5 \text{ m}^{-1}$. In other words, it is more important for the model to predict a representative K_e over the range of $0 \sim 3.5 \text{ m}^{-1}$. Figure 3-32 and relevant plots in Appendix F demonstrate that the model generally does a good job predicting K_e in this practical range, including the Boat Run survey on July 15, 2019, when the model simulation did not reflect an observed algal bloom in the tidal river.

Next, phytoplankton concentrations were regrouped to investigate their seasonal variations against recent 10-year data trend: (1) Season-1: February 1 to April 15 for the late winter and early spring, which is a growing season for the marine diatom (i.e., phytoplankton group 1); (2) Season-2: April 15 to August 31 for the late spring and summer, which is a growing season for both freshwater and marine diatoms (phytoplankton groups 2 and (3)); (3) Season-3: September 1 to October 31 for the fall; and (4) Season-4: November 1 to January 31. Figure 3-33 and Figure 3-34 display predicted concentrations compared with data during growing seasons for the calibration and corroboration periods, respectively. The complete set of comparisons for four seasons are provided in Appendix F. The shaded area in the figures represent seasonal model results between the predicted 25th and 75th percentiles; the box and whiskers depict the recent 10-year Boat Run data trends; and the symbols next to the boxes corresponded to data from 2018–2019 or 2012. Note that Boat Run surveys during 2012 started on April 23 and ended October 22. As a result, there are no 2012 data displayed on the top panel in Figure 3-34. In general, the model reasonably reproduced seasonal variation trends against the recent 10-year data, except in the tidal river during the growing season of late spring and summer 2018–2019.

Additional numerical tests were conducted to: (1) increase boundary loads of phytoplankton, and (2) introduce random variations to the existing light extinction values for reflecting transient variation of light intensity. It was confirmed that these two factors unlikely caused the model under-prediction of the algal bloom in the tidal river. Further comparisons to continuous data and diagnostic analyses (Section 3.2.5) were performed to explore why the model missed the algal blooms in the tidal river during the summer 2018–2019.

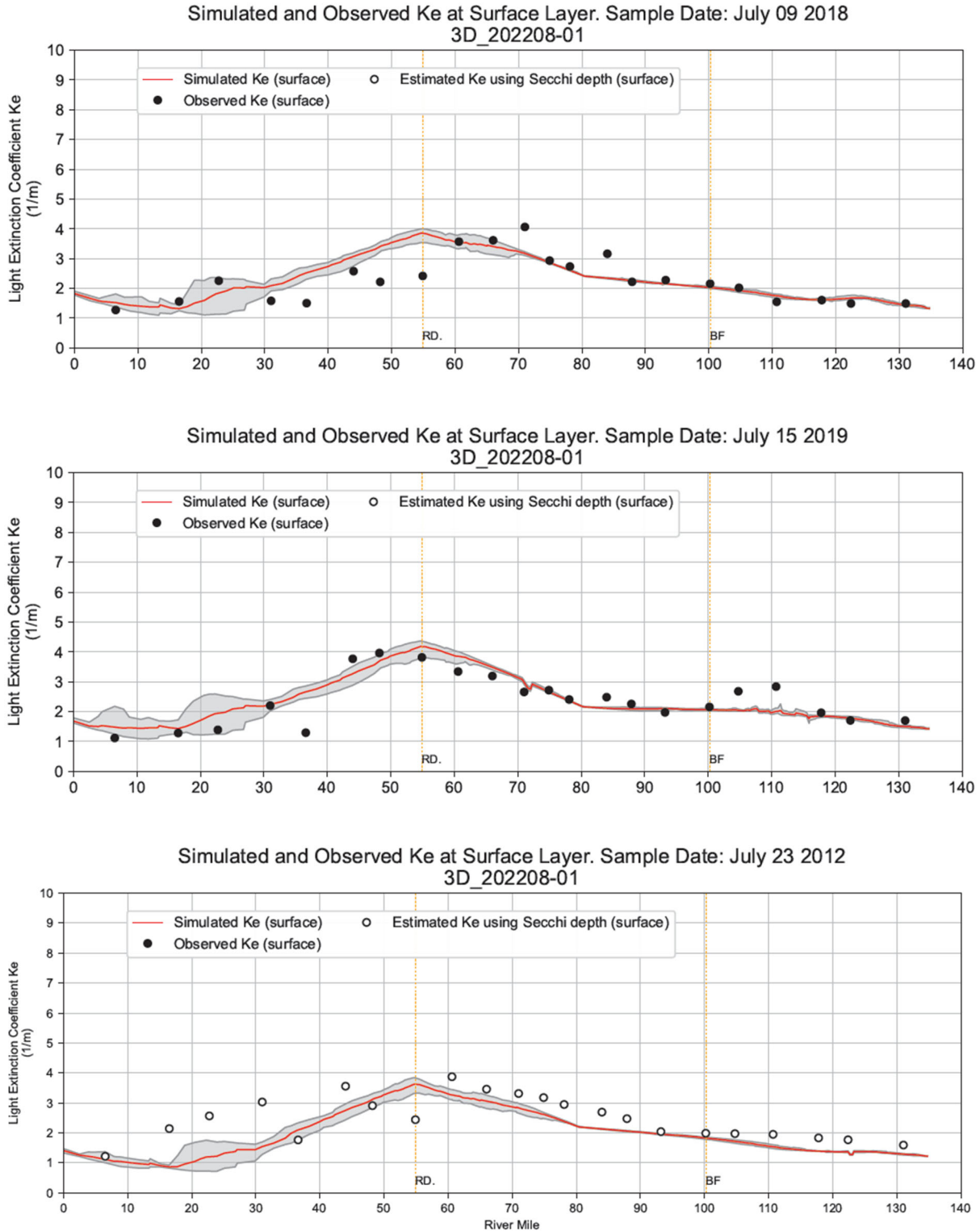
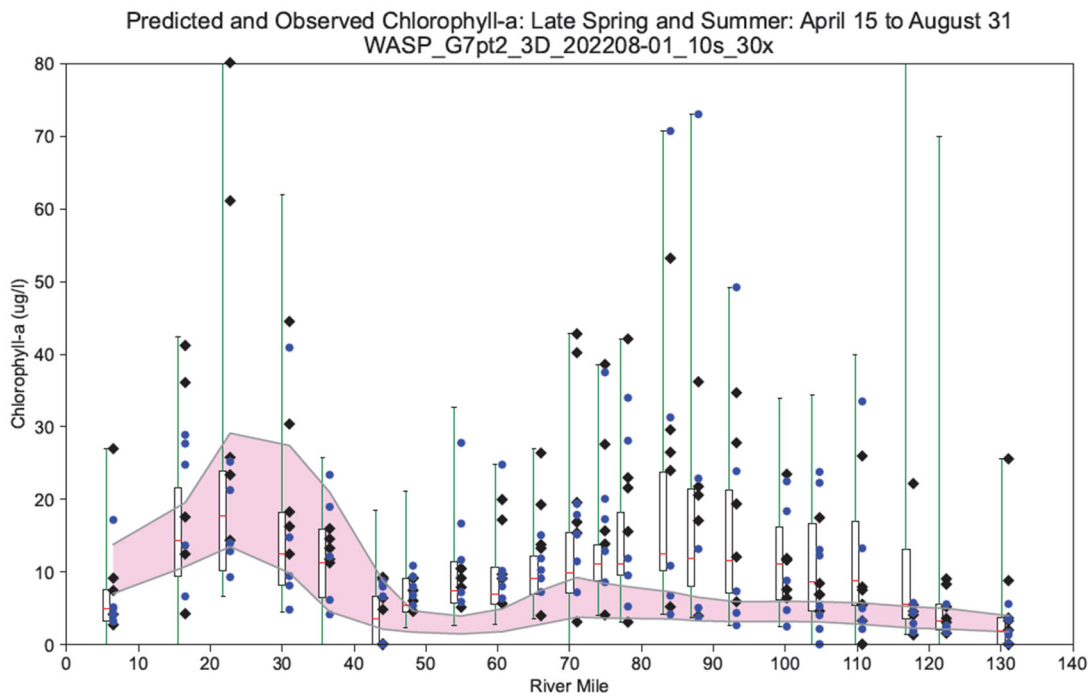
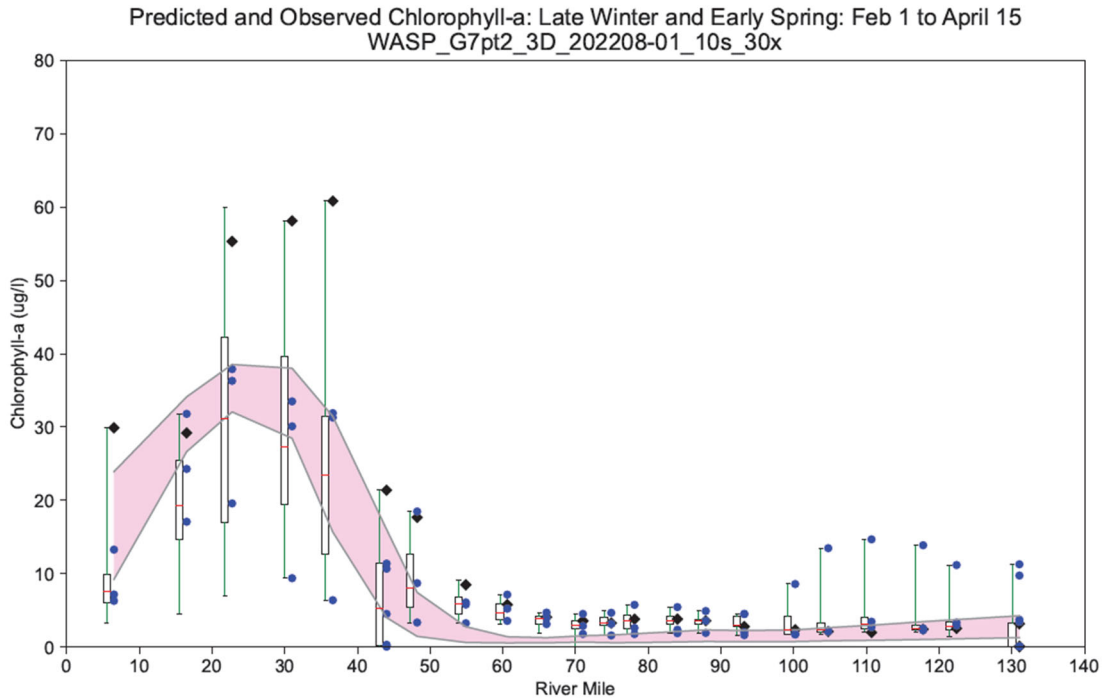


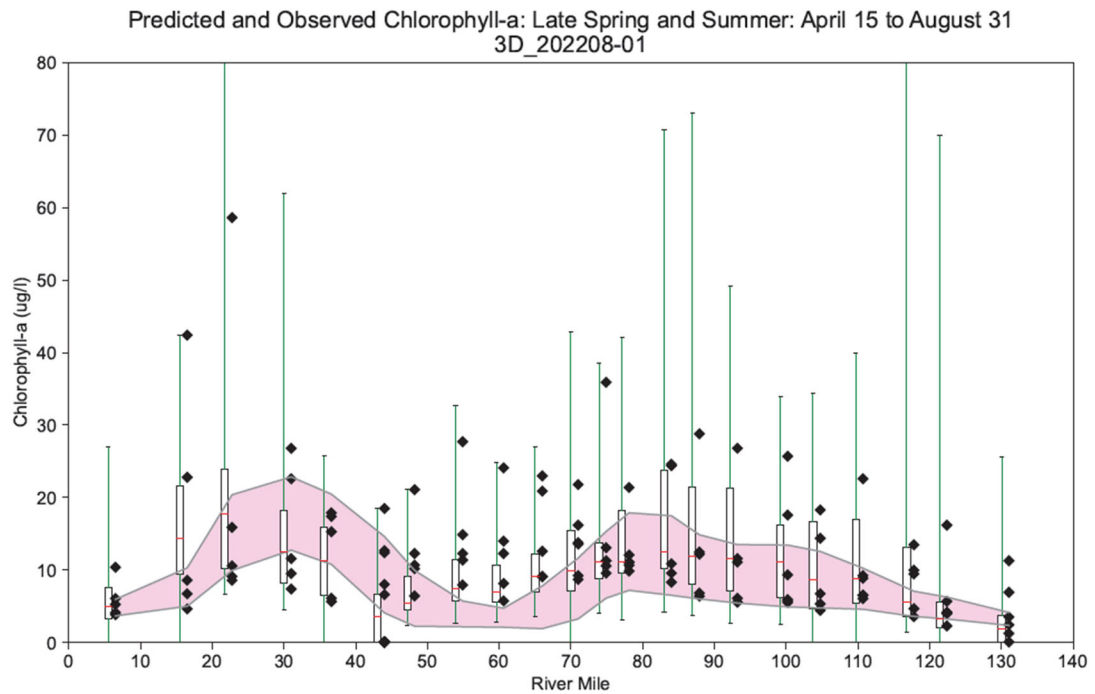
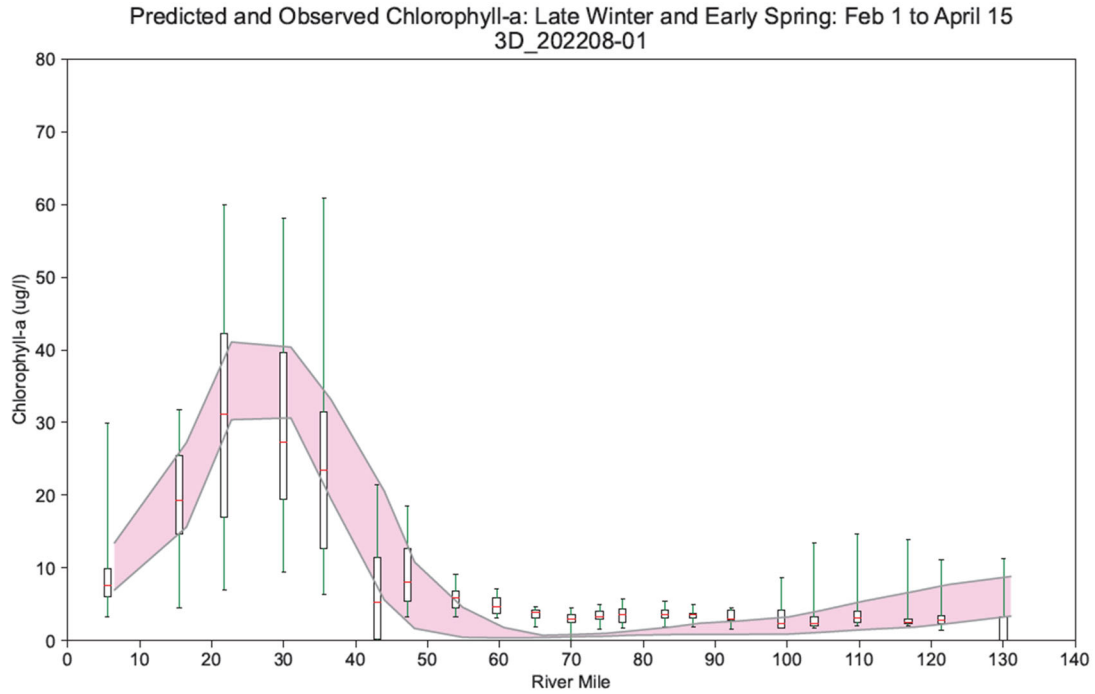
Figure 3-32: Light extinction – July 2018, 2019, and 2012



The symbols next to the box represent data from 2018 and 2019
 The shaded area represent model results between the 25 and 75 percentile.
 The un-colored box was based on 10-year boat-run data.

◆ Data (2018) ● Data (2019)

Figure 3-33: Seasonal phytoplankton comparisons, 2018–2019



The symbols next to the box represent data from 2012
 The shaded area represent model results between the 25 and 75 percentile.
 The un-colored box was based on 10-year boat-run data. ◆ Data (2012)

Figure 3-34: Seasonal Phytoplankton Comparisons, 2012

3.2.4.1.6 Dissolved Oxygen (DISOX)

- Calibration approach: Phytoplankton growth (photosynthesis) and reaeration are sources of dissolved oxygen while respiration, CBOD, nitrification, and SOD are sinks.
- Spatial plots for individual sampling events: The model reasonably well matched the absolute concentrations and spatial patterns of DISOX, including the dissolved oxygen sags around RM 90.
- Temporal plots for individual Boat Run location: The model matched the absolute concentrations, seasonal patterns, and cumulative frequency distributions of DISOX very well. Both observed and computed DISOX concentrations reach minimum values around July-August.

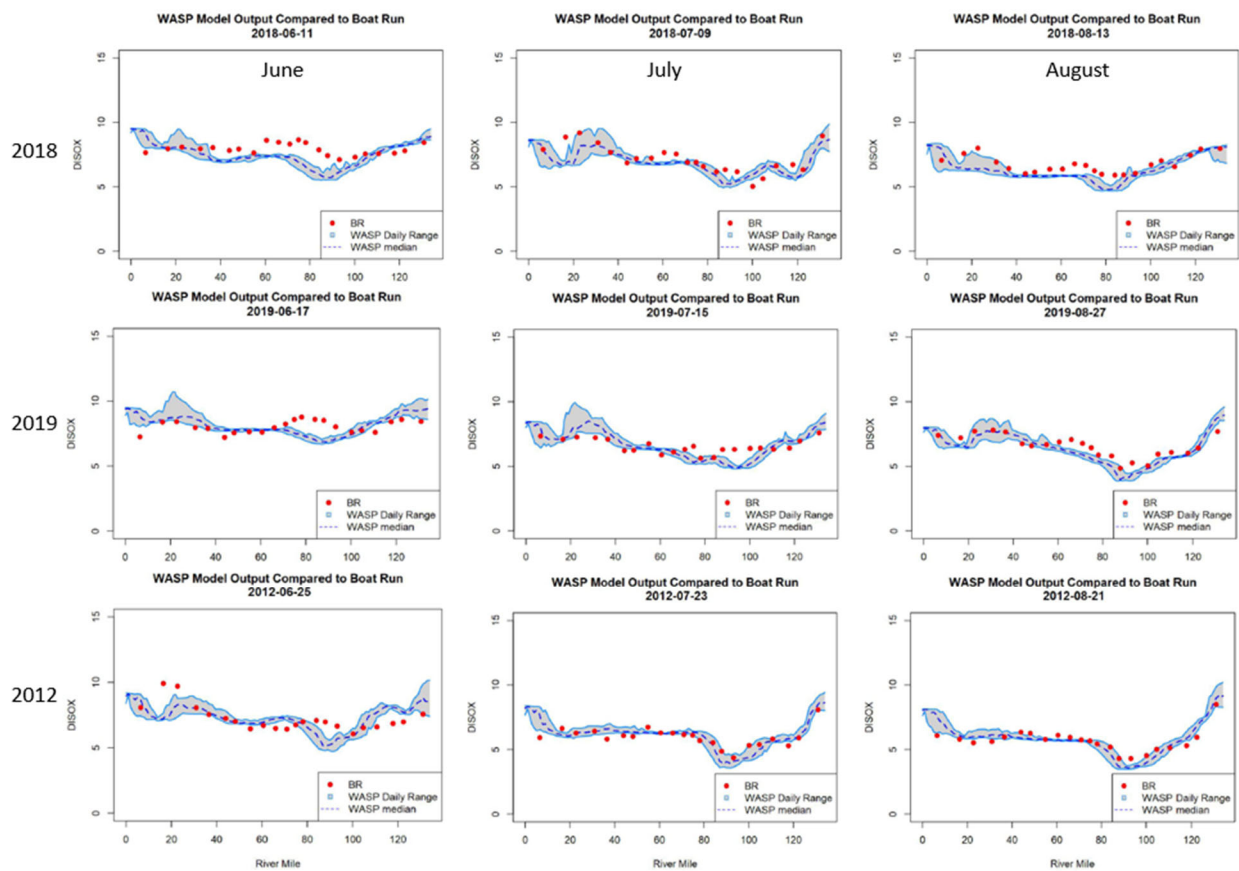


Figure 3-35: Model to Boat Run data comparisons – DISOX during summer

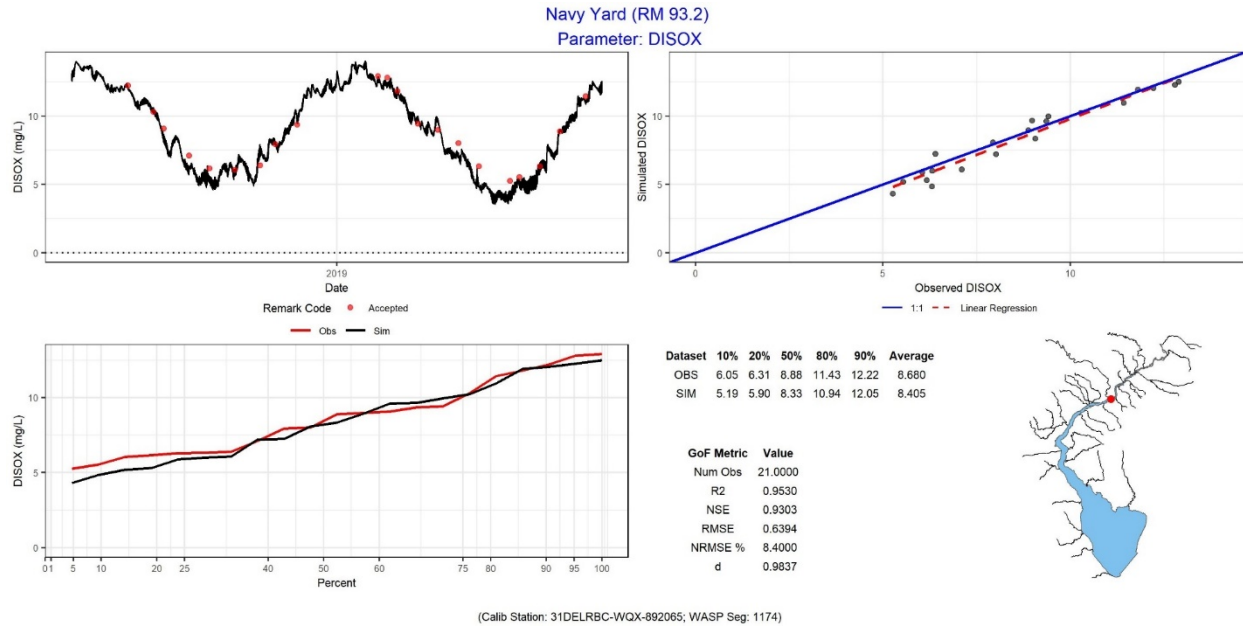


Figure 3-36: Model to Boat Run data comparison – DISOX at Navy Yard, 2018–2019

3.2.4.1.7 Dissolved Oxygen percent saturation (DOSAT)

- Spatial plots for individual sampling events: Model-data comparisons of DOSAT were good in general. Since dissolved oxygen percent saturation was calculated based on salinity and water temperature, their simulation accuracy (as computed by EFDC) affects the model-data comparisons of dissolved oxygen saturation.
- Temporal plots for individual Boat Run location: Model-data comparisons of DOSAT were reasonable, with the model slightly under-estimating the DOSAT concentrations, perhaps due to slightly over-estimation of water temperature.

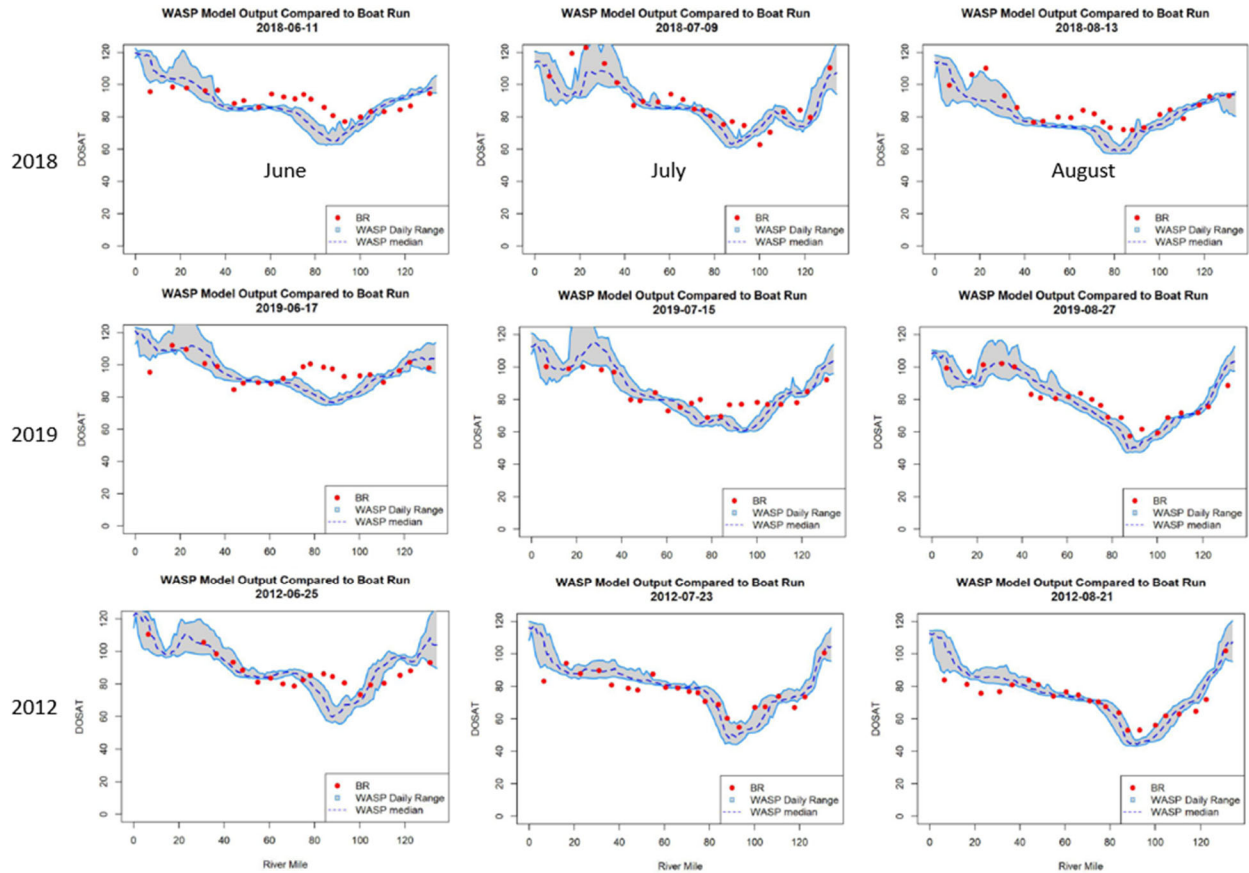


Figure 3-37: Model to Boat Run data comparisons – DOSAT during summer

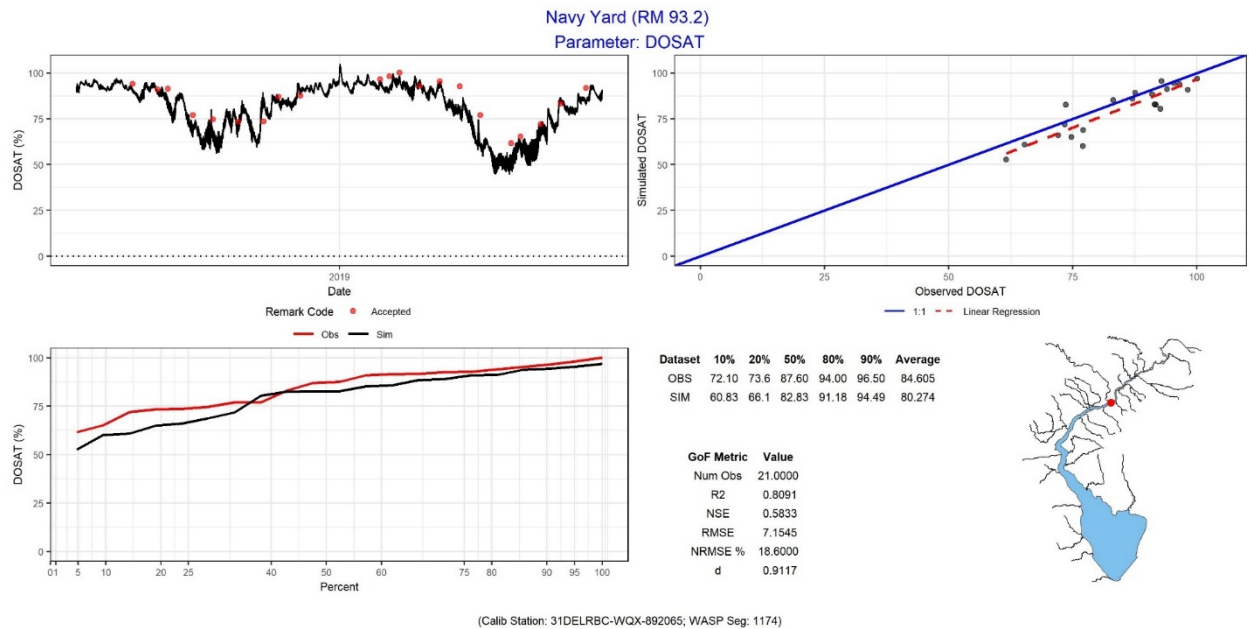


Figure 3-38: Model to Boat Run data comparison – DOSAT at Navy Yard, 2018–2019

3.2.4.2 COMPARISONS TO THE CONTINUOUS DATA AT DISCRETE LOCATIONS

Predicted dissolved oxygen and phytoplankton were compared with continuous data collected at four USGS stations and two PWD buoy stations (Figure 3-15) for both the 2018–2019 two-year model calibration period and the 2012 corroboration year. PWD buoy data were not available for 2012. Sensors at the USGS stations were installed at fixed locations (i.e., two ~ three feet below water surface during low tide), approximately corresponding to the second model vertical layer below the water surface (model vertical layer thickness is about 1.5 m/4.9 feet), whereas sensors at the PWD buoy stations were positioned about one meter below water surface, corresponding to model surface layer. Comparisons to these temporally high-resolution data are invaluable in assessing model performance. **Error! Reference source not found.** Figure 3-39 to Figure 3-44 present the predicted and measured (near-) surface dissolved oxygen concentrations for the calibration period 2018–2019, in the sequence of upstream to downstream stations. Similar figures for the corroboration period 2012 are available in Appendix F. Both the model predictions and data represent instantaneous values paired at two-hour intervals. The top panel in the figures shows the time series model-data comparisons of dissolved oxygen concentrations. DRBC Boat Run data are also displayed as green circles for additional information. The bottom left panel shows comparisons of cumulative frequency distributions, while the bottom right panel shows 1-to-1 comparisons with key statistical metrics displayed. Over the two-year model calibration period, the concentrations, seasonal variations, and cumulative frequency distributions of dissolved oxygen are reproduced well by the model at all stations. Lower dissolved oxygen in the Delaware Estuary occurs around July-August, as a result of lower solubility of oxygen in water column, elevated nitrification, CBODU oxidation, and sediment oxygen demand caused by high water temperatures. During the calibration period of 2018–2019, the predictions match well with the observations at lower dissolved oxygen concentrations (at 0.01 percentile) for most of the monitoring stations with the differences between model and data of about 0.1 ~ 0.3 mg/L. The largest differences (about 0.7 mg/L at 0.01 percentile) between the model predictions and observations of lower end dissolved oxygen occur at the Reedy Island station around RM 54, however, the difference is relatively small (about 0.1 mg/L) at 1st percentile. Spatially, both the model predictions and data indicate the dissolved oxygen sag occurs around Buoy B, RM 93.5, near the Schuylkill River entrance. During the model corroboration period of 2012, the model-data comparisons for lower dissolved oxygen concentrations, spatially and temporally, are not as good as those during the calibration period, due likely to the less frequent data available for specifying boundary conditions during 2012. Overall, the model performs well in representing the observed minimum dissolved oxygen levels and dissolved oxygen sag locations and temporal trends and variations over all three years, indicating that the model captures the principal processes affecting dissolved oxygen in the Delaware Estuary.

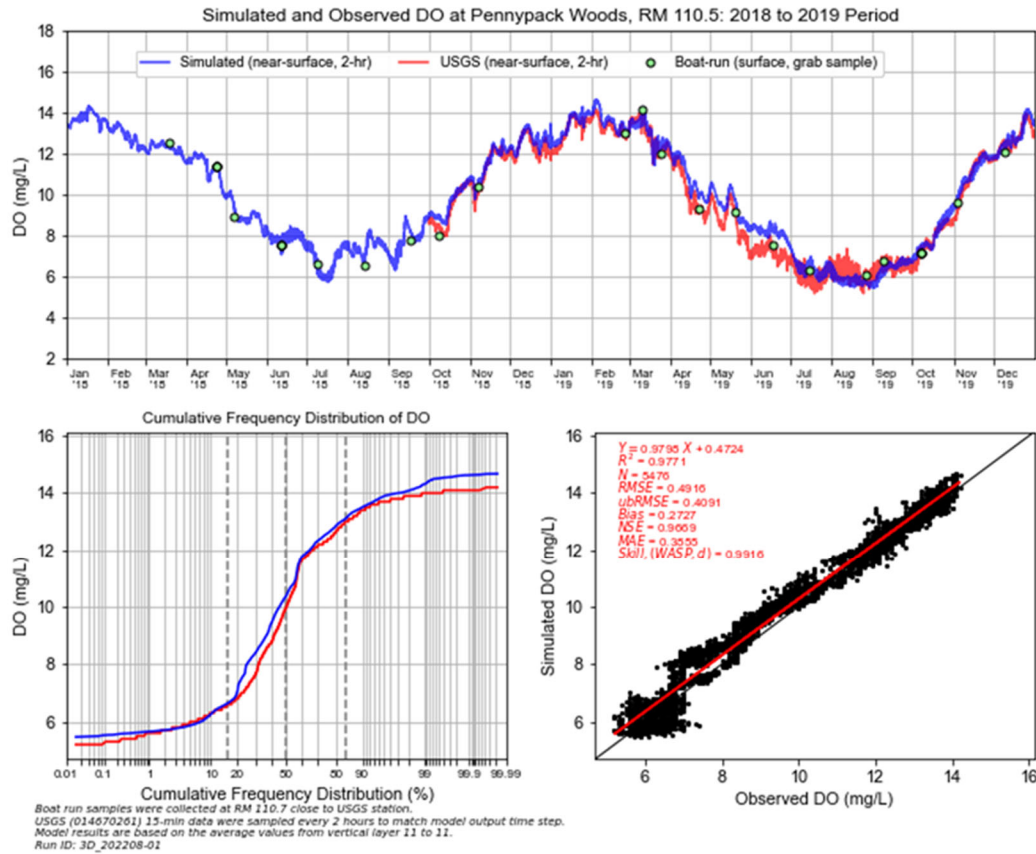


Figure 3-39: Model to Continuous Data Comparison – DO at Pennypack Woods during 2018–2019

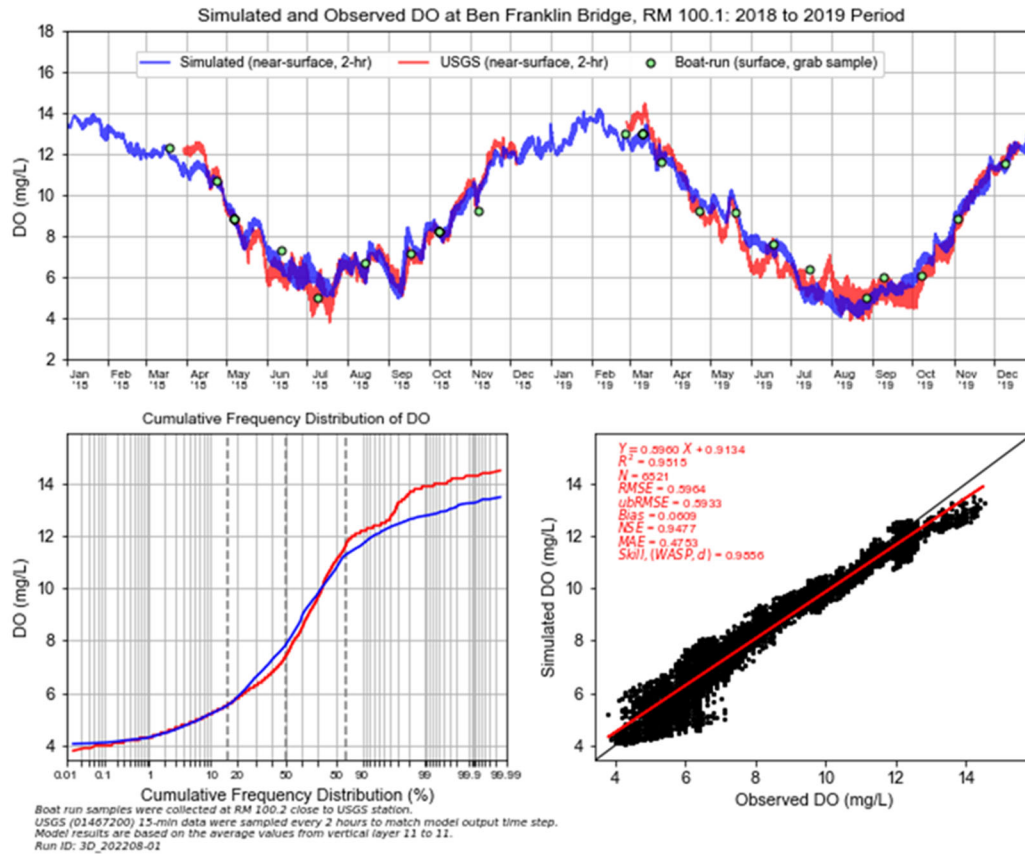


Figure 3-40: Model to Continuous Data Comparison – DO at Ben Franklin Bridge during 2018–2019

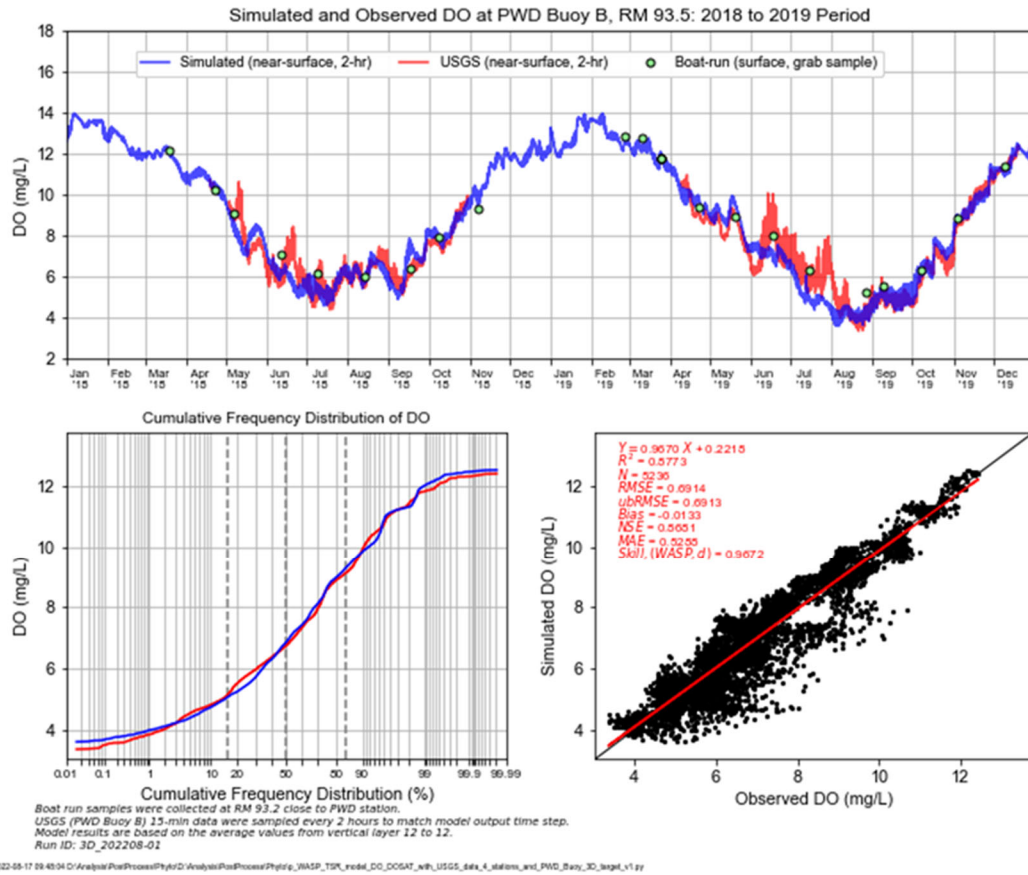


Figure 3-41: Model to Continuous Data Comparison – DO at Buoy B during 2018–2019

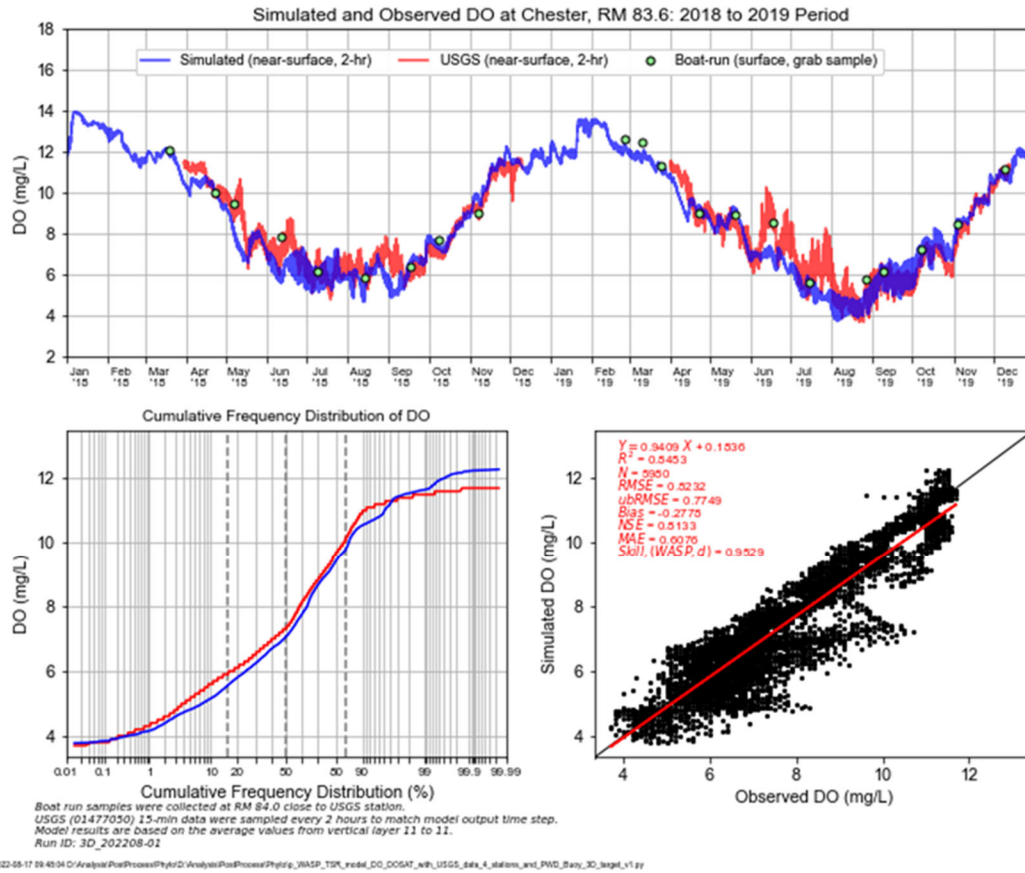


Figure 3-42: Model to Continuous Data Comparison – DO at Chester during 2018–2019

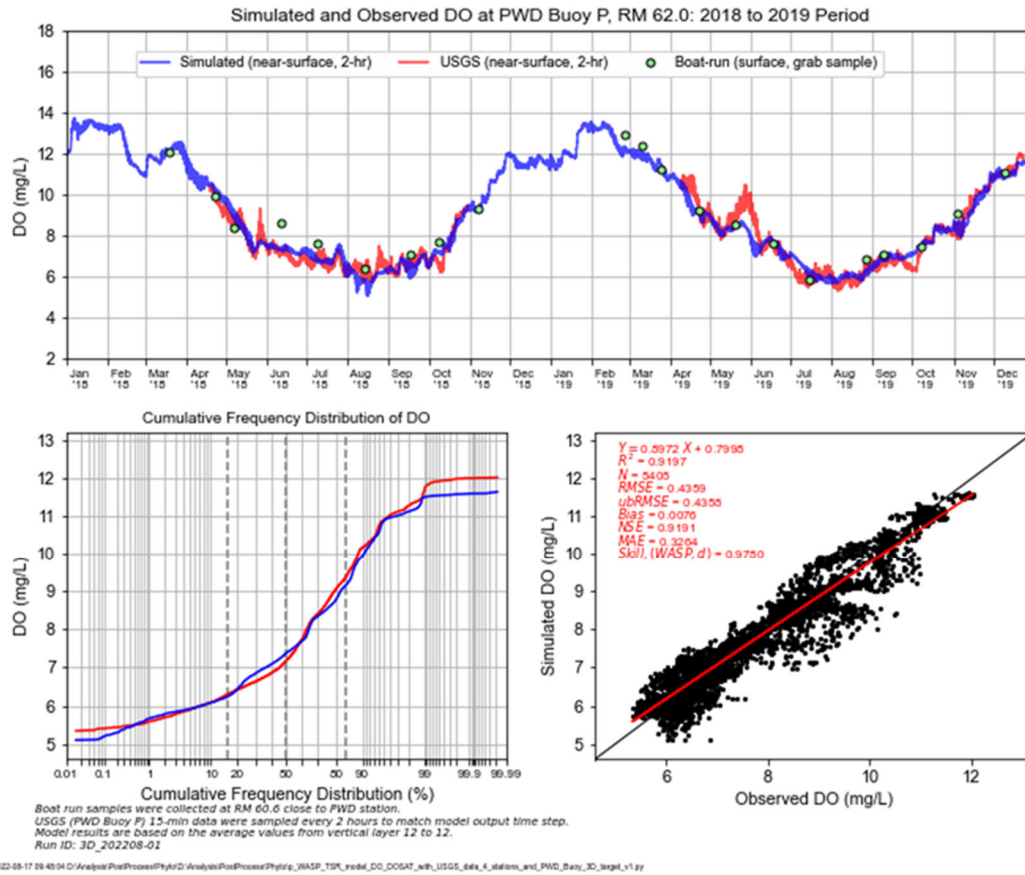


Figure 3-43: Model to Continuous Data Comparison – DO at Buoy P during 2018–2019

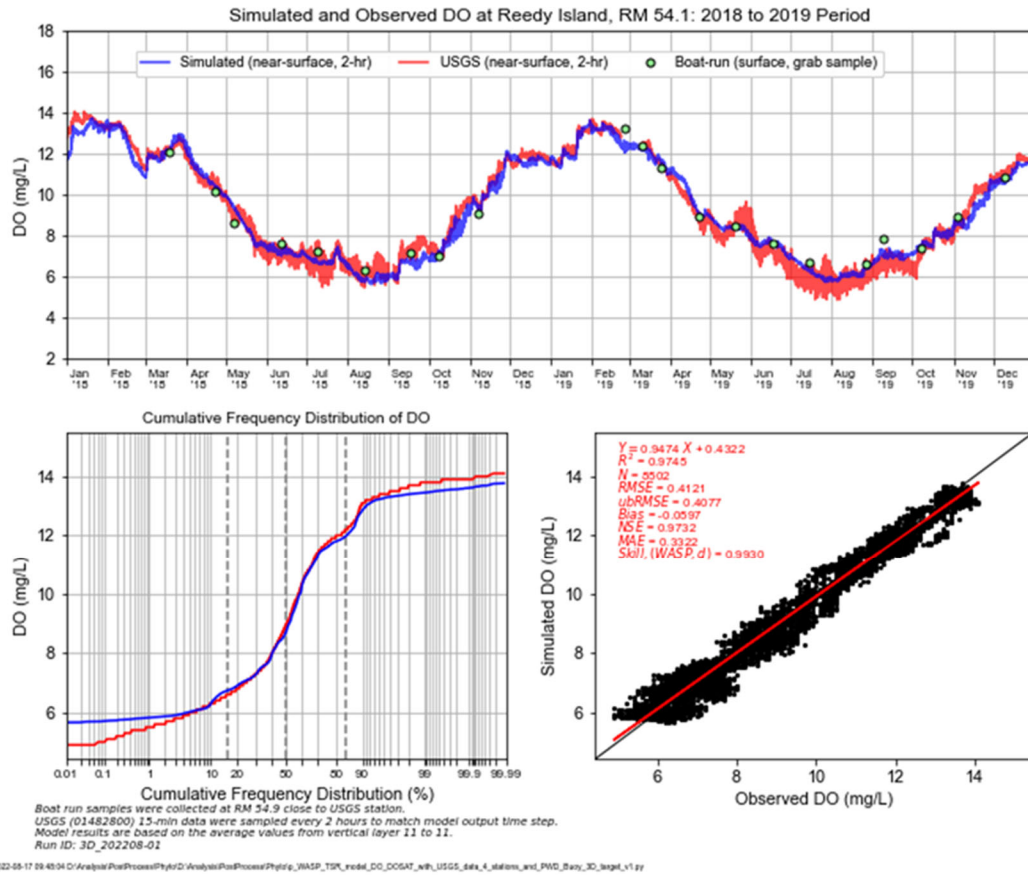


Figure 3-44: Model to Continuous Data Comparison – DO at Reedy Island during 2018–2019

Figure 3-45 to Figure 3-47 illustrate the comparisons of predicted and measured (near-) surface phytoplankton concentrations during the calibration period 2018–2019. The figure formats are the same as those in the dissolved oxygen comparisons. Similar figures for the corroboration period 2012 are available in Appendix F. Daily averaged values were used for both model and data. Continuous phytoplankton data were available only for the USGS station at Ben Franklin Bridge and PWD Buoys B and P during 2018–2019. The pink lines in the top panel of figures represent water age (right y-axis), one of the WASP model output variable, where high values correspond to low flow conditions. Delaware estuary has not been experienced with high algal bloom events but there were times with minor active phytoplankton events. In this document, whenever there is an uprising peak of phytoplankton concentrations we refer it to algal bloom. During the calibration period, model did reasonably well predicting an algal bloom that occurred in the tidal river during June–July 2018, with the maximum observed Chl-a concentration being slightly underestimated and the timing of bloom shifting by about a half-month relative to the data. However, the model simulation was unable to reflect an observed algal bloom that occurred in the tidal river around June–July 2019, as also indicated in the comparisons to Boat Run data. Additionally, at Ben Franklin Bridge and Buoy B, the model simulation under-predicts an observed algal bloom in May 2018 and over-predicts a bloom in September 2018. During the 2012 corroboration period, the model does a reasonable job in predicting the observed phytoplankton concentrations, considering the less frequent data available to describe boundary conditions for input to the model. The impact from phytoplankton on dissolved oxygen is well shown in observed data for June–July of 2019 at Buoy B. As phytoplankton concentration increased to approximately 20 ug/L (Figure 3-46), dissolved oxygen concentrations followed similar trends as shown in Figure 3-41. Under prediction of dissolved oxygen in June–July 2019 at Buoy B can be explained by the under prediction of phytoplankton. At the same time, the observed data at the Ben Franklin Station did not show the phytoplankton impact on dissolved oxygen for the same time period. Further diagnoses were conducted and presented in Section 3.2.5 to investigate potential factors (e.g., nutrient and light limiting factors) that may lead to under-prediction of algal blooms in the tidal river, especially during June–July 2019.

The model calibration statistical metrics are summarized in Table 3-9 and Table 3-10 for dissolved oxygen and phytoplankton, respectively. Definition of the metrics can be found in Equations **Error! Reference source not found.** to (3-54), and Appendix F. In general, the statistical metrics results demonstrate that the model captures the main features of the dissolved oxygen observations exceptionally well. For example, in Table 3-9 the skill factors (or index of agreement) are larger than 0.95 at all stations. Additionally, the R^2 and Nash-Sutcliffe coefficients (NSE) at four out of six stations are greater than 0.92. A value of 1 for skill factor, R^2 , and NSE represents a perfect match between model predictions and observed data (Davis, 2019, Appendix B). On the other hand, the statistical comparisons for phytoplankton are not as good. For example, in Table 3-10 the skill factors range from 0.38 to 0.61, R^2 range from 0.11 to 0.16, and NSE values vary from -0.63 to -0.05, where NSE = 0 indicates that model predictions are only able to accurately represent the mean of observed data (Davis, 2019, Appendix B). Overall, the model performance in predicting dissolved oxygen in the Delaware Estuary is satisfactory.

Next, the model-data comparisons of dissolved oxygen and phytoplankton concentrations during 2018–2019 were evaluated using the target diagrams (Figure 3-48 and Figure 3-49), which provides a summary of model performance at multiple stations and during multiple years. Jolliff et al. (2009) and McWilliams et al. (2015) provided a detailed description of target diagrams and their use in model skill assessment. In short, the bias and the unbiased Root Mean Square Difference (ubRMSD) described in Equations (3-53) and (3-54) are normalized by the observed standard deviation, so the values are comparable among different variables (i.e., to compare model accuracy among group of stations, and/or among different periods, etc.). On the target diagram, the normalized bias is plotted on the Y-axis and the normalized ubRMSD is plotted on the X-axis.

The bias of model estimates is calculated as

$$bias = \frac{1}{N} \sum_{n=1}^N X_{Mi} - \frac{1}{N} \sum_{n=1}^N X_{Oi} \quad (3-53)$$

where subscripts “M” and “O” stand for model and observation values.

Negative bias indicates that the model underpredicts relative to data; positive bias indicates that the model overpredicts relative to data.

The ubRMSD is calculated as

$$ubRMSD = \left[\frac{1}{N} \sum_{n=1}^N [(X_{Mi} - \bar{X}_M) - (X_{Oi} - \bar{X}_O)]^2 \right]^{0.5} \quad (3-54)$$

The ubRMSD metric quantifies the model-data differences with the bias removed. It is similar to a root-mean-square error, but the effects of bias are removed from the calculation. As ubRMSD increases, the difference between oscillations in the predicted and observed variable becomes larger. To indicate whether the modeled variability is greater than or less than the observed variability, the ubRMSD is multiplied by the sign of the difference between the modeled and observed standard deviations in the target diagram.

An ideal model-data comparison would lie on the origin of the target diagram. Jolliff et al. (2009) and McWilliams et al. (2015) recommend that predictions falling outside a radius of 1 are classified as indicating poor agreement between the model predictions and the observed data. They considered this threshold independent of variables (e.g., chlorophyll-a, hydrodynamic parameters, and DO). The target diagram is used as an additional skill assessment tool for evaluating the model performance.

In Figure 3-48, all symbols of dissolved oxygen comparisons fall within the 0.5-radius. The distribution of the symbols indicates: (1) two-hour instantaneous and daily averaged outputs have almost identical patterns and thus share about the same degree of accuracy² (i.e., output positions with respect to the origin where perfect results lie on); (2) model results slightly overestimated dissolved oxygen concentrations, since the count of positive-y symbols is greater than the negative-y ones; and (3) model results slightly underestimate the variability in dissolved oxygen concentrations, considering the count of positive-x symbols is fewer than the negative-x ones. Overall, the target diagram demonstrates that the model performs well in predicting observed dissolved oxygen concentrations at multiple locations throughout the estuary during the calibration period.

In Figure 3-49, phytoplankton comparisons at PWD Buoy-B during 2018–2019 and USGS station at Ben Franklin Bridge during 2019 are located approximately at the 1.0-radius, comparisons at the remaining stations fall beyond the 1.0-radius. The two-hour instantaneous and daily averaged outputs demonstrate about the same degree of accuracy. The model systematically underestimates phytoplankton concentrations since most of symbols are below the x-axis. All symbols are approximately evenly distributed around the y-axis, which suggests that the model does not apparently overestimate or underestimate the variability in phytoplankton. Diagnostic analyses presented in Section 3.2.5 address possible reasons for why the model simulation underestimated algal blooms in the tidal river during summer 2018–2019.

²

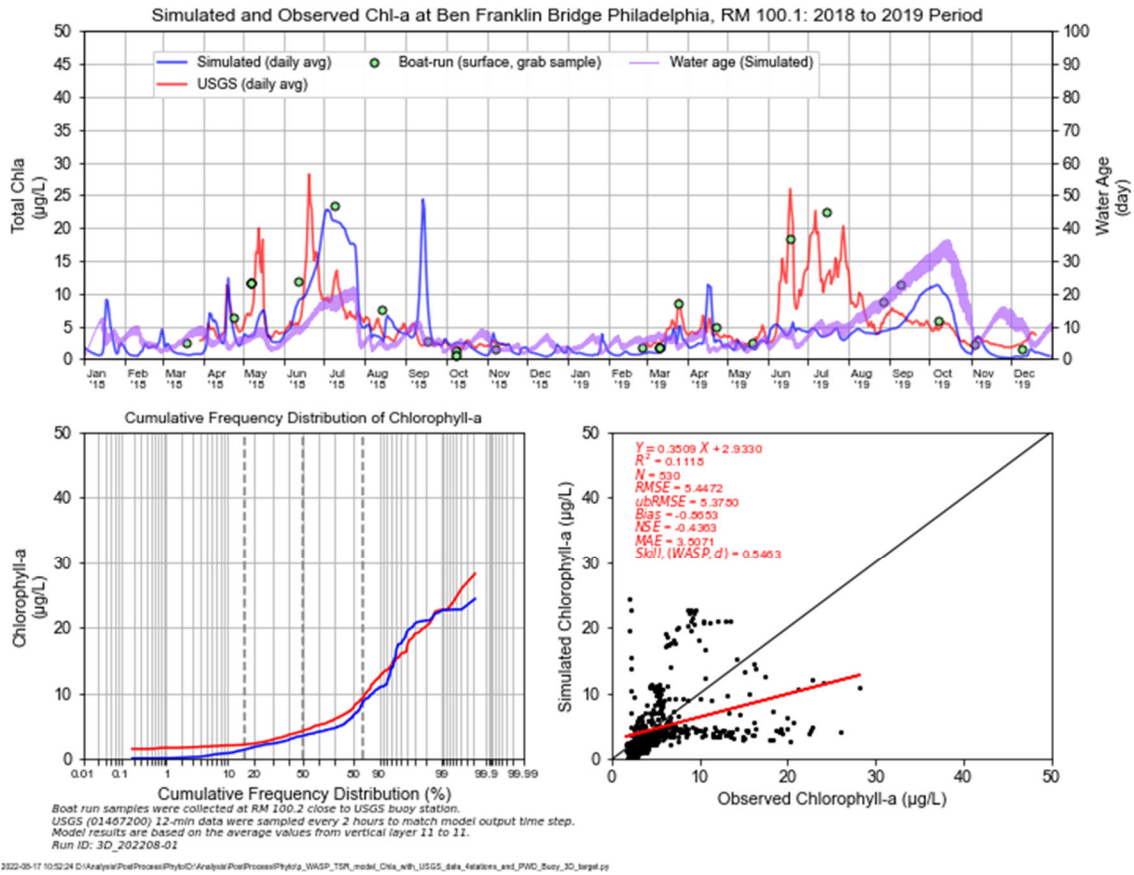


Figure 3-45: Phytoplankton at Ben Franklin Bridge during 2018–2019

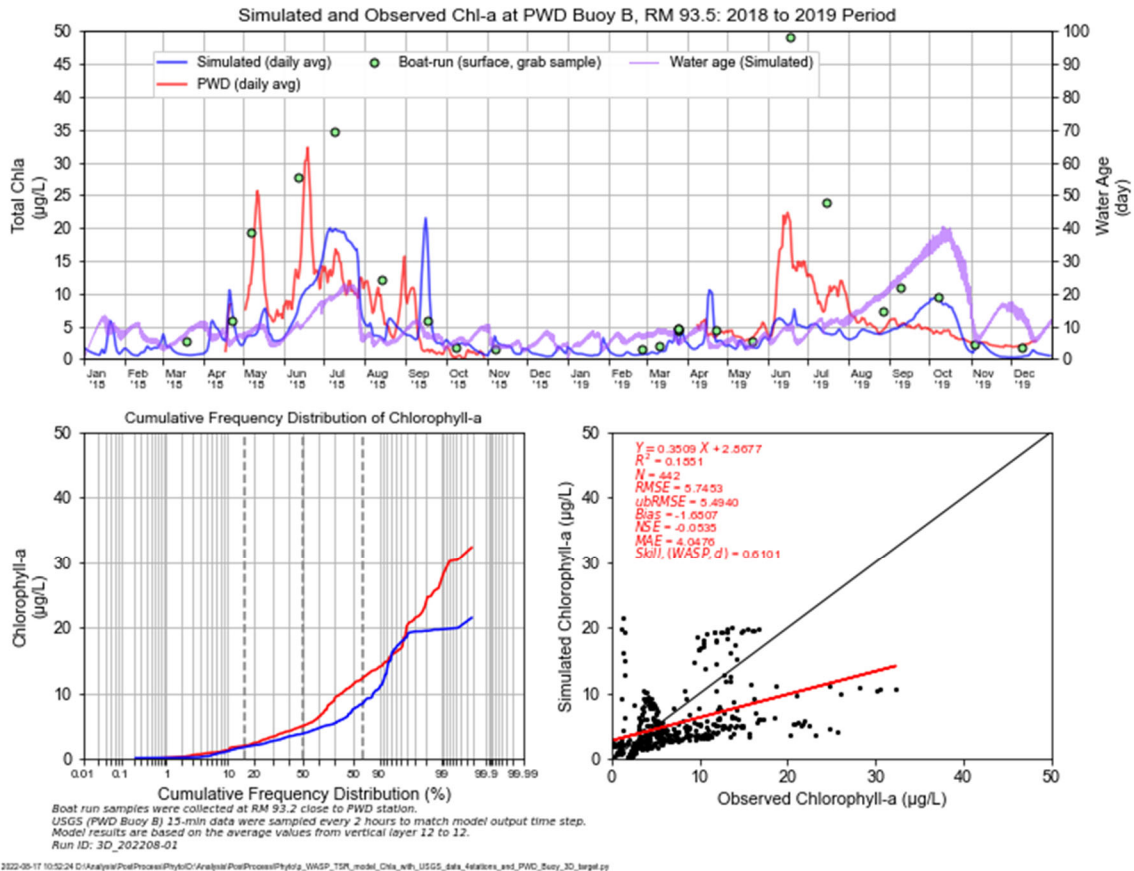


Figure 3-46: Phytoplankton DO at Buoy B during 2018–2019

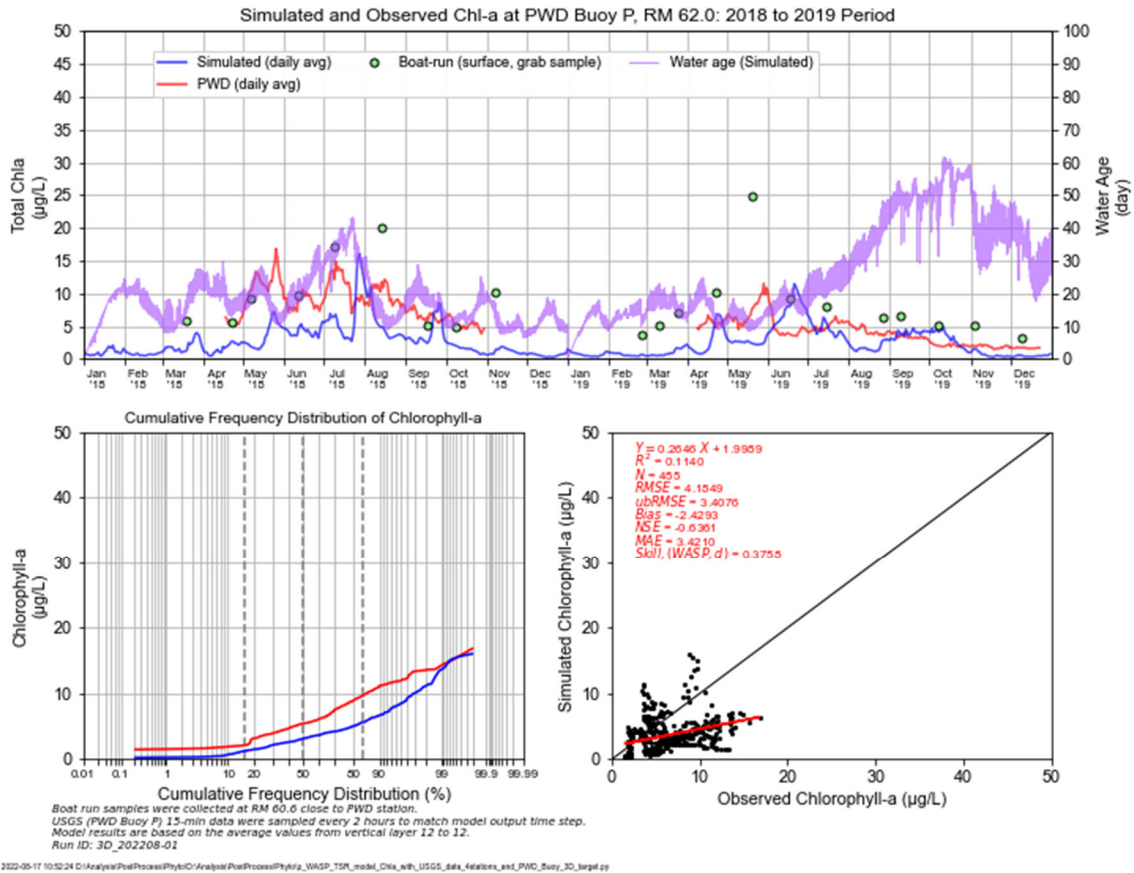


Figure 3-47: Phytoplankton at Buoy P during 2018–2019

Table 3-9: Statistical Metrics of Dissolved Oxygen at USGS Stations and PWD-Buoys, 2018–2019

Metrics	USGS-Pennypack Woods	USGS-Ben Franklin Bridge	USGS-Chester	USGS-Reedy Island	PWD Buoy B	PWD Buoy P
N	5476	6521	5950	8502	5235	5405
R ²	0.98	0.95	0.55	0.97	0.58	0.92
RMSE	0.49	0.60	0.52	0.41	0.69	0.44
ubRMSE	0.41	0.59	0.77	0.41	0.69	0.44
Bias	0.27	0.06	-0.28	-0.06	-0.01	0.01
NSE	0.97	0.95	0.51	0.97	0.57	0.92
MAE	0.36	0.48	0.61	0.33	0.53	0.33
Skill Factor	0.99	0.96	0.95	0.99	0.97	0.98

Note: N stands for Number of observations.

Table 3-10: Statistical Metrics of Phytoplankton at USGS Stations and PWD-Buoys, 2018–2019.

Metrics	USGS-Pennypack Woods	USGS-Ben Franklin Bridge	USGS-Chester	USGS-Reedy Island	PWD Buoy B	PWD Buoy P
N	N/A	530	N/A	N/A	442	455
R ²	N/A	0.11	N/A	N/A	0.16	0.11
RMSE	N/A	5.45	N/A	N/A	5.75	4.15
ubRMSE	N/A	5.38	N/A	N/A	5.49	3.41
Bias	N/A	-0.56	N/A	N/A	-1.65	-2.43
NSE	N/A	-0.43	N/A	N/A	-0.05	-0.63
MAE	N/A	3.51	N/A	N/A	4.05	3.42
Skill Factor	N/A	0.55	N/A	N/A	0.61	0.38

Note: Continuous phytoplankton data are available only at USGS-Ben Franklin Bridge station and PWD Buoys B and P.

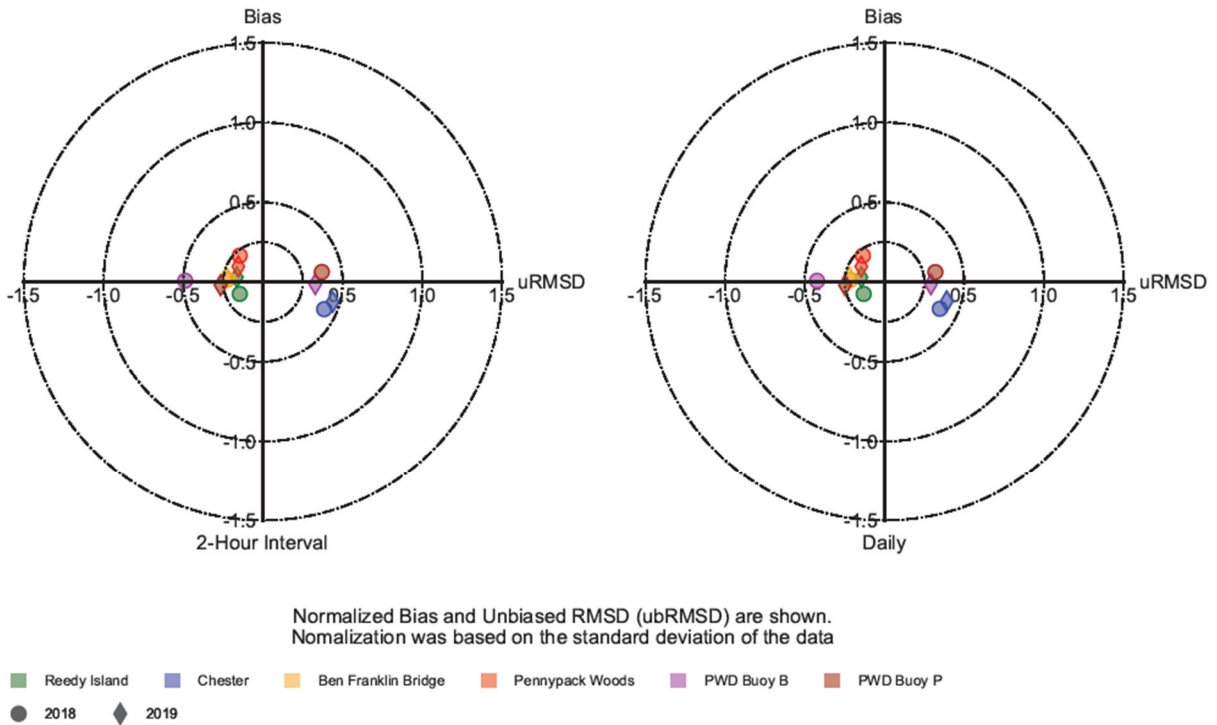


Figure 3-48: Target Diagram for Predicted DO at at Continuous Stations, 2018–2019

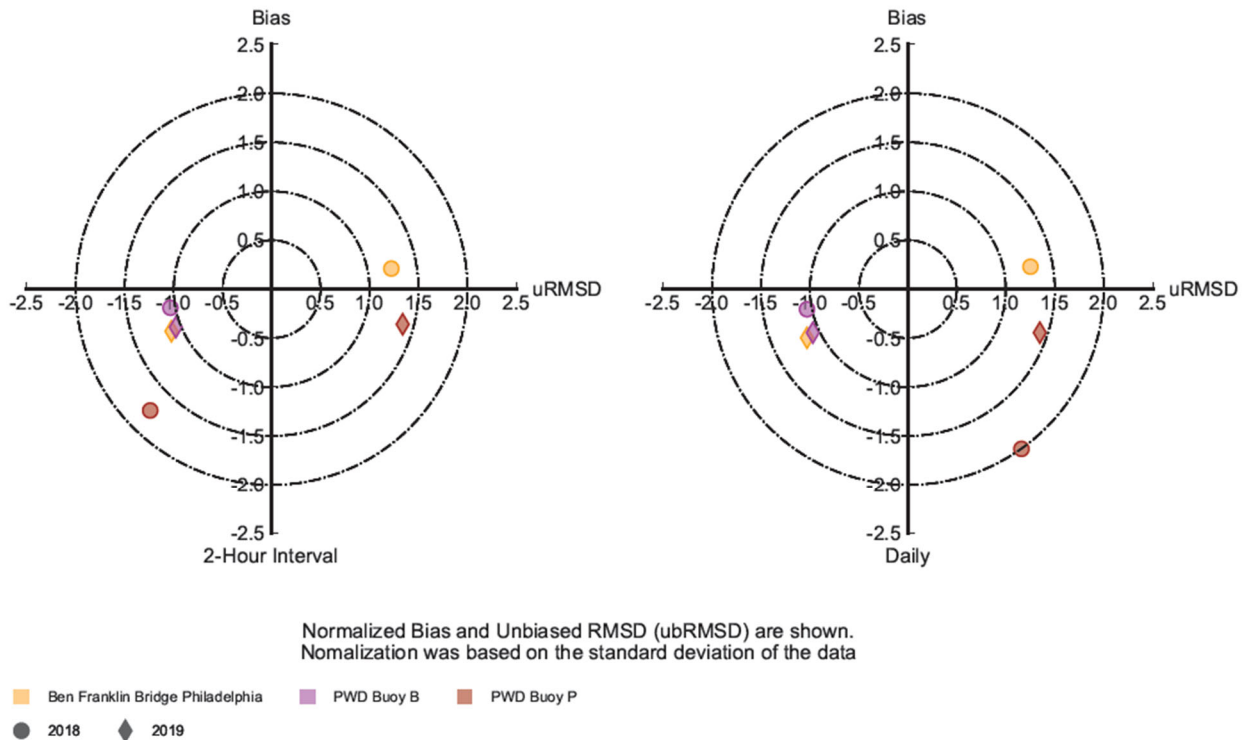


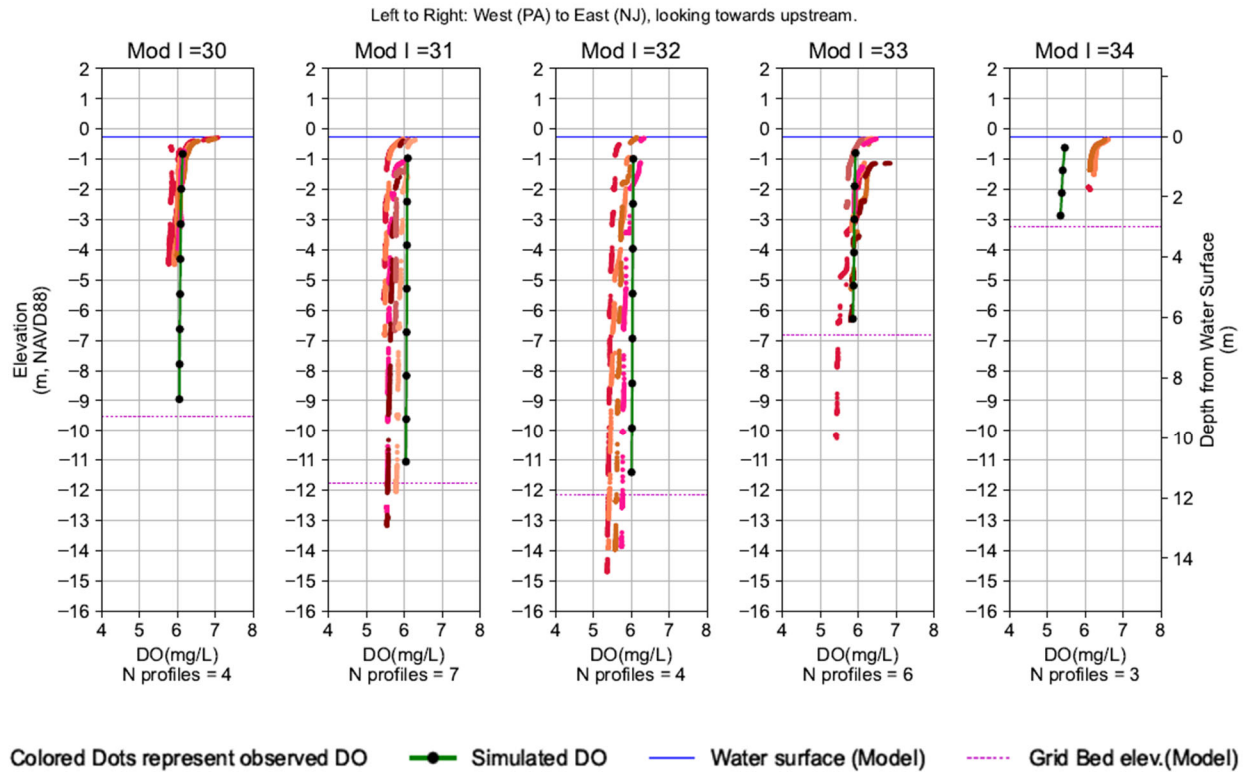
Figure 3-49: Target Diagram for Predicted Phytoplankton at Continuous Stations, 2018–2019

3.2.4.3 COMPARISONS TO TRANSECT DATA

Figure 3-50 through Figure 3-52 illustrate vertical profiles of predicted and measured dissolved oxygen concentrations across five transects near USGS stations during surveys conducted in 2018–2019 and 2012 (Table 3-6). The observed dissolved oxygen concentrations for different vertical profiles are shown as dots and grouped into model grid cells, with different colors (e.g., red, orange, and magenta) representing different measurement profiles (casting of sensors). The values of Mod I represent the model cell IDs across the transects from Pennsylvania shore (the smaller values) to New Jersey shore (the larger ones). These vertical profile data reflect the common perception that the Delaware Estuary is weakly stratified, especially in the urban area, e.g., about 0.5 mg/L differences in dissolved oxygen concentrations from the surface to bottom. Lateral variations show similar ranges of differences in dissolved oxygen concentrations, with New Jersey shore dissolved oxygen levels sometimes being slightly higher than those near the Pennsylvania shoreline.

Model results are shown as lines. The model simulations produced similar vertical and lateral structures to the measured dissolved oxygen profiles, although uncertainties exist in terms of the exact timings and locations for comparing the model-predicted and measured values. Model predictions align nearly on top of measured profiles at the two upstream transects near Pennypack Woods and Ben Franklin Bridge (except at one shallow cell near the New Jersey shore). Additionally, the model over-predicted dissolved oxygen concentrations up to about 0.5 ~ 0.8 mg/L at the two downstream transects near Delaware Memorial Bridge and Reedy Island, perhaps due to insufficient or lack of SOD and benthic flux forcing data to inform the model inputs in those areas. More importantly, the vertical gradients of predicted dissolved oxygen were consistent with those of observation.

Vertical Profile of Simulated and Observed DO at the Cross Section at RM 110.5, Pennypack Woods, 07-24-2019 11:04 to 07-24-2019 13:41



Vertical Profile of Simulated and Observed DO at the Cross Section at RM 100.0, Ben Franklin Bridge, 12-04-2019 10:54 to 12-04-2019 11:43

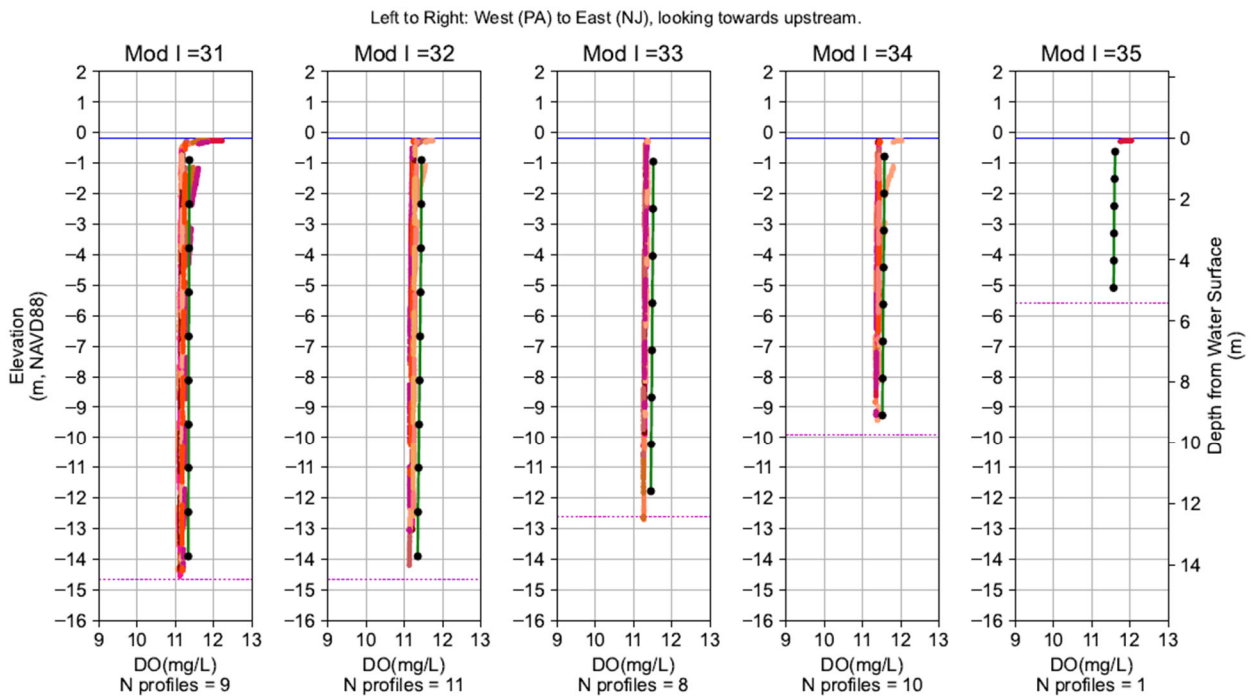
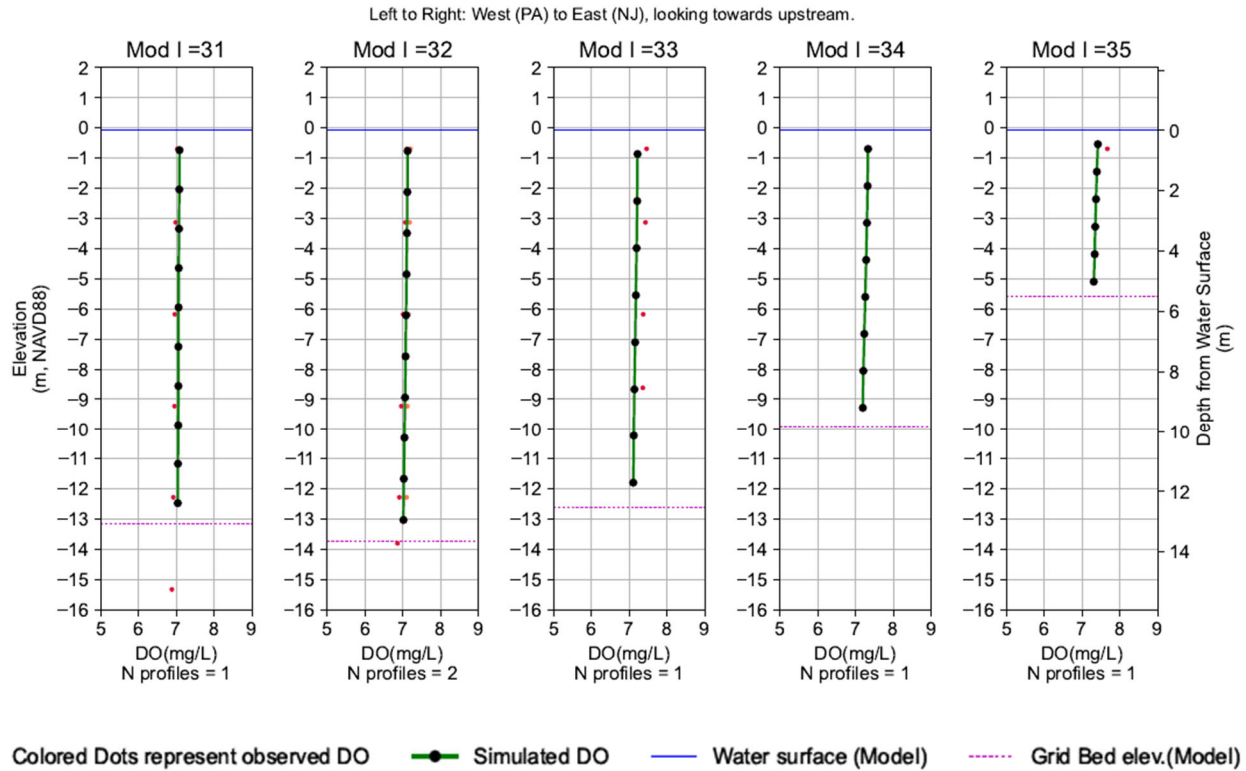


Figure 3-50: Model to Transect Data Comparisons at Pennypack Woods and Ben Franklin Bridge

Vertical Profile of Simulated and Observed DO at the Cross Section at
RM 100, USGS Station at Ben Franklin (RM 100), 10-11-2012 13:05 to 10-11-2012 14:03



Vertical Profile of Simulated and Observed DO at the Cross Section at
RM 68.9, Delaware Memorial Bridge, 07-19-2018 14:43 to 07-19-2018 15:35

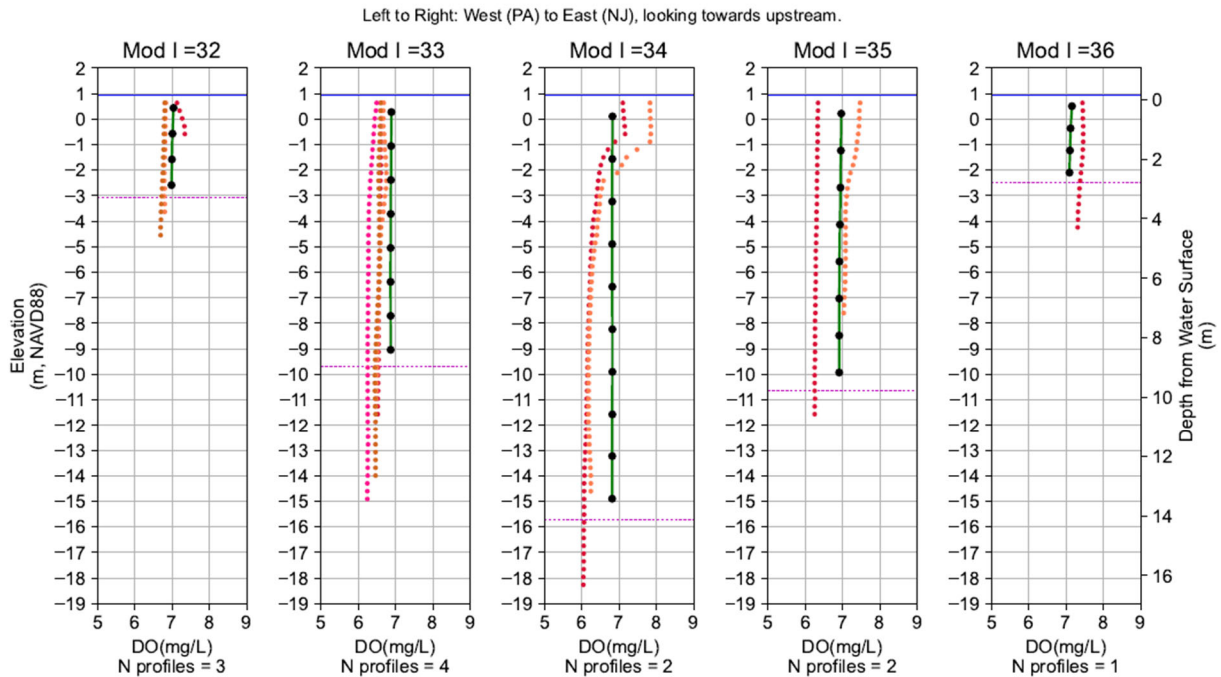


Figure 3-51: Model to Transect Data Comparisons at Ben Franklin and Delaware Memorial Bridges

Vertical Profile of Simulated and Observed DO at the Cross Section at RM 54.0, Reedy Island, 06-07-2019 12:30 to 06-07-2019 14:08

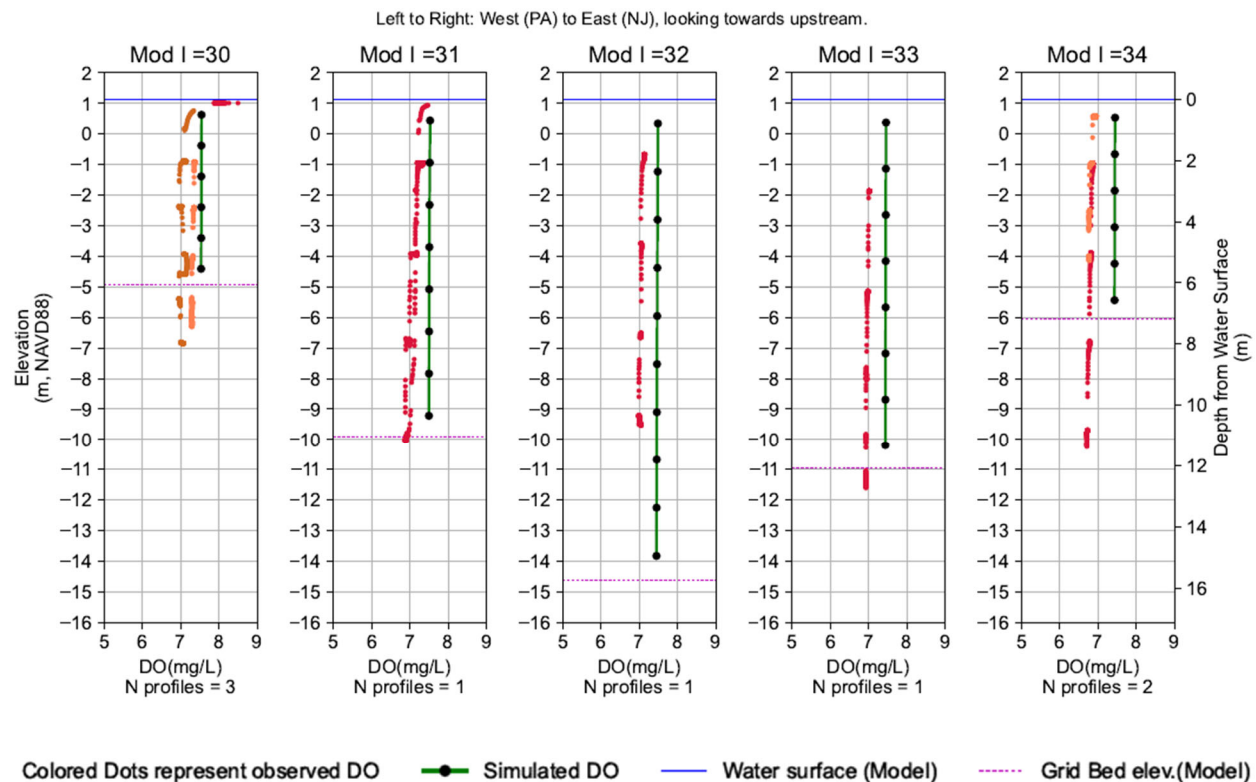


Figure 3-52: Model to Transect Data Comparisons at Reedy Island

3.2.5 DIAGNOSTIC ANALYSES

A series of diagnostic analyses were conducted to gain a better understanding of model performance and reliability and to help inform decisions about model acceptance and usability.

3.2.5.1 DISSOLVED OXYGEN COMPONENT ANALYSIS

The objective of this analysis is to understand what processes controlling dissolved oxygen and by how much. This was accomplished by assessing the WASP model output of dissolved oxygen components associated with different processes along the navigation channel.

Figure 3-53 presents the dissolved oxygen gain (as positive) and loss (as negative) in water column along the navigation channel during February (top panel) and July 2018 (bottom panel). The black solid lines represent the net dissolved oxygen flux (i.e., net impact), and the yellow dash line represents the net algal production (i.e., photosynthesis minus respiration). The complete set of dissolved oxygen component analysis results for the 2018–2019 calibration and the corroboration year of 2012 are provided in Appendix G. The results presented in Figure 3-53, which are monthly-averaged and displayed in a stacked-

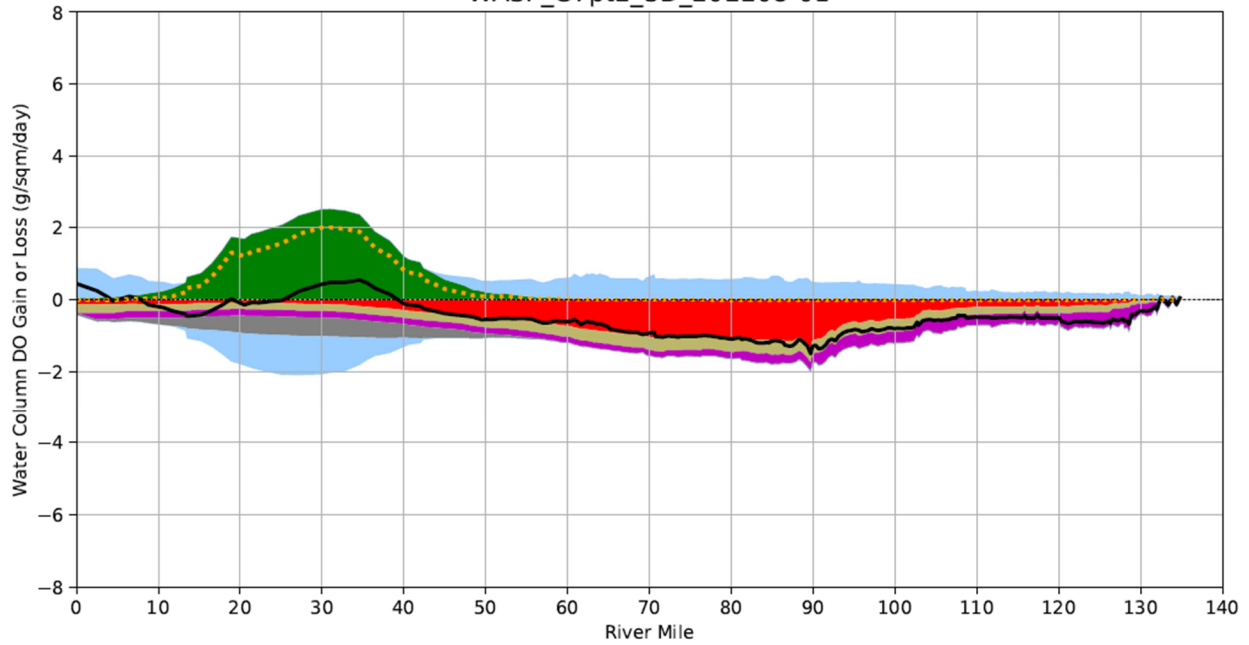
fashion, represent the dissolved oxygen gain/loss over the entire water column from mouth of the Bay (RM 0) to the head of the tide (RM 134).

For the model simulation of February 2018, the predicted major contributor to dissolved oxygen gain in the Bay is algal production (photosynthesis), which caused supersaturation in a portion of the Bay. As a result, reaeration transferred dissolved oxygen from water to atmosphere. Other loss terms in the Bay are algal respiration, followed by SOD and CBOD oxidation. In the tidal river, reaeration is the major contributor to the dissolved oxygen gain in water column. The contribution from algal production by freshwater diatoms is minimal during this wintertime month (i.e., part of the non-growing season). The major dissolved oxygen loss term is the nitrification, with CBOD oxidation and SOD being the second and third largest losses.

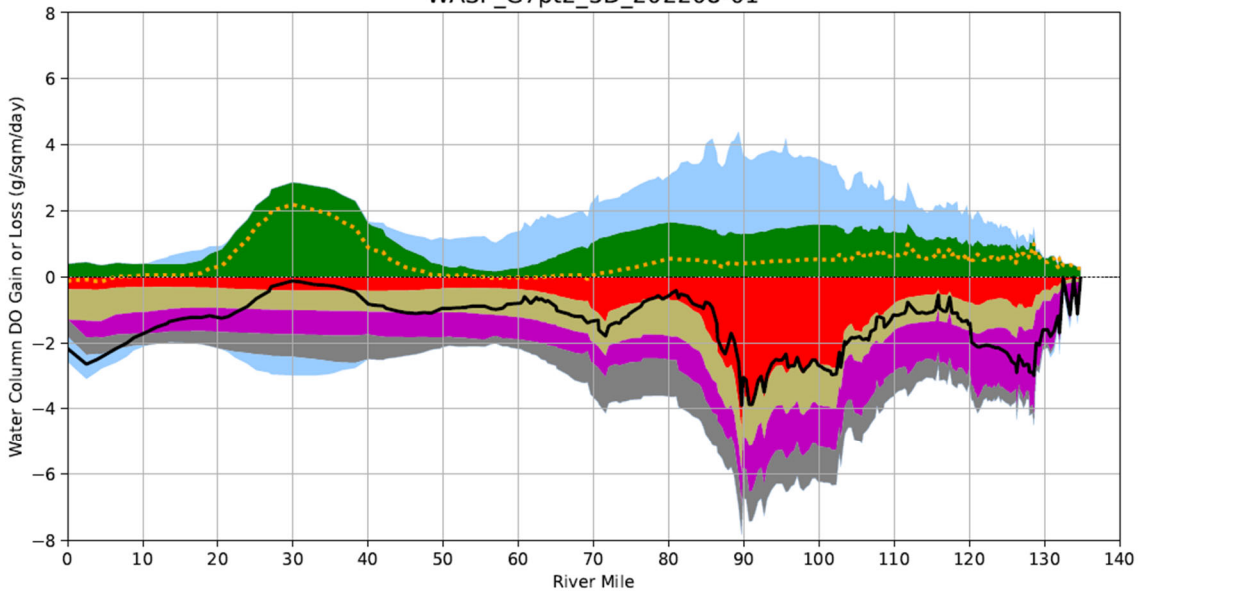
For the model simulation of July 2018, algal production remains the major contributor to the dissolved oxygen gain in the Bay. Major loss terms in the Bay are algal respiration and SOD, followed by CBOD oxidation, nitrification, and reaeration. In the tidal river, reaeration and algal production contribute a similar amount to dissolved oxygen gain. The principal dissolved oxygen loss term in the tidal river for this summer month is dominated by the nitrification, followed by SOD and CBOD oxidation.

This diagnostic analysis of dissolved oxygen components indicates that in the urban estuary, reaeration and photosynthesis are the major processes controlling dissolved oxygen production. The major processes affecting dissolved oxygen consumption within this reach of the urban estuary are nitrification, followed by SOD, CBOD oxidation, and respiration. The analysis also suggests that the dissolved oxygen gain from net algal production (yellow dash line) is much smaller than the dissolved oxygen loss caused by nitrification (red color zone) in the tidal river.

Simulated DO Gain (+) and Loss (-) from Different Processes, February 2018
WASP_G7pt2_3D_202208-01



Simulated DO Gain (+) and Loss (-) from Different Processes, July 2018
WASP_G7pt2_3D_202208-01



- Algae Production
- Nitrification (loss)
- SOD (loss)
- Algae Respiration (loss)
- Net DO Flux
- Net Algae Production
- Reaeration
- CBOD Oxidation (loss)

Figure 3-53: DO Component Analyses – February and July 2018

3.2.5.2 PHYTOPLANKTON LIMITING FACTORS

The objective of this model diagnostic was to ascertain which factors control phytoplankton growth and their relative seasonal importance. This was done by analyzing the growth-limiting factors associated with nutrients, light, and water temperature.

Figure 3-54 and Figure 3-55 present the limiting factors of nutrients (i.e., nitrogen, phosphorus, and silica) and light at Ben Franklin Bridge during 2019 at the water surface and water column depth-averaged, respectively. More figures of limiting factors at other locations and years are provided in Appendix G. Light and nutrient limiting factors were calculated based on Equations (3-11) and (3-12), which are multipliers applied to the user specified maximum growth rates in Equation (3-8). In other words, the values of limiting factors reflect a fraction of maximum growth rates.

Results in Figure 3-54, Figure 3-55, and Appendix G indicate that there is infrequent normal growth limitation associated with nitrogen and silica (i.e., limiting factor close to 1, almost 100% of the maximum growth rates), but some occasional perceptible growth-limitation for phosphorus. Strong vertical mixing in the tidal river results in nearly uniform distribution of nutrient concentrations in the vertical direction. As a result, the nutrient limiting factors at the water surface and depth-averaged are almost identical, as shown in Figure 3-54 and Figure 3-55.

Results in Figure 3-54 and Figure 3-55 suggest that light does constrain the phytoplankton growth as expected. Limiting factors are up to about 0.7 ~ 0.8 (i.e., 70% ~ 80% of the maximum) at water surface, while the depth-averaged values are up to about 0.1. Additional analysis indicates that light limiting factors decrease dramatically through water depth. For example, the light limiting factors may reduce from 0.7 ~ 0.8 at the surface layer to less than 0.2 at the second to the surface layer, and to close to zero at the third layer to the surface. This implies that only the top two layers have enough light to permit phytoplankton growth and the lower layers are almost completely dark. The vertical stratification in light limiting factor is caused by the high turbid environment in the Delaware Estuary. Longitudinally, figures in Appendix G indicate that light limiting factors at upper portion of the estuary are a little larger (e.g., 0.8 ~ 0.9 during summer at Pennypack Woods) than those at the downstream portions (e.g., around 0.7 during summer at Ben Franklin Bridge, Chester, and Reedy Island). In other words, light at the upper portion may be relatively easier to penetrate through water column.

Figure 3-56 illustrates the limiting factors associated with water temperature at Eddystone (RM 84) for three groups of phytoplankton during 2019. The patterns of temperature limiting factors at other locations and years are similar. Temperature limiting factors were calculated based on Equations (3-9) and (3-10). The maximum value of 1.0 corresponds to the optimal temperature for growth, which are part of calibration parameters (see Section 3.2.3): 4.3, 22.5, and 26.3 °C, for phytoplankton group 1, 2, and 3, respectively. When water temperature is not at the relevant optimal temperature, phytoplankton growth is constrained. In other words, temperature always defines the upper bound envelope for phytoplankton growth rate, and light and nutrients control the specific growth rates within this envelope.

This diagnosis indicates that (1) nutrients, light and temperature can all limit phytoplankton growth, consistent with Equation (3-8); and (2) regardless of temperature, phytoplankton is more limited by light than by nutrients.

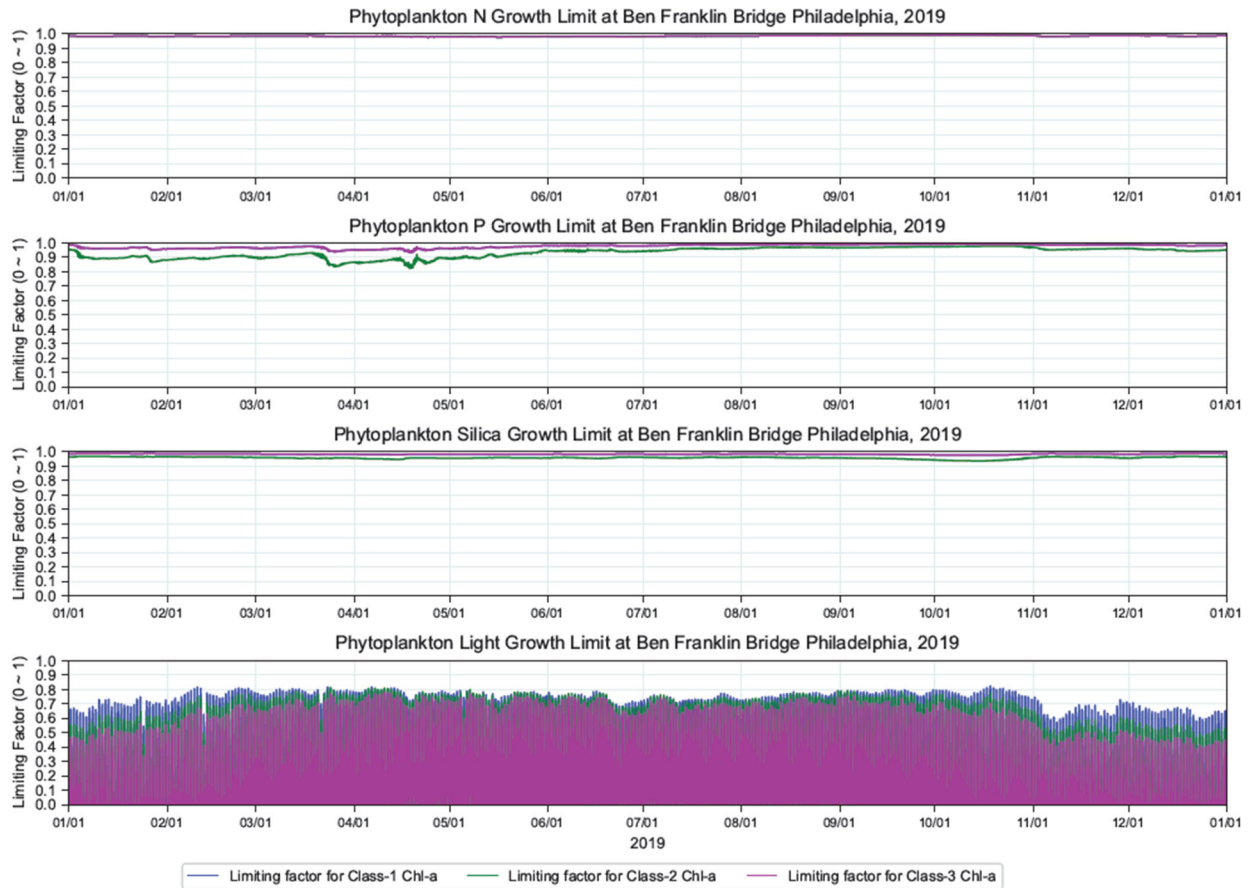


Figure 3-54: Alga Growth Limiting Factors at Ben Franklin Bridge during 2019 – Water Surface

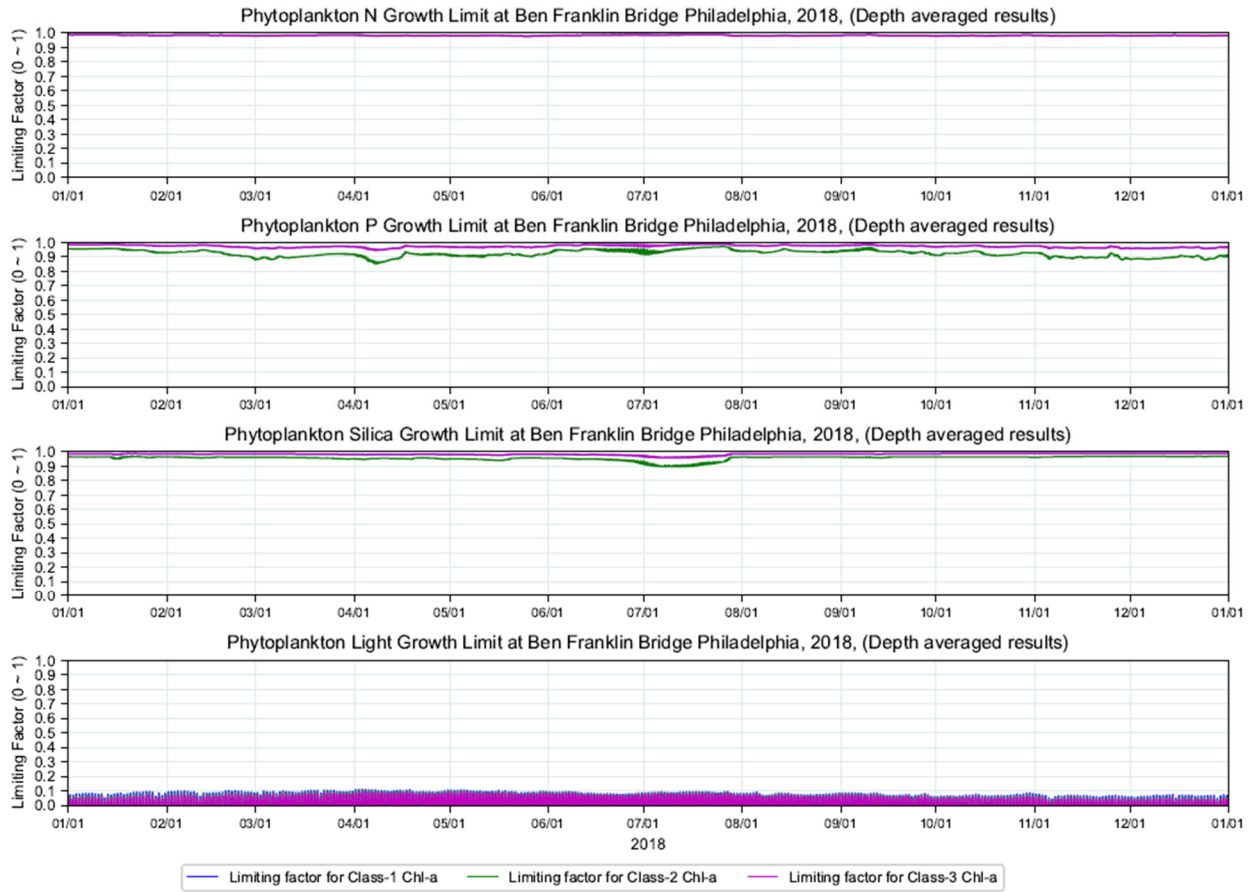


Figure 3-55: Algal Growth Limiting Factors at Ben Franklin Bridge during 2019 – Depth-averaged

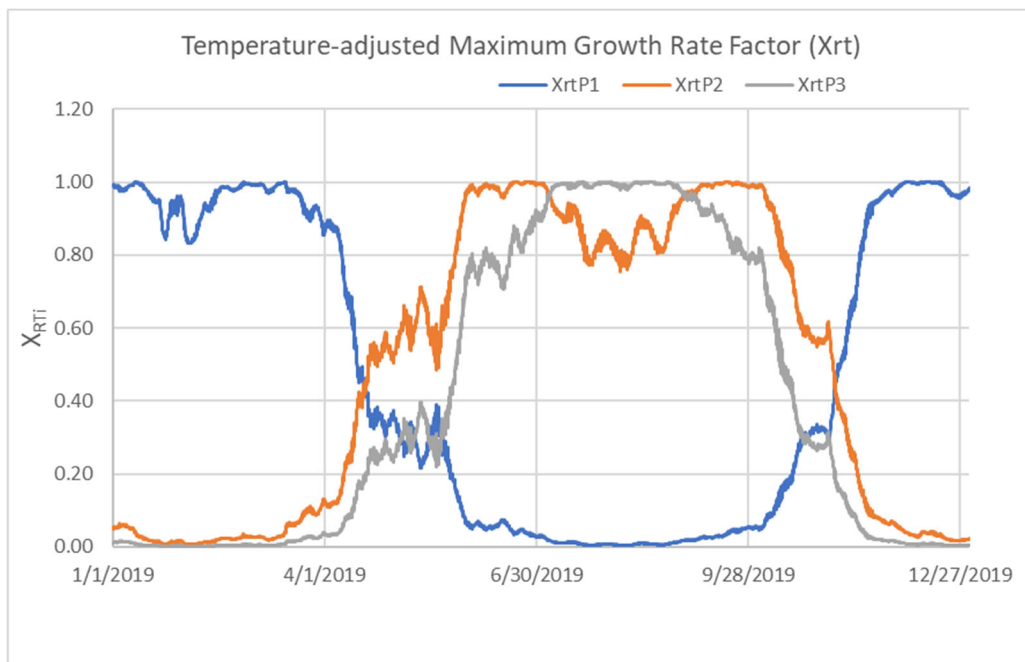


Figure 3-56: Temperature Limiting Factors at Eddystone during 2019

3.2.5.3 ZONE-2 LIGHT ATTENUATION DIAGNOSIS

Previously discussed model diagnostic tests evaluated potential factors causing the under-prediction of algal bloom in the tidal river during June–July 2019, including temperature, boundary loads of phytoplankton, kinetic specifications, random variations to the existing light extinction coefficients, nutrient limiting factors, and hydrodynamics. The conclusion is that these factors are unlikely to be causing the problem. On the other hand, the diagnosis in the previous section indicates that light largely controls the growth of phytoplankton in the Delaware Estuary. One hypothesis is that the existing light extinction formulation may not capture all the necessary mechanisms governing water column light attenuation, although the model generally does a good job reproducing the observed light extinction coefficients K_e during the DRBC Boat Run surveys (Figure 3-32 and Appendix G). In this section, we dig deeper into this issue.

Dr. Chant (one of DRBC expert panel members) and his colleagues have extensively studied the physical and biological processes of Delaware Estuary, which may shed some light on resolving the puzzle. The following two paragraphs are Dr. Chant’s findings:

“It has long been recognized the primary production in Delaware Bay is light limited [Pennock, 1985]. The predominant physical factor limiting light, and thus phytoplankton biomass, is suspended sediment [McSweeney et al., 2017]. In tidal rivers heavy loads of sediment are supplied to the system during high river flow events which are temporarily stored at the bed in the upper reaches of the river. The finer sediments deposited by these events are reworked by tidal currents and remain in suspension [Ralston and Geyer, 2017] and thus persistently limit light levels and primary production. Tidal resuspension, and thus sediment concentration, is proportional to tidal current amplitude. In the Delaware River tidal currents in main channel are between 80-120 cm/s throughout much of the estuary but rapidly fall off to near zero at the head of the estuary at Trenton [Pareja-Roman et al., 2020] thus we expect water clarity to increase in the upper reaches of the river. Indeed, observations of light levels in the upper reach of the river during low flow conditions reveal that the depth penetration of the 1% light level increases from a depth of less than 5 meters at the ETM around km 100 to nearly 10 m at km 200 at Trenton (Figure 3-57). Coincident with the elevated light levels are elevated Chlorophyll concentration (3B) and elevated oxygen levels (3D) all consistent with elevated primary production in this reach of the river. I note that in our field survey in 2011 also observed elevated Chlorophyll in the upper reaches of the river. In an ensuing river flow event these water masses, would be advected down-stream and influence water quality throughout the system.”

“An example of this phenomena occurred in June of 2019 when a series of high river flow events was followed by increased chlorophyll concentrations at Ben Franklin Bridge (Figure 3-58). Here, the model needed to increase water clarity in the upstream reaches of the river to produce this biomass that was produced upstream and later advected down-stream by elevated river flow events.”

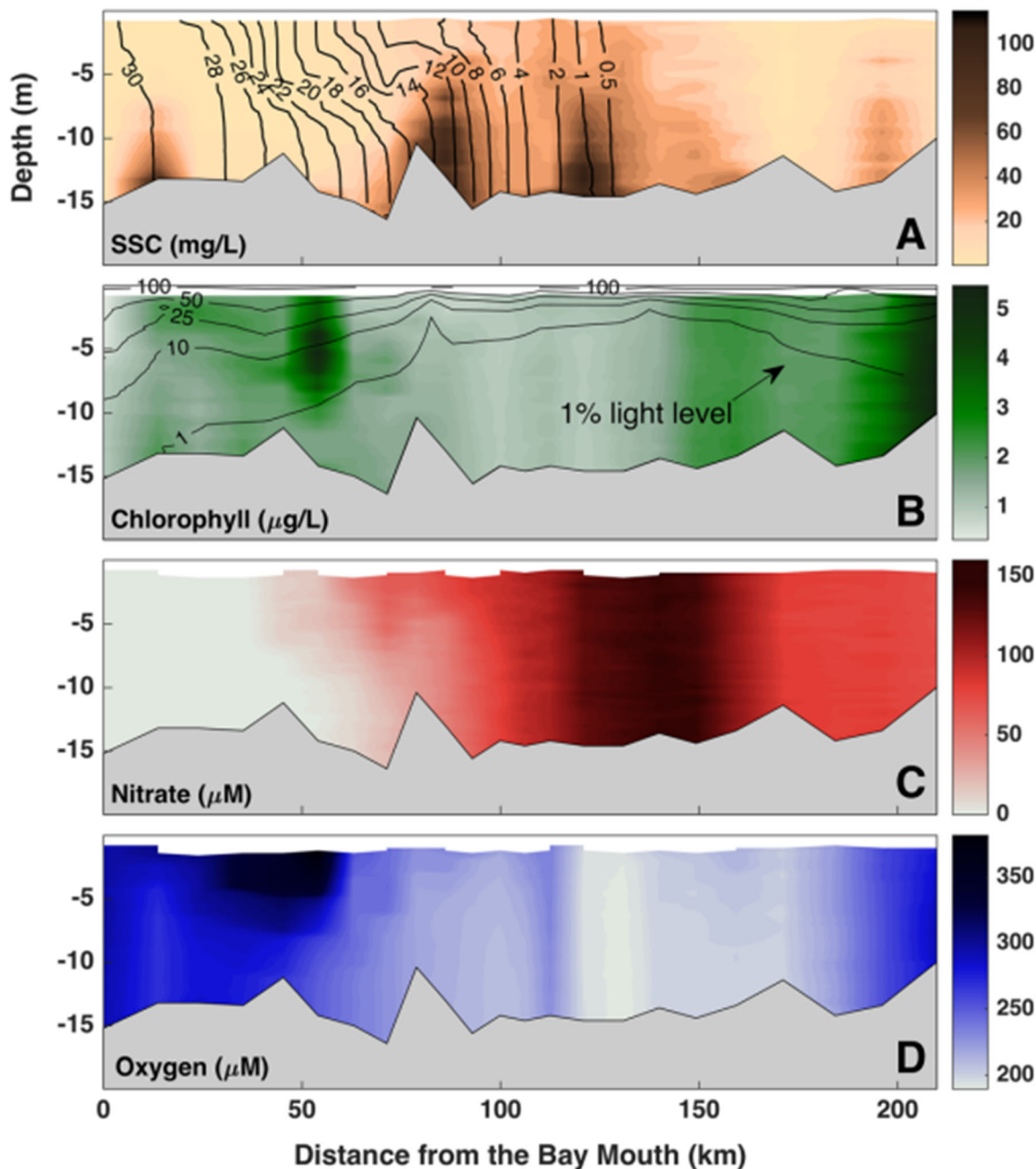


Fig. 3 June 2010 along channel distribution of sediment (mg/L), chlorophyll ($\mu\text{g/L}$), nitrate (μM), and dissolved oxygen (μM). *Black contours in top panel are salinity and contours in second panel are PAR as a percentage of that at the surface*

Figure 3-57: Figure 3 from McSweeney et al. 2017

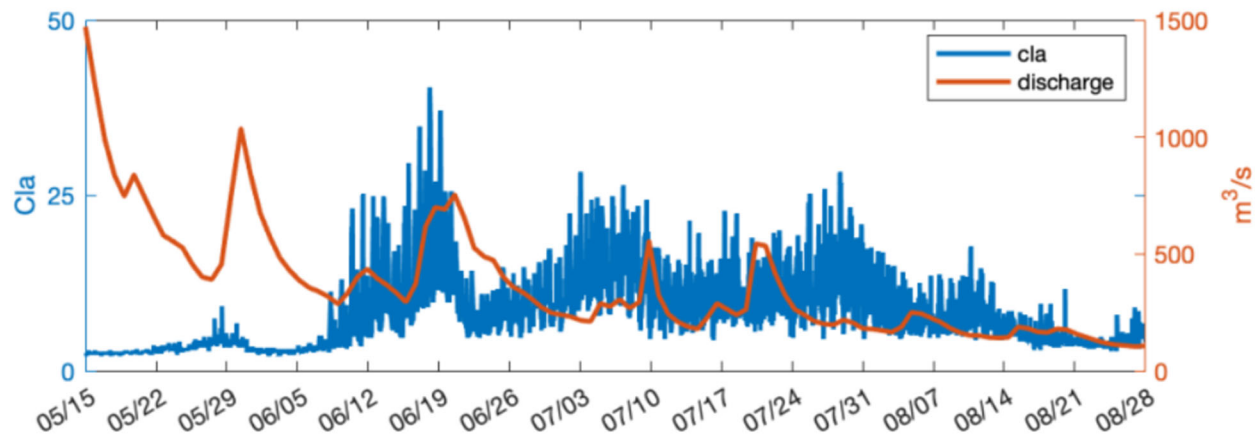


Figure 3-58: Chlorophyll at Ben Franklin Bridge and River Discharge Flow at Trenton, 2019

Upon closer examination, it was determined that the model simulation sometimes does over-predict light extinction coefficient K_e in Zone-2 (RM >108.7), especially during the growing season of freshwater diatom (i.e., April 15 to August 31). Top left panel of Figure 3-59 shows this case for June 2019. To test Dr. Chant's idea, we made a seasonal adjustment to the light extinction coefficient, i.e., multiplied the existing K_e values by 0.55 in Zone-2 for the period of May 1 to July 15.

The complete set of model simulation results for K_e , phytoplankton, and dissolved oxygen from the sensitivity test are provided in Appendix G. Some key results are provided here for discussion.

Figure 3-59 presents the comparisons of K_e between the base case (calibration) and the seasonal adjustment test. The seasonal adjustment forced the predicted K_e to be better matched with data for the Boat Run survey on June 17, 2019.

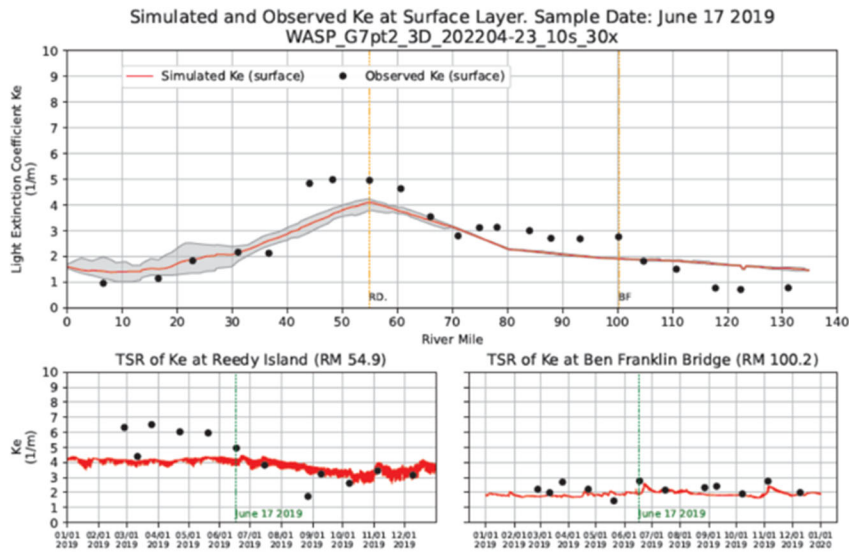
Figure 3-60 shows the comparison of phytoplankton concentrations between the base case and the seasonal adjustment test in three stations (Ben Franklin Bridge, Buoys B and P) with continuous data. With the seasonal adjustment of K_e , the predicted phytoplankton concentrations (blue lines) reflect the blooms that were observed at Ben Franklin Bridge and Buoy B during June–July 2019, but over-predict the blooms during June–July 2018. The model also over-predicted the observed bloom in Buoy P during summer 2019.

Figure 3-61 illustrates the comparison of phytoplankton Chl-a and dissolved oxygen concentrations between the base case and the seasonal adjustment test for the USGS station at Pennypack Woods. The seasonal adjustment caused the model to over-predict phytoplankton Chl-a concentrations and the consequent dissolved oxygen concentrations at this location.

Figure 3-62 presents a comparison of the simulated dissolved oxygen concentrations between the base case and the seasonal adjustment test at the USGS station at Ben Franklin Bridge. With more phytoplankton being introduced by the seasonal adjustment during June–July in 2018–2019, the model over-predicted dissolved oxygen concentrations during these two periods.

The seasonal adjustment confirms Dr. Chant's finding, i.e., the algal blooms in the tidal river could be caused by the growth of phytoplankton at the upper portion of the estuary (e.g., Zone-2) due to more clarity and the subsequent advection to downstream reaches. The results from this diagnosis also indicate that a mechanistic adjustment of K_e may be needed to achieve further improvement in the model representation of summer algal blooms and the associated effect of increasing dissolved oxygen levels.

Calibrated Model



Seasonal adjustment: multiply light extinction coef. by 0.55 for the period of 5/1 ~ 7/15

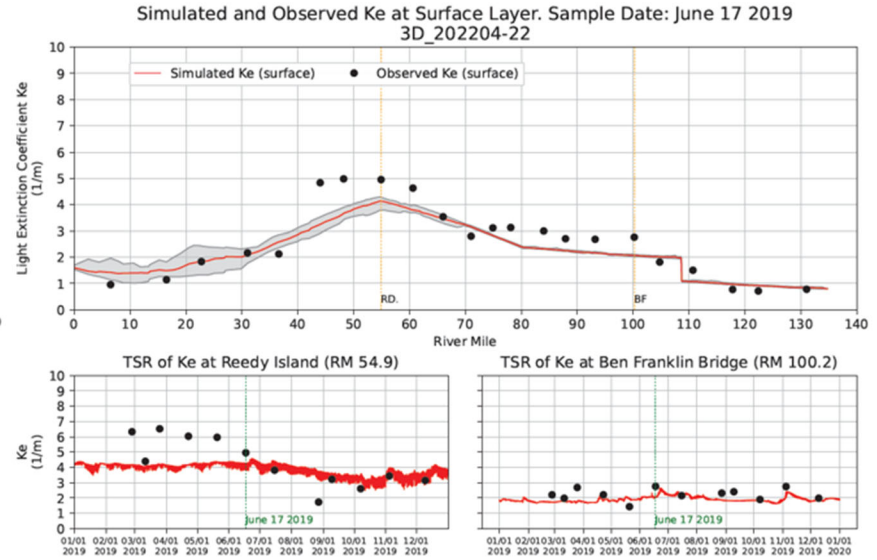


Figure 3-59: Comparisons between Base Case and Seasonal Adjustment – Ke

Note “TSR” stands for Time Series

Calibrated Model

Seasonal adjustment: multiply light extinction coef. by 0.55 for the period of 5/1 ~ 7/15

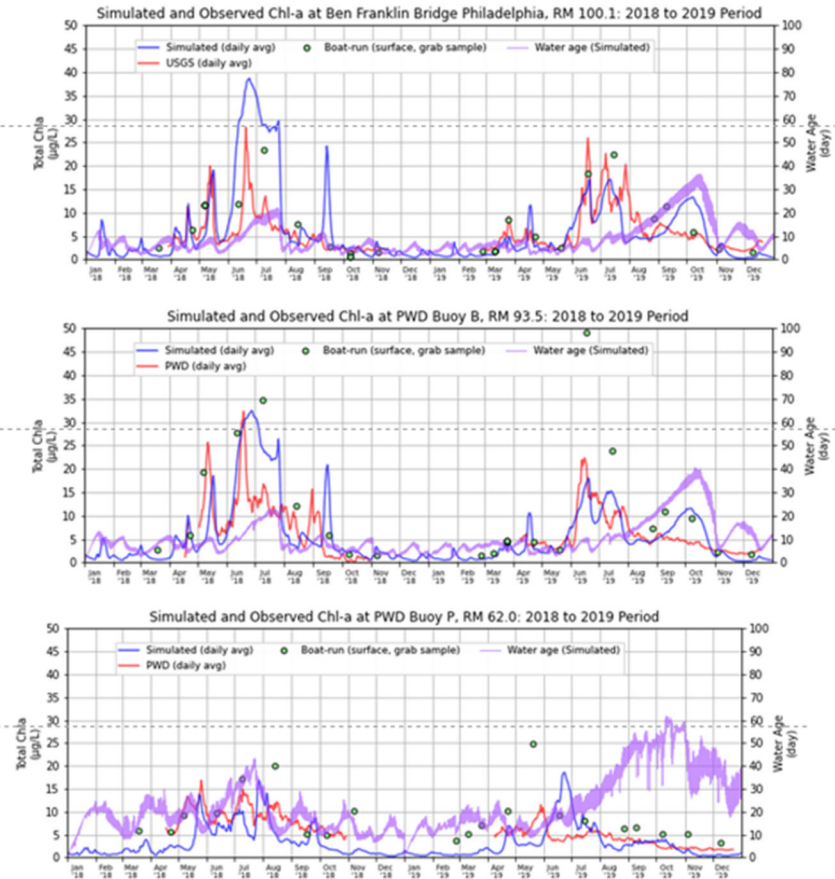
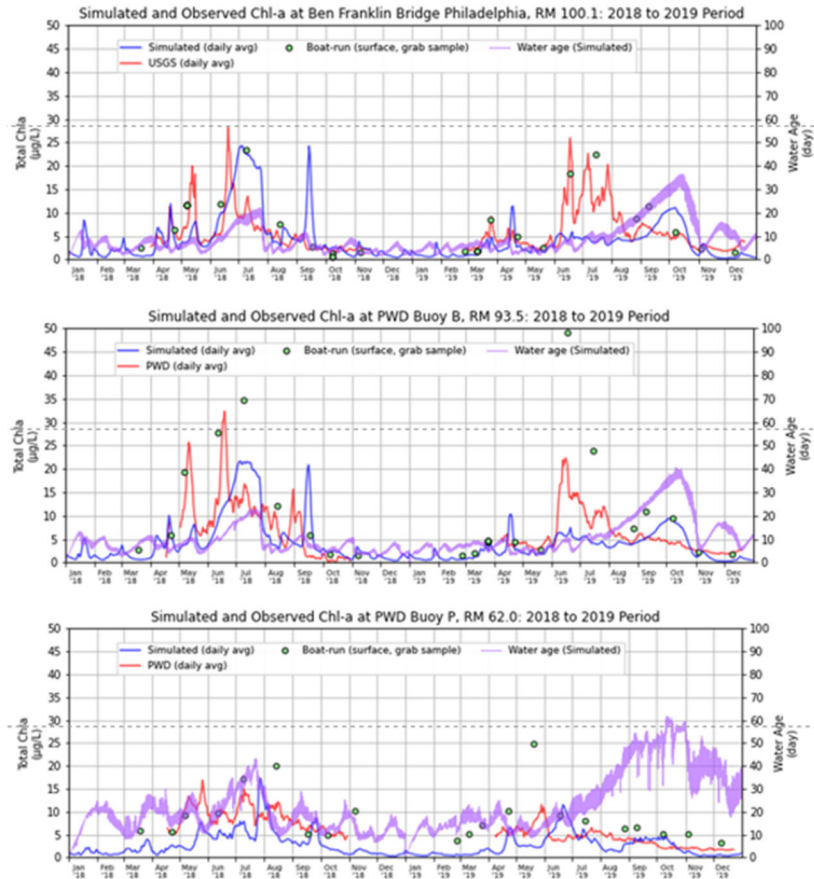
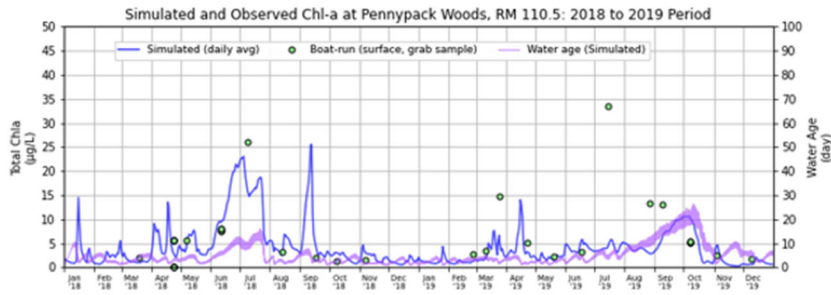


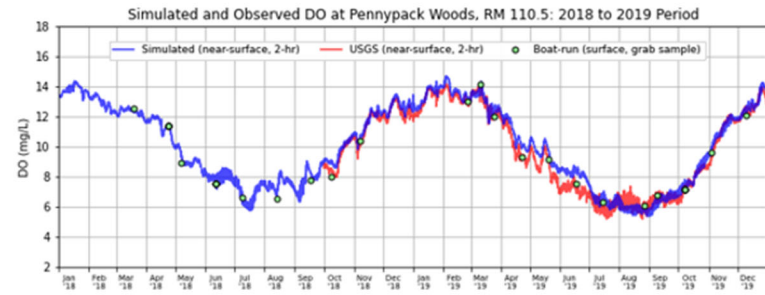
Figure 3-60: Comparisons between Base Case and Seasonal Adjustment - Phytoplankton

Phytoplankton Chl-a



Base Case

Dissolved Oxygen



Zone 2 light sensitivity

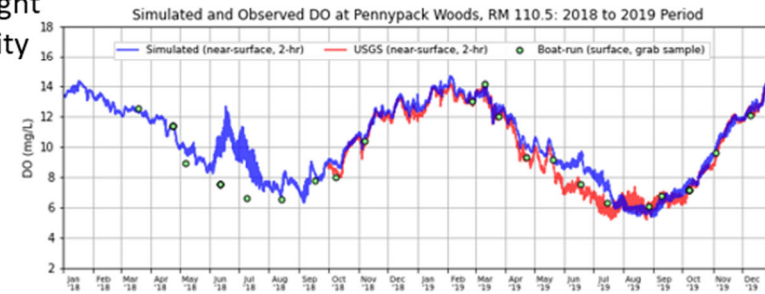
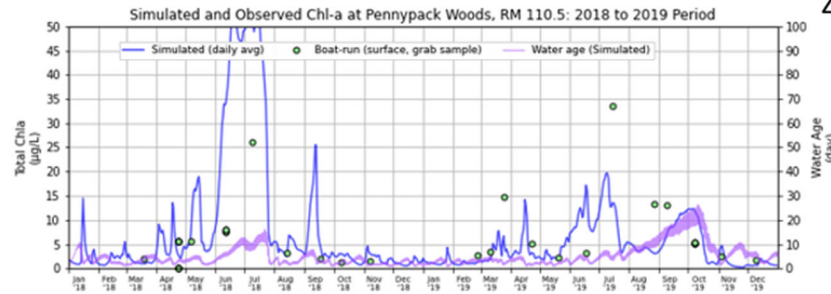
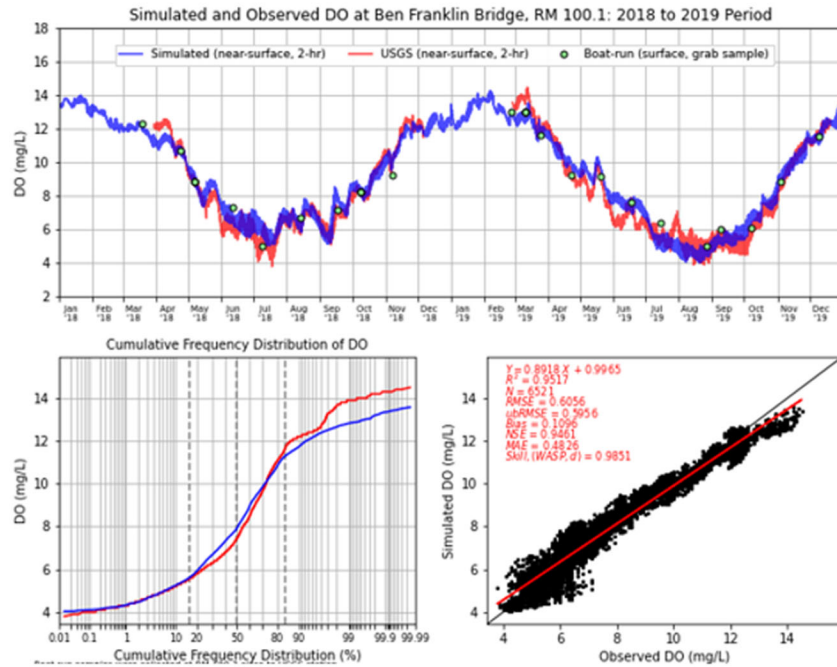


Figure 3-61: Base Case and Seasonal Adjustment Comparisons – Phytoplankton and DO

Calibrated Model



Seasonal adjustment: multiply light extinction coef. by 0.55 for the period of 5/1 ~ 7/15

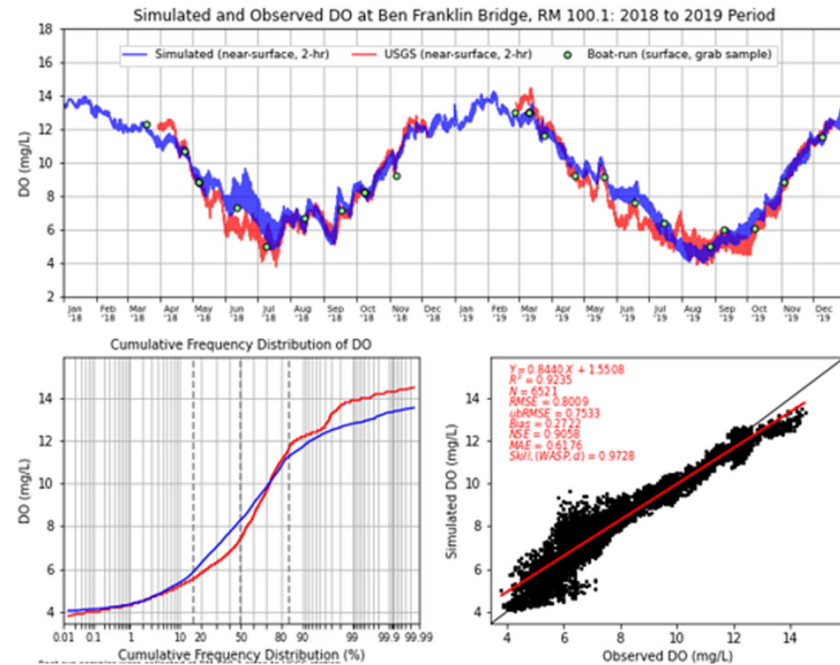


Figure 3-62: Base Case and Seasonal Adjustment Comparisons – DO at Ben Franklin Bridge

3.2.6 EVALUATION OF MODEL ACCURACY, RELIABILITY, AND UNCERTAINTY

Independent data collected over a multi-year period have been used to evaluate the model accuracy and reliability. A variety of comparison plots, together with various statistical metrics, have been generated to thoroughly investigate the model performance. The comparison plots include the formats of spatial distribution, time series, 1-to-1 comparison, cumulative frequency distribution, and target diagram. The model was well-calibrated to the intensive project dataset that is available for 2018–2019, with high flows in 2018 and medium flows in 2019, as well as moderately low dissolved oxygen in both years. One exception to the generally good model-data comparisons is that the model missed the observed algal bloom in the tidal river during summer 2019. The model successfully hindcasted historical conditions in 2012 with low flows and low dissolved oxygen. The model corroboration was performed using 2012 available flows, boundary conditions, and forcing functions without changing calibration coefficients. Model predictions are quantitatively consistent with observed data across a range of flow and dissolved oxygen conditions. The ability of the model to match these year-to-year patterns of data provides strong support that (1) the parameterization and kinetics currently used by the model are effective in representing the most important processes controlling the Delaware Estuary water quality; and (2) the model captures the principal mechanisms affecting dissolved oxygen in the Delaware Estuary.

As with any mathematical model of a natural system, the parameters contain uncertainty, which stems from both incomplete information and natural variability in the data upon which they are based. Ideally, quantitative analyses to evaluate the impact of that uncertainty on model predictions would be conducted. However, something like a comprehensive Monte Carlo uncertainty analysis for the Delaware Estuary water quality model, incorporating each model parameter, is not possible because uncertainty distributions are not known for every parameter and the actual timeframe required for performing the necessary model simulations would be prohibitive (e.g., tens of months and perhaps multiple years of computational time using the same up-to-date computer hardware on which model calibration was conducted). To address this, a series of sensitivity analyses were conducted to evaluate calibration uncertainty. Sensitivity analyses was conducted to identify the extent to which model predictions were affected by uncertainty in the model parameters. Parameters evaluated in the sensitivity analyses were chosen based upon professional judgment, which in turn was based upon a large number of model simulations performed in the process of model calibration. Two criteria were kept in mind: 1) the model is likely to be sensitive to variation in the value of the parameter, within the bounds of its uncertainty; and 2) parameters that are likely to affect the dissolved oxygen should be the primary focus.

Twenty model parameters were chosen for sensitivity analysis (Table 3-11). Each parameter/input was increased or decreased by 10%. The sensitivity of the calibrated model to uncertainty in the parameters was evaluated and quantified by repeating the 2019 simulation in a 2-D mode using the modified input values. The resulting ranges for the model-predicted dissolved oxygen concentration changes relative to the base case are listed column in Table 3-11. The most sensitive parameters are all related to phytoplankton processes, e.g., maximum growth rates, respiration rates, optimal temperature for growth,

and optimal light saturation (Figure 3-63 to Figure 3-67). The complete set of figures for sensitivity analysis is included in Appendix H. Each page of the figures corresponds to a parameter in the sensitivity analysis. The top panels depict the time series of dissolved oxygen concentration changes relative to the base case at four USGS stations and two PWD buoys due to $\pm 10\%$ changes for a given parameter. It is a little hard to identify each line/simulation in the plots, but the line envelopes demonstrate how sensitive the model is to the change of a given parameter. For instance, a $\pm 10\%$ change in the maximum growth rate constants for three phytoplankton groups and group-2 results in dissolved oxygen variations up to 1.2 and 0.5 mg/L or 20% and 8% change in dissolved oxygen concentration, respectively; a $\pm 10\%$ change in the respiration rate constants for three groups generates dissolved oxygen variations up to 1.0 mg/L or 12% change in dissolved oxygen concentration; a $\pm 10\%$ change in the optimal temperature for growth three phytoplankton groups produces dissolved oxygen variations up to 0.4 mg/L or 6% change in dissolved oxygen concentration; a $\pm 10\%$ change in the optimal light saturation for the three phytoplankton groups creates dissolved oxygen variations up to 0.4 mg/L or 5% change in dissolved oxygen concentration; and all other parameter changes cause less changes in dissolved oxygen concentrations. Most of the changes in the dissolved oxygen concentrations happen in the period of June-October 2019, with maximum changes focused on the September-October, when the model predict a phytoplankton bloom.

The bottom panels in the sensitivity plots present the target diagrams of dissolved oxygen model-data comparisons at the USGS stations and PWD buoys for the base case, and the cases with 10% decrease and increase in the parameters. Overall, the patterns in the target diagrams change insignificantly between the base and sensitivity tests, except for the case with maximum growth rate constants for all groups. Detailed information on target diagram is available in Section 3.2.4.2.

Note that another significant uncertainty in the model – light attenuation, was diagnosed and discussed in the previous section and therefore not included here.

Table 3-11: Parameters Chosen in Sensitivity Analysis

Description	Units	Base Value	Increase	Decrease	ΔDO Range	ΔDO Range (%)
Phytoplankton Maximum Growth Rate Constant (Group 2)	per day	3.75	4.125	3.375	0.5	8.0
Phytoplankton Maximum Growth Rate Constant (Group 1,2,3)	per day	3.92	4.308	3.525	1.2	20.0
Phytoplankton Carbon to Chlorophyll Ratio	mg C/mg Chl	40	44	36	0.3	4.1
Phytoplankton Death Rate Constant (Non-Zoo Predation; Group 2)	per day	0.08	0.088	0.072	0.1	2.0
Phytoplankton Respiration Rate Constant (Group 2)	per day	0.05	0.055	0.045	0.1	1.5
Phytoplankton Respiration Rate Constant (Group 1,2,3)	per day	0.037	0.040	0.033	1.0	12.0
Phytoplankton Respiration Temperature Coefficient (Group 2)	dimensionless	1.072	1.079	1.065	~ 0.0	0.5
Optimal Temperature for Growth (Group 2)	deg C	22.5	24.75	20.25	0.2	4.0
Optimal Temperature for Growth (Group 1,2,3)	deg C	17.7	19.47	15.93	0.4	6.0
Phytoplankton Settling Rate (Group 2)	m/day	0.100	0.110	0.090	~ 0.0	0.2
Sediment Oxygen Demand ¹	g/m ² -day	1.012	1.114	0.911	0.2	4.0
Theta -- SOD Temperature Correction	dimensionless	1.065	1.072	1.059	0.1	1.5
Nitrification Rate Constant	per day	0.600	0.660	0.540	0.1	0.8
Dissolved Organic Nitrogen Mineralization Rate Constant	per day	0.010	0.011	0.009	~ 0.0	0.5
CBOD Decay Rate Constant (Watershed)	per day	0.033	0.037	0.030	0.1	1.0
CBOD Decay Rate Constant (Point Source)	per day	0.087	0.0957	0.0783	~ 0.0	0.5
Phytoplankton Optimal Light Saturation (chla 1)	watts/m ²	100	110	90	0.1	0.5
Phytoplankton Optimal Light Saturation (chla 2)	watts/m ²	150	165	135	0.2	3.0
Phytoplankton Optimal Light Saturation (chla 3)	watts/m ²	200	220	180	0.3	4.0
Phytoplankton Optimal Light Saturation ² (chla 1,2,3)	watts/m ²	150	165	135	0.4	5.0

¹ Average rate across bottom segments

² Average optimal light saturation for three classes

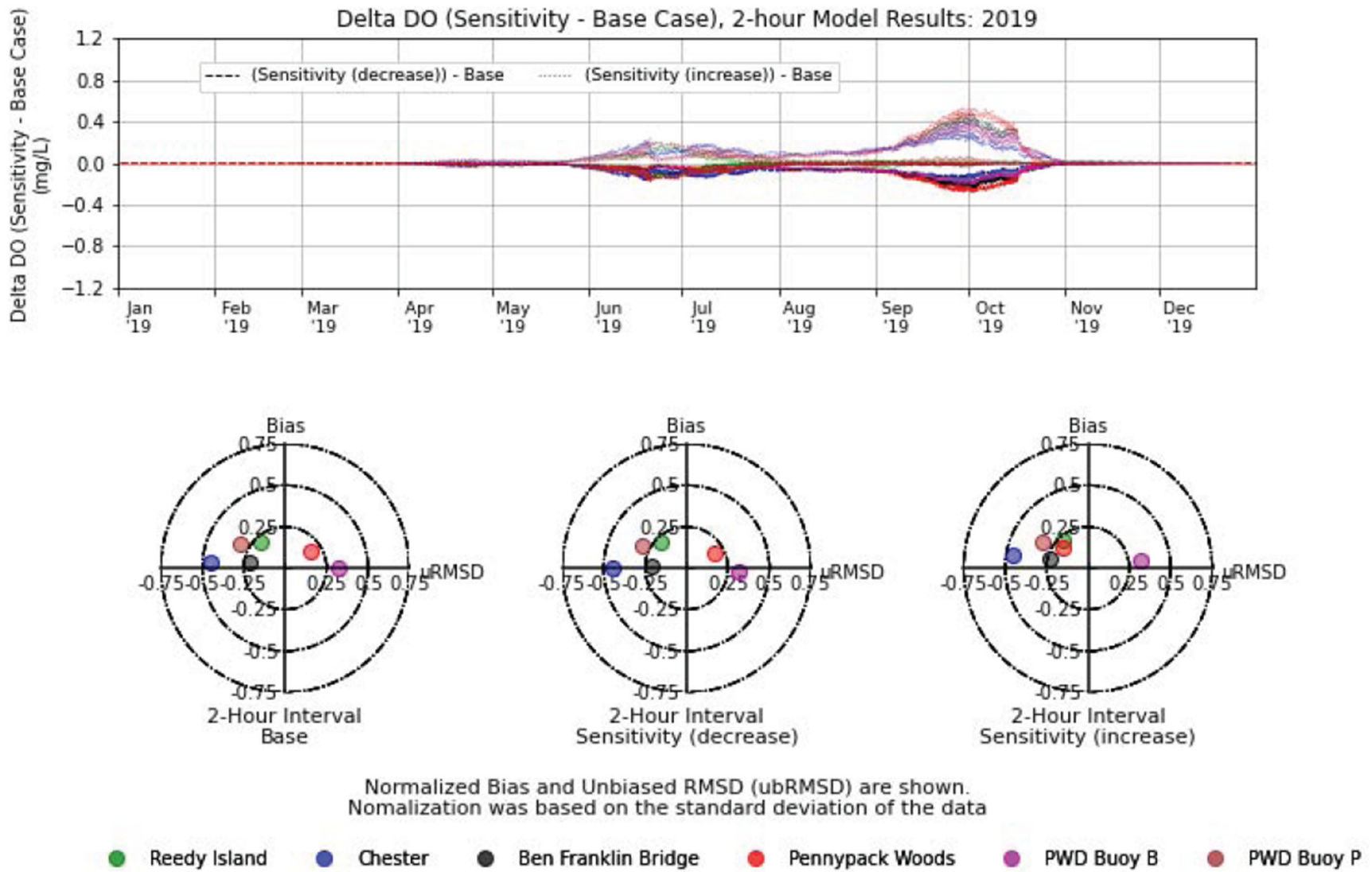


Figure 3-63: Sensitivity Test: Phytoplankton Maximum Growth Rate Constant (Group 2)

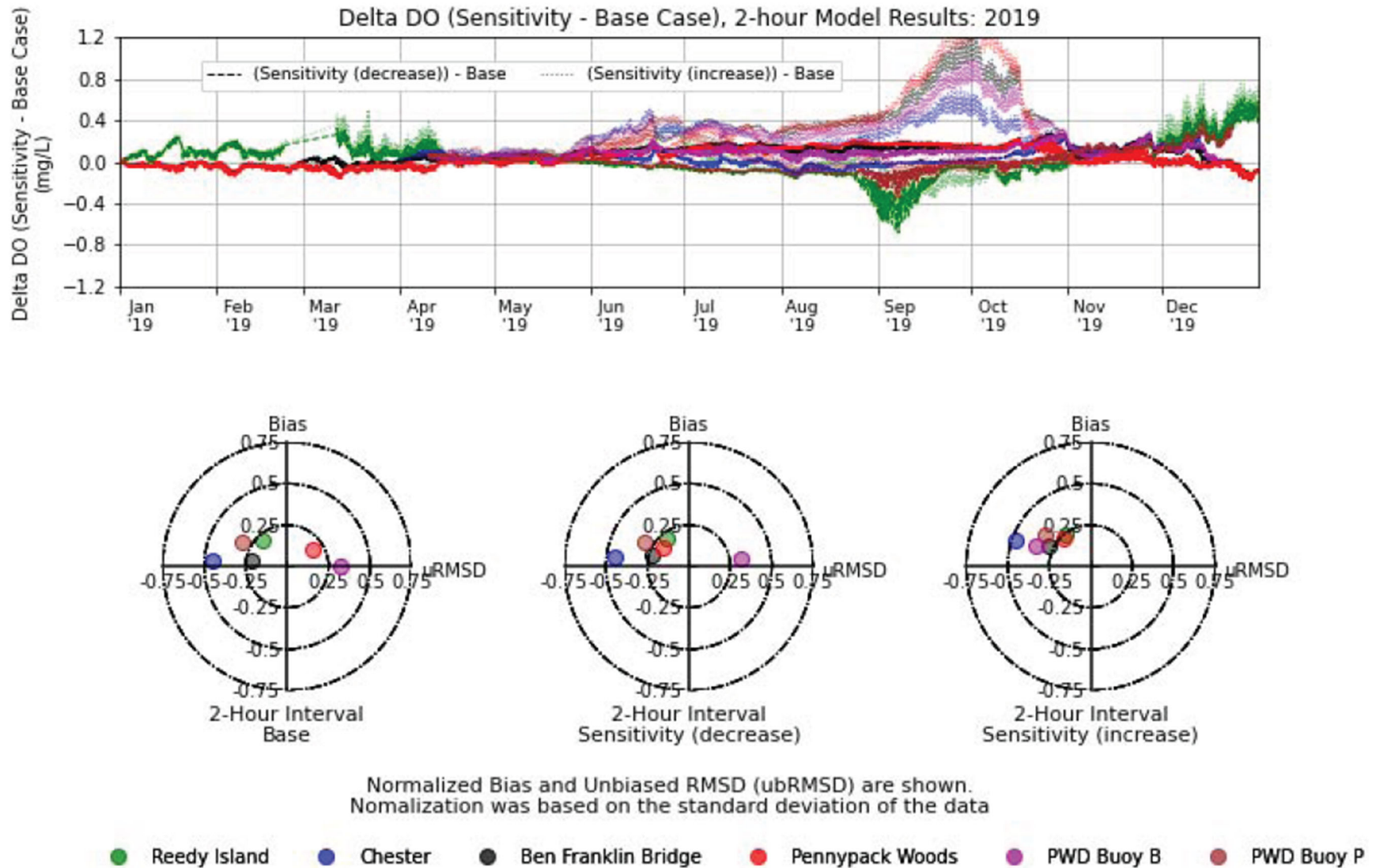


Figure 3-64: Sensitivity Test: Phytoplankton Maximum Growth Rate Constant (Group 1, 2, 3)

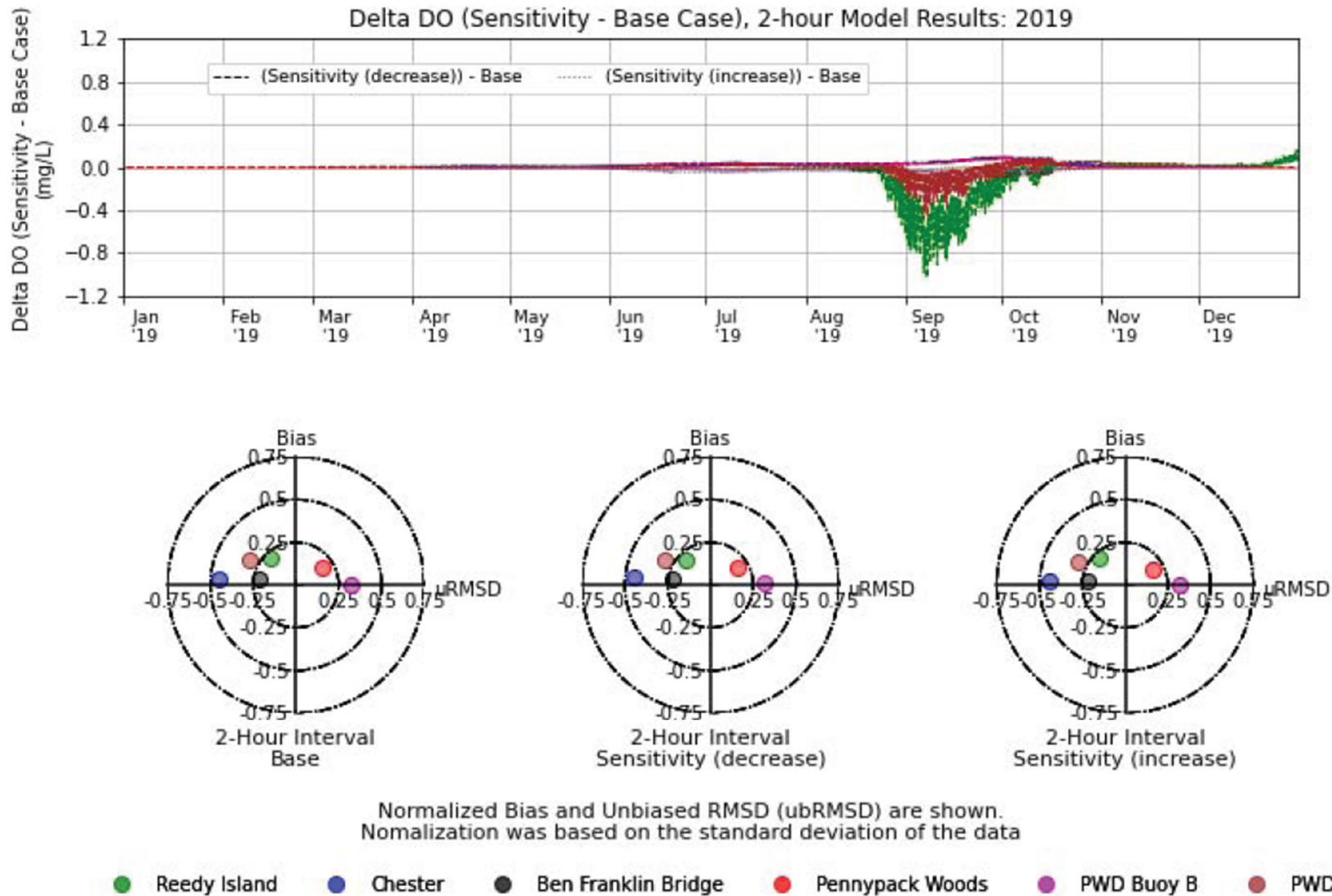


Figure 3-65: Sensitivity Test: Phytoplankton Respiration Rate Constant (Group 1, 2, 3)

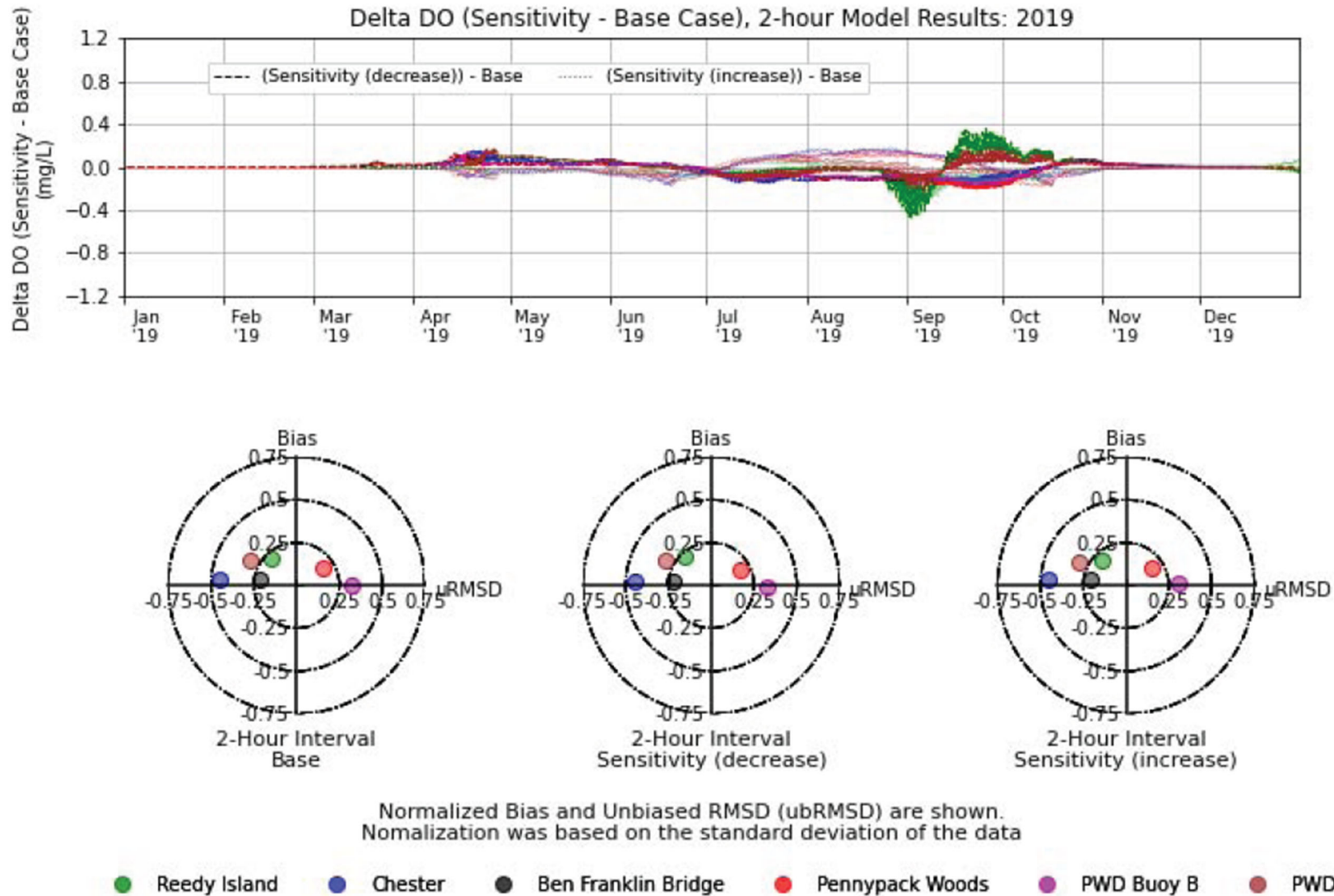


Figure 3-66: Sensitivity Test: Optimal Temperature for Growth (Group 1, 2, 3)

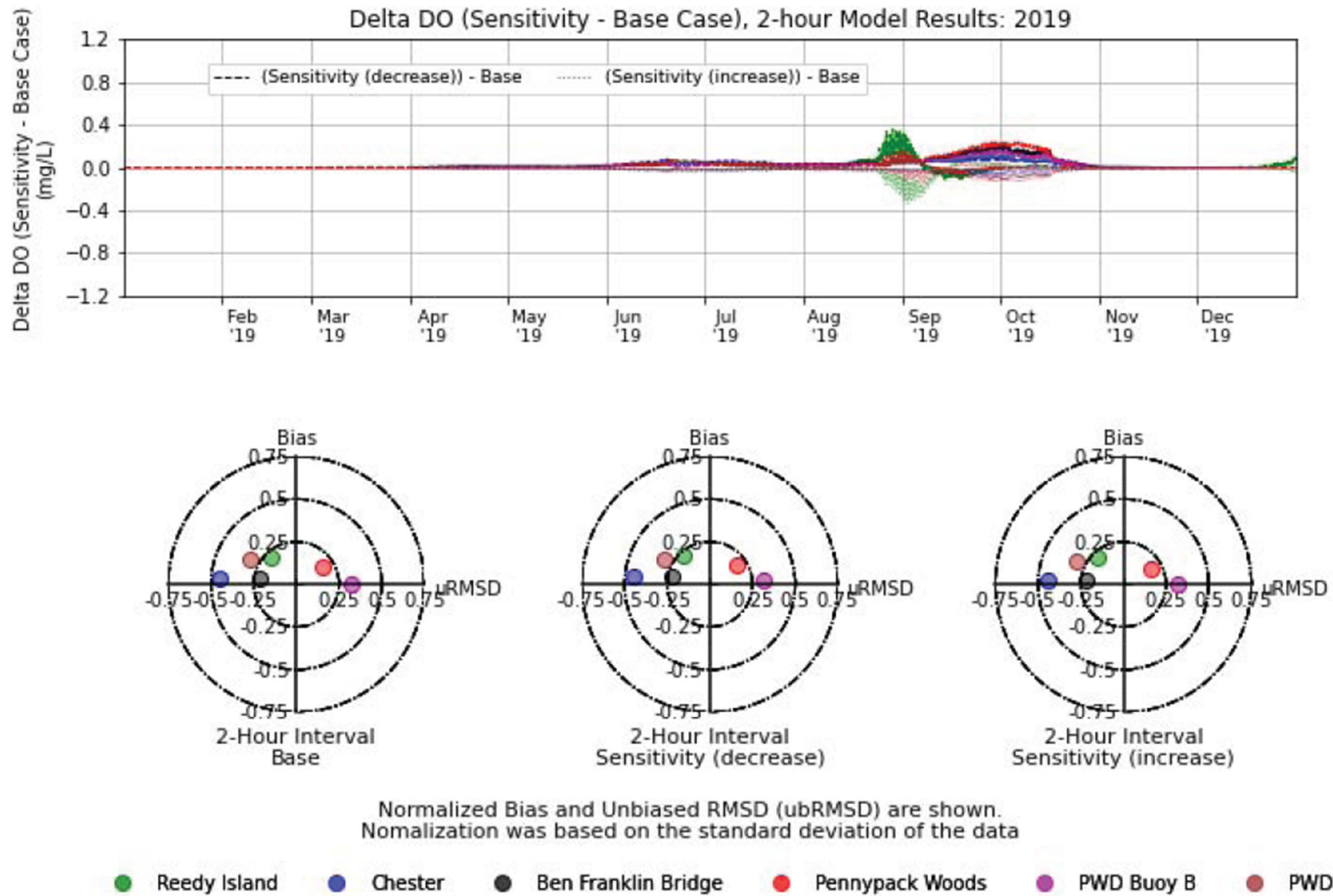


Figure 3-67: Sensitivity Test: Phytoplankton Optimal Light Saturation (Group 1, 2, 3)

3.2.7 MODEL LIMITATIONS

Numerical models are useful tools for testing and refining conceptual models of eutrophication, developing an understanding of the dynamics of the system of study, identifying potential management strategies, and guiding future monitoring efforts. Like any dynamic water-quality model, the Delaware Estuary model has inherent limitations and uncertainties due to data availability and quality, site-specific complexities, parametric uncertainty, and global parameterization.

Model algorithms used to simulate algal communities are simplifications of actual processes and rely on the use of global and lumped parameterization to describe complex interactions and responses to light, nutrients, flow, and vertical mixing, and do not allow for adjustments based on spatial, temporal, or water-quality variability within the estuary. Three general classes of phytoplankton simulated in this study are described by composited properties, and thus the model may predict behavior that is not necessarily representative of algal behavior in the Bay. Sources of error in this model include uncertainties in growth rates, nutrient uptake rates, settling rates, and stoichiometric ratios. In addition, the effects of zooplankton grazing on phytoplankton populations in the estuary were not well known during model construction, and thus were excluded from the study.

Estimation of watershed inputs using statistical techniques presents its own set of limitations on model accuracy. Simple methods for regionalization and transfer of hydrologic and water-quality information to unmonitored areas do not account for attenuation or transformation processes that likely occur during transport to the estuary. Generated time-series inputs may not account for episodic (higher flow) events and may not capture short-term variability in watershed processes and constituent concentrations.

A sediment diagenesis module with the capability of dynamically simulating sediment-water exchanges was tested in this study. However, predicted SOD was substantially lower than indicated by the survey data, which may be attributable to under-prediction/specification of slow reacting organic carbon from tributaries and watersheds and subsequent depletion in the sediment anaerobic layer, especially during heavy storm events. Considering the timeframe of the project, an externally specified option, i.e., specifying SOD and nutrient release rates from sediment based on field survey data, was adopted (see Section 3.1.4.6). Because the descriptive option dissociates diagenesis from water-column dynamics, predicting future conditions under discharge or load reduction scenarios may be problematic. However, the data analysis in Section 3.1.4.6 indicates no apparent temporal trends for SOD or benthic fluxes from 2012 to 2018. In addition, we compare the SOD data collected by PWD during 2012—2018 with historical SOD data collected by DRBC, EPA, and Academy of Natural Sciences in 1986 (DRBC 1987), in which about 35 sediment cores were collected and analyzed along 13 transects in the Delaware Estuary from RM 85 to 118. These data are converted to values at 20°C using the SOD temperature correction of 1.065 (Chapra 1997) employed in this modeling effort and compared to the SOD data collected by PWD from RM 80 to 120 on Figure 3-68 (a). The box plots display the minimum (bottom whisker), 25th-percentile (bottom edge), median (middle line), mean (triangle), 75th-percentile (upper edge), and maximum (upper whisker)

values among data. Generally, the SOD data collected in 1986 are slightly lower than those collected during 2012–2018. Since most of sediment cores collected by PWD are in the near-shore areas, we further excluded the 1986 SOD data collected in the mid-channel (i.e., mainly sand sediment). The revised comparisons are shown on Figure 3-68 (b), which indicates that SOD measurements spanning three decades are comparable. Additionally, the location of maximum SOD data is around RM 125, far away from urban area. These factors tend to moderate the limitations caused by the descriptive option.

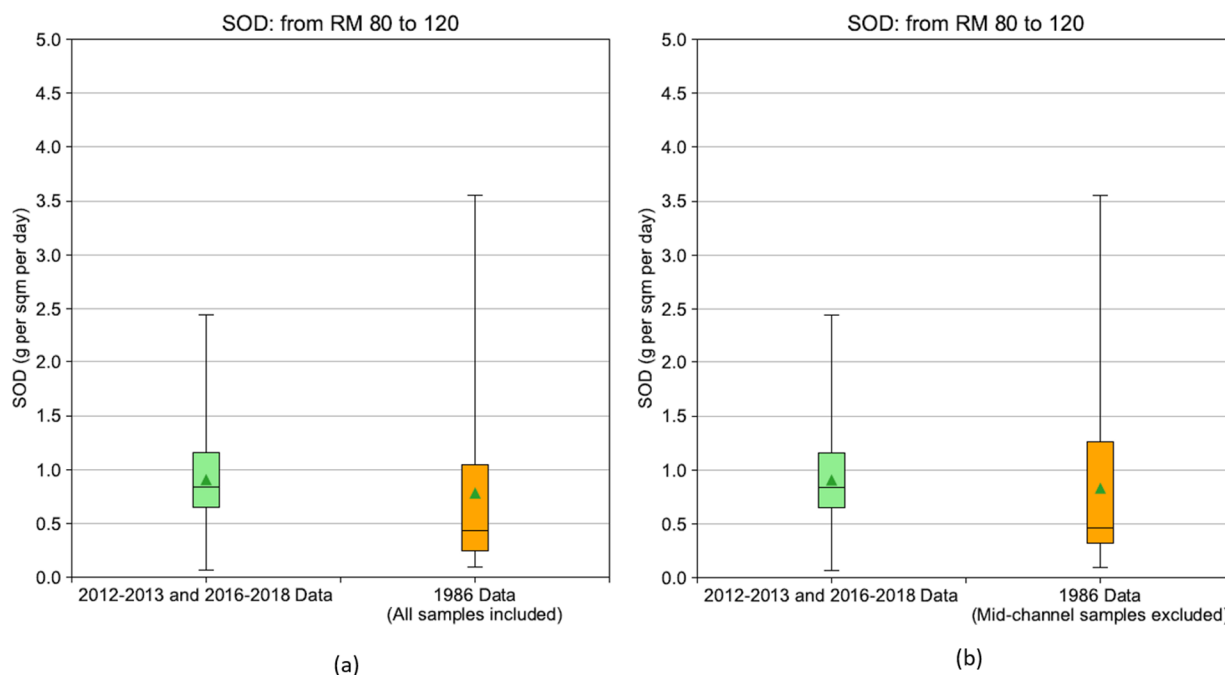


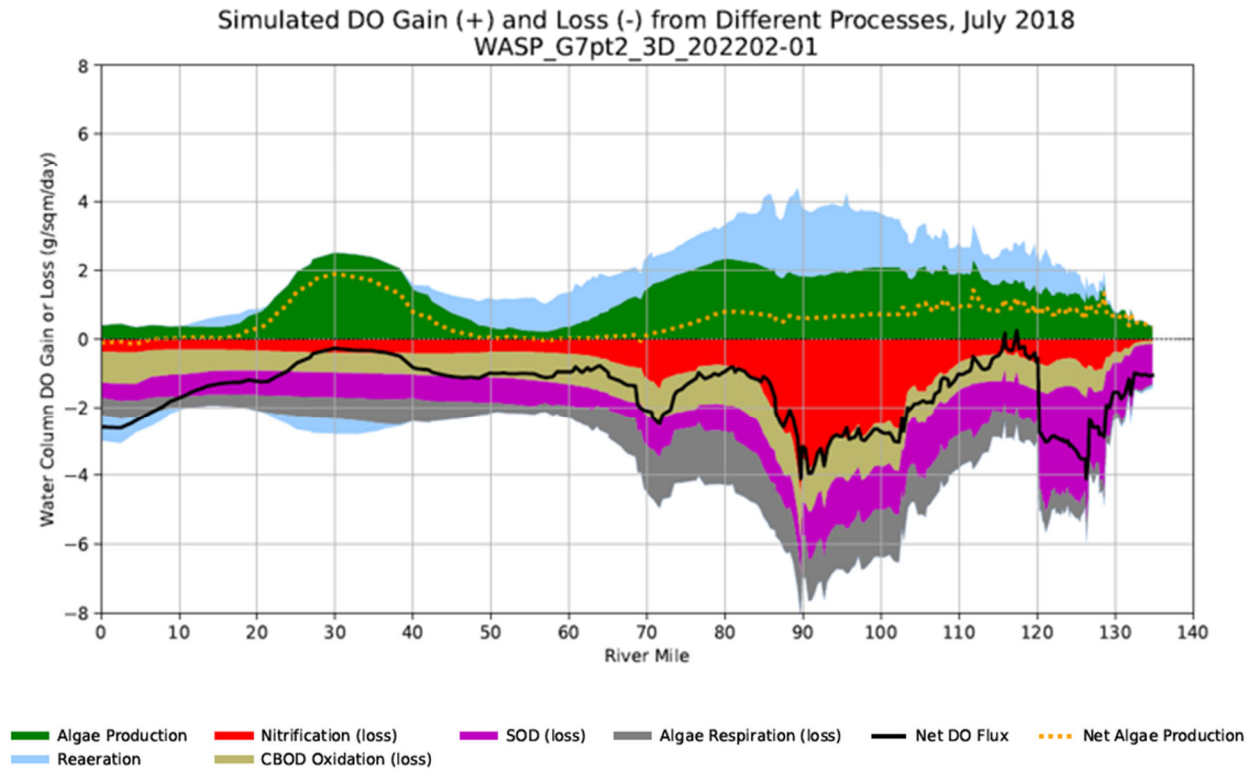
Figure 3-68: Comparisons of SOD Data Collected during 2012–2018 vs. 1986

The light extinction forcing function does not capture all the transient variation in water clarity, especially in the upper portion of the study area as discussed in Section 3.2.5.3. This is in part due to the limitation that a full-scale sediment transport model with resuspension and deposition is not included in this study, and the effect of suspended sediment on light extinction coefficient is not directly incorporated. A refinement to the light extinction forcing function may enhance the predictability of the phytoplankton dynamics.

The model is relatively sensitive to phytoplankton processes (Section 3.2.6), and the photosynthesis is one of the major processes controlling dissolved oxygen production (Section 3.2.5.1), but in some time periods the model under-predicts algal blooms in the tidal river during summer 2019 due to the limitation in light extinction forcing function (Section 3.2.5.3). At the same time, the model is still capable of predicting dissolved oxygen concentrations relatively well. To help explain why this is the case, a numerical test was conducted by turning off growth rates for all three phytoplankton groups to evaluate the influence of phytoplankton on the dissolved oxygen concentration. On Figure 3-69, the top panel shows the spatial dissolved oxygen components averaged over July 2018 from a base case with all parameters turned on,

the bottom panel presents the dissolved oxygen components averaged for the same period from the sensitivity test with zero growth rates for all three phytoplankton groups. On the dissolved oxygen production side when phytoplankton growth rates are zero, the contribution from photosynthesis disappear, meanwhile the reaeration process plays a role in filling many gaps left by the photosynthesis. On the dissolved oxygen loss side when the phytoplankton growth rates are zero, the contribution from respiration is reduced dramatically. Note that a little phytoplankton still exists in the system due to transport from boundaries. As a result of the predicted adjustments between the mechanisms impacting dissolved oxygen, the overall effect of zero phytoplankton growth on dissolved oxygen concentrations tends to be tempered. It is worthy to mention while the net effect of phytoplankton on the dissolved oxygen balance may not always be the largest, phytoplankton dynamics account for most of the temporal (episodic) variability in dissolved oxygen concentrations.

Base case



Numerical test – zero phytoplankton growth rates

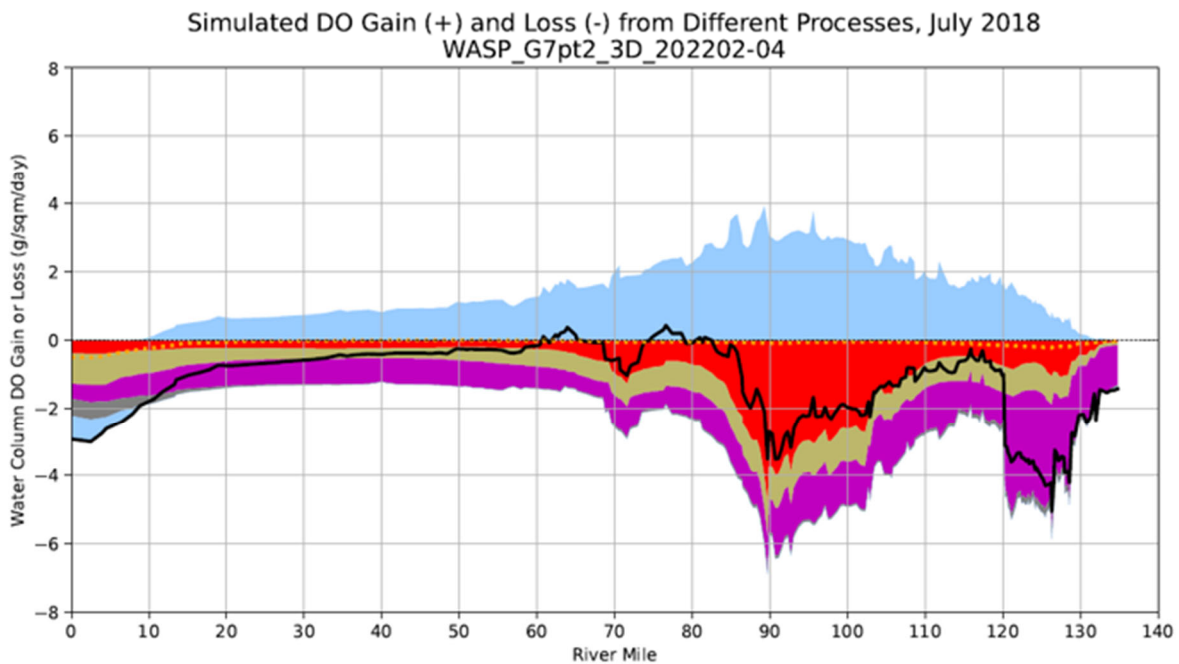


Figure 3-69: DO Components for July 2018: Base case vs. no phytoplankton growth

3.3 MODEL SUMMARY

The Delaware Estuary water quality model was well-calibrated to intensive project dataset for 2018-2019, with high flows in 2018 and medium flows in 2019, as well as moderately low DO in both years. The model corroboration was performed using 2012 available flows, boundary conditions, forcing functions without changing calibration coefficients. The model successfully hindcasted historical conditions in 2012 with low flows and low DO. Overall, the model predictions are quantitatively consistent with observed data across a range of flow and DO conditions.

The DRBC modeling team and the Model Expert Panel that DRBC informed and consulted with throughout the course of this nearly 5 yearlong modeling study conclude that (1) the Delaware Estuary water quality model is scientifically defensible over a wide range of environmental conditions; and (2) the model is appropriate for its intended use - to determine the improvement in dissolved oxygen condition that would result from specific reductions to point and nonpoint source loadings.

With the modelling tool, major processes controlling dissolved oxygen are identified as: reaeration and photosynthesis for production; and nitrification, followed by SOD, CBOD oxidation, and respiration for consumption. The extensive modeling study demonstrates that (1) nitrification is the most important low dissolved oxygen driver and is centered in the urban estuary; (2) low flows and high temperatures, as expected, exacerbate low dissolved oxygen; and (3) photosynthesis from phytoplankton tempers low dissolved oxygen events. The diagnostic analyses suggest that light and temperature control phytoplankton under the current conditions of the estuary and that autochthonous growth during summer periods of high clarity in Zone 2 can impact entire estuary.

REFERENCES

- Agrawal, Y.C., Terray, E.A., Donelan, M.A., Hwang, P.A., Williams III, A.J., Drennan, W.M., Kaham, K.K., Kitaigorodskii, S.A. 1992, Enhanced dissipation of kinetic energy beneath surface waves, *Nature*, 359, 219 – 220.
- Ambrose, R.B., Wool, T.A., and Barnwell, Jr. T.O. 2009. Development of water quality modeling in the United States. *Environ. Engineering Res.*, 14(4), 200-210.
- Brumer, S.E., Zappa, C.J., Anderson, S.P., Dugan, J.P. 2016. Riverine skin temperature response to subsurface processes in low wind speeds. *J. Geophys. Res.: Oceans*. Vol. 121, 1-15.
- Burchard, H. 2001. On the q^2/l Equation by Mellor and Yamada. 1982, *J. Physical Oceanography*, Vol. 31, 1377-1387.
- Burchard, H., Petersen, O., Rippeth, T.P. 1998. Comparing the performance of the Mellor-Yamada and the $k-\epsilon$ two-equation turbulence models. *J. Geophys. Res.* 103 (C5):10,543-10,554.
- Camacho, R.A., Zhang, Z., Chao, X. 2019. Receiving Water Quality Models for TMDL Development and Implementation. *J. Hydrologic Engineering*, Vol. 24, No. 2
- Cerco, C., Cole, T. 1994. Three-dimensional eutrophication model of Chesapeake Bay, Technical Report EL-94-4, US Army Engineer Waterways Experiment Station, Vicksburg, MS.
- Cerco, C.F, Noel, M.R. 2013. Twenty-one-year simulation of Chesapeake Bay water quality using the CE-QUAL-ICM eutrophication model. *J. the American Water Resources Association*. Volume 49, No. 5: 1119-1133.
- Cerco, C.F, Noel, M.R. 2017. The 2017 Chesapeake Bay Water Quality and Sediment Transport Model. A Report to the US Environmental Protection Agency Chesapeake Bay Program, May 2017 Draft, US Army Engineer Research and Development Center, Vicksburg, MS.
- Chapra, S.C. 1997. *Surface Water-Quality Modeling*. Ed., WCB/McGraw-Hill, New York, NY.
- Chapra, S.C. 2022. *Applied Numerical Methods with MATLAB for Engineers and Scientists, 5th Ed.*, WCB/McGraw-Hill, New York, NY.
- Chapra, S.C., Pelletier, G., Tao, H. 2012. QUAL2K: A Modeling Framework for Simulating River and Stream Water Quality (Version 2.12). Documentation.
- Churchill, M. A., Elmore, H.A., Buckingham, R.A. 1962. Prediction of stream reaeration rates." *J. San. Engr. Div., Proc. Amer. Soc. Civil Engr.*, 86(SA4):1-46.

- Cohn, T.A., DeLong, L.L., Gilroy, E.J., Hirsch, R.M., Wells, D.K., 1989. Estimating constituent loads. *Water Resources. Res.* 25 (5), 937–942.
- Connolly, J.P., and R. Winfield, 1984. A User’s Guide for WASTOX, a Framework for Modeling the Fate of Toxic Chemicals in Aquatic Environments. Part 1: Exposure Concentration. U.S. Environmental Protection Agency, Gulf Breeze, FL. EPA-600/3-84-077
- Covar, A. P. 1976. "Selecting the proper reaeration coefficient for use in water quality models." Presented at the U.S. EPA Conference on Environmental Simulation and Modeling, April 19-22, 1976, Cincinnati, OH.
- Davis, J.M. 2019. Instruction manual for R-calibration scripts. USEPA Region 4, Model Calibration Webinar Series. Updated on September 24, 2019.
- Di Toro, D.M., J.J. Fitzpatrick, and R.V. Thomann. 1983. Documentation for water quality analysis simulation program (WASP) and model verification program (MVP) No. EPA-600-3-81-044). U.S. EPA U.S Government Printing Office, Washington DC.
- Di Toro, D. M. 2001. *Sediment flux modeling*, Wiley-Interscience, New York, New York. 624 pp.
- Dolgoplova, E.N. 2014. Sediment Transport and Saltwater Intrusion into the Weakly Stratified Estuary of the Delaware River. *Water Resources* 41(2):143-162.
<https://doi.org/10.1134/S0097807814020067>
- DRBC. December 2021. Draft. *Modeling Eutrophication Processes in the Delaware Estuary: Three-Dimensional Hydrodynamics Model for the Delaware Estuary*. Delaware River Basin Commission. West Trenton, New Jersey.
- DRBC. October 2019. *Modeling eutrophication processes in the Delaware Estuary: quality assurance project plan*. Delaware River Basin Commission. West Trenton, New Jersey.
- DRBC, March 1987. *Sediment oxygen demand study*. Delaware River Basin Commission. West Trenton, New Jersey.
- Fisher, T. R., Gustafson, A.B. 2015. [Concentrations of nutrients and chlorophyll a, and rates of respiration and primary production in samples from Delaware Bay collected in May and July 2014](#). Cambridge, MD.
- Fisher, T. R, Gustafson, A. B. 2019. [Concentrations of nutrients and chlorophyll a, and rates of respiration and primary production in samples from Delaware Bay collected in May and July 2018](#). Cambridge, MD.

- Fisher, T. R, Gustafson, A. B. 2020. [Concentrations of nutrients and chlorophyll a, and rates of respiration and primary production in samples from Delaware Bay collected in May and July 2019.](#) Cambridge, MD.
- Garcia, H.E., Weathers, K.W., Paver, C.R., Smolyar, I., Boyer, T.P., Locarnini, R.A., Zweng, M.M., Mishonov, A.V., Baranova, O.K., Seidov, D., Reagan, J.R. 2019. World Ocean Atlas 2018. Vol. 4: Dissolved Inorganic Nutrients (phosphate, nitrate and nitrate+nitrite, silicate). A. Mishonov Technical Editor, NOAA Atlas NESDIS 84, 35pp.
- Hirsch, R.M., Moyer, D.L., Archfield, S.A., 2010. Weighted Regressions on Time, Discharge, and Season (WRTDS), with an application to Chesapeake Bay River inputs. *J. Am. Water Resour. Assoc.* 46 (5), 857–880.
- Inoue, T., Glud, R.N., Stahl, H., Hume, A. 2011. Comparison of three different methods for assessing in situ friction velocity: A case study from Loch Etive, Scotland. *Limnology and Oceanography: Methods*, 9:275-287.
- Jolliff, J.K., Kindle, J.C., Shulman, I., Penta, B., Friedrichs, M.A.M., Helber, R., and Arnone, R.A. 2009. Summary Diagrams for Coupled Hydrodynamic-Ecosystem Model Skill Assessment. *J. Mar. Syst.*, 76(1–2), 64–82
- Lavallee, H. 2021. Memorandum of Data Delivery to DRBC. Woods Hole Group, February 18, 2021.
- MacWilliams, M.L., Bever, Aaron J., Gross, Edward S., Gerard S. Ketefian², and Wim J. Kimmerer³ (2015). Three-Dimensional Modeling of Hydrodynamics and Salinity in the San Francisco Estuary: An Evaluation of Model Accuracy, X₂, and the Low-Salinity Zone. *San Francisco Estuary and Watershed Science*, 13(1).
- Martin, J.L, Wool, T.A. 2017. Supplement to water analysis simulation program user documentation, WASP Sediment Diagenesis Routines: Model Theory and User’s Guide.
- McSweeney, J. M., Chant, R.J., Wilkin, J.L., Sommerfield, C.K. 2017. Suspended-sediment impacts on light-limited productivity in the Delaware Estuary, *Estuaries and Coasts*, 40(4), 977-993
- Mellor, G.L., Yamada, T., 1982: Development of a turbulence closure model for geophysical fluid problems. *Rev. Geophys. Space Phys.*, 20(4):851-875.
- Moriasi, D. N., Arnold, J. G., Van Liew, M. W., Bingner, R. L., Harmel, R. D., and T. L. Veith. 2007. Model evaluation guidelines for systematic quantification of accuracy in watershed simulations. *Transactions of ASABE*. 50: 885–900.
- O’Connor, D.J. 1983. Wind effects on gas-liquid transfer coefficients. *J. Environ. Eng.*, 109(3):731–752.

- O'Connor, D.J., Dobbins, W. 1958. Mechanism of reaeration in natural streams. *Trans. Am. Soc. Civ. Eng.* 123: 641–684.
- Owens, M., Edwards, R.W., Gibbs, J.W. 1964. Some reaeration studies in streams. *Int. J. Air and Water Poll.*, 8, 469-486.
- Pareja-Roman, L. F., Chant, R.J., Sommerfield, C.K. 2020. Impact of historical channel deepening on tidal hydraulics in the Delaware Estuary, *J. Geophys. Res.: Oceans*, 125(12), e2020JC016256.
- Pennock, J. R. 1985. Chlorophyll distributions in the Delaware estuary: regulation by light-limitation, *Estuarine, Coastal and Shelf Science*, 21(5), 711-725
- Petrus K. 2015. Dissolved Oxygen and Nutrient TMDL for McKay Creek Tidal Segment, WBID 1633. Water quality evaluation and TMDL Program, Division of Environmental Assessment and Restoration, Florida Department of Environment Protection. August 2015
- Philadelphia Water Department, 2015. Green City, Clean Waters. Tidal Waters Water Quality Model – Bacterial and Dissolved Oxygen. Consent Order & Agreement Deliverable IX and X. City of Philadelphia Combined Sewer Overflow Long Term Control Plan Update. Submitted to The Commonwealth of Pennsylvania, Department of Environmental Protection. June 1, 2015.
- Philadelphia Water Department, 2022. Sediment oxygen demand and benthic flux data collected in the Delaware Estuary during 2012-2013 and 2016-2018. Provided by the PWD modeling team.
- Ralston, D. K., Geyer, W.R. 2017. Sediment transport time scales and trapping efficiency in a tidal river, *J. Geophys. Res.: Earth Surface*, 122(11), 2042-2063.
- Runkel, R.L., Crawford, C.G., Cohn, T.A., 2004. Load Estimator (LOADEST): A FORTRAN Program for Estimating Constituent Loads in Streams and Rivers. U. S. Geological Survey Techniques and Methods Book 4, Chapter A5
- Schopp R.D., Firda G.D. 2008. Flood magnitude and frequency of the Delaware River in New Jersey, New York, and Pennsylvania. U.S. Geological Survey Open-File Report 2008–1203.
<https://pubs.usgs.gov/of/2008/1203/>
- Schwede, D.B.; Lear, G.G. A novel hybrid approach for estimating total deposition in the United States; *Atmos. Environ.* 2014, 92, 207-220
- Terray, E.A., Donelan, M.A., Agrawal, Y.C., Drennan, W.M., Kahma, K.K., Kitaigorodskii, S.A., Hwang, P.A., Williams, A.J. 3rd. 1996: Estimates of kinetic energy dissipation under breaking waves. *J. Phys. Oceanogr.*, 26, 792-807.
- Tetra Tech, Inc., 2007. The Environmental Fluid Dynamics Code, Theory and Computation. Volume 1: Hydrodynamics and Mass Transport. 10306 Eaton Place, Suite 340, Fairfax, VA 22030.

- Tetra Tech, Inc., 2015. Final Report, Hydrodynamic and Water Quality Modeling Report for the Savannah Harbor, Georgia. Prepared for the Department of the Army, Savannah District, Corps of Engineers, 100 W Oglethorpe Avenue, Savannah, Georgia 31401-3640. Contract: 100-ATL-T32468.
- Tetra Tech, Inc., 2016. High Rock Lake Hydrodynamic and Nutrient Response Models, Draft Report Prepared by Tetra Tech, Inc under EPA Contract, September 2012. Report Finalized by the North Carolina Division of Water Resources, October 2016.
- Tsivoglou, E. C., Wallace, R. J. 1972. Characterization of stream reaeration capacity. Research Reporting Series. U.S. Environmental Protection Agency, 317.
- Ullman, W.J., J.R. Scudlark and J.A. Volk, 2010. Standard Operating Procedure for the Calculation of N and P Deposition from the Atmosphere to Waters of Delaware’s Inland Bays. Report to the Center for the Inland Bays. 11 p
- USEPA, 2021, “WASP model documentation.” Accessed Nov. 24, 2021.
<https://www.epa.gov/ceam/wasp-model-documentation>.
- Valle-Levinson A. 2009. Definition and classification of estuaries. Chapter 1 in Contemporary Issues in Estuarine Physics, Edited by A. Valle-Levinson. Cambridge University Press. 978-0-521-89967-3.
- Walski, T. May 2019. Why global standards for calibration of water distribution models won’t work. *J. Am. Water Works Assoc.*, v111(5):31-34.
- Wool, T.A., Ambrose, R.B., Martin, J.L. 2004. WASP8 Multiple Algae – Model Theory and User’s Guide. Supplement to Water Quality Analysis Simulation Program (WASP) User Documentation. USEPA Office of Research and Development, Washington, DC.
- Wool, T.A., Ambrose, R.B., Martin, J.L 2018. Water Quality Analysis Simulation Program (WASP 8.2), Water Quality Modeling Workshop Documents, June 11 – 15, 2018. Atlanta, GA.
- Wool, T.A., Ambrose, R.B., Martin, J.L., Comer A. 2020. WASP8: The next generation in the 50-year evolution of USEPA’s water quality model. *Water (Basel)*. 2020, 12(5), 1398.
- Wool, T.A., Ambrose, R.B., Martin, J.L., Comer, E.A. 2006. Water Quality Analysis Simulation Program (WASP), Version 6.0 Draft: User’s Manual. USEPA Environmental Research Laboratory. Athens, GA.
- Wool, T.A., Davie, S.R., Rodriguez, H.N. 2003. Development of three-dimensional hydrodynamic and water quality models to support total maximum daily load decision process for the Neuse River Estuary, North Carolina. *J. Water Resources Planning and Management*, Vol. 129, No. 4.
- Zafer Defne, Spitz, V.J., DePaul, V., Wool, T.A. 2017. Toward a comprehensive water-quality modeling of Barnegat Bay: Development of ROMS to WASP coupler. *J. Coastal Research*. No. 78

Zambrano-Bigiarini, M. 2017. hydroGOF: Goodness-of-fit functions for comparison of simulated and observed hydrological time series. R package version 0.3-10. URL <http://hzambran.github.io/hydroGOF/>

Zappa, C.J., McGillis, W.R., Raymond, P.A., Edson, J.B., Hints E. J., Zemmeling, H.J., Dacey, J.W.H., and Ho, D.T. 2007. Environmental turbulent mixing controls on air-water gas exchange in marine and aquatic system. *Geophysical Research Letters*, Vol. 34. 1-6.

Appendix A: Monitoring Results

- Point source concentrations
- Point source loads
- Tributary concentrations
- Tributary loads

Appendix B: Transect Profile Data

Appendix C: Verification of Transport Fidelity

- Conservative tracer simulations
- Mass balance check
- DO comparisons
- Summary

Appendix D: Enhancement in Reaeration Simulation

1. Impact of Vertical Segmentation on Ammonium and Oxygen Profiles in Estuaries
2. Calculate Mass Transfer Coefficient with Turbulence Dissipation Rate
3. Comparisons of dissolved oxygen results between Zappa's approach and conventional approaches

Appendix E: State Variable Calculation

1. Nitrogen
2. Phosphorous
3. Carbon
4. Silica
5. Suspended solids

Appendix F: Model to Data Comparisons

- WASP calibration parameters
- Boat-run data (Spatial)
- Boat-run data (Time Series, 1-to-1, and CFD)
- Statistical metrics definition
- Boat-run statistical metric summary
- Light extinction (K_e)
- Phytoplankton seasonal variation
- Continuous data comparisons – 2012 DO and DOSAT
- Continuous data comparisons – 2012 Phytoplankton

Appendix G: Diagnostic Analyses

- DO component analysis
- Phytoplankton limiting factors
- Zone-2 light attenuation diagnosis – K_e
- Zone-2 light attenuation diagnosis - DO
- Zone-2 light attenuation diagnosis - Phytoplankton

Appendix H: Sensitivity Analysis

End of Document